Suivi de santé structurale basé sur l'identification modale opérationnelle

Duc Tuan Ta

université PARIS-SACLAY

Structural health monitoring based on operational modal analysis

Suivi de santé structurale basé sur l'identification modale opérationnelle

Thèse de doctorat de l'Université Paris-Saclay

École doctorale n° 579, Sciences Mécaniques et Énergétiques, Matériaux et Géosciences (SMEMAG)
Spécialité de doctorat: Génie civil
Graduate School : Sciences de l'ingénierie et des systèmes. Référent: Université d'Évry Val-d'Essonne

Thèse préparée dans l'unité de recherche LMEE (**Université Paris-Saclay, Univ Evry**), sous la direction de **Thien-Phu LE**, Maître de conférences-HDR, le co-encadrement de **Michael BURMAN**, Maître de conférences

Thèse soutenue à Paris-Saclay, le 13/10/2022, par

Duc Tuan TA

Composition du jury:

Alexis Béakou Professeur, Institut national polytechnique Clermont-Auvergne (Sigma Clermont)	Président
Pierre Argoul Chercheur - HDR, Gustave Eiffel University	Rapporteur
Luigi Garibaldi Professeur, Politecnico di Torino	Rapporteur
Jean Lerbet Professeur, Université d'Évry, Paris-Saclay	Examinateur
Thien Phu Le Maître de conférences - HDR, Université d'Évry, Paris-Saclay	Directeur de thèse

Thèse de doctorat

NNT: 2022UPAST120

Acknowledgments

In writing this thesis, I received a lot of support from everyone, including supervisors, family, friends, and colleagues.

I would like to express my deep gratitude to my supervisors Thien-Phu Le and Michael Burman. I had the pleasure of getting to know them and working with them. Thanks to their exceptional responsiveness, great patience and availability throughout my thesis, I have benefited greatly from exceptionally effective supervision. Their scientific skills, as well as their human qualities allowed me to complete this thesis.

I express my deepest gratitude to the members of the Committee. I sincerely thank Dr. Pierre Argoul, Chargé de recherche at Université Gustave Eiffel and Dr. Luigi Garibaldi, Professor at Politecnico di Torino for devoting their time to carefully reading and evaluating my dissertation as reviewers. Their comments helped me to improve this manuscript. I sincerely thank Dr. Alexis Béakou, Professor at Institut national polytechnique Clermont-Auvergne (Sigma Clermont) and Dr. Jean Lerbet, Professor at Université de Évry Val d'Essonne for kindly agreeing to be examiners.

I am sincerely grateful to the French government for providing financial assistance through the Excellence Scholarship Program.

I express my sincere gratitude to Dr. Minh-Ngoc Vu for helping me from the first days of my stay in France. His knowledge and kindness have always been a source of inspiration.

I would also like to thank the director of the laboratory, Professor Olivier Quemener, and the current and former members of Laboratoire de Mécanique et d'Energétique d'Evry (LMEE) for their friendship, understanding and support.

I would like to take this opportunity to thank my parents for their support. Words can not express my gratitude for all their support and self-sacrifice. Special thanks to my sister Thu-Hien. She has provided me with a tremendous emotional and psychological support throughout these years, and for that I am eternally grateful for her.

I am especially grateful to my friend Ngoc-Anh. Her smile and jokes always bring so much joy and support for any occasion. Her support is a great comfort and contributes to the success of this work.

Abstract

Structural health monitoring (SHM) is primordial for safe use and is essential for sustainable development. Among existing methods for SHM, vibration-based methods are the most commonly used. Operational modal analysis (OMA) is suitable for real structures as it offers several advantages: low cost, normal use of structures, and continuous monitoring. However, it has some main obstacles: (i) uncertainty in identified modal parameters due to unmeasured and uncontrolled operational excitations; (ii) underdetermined problems when the number of measured responses is less than that of active modes; (iii) the relationship between the damage in terms of change in mechanical properties like mass and stiffness and the change in modal parameters, is not straightforward, and it often goes through finite element update steps resulting in computational burden; (iv) in reality, there may be several damages in a structure, and the detection of multiple damages is not obvious. Therefore, the objectives of the thesis are: (i) overview of efficient and popular methods for operational modal analysis and damage identification; (ii) propose improvements to existing methods or a novel method that can deal with underdetermined cases; (iii) develop a procedure for rapid damage detection based on a simplified relationship between damage and changes in modal parameters; (iv) introduce an enhanced procedure for multiple damage detection in structures. To achieve these objectives, the obtained results of the thesis can be briefly summarized in the following four contributions.

The first contribution is an improvement of the existing modal identification technique based on the PARAllel FACtor (PARAFAC) decomposition in time domain. The third-order tensor of the covariance of responses is first decomposed into components corresponding to structural modes or harmonic components. A minimum length of autocovariance functions using natural periods and damping factors is suggested to distinguish between harmonics and structural modes accurately.

The second contribution is the development of a novel method for modal identification based on PARAFAC decomposition in frequency domain. Using the PARAFAC decomposition, a third-order tensor in frequency constructed from Power Spectral Density (PSD) of responses is first decomposed into rank-1 tensors that can be structural modes or harmonic components. The auto-PSD function of each rank-1 tensor is then used to identify modal parameters, while spectral kurtosis values are used for the distinction of structural modes and harmonics.

The third contribution is devoted to the proposal of an efficient method for the rapid detection and quantification of a single local change in the mass and/or stiffness of like-beam structures using identified modal parameters. This contribution considers the relationship between local changes in the mass and/or stiffness of a beam and its natural frequency shift

and mode shape, and explicitly gives an analytical expression. Based on the proposed expression, linear regression is applied to obtain accurate results of the change in the mass/stiffness of the beam.

The fourth contribution aims to extent the previous damage identification procedure for multiple damage detection. Comparison between natural frequency shifts obtained directly from the analytic expression established in the former contribution instead of using FEM and measured ones allows multiple damages to be identified using Bayesian inference. The proposed identification of damages becomes rapid because it skips the computational cost caused by FEM simulations.

All the above contributions have been validated by numerical simulations and experimental laboratory tests.

Contents

List of Abbreviations **ix**

List of Symbols **xi**

1 Introduction to structural heath monitoring **1**
1.1 General introduction . . . 1
1.2 Modal analysis . . . 3
1.2.1 Dynamics of structures . . . 3
1.2.2 Classical experimental modal analysis . . . 4
1.2.3 Operational modal analysis . . . 7
1.3 Blind source separation . . . 8
1.3.1 Independent component analysis . . . 11
1.3.2 Second-order blind identification . . . 11
1.3.3 Sparse component analysis . . . 12
1.3.4 Tensor decomposition . . . 12
1.4 Harmonic detection in modal analysis . . . 14
1.4.1 Histograms and kurtosis values . . . 15
1.4.2 Spectral kurtosis . . . 16
1.5 Structural damage detection . . . 17
1.5.1 Traditional non-destructive testing methods . . . 18
1.5.2 Vibration-based damage identification methods . . . 19
1.6 Challenges and objectives . . . 25
1.7 Organization . . . 26
1.8 Publications . . . 27

2 Operational modal analysis in the time domain **39**
2.1 An enhanced method for modal analysis in the time domain (Article 1) . . . 39

3 Operational modal analysis in the frequency domain **59**
3.1 A novel method for modal analysis in the frequency domain (Article 2) . . . 59

4 Single damage detection **93**
4.1 Single damage detection using natural frequency shifts and mode shapes (Article 3) . . . 94

5 Multiple damage detection **131**
5.1 A enhance method for multiple damage detection (Article 4) . . . 132

6 General conclusions and perspectives **155**
6.1 Conclusions 155
6.2 Perspectives 157

A Résumé étendu en Français **159**

List of Abbreviations

SHM	Structural Health Monitoring
EMA	Experimental Modal Analysis
OMA	Operational Modal Analysis
FRFs	Frequency Response Functions
IRFs	Impulse Response Functions
DOF	Degree-Of-Freedom
PSD	Power Spectral Densitiy
SVD	Singular Value Decomposition
EMD	Empirical Modal Decomposition
FFT	Fast Fourier Transform
DFT	Discrete Fourier Transform
STFT	Short Time Fourier Transform
WPT	Wavelet Packet Transform
CWT	Continuous Wavelet Transform
HHT	Hilbert–Huang Transform
PDF	Probability Density Function
ALS	Alternating Least Square
SISO	Single-Input-Single-Output
SIMO	Single-Input-Multiple-Output
SISO	Multiple-Input-Single-Output
MIMO	Multiple-Input-Multiple-Output
MAC	Modal Assurance Criterion
CEA	Complex Exponential Algorithms
LSCE	Least-Squares Complex Exponential

PTD	Polyreference Time Domain
HPB	Half-Power Bandwidth
ITD	Ibrahim Time Domain
ERA	Eigen Realization Algorithm
SSI	Stochastic Subspace Identification
PP	Peak-Picking
FDD	Frequency Domain Decomposition
CMIF	Complex Mode Indicator Function
RFP	Rational Fraction Polynomial
BSS	Blind Source Separation
ICA	Independent Component Analysis
SOBI	Second Order Blind Identification
JAD	Joint Approximate Diagonalization
SCA	Sparse Component Analysis
SK	Spectral Kurtosis
SDD	Structural Damage Detection
NDT	Non-Destructive Testing
GPS	Global Positioning System
FEM	Finite Element Method
ML	Machine Learning
ANNs	Artificial Neural Networks

List of Symbols

$\mathbf{M}$	Mass matrix
$\mathbf{C}$	Damping matrix
$\mathbf{K}$	Stiffness matrix
$\mathbf{x}(t)$	Vector of displacements
$\mathbf{s}(t)$	Vector of sources
n_x	Number of measurement signals
n_s	Number of sources
$\mathbf{f}(t)$	Excitation
$\mathbf{\Phi}$	Mode shape matrix
ξ	damping ratio
ω	angular frequency
f	natural frequency
$\mathbf{q}(t)$	Vector of modal coordinates
$\mathbf{H}(\omega)$	Frequency response function
$\mathbf{h}(t)$	Impulse response function
$\mathbf{A}$	Mixing matrix
E	Expectation operator
τ	Time lag
k	Kurtosis value
$\mathbf{C}_x$	Correlation matrix of measurement signals
$\mathbf{C}_q$	Correlation matrix of modal coordinates
$*$	Convolution operator
$\odot$	Khatri-Rao product
$\circ$	Tensor outer product
$\|\|.\|\|$	Frobenius norm
$\mathbb{N}$	The set of natural numbers
$\mathbb{C}^{n_1}$	n-dimensional vector space over the field of the complex numbers

1 Introduction to structural heath monitoring

Chapter abstract

Structural Health Monitoring (SHM) is process of in-service health assessment for a structure through a monitoring system. It is a key element of cost-effective maintenance strategies. A complete SHM system includes many components: sensor networks, modal analysis, damage assessment, and decision making. Modal identification and damage detection are considered to be the most important components of a SHM system. The general principle of SHM is that modal parameters are first determined from vibration measurements using modal analysis methods. The obtained modal parameters are then associated with a change in structure's parameters, such as a decrease in stiffness or a change in mass, due to structural damage. Therefore, it is natural to use the measured change in dynamic behavior to determine structural damage. The main advantage of the vibration-based approach is that damage can be determined globally, even if the damage site cannot be reached.

This chapter is constructed as follows. First, a general introduction of Structural Health Monitoring is presented in Section 1.1. Then, the most common methods used in modal analysis are briefly described in Sections 1.2-1.4. Next, several Structural Damage Detection (SDD) methods are summarized in Section 1.5. The challenges, objectives and the organization are highlighted in Sections 1.6-1.7, respectively. Finally, Section 1.8 lists the main contributions of the research presented in this dissertation, which addresses the issues discussed in this chapter.

1.1 General introduction

The health of a structure can be stated as its current ability to safely and effectively provide the intended level of service against expected hazards during its service life [1]. SHM performs health assessment of engineering structures using a system of sensors, associated hardware and software to monitor the performance and the operational environment of engineering structures. It provides useful information for optimizing the maintenance planning of engineering structures for reliable operation, cost-effectively schedule maintenance planning and repair. Therefore, over the past decades, this topic has attracted considerable attention

of researchers. Comprehensive reviews of SHM development can be found in studies [2, 3, 4]. A schematics of a structural health monitoring system is shown in Fig. 1.1.

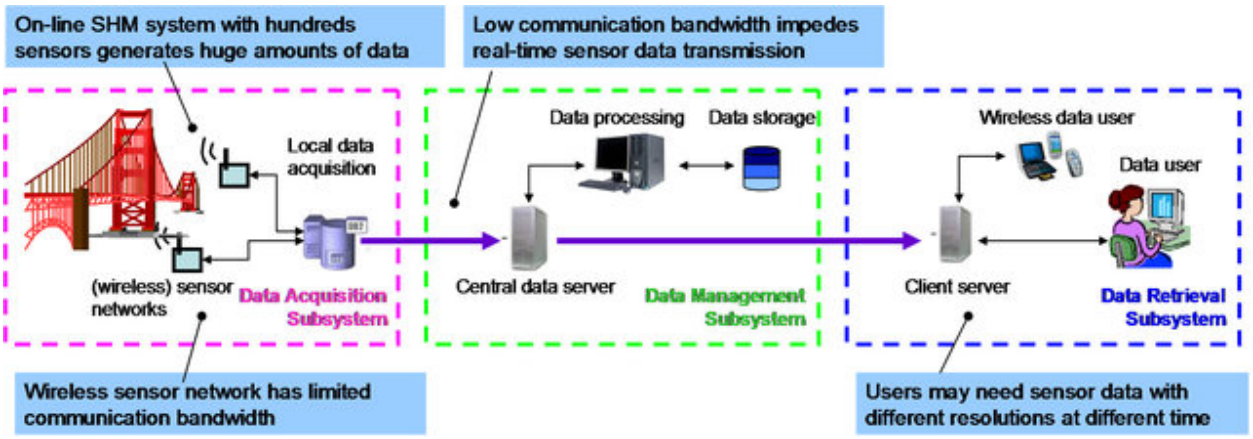

FIGURE 1.1: Schematics of a structural health monitoring system [5]

Engineering infrastructure includes bridges, buildings, towers, pipelines, tunnels, dams, and other structures. Although the necessary design methods were initially adopted, these engineering structures will degrade over time. This deterioration is due to a variety of causes, including structural aging, cyclic loading and environmental factors (e.g. steel corrosion, concrete carbonation) [6]. In addition, degradation can be caused by infrequent natural disasters such as earthquakes, hurricanes, and floods. All these factors are uncertain variables, so it is difficult to determine the health state of a structure according to its age as well as its use and safety against the harsh effects of nature.

(a) Tacoma bridge **(b)** Sampoong Department Store

FIGURE 1.2: Examples of structural failure [7]

Several case studies have reported collapse and damage of civil engineering structures due to insufficient SHM [8, 9, 10]. Here are some illustrative examples to prove this fact. In the study [1] the catastrophic structural failure of the I-35 highway bridge due to aging was highlighted as a critical civilian infrastructure problem. The collapse of the Tacoma Narrows Bridge (TNB) in 1940 is undoubtedly the most famous structural failure attributed to a the sudden change from a vertical to a torsional mode of oscillation [11]. In 1864, Dale Dyke Dam in the United Kingdom collapsed due to the formation of cracks in the embankment

[12]. The Sampoong Department Store collapsed in 1989, along with 1,500 employees inside, due to massive cracks that were noticed but ignored. Similarly, in recent years, the Florida International University pedestrian bridge suffered structural damage due to crack growth in 2018 [13], and the Xinjia Express Hotel due to the unauthorized construction of an additional floor in 2020 [14]. Thus, the above examples highlight the importance of SHM, since the long-term safe and economical use of civil structures depends largely on proper maintenance and use management [15].

The development of SHM technology for cost-effective infrastructure management has attracted significant attention from the engineering community as tt is essential to identify damages in structures as early as possible. In SHM, vibration-based methods are generally more commonly used for modal analysis and damage detection, as they offer advantages such as low cost, applicability during normal operation of structures, and continuous monitoring [16]. However, the application of these methods also have some limitations, which have stimulated research and development based on the continuous observation and interpretation of the comprehensive performance of engineering structures during use. It is clear that SHM technology can bring enormous security and economic benefits. The future development of the SHM strategy requires a multidisciplinary research effort involving areas such as sensing, signal processing, data interpretation, numerical modeling, and computational hardware.

1.2 Modal analysis

The design and construction of large engineering structures, such as long bridges and high-rise buildings, is becoming more common. This requires the development of reliable methods to accurately identify the most relevant dynamic characteristics: natural frequency, mode shape, and damping ratio. Such modal identification methods can provide reliable information to support validation of models used during the design phase. These methods also provide up-to-date information to help identify damage in engineering structures through structural health monitoring systems.

1.2.1 Dynamics of structures

Consider a classically damped system with n Degree-Of-Freedom (DOF) subjected to an excitation $\mathbf{f}(t)$ as follows:

$$\mathbf{M}\ddot{\mathbf{x}}(t) + \mathbf{C}\dot{\mathbf{x}}(t) + \mathbf{K}\mathbf{x}(t) = \mathbf{f}(t) \tag{1.1}$$

where $\mathbf{x}(t)$ is the vector of displacements. $\mathbf{M}$, $\mathbf{C}$, $\mathbf{K}$ are mass, damping and stiffness matrices, respectively.

For the viscous damping model, the damping force is assumed to be proportional to the velocity. For systems with external dampers, or with energy dissipation devices, or made of various materials differ significantly in properties from viscous damping, the resulting damping matrix is non-proportional. For such systems, each component of a given mode shape is characterized by its amplitude and phase [17].

A damping matrix is proportional to the mass and/or stiffness matrix and it satisfies the orthogonality conditions.

$$\mathbf{C} = a_0\mathbf{M} + a_1\mathbf{K} \tag{1.2}$$

where a_0 and a_1 are arbitrary coefficients. The orthogonality properties of mode shapes can be applied to the damping matrix:

$$\begin{cases} \mathbf{\Phi}_i^T\mathbf{C}\mathbf{\Phi}_j = 0, & i \neq j \\ \mathbf{\Phi}_i^T\mathbf{C}\mathbf{\Phi}_i = 2\xi_i\omega_i \end{cases} \tag{1.3}$$

where $\mathbf{\Phi}, \xi_i, \omega$ are mode shape matrix, damping ratio and angular frequency, respectively.

In the case of proportional damping, $\mathbf{\Phi}$ are real values while $\mathbf{\Phi}$ are complex values if damping is not proportional.

The vector of displacements $\mathbf{x}(t)$ can be represented in the form of a modal superposition of the vibration modes:

$$\mathbf{x}(t) = \mathbf{\Phi}\mathbf{q}(t) \tag{1.4}$$

where $\mathbf{\Phi}$ is the mode shape matrix and $\mathbf{q}(t)$ is a column vector of modal coordinates.

Relation (1.4) shows that the measured responses can be used to determine the modal parameters of the system. The process of correlating the dynamic characteristics of a mathematical model with the physical properties of the system derived from experimental measurements called modal identification of an engineering structure [18].

A huge number of modal identification methods have been developed for this area, and they can be divided into two groups depending on what data they use: input-output identification methods and output-only identification methods [18]. Input-output methods, known as classical modal testing methods or Experimental Modal Analysis (EMA), require both input and output information (excitations and responses). Output-only identification methods, also known as Operational Modal Analysis (OMA), require only response measurements of the structure under operational conditions. These methods can be performed in either the time domain or in the frequency domain. The most common methods will be briefly reviewed in the following subsections.

1.2.2 Classical experimental modal analysis

Classical modal testing methods are known as input-output methods or Experimental Modal Analysis (EMA), which is based on controlled input that is measured and used in the identification process. In classical modal analysis, Frequency Response Functions (FRFs) or Impulse Response Functions (IRFs) are constructed from the relationship between the applied external force and the corresponding responses at predetermined points on the structure. Many techniques have been developed for input-output modal identification, based on estimating a set of FRFs or corresponding IRFs. Comprehensive reviews of input-output modal identification methods can be found in [19, 20, 21, 22].

The frequency response function can be represented as follows:

$$\mathbf{H}(\omega) = \sum_{1}^{n} \frac{\mathbf{\Phi}_i \mathbf{\Phi}_i^T}{\omega_i^2 - \omega^2 - 2j\omega_i\omega} \tag{1.5}$$

where ω_i is the i^{th} frequency of structure.

Classical EMA methods are generally used to determine the dynamic characteristics of small and medium-size structures. On rare occasions, these methods are used on large structures because of the complexity of providing significant excitation levels to a large, massive structure. In these tests, artificial excitation is applied to structures to induce vibrations. By measuring the response of structure to these known forces, the dynamic characteristics of the structure can be determined. The measured excitation and response time histories are used to estimate FRFs, or IRFs between measured outputs and measured inputs, as it shown on the Figure .1.3

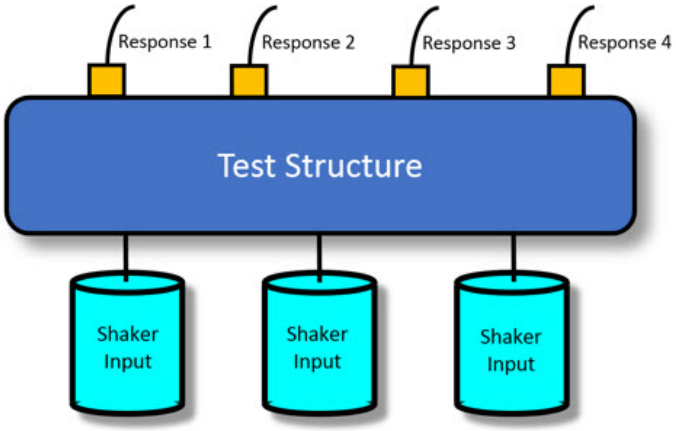

FIGURE 1.3: An example of a MIMO system

The developments in these methods progressed from Single-Input-Single-Output (SISO) systems through Single-Input-Multiple-Output (SIMO) systems, then through Multiple-Input-Single-Output (SISO) systems to the general case of Multiple-Input-Multiple-Output (MIMO) systems. These methods can work in both time and frequency domain.

- **Classical time domain identification methods**

Time domain identification methods have been developed and become widely available over the past decades. Logarithmic decrement technique was introduced by Rayleigh [23]. The measure of damping is the reduction in amplitude of the response after several cycles of free response, as shown in Figure. 1.4. This technique is considered standard work and provides the basis for many modern techniques.

Complex Exponential Algorithms (CEA) is one of the earliest modal analysis methods based on the curve fitting of the response properties of the system, represented as time-domain data [24]. It was first used to extract frequency and damping using IRF for SISO systems. Although the method is simple, it is very sensitive to noise.

Brown et al. [25] developed the Least-Squares Complex Exponential (LSCE) method for SIMO systems using multiple IRFs and the least square (LS) procedure to extract frequencies

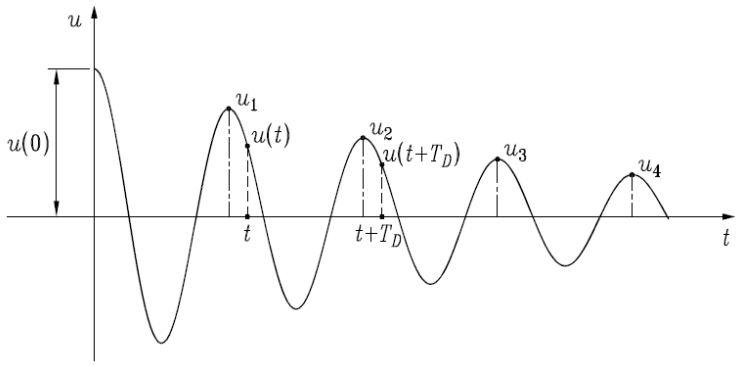

FIGURE 1.4: Free response

and dampings. The method can deal with noise due to the LS procedure, but it requires selecting mode numbers in advance.

Vold et al. [26] presented the Polyreference Time Domain (PTD) for MIMO systems. It was formulated as an extension of the LSCE method. By using several references, the chances of missing a mode of the structure are reduced.

Juang and Pappa [27] proposed the Eigen Realization Algorithm (ERA) method based on the general state-space description using the IRFs. However, the disadvantage of this method is that it has the need to obtain free or impulsive responses of structure, which is not always available in civil engineering applications.

- **Classical frequency domain identification methods**

Frequency domain methods are based on frequency response functions as shown in Figure. 1.5. The Half-Power Bandwidth (HPB) method is one of the most common methods [28, 29, 30, 31]. It is used to estimate damping ratios from the frequency response function of a structure. However, this method gives large errors for highly damped modes and is inapplicable for closely spaced modes.

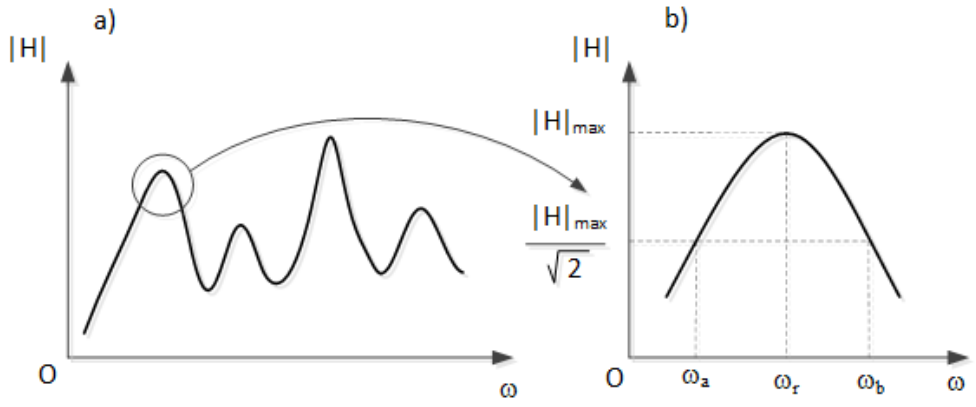

FIGURE 1.5: Frequency Response Functions (FRFs)

Formenti and Richardson [32] developed the Rational Fraction Polynomial (RFP) method for SIMO systems using FRF measurements. The FRFs are given in partial fraction form. It is one of the most widely used methods in the frequency domain. In addition, it has

been adopted and implemented by commercial modal analysis software. This method has been verified to be effective for many cases, even with closely spaced modes. Later, the author introduced the global rational fraction polynomial (GRFP) method to obtain global estimates of modal frequency and damping from a set of FRF measurements [33]. This method can provide some advantages, but it requires selection of an appropriate number of modes as its prerequisite.

Complex Mode Indicator Function (CMIF) was introduced based on Singular Value Decomposition (SVD) applied to multiple reference FRF measurements [34]. It was first developed for traditional FRF data in order to identify the proper number of modal frequencies, particularly when there are closely spaced.

Peeters et al. [35] developed the PolyMax or polyreference least-squares complex frequency-domain method. It is implemented in a very similar way as the industry standard polyreference (time-domain) least-squares complex exponential method. It offer even greater promise for obtaining accurate modal parameter estimates by using FRF measurements. It uses a stabilization diagram to estimate frequency, damping and participation information. This method can handle difficult estimation cases such as high-order systems or highly damped systems with modal overlap.

- **Main drawbacks of the above classical methods**
  - Require both input and output information, so are generally applicable to small and medium-size structures.
  - High cost and are time-consuming due to the installation of artificial excitations.

1.2.3 Operational modal analysis

In contrast to EMA, Operational Modal Analysis (OMA) is the engineering field that studies the modal characteristics of structures under ambient vibration, or normal operational conditions. It does not require any controlled excitation as artificial stimuli such as sharkers and impact hammers may not be suitable for large engineering structures such as high-rise buildings and long-span bridges. Instead, the response of structures to ambient excitations such as wind, traffic, and human-induced loadings are recorded.

OMA techniques have become very attractive due to their relatively low cost and speed of implementation, as well as recent improvements in recording equipment and calculation methods. It offers many advantages for modal identification of mechanical systems as it does not require to measure external excitation and allows to estimate modal parameters under actual boundary conditions.

Various modal identification techniques have been developed for engineering systems in OMA. They perform identification either in the time domain or in the frequency domain. As a rule, identification methods are aimed at obtaining physical information related to structures from correlation functions or spectral densities [36, 18]. Time-domain identification methods obtain this physical information from the correlation functions, while frequency-domain identification methods derive it from the Power Spectral Densitiy (PSD) functions.

1.2.3.1 Time domain methods

Time domain methods apply an appropriate mathematical model to idealize the dynamic structural behavior for the output-only modal identification, e.g. time-discrete or state-space stochastic models [37].

Ibrahim Time Domain (ITD) method was introduced in [38, 39]. It is one of the first techniques developed for the modal identification of multiple-output systems. The method uses free responses to estimate the modal parameters. However, it requires free-response inputs, and an appropriate selection of modal order is a prerequisite.

Stochastic Subspace Identification (SSI) method was proposed by Overschee and Moor [40]. This is an output-only system identification method and has been quite popular over the past decades. The basic idea of the data-driven SSI is to form the block Hankel matrix based directly on the measured responses. However, this method seems to be computationally expensive and time consuming due to the projection calculation and the use of a stability diagram.

1.2.3.2 Frequency domain methods

Along with the development of time domain identification methods, frequency domain methods have been introduced for operational modal analysis [41]. Typical frequency domain methods are described as follows:

Peak-Picking (PP) method is the basic frequency domain method for estimating the modal parameters of a structure. The basic idea of peak-peaking is that when a structure is subjected to ambient excitations, it will have strong responses close to its natural frequency. These frequencies can be determined from the peaks in the PSD calculated from the time history recorded at the measurement points.

Frequency Domain Decomposition (FDD) was introduced by Brincker, Zhang, and Andersen [42] in 2000. The method is based on SVD of spectral density matrices. It is closely related to the CMIF method introduced by C.Y.Shih et al. [34], which was based on an SVD of the FRF matrix. This method is relatively intuitive and user-friendly, but it can give unreliable damping estimates in the case of heavily damped and closely spaced modes.

1.3 Blind source separation

Blind Source Separation (BSS) emerged in the 1990s in the audio domain to recover original sources from the records. They are output-only methods. The separation can be achieved without any knowledge of the mixing process. A detailed description of the fundamental principles of BSS can be found in the reference [43]. The BSS has been used extensively in speech and audio processing [44, 45, 46, 47]. A typical example of a source separation problem is the cocktail party problem, where several people are talking simultaneously at a cocktail party in a room, and a listener is trying to follow one of the discussions. The term *blind* is commonly used because BSS methods aim to recover the mixing matrix $\mathbf{A}$ and the corresponding source $\mathbf{s}$ without knowing the mixing process. An illustration of the BSS problem can be represented as in Figure. 1.6.

Depending on the relation between the number of measurements n_x and the number of sources n_s, BSS problems can be classified as overdetermined case when $n_x > n_s$, determined case when $n_x = n_s$, or underdetermined case when $n_x < n_s$.

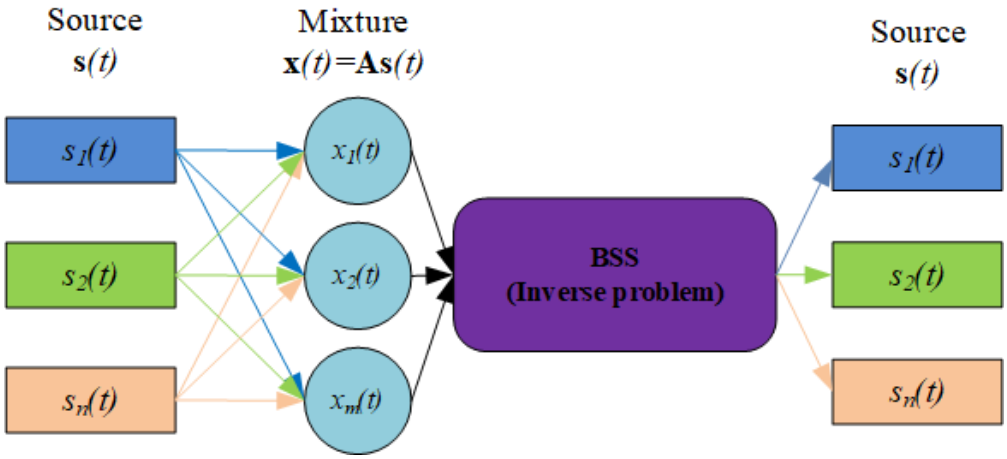

FIGURE 1.6: Blind source separation scheme

Over the last decade, blind separation techniques have widely employed in different research areas [48, 49, 50, 51, 52, 53, 54]. It has attracted considerable interest in OMA as a non-parametric alternative to modal identification from output-only measurements. In general, the BSS models can be divided into two groups depending on the mixing structure of the sources: the instantaneous model and the convolutive mixed model. More detailed information about BSS models can be found in reference [55].

- **Instantaneous mixture**

The instantaneous model is most commonly used in BSS problems as well as in modal analysis where sources arrive simultaneously at the sensors but with different intensities, and is expressed as follows:

$$\mathbf{x}(t) = \mathbf{A}\mathbf{s}(t) + \mathbf{n}(t) \tag{1.6}$$

where $\mathbf{x}(t) = [x_1(t), x_2(t), \ldots, x_m(t)]^T$ contains m measurements, $\mathbf{s}(t) = [s_1(t), s_2(t), \ldots, s_n(t)]^T$ contains n sources, $\mathbf{n}(t) = [n_1(t), n_2(t), \ldots, n_m(t)]^T$ is the noise vector and $\mathbf{A}$ is the static mixing matrix.

The output of the i^{th} measurement can be represented as:

$$x_i(t) = \sum_{j=1}^{n} a_{ij} s_j(t) + n_i(t) \tag{1.7}$$

Without consideration of observation noise, the equation (1.6) can be expressed as follows:

$$\mathbf{x}(t) = \mathbf{A}\mathbf{s}(t) \tag{1.8}$$

Eq. (1.8) is similar to the classical modal superposition model in Eq. (1.4). This provides a basic equivalence model for using BSS as an identification method. Once the sources and

the mixing matrix are recovered using BSS, the natural frequencies and the damping ratios can be identified from the recovered sources.

- **Convolutive mixture**

The validity of the instantaneous model has been questioned in the processing of data obtained by wireless sensors [56], where data from multiple locations does not arrive simultaneously or the mixing matrix coefficients are time-varying. This problem led to the development of a convolution BSS solution that takes into account the time lag in modeling [57, 58, 59].

A convolutive mixture can be expressed as follows [46]:

$$\mathbf{x}(t) = \mathbf{A}(\tau) * \mathbf{s}(t-\tau) + \mathbf{n}(t) \tag{1.9}$$

where * is the convolution operator, $\mathbf{A}$ is the mixing filter matrix containing the coefficients of finite impulse response (FIR) filter.

$$\mathbf{A}(\tau) = \begin{bmatrix} a_{11}(\tau) & a_{12}(\tau) & \cdots & a_{1n}(\tau) \\ a_{21}(\tau) & a_{12}(\tau) & \cdots & a_{2n}(\tau) \\ \vdots & \vdots & \cdots & \vdots \\ a_{m1}(\tau) & a_{m2}(\tau) & \cdots & a_{1n}(\tau) \end{bmatrix} \tag{1.10}$$

where $a_{ij}(\tau)$ is the impulse response of the filter characterizing the propagation of the signal from the j^{th} source to the i^{th} sensor with τ delay.

In order to separate mixed sources in a convolution scenario, several BSS solutions have been developed. They allow to take into account time lags in the model. This convolutive model can be transformed into an equivalent static mixing problem in a transformed domain using Short Time Fourier Transform (STFT) [59, 58]. However, this issue has received less attention because the superposition model is widely used and is accepted in structural dynamics as an equivalent instantaneous mixing model.

Solutions to the BSS problem have been applied to modal identification. Independent component analysis (ICA) [48] is one of the first application of BSS in structural dynamics that deals with overdetermined or determined problems. This method assumes that the observed data are a linear combination of statistically independent sources. The next advent of Second Order Blind Identification (SOBI) [49], which is based on cross-correlation of data, improves the separation performance compared to Independent Component Analysis (ICA).These methods have been successfully applied to perform output-only modal identification [60, 61, 62, 63, 64].

One of the main challenges of BSS-based modal identification methods is to deal with underdetermined problems where the number of mixtures (registered system responses) is less than the number of sources (active modes). Conventional BSS algorithms such as ICA or SOBI can only handle the overdetermined or determined problems that require the number of mixtures equal or greater the number of sources. This requirement may not be satisfied in many practical applications with limited sensors; for example, for large-scale or complex structures, where the sensors may be less than the number of structural modes. This poses a serious limitation in practical applications of these methods, which has been reported many

times in the literature. A few BSS approaches have been developed in the literature to handle the underdetermined case, but they seem to be very restricted. So far, two approaches seem to be the most popular and efficient: the first exploits the sparseness of the source, and the second involves tensor decomposition. A recent review of BSS methods in structural dynamics is presented by Sadhu, Narasimhan, and Antoni [65].

1.3.1 Independent component analysis

Independent Component Analysis (ICA) is one of the earliest BSS methods in the literature for determined cases. The ICA method uses the following assumptions:

- A statistical independence. It means that the general probability density can be decomposed into the product of the probability density of the component sources:

$$P(s_1, s_2, ..., s_n) = P(s_1)P(s_2)...P(s_n) \tag{1.11}$$

- A is non-Gaussian distribution.

- The unknown mixing matrix is square, i.e., the number of independent components equals the number of observed mixture signals.

From the above three assumptions, the independent components $\mathbf{s}(t)$ can be estimated by transforming the observed signals $\mathbf{x}(t)$ into the components $\mathbf{s}(t)$.

$$\mathbf{s}(t) = \mathbf{B}\mathbf{x}(t) \tag{1.12}$$

The basic idea of the ICA algorithm is to construct an objective function that measures mutual information [48], non-Gaussianity [66] or entropy [67] of the demixed signals $\mathbf{s}(t)$.

1.3.2 Second-order blind identification

In the second-order method, sources are assumed to be spatially uncorrelated, but temporally correlated as determined by the diagonal correlation matrix [49]. The SOBI method does not make any prior assumptions about the statistical independence or non-gaussianity of the sources. It improves separation performance compared to ICA. The basic assumptions are that the sources are assumed to be stationary and the measured noise is assumed to be uncorrelated. The correlation matrix is built from the measurement $\mathbf{x}(t)$ as follows:

$$\mathbf{R}_x(\tau) = E\{\mathbf{x}(t)\mathbf{x}^T(t+\tau\} = \mathbf{A}\mathbf{R}_s(\tau)\mathbf{A}^T + \sigma^2\delta(\tau)\mathbf{I} \tag{1.13}$$

where $\mathbf{R}_s(\tau)$ is the correlation matrix of sources, δ is the standard deviation of the additive noise which is assumed to be stationary, white and uncorrelated to the sources , $\delta(\tau)$ is the Kronecker delta, and $\mathbf{I}$ is the identity matrix.

Source separation by SOBI consists of two main steps: (i) whitening of the measured signal and (ii) Joint Approximate Diagonalization (JAD) that can be accomplished with the Jacobi method [68].

1.3.3 Sparse component analysis

Sparse Component Analysis (SCA) has experienced considerable development in the early 1990s. Sparsity means a domain of representation where the sources tend to occupy different regions of the space, with a reduced degree of overlap [53, 69, 46]. This approach has proven to be more promising. By far, this technique began to be fully exploited for blind source separation [70, 71, 72, 53, 73]. It can implement a relatively simple framework for underdetermined cases when the number of sources exceeds the number of observed mixtures.

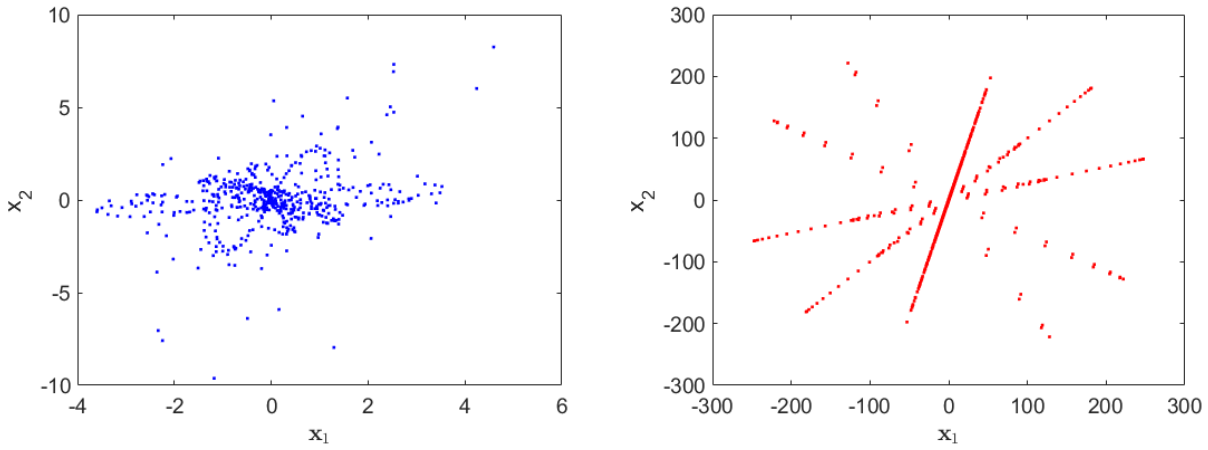

(a) Time domain **(b)** Frequency domain

FIGURE 1.7: Scatter plot $\mathbf{x}_1$ vs. $\mathbf{x}_2$ of five sources mixed into two mixtures in the time (left) and frequency (right) domains

It is shown that the time domain representation for a signal cannot be sparse enough, but sparsity can still be achieved in a transformed domain [53]. Sparsity can be achieved in the frequency or time-frequency domain using Fast Fourier Transform (FFT) [74], Short Time Fourier Transform (STFT) [75], Wavelet Packet Transform (WPT) [76], etc., when they are not directly achievable in the time domain. The mixing matrix is then estimated using clustering algorithms such as K-means clustering [77], hierarchical clustering [78], fuzzy C-mean clustering [79], etc. From the estimated mode shapes, the modal coordinates can be recovered by methods such as the least square method [80], l_1-norm [79].

The benefit of such an approach is clearly shown in Fig. 1.7. The five simulated signals are combined into two mixtures. Fig. 1.7a presents a scatter plot of the resulting data (x_1 against x_2), showing a mess cloud. As can be seen, the sources are indistinguishable in the time domain. Then each mixture was transformed to the frequency domain and the scatter plot of the frequency domain data is shown in Fig. 1.7b. However, the accuracy of the estimated mode shape of these methods depends on the clustering technique, and the recovered modal coordinates are less accurate in the case of poor clustering performance.

1.3.4 Tensor decomposition

The tensor decomposition technique was recently employed in operation modal analysis as one of the BSS family methods. It has been proven to effectively treat different types of excitations such as ambient vibrations, earthquakes, or human-induced vibrations [81, 82, 83, 84, 85, 86, 87, 88].

A multidimensional signal can be expressed as a tensor using multi-linear algebra tools, which are more efficient and powerful than linear algebra tools (e.g. principal component analysis) [89].

For example, a vector $\mathbf{t} = t_i \in \mathbb{C}^{n_1}$ is a first-order tensor, a matrix $\mathbb{T} = t_{ij} \in \mathbb{C}^{n_1 \times n_2}$ is a second-order tensor. pth-order tensor is written as $\mathbb{T} = t_{ij\ldots p} \in \mathbb{C}^{n_1 \times n_2 \times \ldots \times n_p}$

A third order tensor can be decomposed into a sum of outer products triple vectors as follows [90]:

$$\mathbb{T} = \sum_{r=1}^{R} \mathbf{a}_r \circ \mathbf{b}_r \circ \mathbf{c}_r \Leftrightarrow T_{ijk} = \sum_{r=1}^{R} a_{ir} b_{jr} c_{kr} \tag{1.14}$$

where $\circ$ denotes the tensor outer product, R is the number of rank-1 tensor present in $\mathbb{T}$. This is termed as a trilinear model of $\mathbb{T}$, $\mathbb{T} = [[\mathbf{a}, \mathbf{b}, \mathbf{c}]]$ with the matrices $\mathbf{a} = (\mathbf{a}_1, \mathbf{a}_2, ..., \mathbf{a}_R)$, $\mathbf{b} = (\mathbf{b}_1, \mathbf{b}_2, ..., \mathbf{b}_R)$, and $\mathbf{c} = (\mathbf{c}_1, \mathbf{c}_2, ..., \mathbf{c}_R)$.

The geometric interpretation for the above equation can be represented as shown in Figure 1.8.

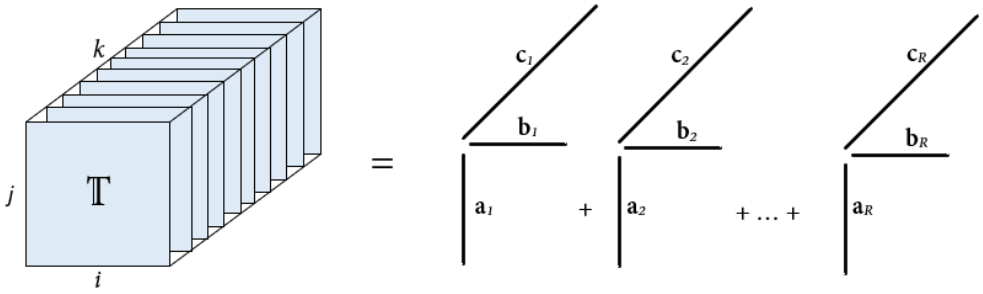

FIGURE 1.8: Geometric interpretation for PARAFAC decomposition [89]

In this work, the third-order tensor is used as the fact that the signals are represented and processed in a three-dimensional array. The factor matrices can be obtained by optimizing the following cost function:

$$\min_{\mathbf{a},\mathbf{b},\mathbf{c}} \left\| \mathbb{T} - \sum_{r=1}^{R} \mathbf{a}_r \circ \mathbf{b}_r \circ \mathbf{c}_r \right\|^2 \tag{1.15}$$

This technique was introduced by PARAllel FACtor (PARAFAC) decomposition [91] and canonical decomposition [92]. Several algorithms have been developed to fit a PARAFAC model, which can be classified into three categories [93, 94]: Alternating Least Square (ALS) algorithm, derivative based algorithms, and non-iterative algorithms. The derivative based algorithms seek an update for all the parameters simultaneously by successive approximations while non-iterative algorithms have one matrix factor with a Toeplitz structure which are somewhat complicated. In this work, the ALS algorithm is applied because of its simpler implementation, and guaranteed convergence [95].

The ALS algorithm is mainly comprised of the following key steps to undertake simultaneous unfolding of three model matrices:

1. Fix $\mathbf{a}$ and $\mathbf{b}$. $\mathbf{c}$ is solved using:

$$\min_{\mathbf{c}} \|\mathbb{T} - [[\mathbf{a},\mathbf{b},\mathbf{c}]]\|^2 = \min_{\mathbf{c}} \left\|\mathbb{T}_{(3)} - \mathbf{c}(\mathbf{a}\odot\mathbf{b})^T\right\|^2 \tag{1.16}$$

where $\odot$ represents Khatri-Rao product. Given $\mathbf{a} \in \mathbb{C}^{I\times R}$ and $\mathbf{b} \in \mathbb{C}^{J\times R}$, then $\mathbf{a}\odot\mathbf{b}$ is a matrix with IJ rows and R columns and is expressed as:

$$\mathbf{a}\odot\mathbf{b} = \begin{bmatrix} a_{11} & a_{12} & \dots & a_{1R} \\ a_{21} & a_{22} & \dots & a_{2R} \\ \vdots & \vdots & \dots & \vdots \\ a_{I1} & a_{I2} & \dots & a_{IR} \end{bmatrix} \odot \begin{bmatrix} b_{11} & b_{12} & \dots & b_{1R} \\ b_{11} & b_{12} & \dots & b_{1R} \\ \vdots & \vdots & \dots & \vdots \\ b_{J1} & b_{J2} & \dots & b_{JR} \end{bmatrix} = \begin{bmatrix} a_{11}b_{:1} & a_{12}b_{:2} & \dots & a_{1R}b_{:R} \\ a_{21}b_{:1} & a_{22}b_{:2} & \dots & a_{2R}b_{:R} \\ \vdots & \vdots & \dots & \vdots \\ a_{I1}b_{:1} & a_{I2}b_{:2} & \dots & a_{IR}b_{:R} \end{bmatrix} \tag{1.17}$$

where $b_{:k}$ denotes kth column of matrix $\mathbf{b}$.

2. Successively solve for $\mathbf{a},\mathbf{b}$ and $\mathbf{c}$, until the desired convergence is achieved

3. Finally, a tensor $\bar{\mathbb{T}} = \sum_{r=1}^{R} \mathbf{a_r}\circ\mathbf{b_r}\circ\mathbf{c_r}$ is obtained such that the cost function is minimized:

$$f(\mathbf{a},\mathbf{b},\mathbf{c}) = ||\mathbb{T} - \bar{\mathbb{T}}||^2 \tag{1.18}$$

A unique decomposition is obtained if the Kruskal condition [96] is satisfied:

$$k_{\mathbf{a}} + k_{\mathbf{b}} + k_{\mathbf{c}} \geq 2R + 2 \tag{1.19}$$

where $k_{\mathbf{a}}, k_{\mathbf{b}}$ and $k_{\mathbf{c}}$ are $k-$rank of the matrices $\mathbf{a},\mathbf{b}$ and $\mathbf{c}$ respectively, where $k-$rank is defined as maximum number k such that every set of k columns of the matrix is linearly independent.

The PARAFAC decomposition offers a unique decomposition even if its rank order is greater than the smallest dimension of the tensor. Therefore, this decomposition can be utilized to handle underdetermined cases. The constrained decomposition in Eq. (1.14) is essentially unique under the following condition [97]:

$$2n_s(n_s-1) \leq n_x^2(n_x-1)^2 \tag{1.20}$$

where n_s is the number of sources, and n_x is number of measurements.

The relationship between the number of measurements and the maximum number of identifiable sources extracted by PARAFAC decomposition is given in Table. 1.1. It can be noted that the number of identifiable modes for complex tensor cases is higher than for real-valued tensors.

1.4 Harmonic detection in modal analysis

Engineering structures are subjected to ambient and human-induced vibrations during normal operational conditions. In general, a fundamental assumption of operational modal

TABLE 1.1: Source separation capability for PARAFAC decomposition [97]

Number of measurements n_x	2	3	4	5	6	7	8
Number of identifiable modes $n_s^{\max}$ (real-valued case)	2	4	6	10	15	20	26
Number of identifiable modes $n_s^{\max}$ (complex case)	2	4	9	14	21	30	40

analysis methods is that the external excitation is white noise. This assumption implies that the excitations are not driving the system at any particular frequency, and therefore any identified active frequency reflects structural modal response. However, in reality, some of the harmonic disturbances, for instance, an adjacent machine operating at a particular frequency, may drive the structure at that frequency. Thus, these components need to be detected and eliminated in the modal identification process. A direct approach for processing these harmonic components is to consider them as zero-damping modes [98]. Besides, kurtosis can also be used as a harmonic indicator. It was used in the time domain or in the frequency domain to distinguish structural modes from periodic excitations [99, 100, 101, 102].

1.4.1 Histograms and kurtosis values

In BSS methods, the conventional kurtosis value can be used to distinguish modal responses and harmonic components. Kurtosis is a measure of the tailedness of the probability distribution of a real-valued random variable. The kurtosis is defined as the fourth central moment of the stochastic variable as follows [103]:

$$k = \frac{E\left\{x^4\right\}}{\left(E\left\{x^2\right\}\right)^2} \tag{1.21}$$

where E is the expectation operator.

For sampled data with K samples, the expectation can be computed statistically as follows:

$$E\{x\} = \frac{1}{K}\sum_{k=1}^{K} x(k) \tag{1.22}$$

The Probability Density Function (PDF) of the response of a structural mode will be normally distributed (Fig. 1.9a), and the kurtosis $k = 3$. The PDF p is given as follows:

$$p(x|\mu,\delta) = \frac{1}{\delta\sqrt{2\pi}}\mathrm{e}^{-\frac{(x-\mu)^2}{2\delta^2}} \tag{1.23}$$

where μ and δ are the mean and standard deviation of x, respectively.

In the case of a pure harmonic component, the PDF will have two distinct peaks (Fig. 1.9b) and the kurtosis $k = 1.5$. The PDF p is given as follows:

$$p(x,a) = \begin{cases} 0, & |x| > a \\ \dfrac{1}{\pi \cos\left(\arcsin\left(\dfrac{x}{a}\right)\right)}, & |x| \leq a \end{cases} \tag{1.24}$$

where a is the amplitude of the harmonic component.

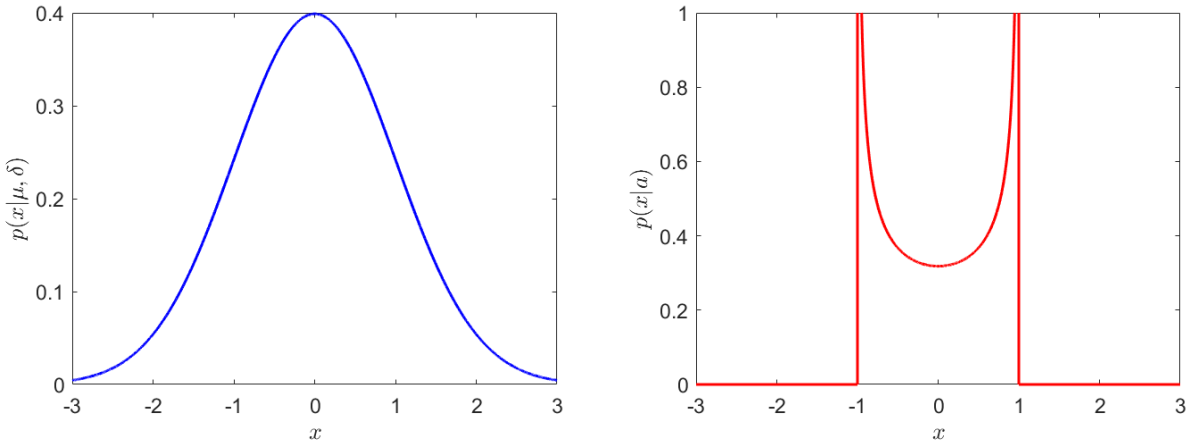

(a) Structural mode **(b)** Harmonic component

FIGURE 1.9: Normalized PDF of the response of a structural mode and a harmonic component

1.4.2 Spectral kurtosis

In the frequency domain, the Spectral Kurtosis (SK) of a signal is defined as the kurtosis value of its frequency component. It has been applied to the detection of harmonics in studies [102, 104, 105, 106]. A remarkable advantage of this approach is that the information for each frequency component can be indicated in the frequency range of interest.

Let $X(f)$ be the Discrete Fourier Transform (DFT) of signal $x(t)$. The original SK can be defined as follows [102]:

$$SK(f) = \frac{E\left\{|X(f)|^4\right\} - 2\left[E\left\{|X(f)|^2\right\}\right]^2}{\left[E\left\{|X(f)|^2\right\}\right]^2} \tag{1.25}$$

where $E\{.\}$ denotes the operator of expectation and $|.|$ represents the modulus operator.

In practice, the signal $x(t)$ is divided into M blocks to obtain an unbiased estimator of the SK by using the k-statistics as in [107]:

$$SK(f) = \frac{M}{M-1}\left[\frac{(M+1)\sum_{i=1}^{M}\left|X^i(f)\right|^4}{\left(\sum_{i=1}^{M}\left|X^i(f)\right|^2\right)^2} - 2\right] \tag{1.26}$$

where the vector $X^i(f)$ is a DFT of the i-th block.

According to the statistical characteristic [102], the SK of a synthetic signal always equals to –1 for the harmonic frequency. However, this value for a random process equals to zero. In the case of $\mathbf{x}(t)$ mixing with a harmonic signal, its SK can be comprehensively described as:

$$\begin{cases} SK(f) = -1, & f = f_h \\ SK(f) = 0, & f \neq f_h \end{cases} \tag{1.27}$$

where f_h is a harmonic frequency.

Consequently, harmonic components will be detected by estimating the values of SK at each frequency through Eq. (1.26) and Eq. (1.27).

1.5 Structural damage detection

Structural Damage Detection (SDD) is one of the most important part of the health assessment for a structure. In the functional time, damage may accumulate on structures due to environmental and human-induced factors. Damage is interpreted as a change in a system's geometric or material characteristics that can adversely affect its performance, safety, reliability, and longevity. A structural failure can be catastrophic if it is not detected or repaired in time. Therefore, Structural Damage Detection is essential, especially in the early damage state, to avoid sudden failures and improve the safety and longevity of structures [1].

In general, the identification of the damage can be classified into four levels [108]. Most current research focuses on the first three levels [109]:

- Level 1: Damage detection. It gives a qualitative indication that damage might be present in the structure.
- Level 2: Damage localization, providing information on the location of possible damage
- Level 3: Damage quantification, give an estimate of damage
- Level 4: Damage prognosis, providing information about the safety of the structure.

SDD methods have been the subject of numerous research projects in recent decades [1, 3, 109, 110, 111]. In general, damage identification methods can broadly be categorized into two groups [1]: traditional Non-Destructive Testing (NDT) methods (local methods) and modern vibration-based methods (global methods). Both global and local methods provide different types of information and support different types of analysis. The local ones detect and quantify structural damage on a relatively smaller scale without using the responses of structures. The detection area for local methods is relatively small. Therefore, most of NDT methods are considered as local methods. In contrast, vibration-based damage methods examine changes in the global vibration characteristics of the structure and are therefore considered global methods.

The manipulations of NDT methods are usually manual and relatively simple. They are often localized and require prior knowledge of the damage location in a structure. Modal

analysis is not very useful for NDT methods. Due to their local nature, the assessment of the overall structure may not be resolved.

In contrast to the NDT methods, vibration-based damage methods often use sensor networks that can be automated. They can cover large areas and do not require prior knowledge of the damage location. Modal analysis is an integral part of most these methods, and they are used to determine modal parameters based on ambient measurements.

1.5.1 Traditional non-destructive testing methods

Non-Destructive Testing methods have been extensively employed for detecting damage in engineering structures [112, 113, 114], including acoustic emission, ultrasound, lamb waves, laser vibrometer, thermal imaging, and Global Positioning System (GPS). Studies [115, 116] present a detailed literature review of the most widely used NDT methods applied to engineering structures.

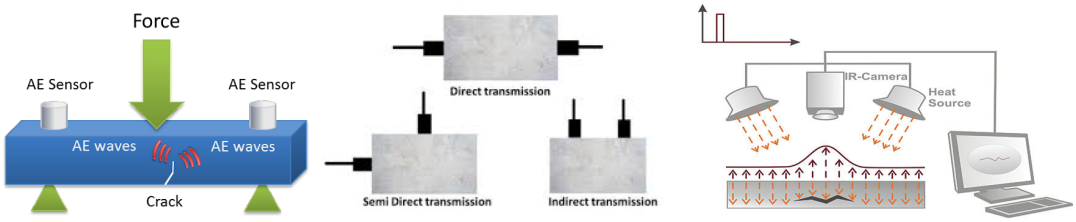

(a) AE **(b)** Ultrasound **(c)** Thermography

FIGURE 1.10: Some examples of non-destructive testing methods

Acoustic emission (AE) is used as an NDT method. This theory is that damage events in a material or structure create stress waves that propagate throughout the structure (Figure. 1.10a). These stress waves are called acoustic emissions with a frequency range typically from 20 kHz to 1.0 MHz. The properties of these stress waves depend on the nature of damages and structures. Therefore, by analyzing the measured acoustic emission signals, structural damage can be detected, and the state of the structure can be estimated. This is a passive NDT method, and depends on the propagation of damage signals.

Ultrasound is a prevalent NDT method for investigating the inner structure in a solid test object. In ultrasound scanning, the transmitter send ultrasound waves into the material, and the receiver collects its signal once the transmitter signal has passed through the material (Figure. 1.10b). Then, the signals collected by the receiver can be processed, and the damage in the test object can be detected. The ultrasound technique is an active method, and it generates signals and monitors the interaction of the signals with test objects.

Thermal imaging is a subsurface defect detection method based on temperature variations measured on the examined surface during monitoring using infrared sensors or cameras (Figure. 1.10c).

Besides, the magneto-inductive method arises in the cableways sector in the first half of the 20th century. The magneto-inductive test method is based on an electromagnetic field generated by a field coil and modified by the presence of a test piece with conductivity and permeability. This method can be applied to different sectors and applications. Such characteristics as the surface hardness and case hardening depth can be identified without

destruction. However, the method can be affected by metal structures in near-field magneto-inductive communication systems.

In general, these above methods give effective damage detection results in local areas when these locations are known. However, these NDT methods differ significantly in their range of applicability and may only be suitable for damage assessment in local areas. In addition, they have certain kinds of limitations in practical applications, particularly for large complex engineering structures.

1.5.2 Vibration-based damage identification methods

It is clear from the previous discussion that a reliable and ongoing assessment of the integrity of structures is required. The need for effective damage detection in engineering structures has stimulated the development of SHM methods. As a result, SHM is an emerging method for assessing the current health and predicting the future performance of engineering structures. Vibration-based damage identification techniques show great promise for damage assessment in engineering structures [117]. These methods are based on vibration measurements, such as the acceleration, which are related to damage in the structure. Thus, from vibration measurements, these techniques can be applied to detect structural damage directly.

The underlying principle behind these methods is that the vibration signature, such as modal parameters, is a sensitive indicator of a structure's physical integrity [109, 118]. When a damage occurs in a structure, the structural parameters, such as stiffness, flexibility, and strain energy, are altered, and consequently, the modal parameters, such as natural frequency, mode shape, and damping, will also be changed. Modal parameters can be derived from vibration measurements of the structure under consideration using modal analysis. Therefore, it is reasonable to use the measured change in dynamic behavior to identify structural damage.

Since the number of published studies related to damage identification is huge, damage identification in a structure can be performed using various system properties. These damage identification methods can be classified into following main groups [111]: modal parameter based methods, signal processing based methods, finite element model updating methods and machine learning methods.

1.5.2.1 Modal parameter based methods

Modal parameters, such as natural frequencies, mode shapes and damping ratios are global properties of an engineering structure. Damage identification methods based on the change of modal parameters do not require the measurements at the damage location. Instead, they assume that damages can be identified by comparing the current modal parameters with those of the undamaged state.

a. Natural frequency based methods

In damage identification techniques, natural frequencies are the easiest to measure and are independent of the measurement location. Since changes in stiffness due to damages in a structure, whether local or distributed, cause a change in the natural frequency of the

structure, the presence of these failures can be detected using the change in natural frequency. Cawley and Adams [119] introduced the relationship between the change of natural frequencies and the change in stiffness as follows:

$$\Delta\omega_i^2 = \frac{\mathbf{\Phi}_i^T \Delta\mathbf{K} \mathbf{\Phi}_i}{\mathbf{\Phi}_i^T \mathbf{M} \mathbf{\Phi}_i} \tag{1.28}$$

where $\Delta\omega_i$ and $\Delta\mathbf{K}$ are the i^{th} natural frequency change and the stiffness change, respectively, $\mathbf{\Phi}_i$ is the i^{th} mode shape of the undamaged structure and $\mathbf{M}$ is the global mass matrix.

This simple relationship is not sensitive enough for damage detection and it is of little use for damage detection in practice.

b. Mode shape based methods

Mode shape changes are also discovered to be sensitive to damages in structures, in particular, when higher-order modes are utilized. Therefore, mode shape changes can directly provide damage location information [120]. However, the mode shape measurements of an engineering structure require a high number of spatial sensors. The commonly used ways to compare two sets of mode shapes include the Modal Assurance Criterion (MAC) and the coordinate modal assurance criterion (COMAC).

The MAC can be used to detect the existence and the location of structural faults. The MAC value is a scale quantity ranging from 0 to 1. Low MAC values close to zero indicate possible damage in the structure. When applied to damage detection, the MAC can be defined as follows:

$$\mathrm{MAC}_i = \frac{\left|\mathbf{\Phi}_i^{hT} \mathbf{\Phi}_i^d\right|^2}{\mathbf{\Phi}_i^{hT} \mathbf{\Phi}_i^h \mathbf{\Phi}_i^{dT} \mathbf{\Phi}_i^d} \tag{1.29}$$

where $\mathbf{\Phi}_i^h$ and $\mathbf{\Phi}_i^d$ are the i^{th} mode shape vectors of the intact and damaged structure, respectively.

The COMAC is a point-wise measure of the difference between two sets of mode shapes [121]. It ranges from 0 to 1. The COMAC spatially correlates two sets of mode shapes and identifies the DOFs with maximum disagreement between the mode pair. The COMAC value at location j can be represented as follows:

$$\mathrm{COMAC}_{i,j} = \frac{\sum_{i=1}^{n} \left(\mathbf{\Phi}_{i,j}^h \mathbf{\Phi}_{i,j}^d\right)^2}{\left(\sum_{i=1}^{n} \left(\mathbf{\Phi}_{i.j}^h\right)^2\right)\left(\sum_{i=1}^{n} \left(\mathbf{\Phi}_{i.j}^d\right)^2\right)} \tag{1.30}$$

where n is the number mode shapes, $\mathbf{\Phi}_{i.j}^h$ and $\mathbf{\Phi}_{i.j}^d$ denote the values of i^{th} mode shape at a point j for healthy and damaged states,respectively.

The MAC and COMAC have been successfully applied for many damage detection studies [122, 123]. However, they are highly dependent on the geometry of the structure and the damage location. Sufficient sensors must be used to ensure that these values are a meaningful

indicator. These criteria are not sensitive enough to detect damages in the early stages of their growth.

c. Mode shape curvature based methods

Pandey, Biswas, and Samman [124] used the change of mode shape curvature to detect and locate damage in structures. The mode shape curvature of the undamaged and damaged structure can be calculated from the displacement mode shapes using a central difference approximation technique.

$$\Phi_{i,j}^{h''} = \frac{\Phi_{i,j+1}^{h} - 2\Phi_{i,j}^{h} + \Phi_{i,j-1}^{h}}{p^2} \tag{1.31}$$

$$\Phi_{i,j}^{d''} = \frac{\Phi_{i,j+1}^{d} - 2\Phi_{i,j}^{d} + \Phi_{i,j-1}^{d}}{p^2} \tag{1.32}$$

where i is the i^{th} mode, j is the j^{th} point, and p is the distance between two consecutive mode shape points.

The modal curvature change rate index $\beta_{i,j}$ for the i^{th} mode is defined as follows:

$$\beta_{i,j} = \frac{\left|\Phi_{i,j}^{h''} - \Phi_{i,j}^{d''}\right|}{\sum_{j}\left|\Phi_{i,j}^{h''} - \Phi_{i,j}^{d''}\right|} \tag{1.33}$$

The mode shape curvature (MSC) damage index is defined as the average of the mode curvature change rates for the total n modes:

$$MSC_{i,j} = \frac{1}{n}\sum_{i=1}^{n}\beta_{i,j} \tag{1.34}$$

Methods based on mode shapes and their derivatives are more sensitive to damage identification than methods based on changes in natural frequencies. However, the measurement of mode shapes for damage detection requires a large number of spatial measurements.

d. Damping ratio

Compared to natural frequency and mode shape, damping is less commonly used for damage detection in the literature. The existence of damages in a structure can cause changes in the damping of a structure Rytter [108]. However, these changes are highly dependent on ambient factors, such as temperature, humidity, or uncertainty in boundary conditions. The damping ratio variation given in modal parameter variations is inapplicable since the ratio variance in actual measurement is entirely masking any large damage effect.

1.5.2.2 Signal processing based methods

These damage detection methods are based on the measurement and analysis of signals collected from sensors. The measured signals are usually analyzed in a transformed domain by transforming the signal from the time domain, since the damage characteristics can be displayed more clearly. Some signal processing approach includes methods of damage identification based on signal processing such as Wavelet [125], Hilbert-Huang transform [126] or fractal dimension [127].

a. Wavelet transforms

Wavelet transforms are one of the common tools for signal processing. They are mathematical functions that can slice data into different frequency components, then study each component with a resolution appropriate to its scale [125]. Wavelet transforms have advantages over traditional Fourier methods in analyzing physical situations where the signal has discontinuities and spikes.

The Continuous Wavelet Transform (CWT) of a signal $x(t)$ can be represented as:

$$cwt(s,\tau) = \frac{1}{\sqrt{s}} \int_{-\infty}^{+\infty} x(t)\psi(\frac{t-\tau}{s})dt \tag{1.35}$$

where the basic function (wavelet function) $\psi(s,\tau,t)$ includes a scaling variable (s) and a translation variable (τ).

Wavelet analysis is suitable to the analysis of non-stationary signals, so it can be used as a feasible method for signal processing to construct an intended index of structural damage. In addition, the spectrum obtained using the Wavelet transforms can directly indicate the presence of damage. Applications of wavelet analysis for structural damage detection are discussed in [128].

b. Hilbert–Huang transform

The Hilbert–Huang Transform (HHT) [126] is a famous signal processing technique that is applicable for non-stationary and nonlinear signals. It is a combination of two methods, which are Empirical Modal Decomposition (EMD) and Hilbert Transform (HT).

The HT of a signal $x(t)$ can be represented as:

$$\hat{x}(t) = \frac{1}{\pi} P \int_{-\infty}^{+\infty} \frac{x(\tau)}{t-\tau} d\tau \tag{1.36}$$

where P is the Cauchy principal value.

The HHT offers many advantages, such as being applicable to non-stationary signals or non-linear problems. It can produce more physically meaningful results than other transformations. This method performs empirical mode decomposition of the time signal into narrow-band components with zero mean. These components can be associated with a physical meaning. HHT-based structural damage detection methods have been reviewed in study [129].

In general, these signal processing methods are typically non-parametric methods. They only require the measurement of signals from a damaged structure. While these methods are effective for practical application without requiring a baseline model, they are generally limited to a low level of damage identification, such as damage localization only. This limitation is due to the lack of relationship between the measured signal and the severity of damage.

1.5.2.3 Finite element model updating methods

The Finite Element Method (FEM) is a popular tool for structural damage detection in civil engineering. In finite element model updating methods, the finite element model can provide baseline information, which can then be updated with new information received from the monitoring system to detect structural damage and predict future performance [109].

Many studies have been conducted in model updating using vibration measurements over the past several decades [130, 131, 132, 133]. According to their approach, they can be broadly classified into two main groups: direct methods and iterative methods. In the first approach, direct methods are a one-step approach that directly updates the elements of the stiffness and mass matrix [134]. They allow the updated model to reproduce the measured modal data, but there is no guarantee that the updated model truly represents the physical properties of the actual structure. In the second approach, iterative methods use the sensitivity of the parameters to update the analytical model [135]. These methods use the error between the analytical data and the measurement data as an objective function. They then minimize the selected objective function by adjusting a preselected set of physical parameters of the analytical model.

Within these groups, iterative methods are more popular in many applications for model update problems. The update parameters can be material properties, geometric properties, and non-dimensional scaling multipliers applied at the element level. The performance of iterative methods extensively depends on the selection of updating parameters and optimization techniques [136]. Their objective function can be the residual between the measured and predicted modal data from the original FE model, for example, the difference in frequency and mode shape.

Although the application of FE model update methods for damage detection has developed significantly, these methods have certain limitations. These methods require a large amount of computational time to process the data and update the model. This will delay the identification process for real-time damage detection. Besides, the performance of these methods largely depends on the accuracy of the FE model. Practical applications often show considerable discrepancy between the predictions of the FE model and the tested results. Two main sources of error are popular in the finite element model: discretization error and modeling error. Due to various assumptions, idealizations, customizations and parameterizations introduced into the numerical model, it may not reflect the actual behavior of the structure. Furthermore, the update process often requires expert intervention, which can prevent the automation of update-based methods for SHM.

1.5.2.4 Machine learning methods

Significant improvements in computing power and advances in technology have enabled the use of Machine Learning (ML) methods in engineering applications. ML includes intelligent algorithms capable of automatically gathering knowledge from available data. These algorithms are intended to give machines the ability to learn by example and recognize patterns. A general overview of the use of ML in damage detection is presented in [110]. These ML algorithms can be broadly divided into supervised, unsupervised, and semi-supervised learning.

a. Supervised learning

Most ML algorithms are supervised learning, which requires features of both the damaged and undamaged states of the structure. These features are used to establish a statistical model during the training process [137].

One of the widely used ML algorithms is Artificial Neural Networks (ANNs). ANNs were initially developed to simulate the function of the human brain or neural system. Consequently, they have been widely applied to various fields ranging from biology to many areas of engineering [138]. For structural damage detection, ANN is used to establish a representative model of the relationship between features extracted from vibration data and structural parameters through a training process [139].

Supervised ML methods require data from damaged and undamaged structures for the training process. However, data regarding damage situations may not be available in practical applications and it is often generated through laboratory testing or numerical simulation. Therefore, the effectiveness of supervised learning techniques depends on the accuracy of the numerical model.

b. Unsupervised learning

Unsupervised learning methods only require data from the intact state for the training process. The trained model is used to evaluate the current structural state when new data are available. If the difference between the predicted data from the trained model and the measured data exceeds the threshold, the structure is considered abnormal and may be damaged [140, 141].

While unsupervised learning methods are preferred for actual damage detection, they are usually limited to level 1 of damage identification - whether there is a damage or not. They could not provide further information on the location and severity of the damage.

c. Semi-supervised learning

In practical applications, it is not feasible to collect fully labeled data for training, while it is possible to have a small amount of labeled data. In such situations, semi-supervised learning methods may make more practical sense as they use both labeled and unlabeled data for the learning process [3]. Many researchers have found that using unlabeled data in combination with small amounts of labeled data can significantly improve the accuracy of ML algorithms [142, 143].

Semi-supervised learning can provide more information than pure novelty detection in unsupervised learning. It can detect and quantify structural damage. However, the use of semi-supervised ML algorithms for damage identification is very limited in the literature.

Despite the fact that ML methods are developing at a fast pace, there are still some challenges and difficulties. The quality of the training data set is extremely important for the performance of ML algorithms. The training process is computationally heavy and labor-intensive. A well-trained and validated model can only work well for a specific type of structure and a specific type of damage.

1.6 Challenges and objectives

In Structural Health Monitoring (SHM), measurement data from the operational responses are used to estimate the parameters of structures, which are a sensitive indicator of structural physical integrity. An approach that studies modal properties of structures under ambient vibrations or under normal operating conditions is called Operational Modal Analysis (OMA). This approach has become quite attractive as it offers several advantages: relatively low cost, speed of implementation, and continuous monitoring during normal use of structures. However, it has some major challenges:

- In modal analysis, the fundamental assumption of the analysis of these ambient vibrations is that the inputs causing motion have white noise characteristics in the frequency range of interest. This assumption implies that the input loads do not drive the system at any particular frequency, and hence any identified frequency associated with an active response reflects a structural modal response. However, in reality, civil engineering structures are exposed to environmental vibrations generated by wind, occupants, ventilation equipment..., under normal operating conditions. For example, a nearby machine operating at a certain frequency may drive the structure at that frequency. This causes uncertainty in modal identification.
- Another limitation of current BSS based modal identification methods is that they can only handle a number of active modes equal to or less than that of measured responses known as overdetermined or determined problems. These methods cannot solve underdetermined problems when the number of measured responses is less than that of active modes. However, it should also be noted that underdetermined problems are quite common in practice when the measurements are smaller than the number of active modes or in the presence of harmonic excitations.
- In Structural Damage Detection (SDD), the relationship between damage due to changes in mechanical properties such as mass and stiffness and changes in modal parameters is not straightforward, and often goes through finite element model updating procedures. The Finite element (FE) modeling is based on the direct assembly of all critical structural components that will involve a large number of degrees of freedom (DOFs) and thus become computationally burden. This also causes a critical problem that the number of DOFs in the finite element model is much higher than the number of DOFs measured in modal testing. In addition, these methods do not provide much-needed rapid assessment of structural integrity after extreme events, such as an earthquake or blast loading.

- In reality, there may be several damages in a structure, and detecting multiple damage is more challenging than detecting a single damage. Although FEM updating and optimization methods can be applied to detect multiple damages, they often cause computational burden or difficulty in achieving convergence of optimization procedures.

Summarizing the above challenges, the objectives of the thesis are as follows:

- Review efficient and popular methods for operational modal analysis and structural damage identification.
- Propose improvements to existing methods or a novel method that can deal with underdetermined cases and uncertainty due to unmeasured and uncontrolled operational excitations.
- Develop a procedure for rapid damage detection based on a simplified relationship between damage and changes in modal parameters.
- Introduce an enhanced procedure for multiple damage detection in structures.

1.7 Organization

This thesis consists of four chapters and is organized as follows:

Chapter 1: This chapter provides a brief introduction to the general principle of structural health monitoring.

- It summarizes the background of various modal identification and damage detection methods for structural health monitoring.
- It highlights the challenges, objectives and main contributions of this thesis.

Chapter 2: This chapter presents an enhanced procedure for modal analysis in the time domain.

- The chapter presents an enhanced procedure of the PARAFAC decomposition-based method used for the operational modal analysis. The minimum length of autocovariance functions using natural periods and damping factors are suggested to distinguish between harmonic and modal components accurately. This modification allows to effectively distinguishing separated structural modes and harmonic ones. The effectiveness of the proposed procedure has been validated by numerical simulations and experimental tests

Chapter 3: In this chapter, a new method of modal analysis in the frequency domain is developed.

- A novel modal identification method based on tensor decomposition in the frequency domain has been developed. A PARAFAC decomposition is used to decompose a third-order tensor constructed from power spectral density matrices of response signals. The decomposition results in the mode shape and the auto-PSD matrix of the modal coordinates. Then natural frequencies and damping ratios can be estimated from the estimated auto-PSD functions. Numerical simulation and experimental tests show that the presented method is efficient when applied to determined and underdetermined

problems in identifying mechanical systems with normal modes, with complex modes, closely-spaced modes and for cases with the presence of harmonic excitations.

Chapter 4: This chapter presents a suggested procedure for single damage detection.

- This chapter presents a procedure for detecting changes in the beam structures using dynamic analysis. A simplified relationship between local changes in mass and/or stiffness and variations in modal parameters is established for damage identification procedure. This procedure allows to determine the location of structural changes and the degree of their severity by analyzing the variations of natural frequencies, the mode shape and the curvature of the intact and damaged states. The effectiveness of the proposed procedure was confirmed by numerical simulations followed by experiment investigation.

Chapter 5: This chapter presents an improvement to the multiple damage detection procedure.

- This chapter presents a enhanced procedure for multi-damage identification using natural frequency shifts, mode shape curvature and Bayesian inference. Comparison between natural frequency shifts obtained directly from the analytic expression established in the previous chapter, instead of using FEM, and measured ones, allows multiple damages to be identified using Bayesian inference. The effectiveness of the proposed method is demonstrated by numerical simulation and then experimental study of beams with the different number of cracks and different boundary conditions.

Chapter 6: This chapter provides some concluding remarks as well as perspectives.

1.8 Publications

Published articles

1. **Duc-Tuan Ta**, Thien-Phu Le, Michael Burman. Operational modal identification based on parallel factor decomposition with the presence of harmonic excitation. *Comptes Rendus. Mécanique*, Volume 349 (2021) no. 3, pp. 435-452. doi: 10.5802/crmeca.90.

To be submitted

2. A novel method for modal analysis using parallel factor decomposition in the frequency domain.

3. Single damage detection using natural frequencies and mode shapes.

4. Multiple damage detection on beams using relative natural frequency shifts and Bayesian inference.

Bibliography

[1] Hua-Peng Chen and Yi-Qing Ni. *Structural Health Monitoring of Large Civil Engineering Structures*. UK: John Wiley & Sons Ltd, 2018.

[2] Charles Farrar, Francois Hemez, D. Shunk, D. Stinemates, and Brett Nadler. "A Review of Structural Health Monitoring Literature: 1996–2001". In: (Jan. 2004).

[3] Charles R Farrar and Keith Worden. *Structural health monitoring: a machine learning perspective*. John Wiley & Sons, 2012.

[4] Mayank Mishra, Paulo B. Lourenço, and G.V. Ramana. "Structural health monitoring of civil engineering structures by using the internet of things: A review". In: *Journal of Building Engineering* 48 (2022), p. 103954. ISSN: 2352-7102. DOI: https://doi.org/10.1016/j.jobe.2021.103954.

[5] Jian Li, Jun Deng, and Weizhi Xie. "Damage Detection with Streamlined Structural Health Monitoring Data". In: *Sensors* 15 (Apr. 2015), pp. 8832–8851. DOI: 10.3390/s150408832.

[6] Diogo Montalvão, N. Maia, and A. Ribeiro. "A Review of Vibration-based Structural Health Monitoring with Special Emphasis on Composite Materials". In: *The Shock and Vibration Digest* 38 (July 2006), p. 295. DOI: 10.1177/0583102406065898.

[7] *Ten Worst Building Collapses in the World*. https://www.arch2o.com/10-worst-building-collapses-in-the-world/. Accessed: 2022-05-19.

[8] Peter E.D. Love, Robert Lopez, and David J. Edwards. "Reviewing the past to learn in the future: making sense of design errors and failures in construction". In: *Structure and Infrastructure Engineering* 9.7 (2013), pp. 675–688. DOI: 10.1080/15732479.2011.605369.

[9] Norbert J Delatte Jr. "Beyond failure: Forensic case studies for civil engineers". In: *Civil and Environmental Engineering Department Books*. American Society of Civil Engineers. ASCE Press, 2008.

[10] Mayank Mishra. "Machine learning techniques for structural health monitoring of heritage buildings: A state-of-the-art review and case studies". In: *Journal of Cultural Heritage* 47 (2021), pp. 227–245. ISSN: 1296-2074. DOI: https://doi.org/10.1016/j.culher.2020.09.005.

[11] Richard Scott. "In the wake of Tacoma". In: *Suspension bridges and the quest for aerodynamic stability. ASCE, Reston* (2001).

[12] James MW Brownjohn. "Structural health monitoring of civil infrastructure". In: *Philosophical Transactions of the Royal Society A: Mathematical, Physical and Engineering Sciences* 365.1851 (2007), pp. 589–622.

[13] Ran Cao, Sherif El-Tawil, and Anil Kumar Agrawal. "Miami Pedestrian Bridge Collapse: Computational Forensic Analysis". In: *Journal of Bridge Engineering* 25.1 (2020), p. 04019134.

[14] S Yu Savin. "Influence of Shear Deformations on the Buckling of Reinforced Concrete Elements". In: *International Scientific Conference on Innovations and Technologies in Construction*. Springer. 2021, pp. 195–200.

[15] M.M. Ettouney and S. Alampalli. *Infrastructure Health in Civil Engineering: Theory and Components*. Infrastructure Health in Civil Engineering. CRC Press, 2012.

[16] J.M.W. Brownjohn, A. De Stefano, Y.L. Xu, H. Wenzel, and A.E. Aktan. "Vibration-based monitoring of civil infrastructure: challenges and successes". In: *Journal of Civil Structural Health Monitoring* 1.3-4 (2011), pp. 79–95. DOI: https://doi.org/10.1007/s13349-011-0009-5.

[17] Patrick Paultre. *Dynamics of Structures*. USA: John Wiley & Sons, Inc, 2013. DOI: 10.1002/9781118599792.

[18] Rune Brincker and Carlos E. Ventura. *Introduction to Operational Modal Analysis*. UK: John Wiley and Sons, 2015. DOI: 10.1002/9781118535141.

[19] Nuno Manuel Mendes Maia and Júlio Martins Montalvão Silva e Silva. *Theoretical and experimental modal analysis*. UK: Research Studies Press, 1997.

[20] R.J.Allemang and D.L.Brown. "A unified matrix polynomial approach to modal identification". In: *Journal of Sound and Vibration* 211.3 (1998), pp. 301–322. ISSN: 0022-460X. DOI: https://doi.org/10.1006/jsvi.1997.1321.

[21] D. J. Ewins. *Modal Testing: Theory, Practice and Application*. UK: Wiley, 2000.

[22] Lingmi Zhang, R. Brincker, and P. Andersen. "An overview of operational modal analysis: Major development and issues". In: *Proceedings of the 1st International Operational Modal Analysis*. Copenhagen: Aalborg Universitet, 2005.

[23] Baron Rayleigh. *The theory of sound*. Vol. 1. Cambridge: Cambridge University Press, 1877.

[24] Frank R. Spitznogle and Azizul H. Quazi. "Representation and analysis of time-limited signals using a complex exponential algorithm". In: *The Journal of the Acoustical Society of America* 47 (1970), pp. 1150–1155. DOI: https://doi.org/10.1121/1.1912020.

[25] D. Brown, R. Allemang, R. Zimmerman, and M. Mergeay. "Parameter estimation techniques for modal analysis". In: *SAE Technical Paper* 88 (1979), pp. 828–846. DOI: https://doi.org/10.4271/790221.

[26] H. Vold, J. Kundrat, G. Rocklin, and R. Russell. "A Multi-Input Modal Estimation Algorithm for Mini-Computers". In: *SAE International Congress and Exposition* 91 (1982), pp. 815–821. DOI: https://doi.org/10.4271/820194.

[27] J.N. Juang and R.S. Pappa. "An eigen system realization algorithm for modal parameter identification and modal reduction". In: *Journal of Guidance Control and Dynamics* 8 (1985), 620–627.

[28] Ivan Wang. "An Analysis of Higher Order Effects in the Half Power Method for Calculating Damping". In: *Journal of Applied Mechanics* 78 (2011), p. 014501. DOI: https://doi.org/10.1115/1.4002208.

[29] Jin-Ting Wang, Feng Jin, and Chu-Han Zhang. "Estimation error of the half-power bandwidth method in identifying damping for multi-DOF systems". In: *Soil Dynamics and Earthquake Engineering* 39 (2012), pp. 138–142. DOI: https://doi.org/10.1016/j.soildyn.2012.02.008.

[30] Jinting Wang, Dandan Lü, Feng Jin, and Chuhan Zhang. "Accuracy of the half-power bandwidth method with a third-order correction for estimating damping in multi-DOF systems". In: *Earthquake Engineering and Engineering Vibration* 12 (2013), pp. 33–38. DOI: 10.1007/s11803-013-0149-1.

[31] Baisheng Wu. "A correction of the half-power bandwidth method for estimating damping". In: *Archive of Applied Mechanics* 85 (2015), pp. 315–320. DOI: https://doi.org/10.1007/s00419-014-0908-0.

[32] Dave Formenti and Mark Richardson. "Parameter estimation from frequency response measurements using rational fraction polynomials". In: *Proceedings of the first International Modal Analysis Conference*. Orlando, Florida: Union College, 1982, pp. 167–182.

[33] Richardson M. H. and Formenti D. L. "Global Frequency and Damping from Frequency Response Measurements". In: *Proceedings of the 4th International Modal Analysis Conference*. Los Angeles, California, 1986, pp. 1–7.

[34] C.Y.Shih, Y.G.Tsuei, R.J.Allemang, and D.L.Brown. "Complex mode indication function and its applications to spatial domain parameter estimation". In: *Mechanical Systems and Signal Processing* 2 (1988), pp. 367–377. DOI: https://doi.org/10.1016/0888-3270(88)90060-X.

[35] B. Peeters, H. Auweraer, P. Guillaume, and J. Leuridan. "The PolyMAX frequency-domain method: a new standard for modal parameter estimation?" In: *Shock and Vibration* 11 (2004), pp. 395–409.

[36] Julius S. Bendat and Allan G. Piersol. *Engineering Applications of Correlation and Spectral Analysis*. John Wiley & Sons, Inc, 2013.

[37] Bart Peeters and Guido De Roeck. "Stochastic System Identification for Operational Modal Analysis: A Review ". In: *Journal of Dynamic Systems, Measurement, and Control* 123.4 (Feb. 2001), pp. 659–667. ISSN: 0022-0434. DOI: 10.1115/1.1410370.

[38] S.R. Ibrahim and E.C. Mikulcik. "A time domain modal vibration test technique". In: *Shock and Vibration Bulletin* 43(4) (1973), pp. 21–37.

[39] S. R. Ibrahim and E. Mikulcik. "A method for the direct identification of vibration parameters from the free response". In: *The Shock and Vibration Bulletin* 47 (1977), 183–196.

[40] Peter van Overschee and B.L. de Moor. *Subspace identification for linear systems, theory, implementation, application*. Netherlands: Kluwer Academic Publishers Group, 1996. DOI: 10.1007/978-1-4613-0465-41.

[41] B. Peeters and C.E. Ventura. "Comparative study of modal analysis techniques for bridge dynamic characteristics". In: *Mechanical Systems and Signal Processing* 17.5 (2003), pp. 965–988. ISSN: 0888-3270. DOI: https://doi.org/10.1006/mssp.2002.1568.

[42] R. Brincker, L. Zhang, and P. Andersen. "Output-only Modal Analysis by Frequency Domain Decomposition". In: *Proceedings of ISMA25: 2000 International Conference on Noise and Vibration Engineering*. Leuven: Katholieke Universiteit, 2000, pp. 717–723.

[43] J.-F. Cardoso. "Blind signal separation: statistical principles". In: *Proceedings of the IEEE*. Vol. 86. IEEE, 1998. DOI: 10.1109/5.720250.

[44] Andrzej Cichocki and Shun-ichi Amari. *Adaptive blind signal and image processing: learning algorithms and applications*. John Wiley & Sons, 2002.

[45] Seungjin Choi, Andrzej Cichocki, Hyung-Min Park, and Soo-Young Lee. "Blind source separation and independent component analysis: A review". In: *Neural Inf. Process. Lett. Rev* 6 (Nov. 2004).

[46] P. Comon and C. Jutten. *Handbook of Blind Source Separation: Independent Component Analysis and Applications*. Elsevier Ltd, 2010.

[47] Jen-Tzung Chien. *Source Separation and Machine Learning*. Elsevier Ltd, 2019.

[48] Pierre Comon. "Independent component analysis, A new concept?" In: *Signal Processing* 36.3 (1994), pp. 287 –314. DOI: https://doi.org/10.1016/0165-1684(94)90029-9.

[49] A. Belouchrani, K. Abed-Meraim, Jean-François Cardoso, and E. Moulines. "A blind source separation technique using second-order statistics". In: *IEEE Trans. Signal Process.* IEEE, 1997. DOI: https://doi.org/10.1109/78.554307.

[50] A. Hyvärinen and E. Oja. "Independent component analysis: algorithms and applications". In: *Neural Networks* 13.4 (2000), pp. 411–430. ISSN: 0893-6080.

[51] Puskal P. Pokharel, Umut Ozertem, Deniz Erdogmus, and Jose C. Principe. "Recursive complex BSS via generalized eigendecomposition and application in image rejection for BPSK". In: *Signal Processing* 88.6 (2008), pp. 1368–1381. ISSN: 0165-1684. DOI: https://doi.org/10.1016/j.sigpro.2007.12.001.

[52] S. Xie, L. Yang, J.-M. Yang, G. Zhou, and Y. Xiang. "Time-frequency approach to underdetermined blind source separation". In: *IEEE Transactions on Neural Networks and Learning Systems* 23.2 (2012), pp. 306–316. DOI: https://doi.org/10.1109/TNNLS.2011.2177475.

[53] Pau Bofill and Michael Zibulevsky. "Underdetermined blind source separation using sparse representations". In: *Signal Processing* 81.11 (2001), pp. 2353–2362. ISSN: 0165-1684.

[54] Jérôme Antoni. "Blind separation of vibration components: Principles and demonstrations". In: *Mechanical Systems and Signal Processing* 19 (2005), pp. 1166–1180.

[55] P.D. O'Grady, Barak A. Pearlmutter, and Scott T. Rickard. "Survey of sparse and non-sparse methods in source separation". In: *International Journal of Imaging Systems and Technology* 15 (2005).

[56] Bharath Sundararaman, Ugo Buy, and Ajay D. Kshemkalyani. "Clock synchronization for wireless sensor networks: a survey". In: *Ad Hoc Networks* 3.3 (2005), pp. 281–323. ISSN: 1570-8705. DOI: https://doi.org/10.1016/j.adhoc.2005.01.002.

[57] Mohammed El Rhabi, Guillaume Gelle, H. Fenniri, and Georges Delaunay. "A penalized mutual information criterion for blind separation of convolutive mixtures". In: *Signal Processing* 84 (Oct. 2004), pp. 1979–1984. DOI: 10.1016/j.sigpro.2004.06.015.

[58] Lars Omlor and Martin A. Giese. "Anechoic Blind Source Separation Using Wigner Marginals". In: *J. Mach. Learn. Res.* 12.null (2011), 1111–1148. ISSN: 1532-4435.

[59] Paris Smaragdis. "Blind separation of convolved mixtures in the frequency domain". In: *Neurocomputing* 22.1 (1998), pp. 21–34. ISSN: 0925-2312. DOI: https://doi.org/10.1016/S0925-2312(98)00047-2.

[60] S Chauhan, R Martell, RJ Allemang, and DL Brown. "Application of independent component analysis and blind source separation techniques to operational modal analysis". In: *Proceedings of the 25th IMAC, Orlando (FL), USA*. 2007.

[61] G. Kerschen, F. Poncelet, and J.-C. Golinval. "Physical interpretation of independent component analysis in structural dynamics". In: *Mechanical Systems and Signal*

Processing 21.4 (2007), pp. 1561–1575. ISSN: 0888-3270. DOI: https://doi.org/10.1016/j.ymssp.2006.07.009.

[62] Yongchao Yang and Satish Nagarajaiah. "Time-Frequency Blind Source Separation Using Independent Component Analysis for Output-Only Modal Identification of Highly Damped Structures". In: *ASCE Journal of Structural Engineering* 139.10 (2013). DOI: https://doi.org/10.1061/(ASCE)ST.1943-541X.0000621.

[63] F. Poncelet, G. Kerschen, J.-C. Golinval, and D. Verhelst. "Output-only modal analysis using blind source separation techniques". In: *Mechanical Systems and Signal Processing* 21.6 (2007), pp. 2335–2358. ISSN: 0888-3270. DOI: https://doi.org/10.1016/j.ymssp.2006.12.005.

[64] Yongchao Yang and Satish Nagarajaiah. "Blind identification of damage in time-varying systems using independent component analysis with wavelet transform". In: *Mechanical Systems and Signal Processing* 47.1 (2014). MSSP Special Issue on the Identification of Time Varying Structures and Systems, pp. 3–20. ISSN: 0888-3270. DOI: https://doi.org/10.1016/j.ymssp.2012.08.029.

[65] A. Sadhu, S. Narasimhan, and J. Antoni. "A review of output-only structural mode identification literature employing blind source separation methods". In: *Mechanical Systems and Signal Processing* 94 (2017), pp. 415–431. ISSN: 0888-3270. DOI: https://doi.org/10.1016/j.ymssp.2017.03.001.

[66] Aapo Hyvarinen, Juha Karhunen, and Erkki Oja. "Independent component analysis". In: *Studies in informatics and control* 11.2 (2002), pp. 205–207.

[67] Anthony J. Bell and Terrence J. Sejnowski. "An Information-Maximization Approach to Blind Separation and Blind Deconvolution". In: *Neural Computation* 7.6 (Nov. 1995), pp. 1129–1159. ISSN: 0899-7667. DOI: 10.1162/neco.1995.7.6.1129.

[68] Jean-François Cardoso and Antoine Souloumiac. "Jacobi Angles for Simultaneous Diagonalization". In: *SIAM Journal on Matrix Analysis and Applications* 17.1 (1996), pp. 161–164. DOI: 10.1137/S0895479893259546.

[69] Abdeldjalil Aissa-El-Bey, Nguyen Linh-Trung, Karim Abed-Meraim, Adel Belouchrani, and Yves Grenier. "Underdetermined Blind Separation of Nondisjoint Sources in the Time-Frequency Domain". In: *IEEE Transactions on Signal Processing* 55.3 (2007), pp. 897–907. DOI: 10.1109/TSP.2006.888877.

[70] J. Lin, D. Grier, and J. Cowan. "Faithful representation of separable distributions". In: *Neural Computation* 9 (1997)), 1305–1320.

[71] M. Van Hulle. "Clustering approach to square and non-square blind source separation". In: *IEEE Workshop on Neural Networks for Signal Processing*. IEEE, 1999, 315–323.

[72] T.-W. Lee, M.S. Lewicki, M. Girolami, and T.J. Sejnowski. "Blind source separation of more sources than mixtures using overcomplete representations". In: *IEEE Signal Processing Letters* 6 (1999)), 87–90.

[73] S. Rickard O. Yilmaz. "Blind separation of speech mixtures via time-frequency masking". In: *IEEE Transactions on Signal Processing* 52 (2004)), 1830–1847.

[74] Roberto Castiglione, Jerome Antoni, and Luigi Garibaldi. "Separation and identification of structural modes in largely underdetermined scenarios using frequency banding". In: *Journal of Sound and Vibration* 414 (2018), pp. 192–217. ISSN: 0022-460X. DOI: https://doi.org/10.1016/j.jsv.2017.10.033.

[75] Fereidoun Amini and Yousef Hedayati. "Underdetermined blind modal identification of structures by earthquake and ambient vibration measurements via sparse component analysis". In: *Journal of Sound and Vibration* 366 (2016), pp. 117–132. ISSN: 0022-460X. DOI: https://doi.org/10.1016/j.jsv.2015.10.028.

[76] Yuanqing Li, Andrzej Cichocki, and Shun-ichi Amari. "Sparse component analysis for blind source separation with less sensors than sources". In: *4th International Symposium on Independent Component Analysis and Blind Signal Separation*. 2003, 89–94.

[77] Kaiping Yu, Kai Yang, and Yunhe Bai. "Estimation of modal parameters using the sparse component analysis based underdetermined blind source separation". In: *Mechanical Systems and Signal Processing* 45.2 (2014), pp. 302–316. ISSN: 0888-3270. DOI: https://doi.org/10.1016/j.ymssp.2013.11.018.

[78] Xiao-Jun Yao, Ting-Hua Yi, Chunxu Qu, and Hong-Nan Li. "Blind Modal Identification Using Limited Sensors through Modified Sparse Component Analysis by Time-Frequency Method". In: *Computer-Aided Civil and Infrastructure Engineering* 33.9 (2018), 769–782. DOI: https://doi.org/10.1111/mice.12372.

[79] Yongchao Yang and Satish Nagarajaiah. "Output-only modal identification with limited sensors using sparse component analysis". In: *Journal of Sound and Vibration* 332.19 (2013), pp. 4741–4765. ISSN: 0022-460X. DOI: https://doi.org/10.1016/j.jsv.2013.04.004.

[80] Wei Guan, Longlei Dong, Yinshan Cai, Jian Yan, and Yi Han. "Sparse component analysis with optimized clustering for underdetermined blind modal identification". In: *Measurement Science and Technology* 30.12 (2019), 125011 (16pp). DOI: https://doi.org/10.1088/1361-6501/ab3054.

[81] Duc-Tuan Ta, Thien-Phu Le, and Michael Burman. "Operational modal identification based on parallel factor decomposition with the presence of harmonic excitation". en. In: *Comptes Rendus. Mécanique* 349.3 (2021), pp. 435–452. DOI: 10.5802/crmeca.90.

[82] J. Antoni and S. Chauhan. "An Alternating Least Squares (ALS) based Blind Source Separation Algorithm for Operational Modal Analysis". In: *Proceedings of the 29th IMAC, A Conference and Exposition on Structural Dynamics*. Vol. 3. Conference Proceedings of the Society for Experimental Mechanics Series. New York, United States: Springer, 2011. DOI: https://doi.org/10.1007/978-1-4419-9299-4_15.

[83] Fariba Abazarsa, Fariborz Nateghi, S. Farid Ghahari, and Ertugrul Taciroglu. "Blind Modal Identification of Non-Classically Damped Systems from Free or Ambient Vibration Records". In: *Earthquake Spectra* 29 (2013), pp. 1137–1157. DOI: https://doi.org/10.1193/031712EQS093M.

[84] F. Abazarsa, S. F. Ghahari, F. Nateghi, and E. Taciroglu. "Response-only modal identification of structures using limited sensors". In: *Structural Control and Health Monitoring* 20 (2013), pp. 987–1006. DOI: https://doi.org/10.1002/stc.1513.

[85] P. Friesen and A. Sadhu. "Performance of tensor decomposition-based modal identification under nonstationary vibration". In: *Smart Materials and Structures* 26 (2017), pp. 1–19. DOI: https://doi.org/10.1088/1361-665X/aa5438.

[86] Scot I. McNeill. "Extending Blind Modal Identification to the Underdetermined Case for Ambient Vibration". In: *ASME 2012 International Mechanical Engineering Congress and Exposition*. Texas, USA: The American Society of Mechanical Engineers, 2012. DOI: https://doi.org/10.1115/IMECE2012-93140.

[87] A. Sadhu, A. Goldack, and S. Narasimhan. "Ambient modal identification using multi-rank parallel factor decomposition". In: *Structural Control and Health Monitoring* 22 (2015), pp. 595–614. DOI: https://doi.org/10.1002/stc.1706.

[88] A. Sadhu, B. Hazra, and S. Narasimhan. "Decentralized modal identification of structures using parallel factor decomposition and sparse blind source separation". In: *Mechanical Systems and Signal Processing* 41 (2013), pp. 396–419. DOI: https://doi.org/10.1016/j.ymssp.2013.06.031.

[89] A. Smilde, Rasmus Bro, and P. Geladi. *Multi Way Analysis — Applications in Chemical Sciences*. England: John Wiley Sons, Ltd, 2004.

[90] Rasmus Bro. "PARAFAC. Tutorial and applications". In: *Chemometrics and Intelligent Laboratory Systems* 38.2 (1997), pp. 149–171. ISSN: 0169-7439. DOI: https://doi.org/10.1016/S0169-7439(97)00032-4.

[91] Richard A. Harshman. *Foundations of the PARAFAC Procedure: Models and Conditions for an explanatory Multi-modal Factor Analysis*. University of California at Los Angeles, 1970.

[92] J. Carroll and J. Chang. "Analysis of individual differences in multidimensional scaling via an n-way generalization of "Eckart-Young" decomposition". In: *Psychometrika* 35 (1970), pp. 283–319. DOI: https://doi.org/10.1007/BF02310791.

[93] Giorgio Tomasi and Rasmus Bro. "A comparison of algorithms for fitting the PARAFAC model". In: *Computational Statistics and Data Analysis* 50.7 (2006), pp. 1700 –1734. DOI: https://doi.org/10.1016/j.csda.2004.11.013.

[94] Pierre Comon, Xavier Luciani, and André de Almeida. "Tensor Decompositions, Alternating Least Squares and other Tales". In: *Journal of Chemometrics* 23 (July 2009), pp. 393–405. DOI: https://doi.org/10.1002/cem.1236.

[95] Dimitri Nion and Lieven De Lathauwer. "An enhanced line search scheme for complex-valued tensor decompositions. Application in DS-CDMA". In: *Signal Processing* 88.3 (2008), pp. 749–755. ISSN: 0165-1684. DOI: https://doi.org/10.1016/j.sigpro.2007.07.024.

[96] Joseph B. Kruskal. "Three-way arrays: rank and uniqueness of trilinear decompositions, with application to arithmetic complexity and statistics". In: *Linear Algebra and its Applications* 18.2 (1977), pp. 95–138. ISSN: 0024-3795. DOI: https://doi.org/10.1016/0024-3795(77)90069-6.

[97] Lieven De Lathauwer and JosÉphine Castaing. "Blind Identification of Underdetermined Mixtures by Simultaneous Matrix Diagonalization". In: *IEEE Transactions on Signal Processing* 56 (2008), pp. 1096 –1105. DOI: https://doi.org/10.1109/TSP.2007.908929.

[98] Vincent Gagnol, Thien-Phu Le, and Pascal Ray. "Modal identification of spindle-tool unit in high-speed machining". In: *Mechanical Systems and Signal Processing* (2011), pp. 2388–2398. DOI: https://doi.org/10.1016/j.ymssp.2011.02.019.

[99] T. Lago. "The difference between harmonics and stochastic narrow band responses". In: *Presentation at the SVIBS symposium*. Stockholm: Structural Vibration Solution, 1997.

[100] Niels-Jørgen Jacobsen, Palle Andersen, and Rune Brincker. "Eliminating the Influence of Harmonic Components in Operational Modal Analysis". In: *The International Modal Analysis Conference IMAC-XXIV: A Conference & Exposition on Structural Dynamics*. Society for Experimental Mechanics, 2007.

[101] Rune Brincker, Palle Andersen, and N. B. Møller. "An Indicator for Separation of Structural and Harmonic Modes in Output-only Modal Testing". In: *Proceedings of SPIE - The International Society for Optical Engineering*. Madrid, Spain: Aalborg University, 2000.

[102] Valeriu Vrabie, Pierre Granjon, and Christine Serviere. "Spectral kurtosis: from definition to application". In: *Proceedings of the 6th IEEE NSPI Grado-Trieste*. Italy, 2003.

[103] Kevin P. Balanda and H. L. MacGillivray. "Kurtosis: A Critical Review". In: *The American Statistician* 42.2 (1988), pp. 111–119.

[104] J.-L. Dion, I. Tawfiq, and G. Chevallier. "Harmonic component detection: Optimized Spectral Kurtosis for operational modal analysis". In: *Mechanical Systems and Signal Processing* 26 (2012), pp. 24–33. ISSN: 0888-3270. DOI: https://doi.org/10.1016/j.ymssp.2011.07.009.

[105] Tong Wang, Zunping Xia, and Lingmi Zhang. "Detection and removal of harmonic components in operational modal analysis". In: *Journal of Vibroengineering* 19.7 (2017), pp. 5278–5289. DOI: https://doi.org/10.21595/jve.2017.17725.

[106] Jérôme Antoni. "The spectral kurtosis: a useful tool for characterising non-stationary signals". In: *Mechanical Systems and Signal Processing* 20 (2006), pp. 282–307. DOI: https://doi.org/10.1016/j.ymssp.2004.09.001.

[107] Maurice George Kendall and Alan Stuart. *Advanced Theory of Statistics, Volume 1, Distribution Theory, Second Edition*. London: Charles Griffin and Company Limited, 1963.

[108] Anders Rytter. "Vibrational Based Inspection of Civil Engineering Structures". PhD thesis. University of Aalborg, Denmark, 1993.

[109] Scott W Doebling, Charles R Farrar, Michael B Prime, and Daniel W Shevitz. "Damage identification and health monitoring of structural and mechanical systems from changes in their vibration characteristics: a literature review". In: *Technical Report* (1996).

[110] Onur Avci, Osama Abdeljaber, Serkan Kiranyaz, Mohammed Hussein, Moncef Gabbouj, and Daniel J. Inman. "A review of vibration-based damage detection in civil structures: From traditional methods to Machine Learning and Deep Learning applications". In: *Mechanical Systems and Signal Processing* 147 (2021), p. 107077. ISSN: 0888-3270. DOI: https://doi.org/10.1016/j.ymssp.2020.107077.

[111] Rongrong Hou and Yong Xia. "Review on the new development of vibration-based damage identification for civil engineering structures: 2010–2019". In: *Journal of Sound and Vibration* 491 (2021), p. 115741. ISSN: 0022-460X. DOI: https://doi.org/10.1016/j.jsv.2020.115741.

[112] C.J. Heller. *Handbook of Non-Destructive Evaluation*. NY, USA: McGraw-Hill, 2001.

[113] M.M. Ettouney and S. Alampalli. *Infrastructure Health in Civil Engineering*. London, UK: CRC Press, 2012.

[114] Thomas E. Michaels and Jennifer E. Michaels. "Application of acoustic wavefield imaging to non-contact ultrasonic inspection of bonded components". In: *Review of progress in quantitative nondestructive Evaluation*. Vol. 25. 2006, 1484–1491.

[115] Kevin L. Rens, Terry J. Wipf, and F. Wayne Klaiber. "Review of Nondestructive Evaluation Techniques of Civil Infrastructure". In: *Journal of Performance of Constructed Facilities* 11.4 (1996). DOI: https://doi.org/10.1061/(ASCE)0887-3828(1997)11:4(152).

[116] Peter C. Chang and S. Chi Liu. "Recent Research in Nondestructive Evaluation of Civil Infrastructures". In: *Journal of Materials in Civil Engineering* 15.3 (2003). DOI: https://doi.org/10.1061/(ASCE)0899-1561(2003)15:3(298).

[117] D. Montalvão, N. Maia, and A. R. Ribeiro. "A review of vibration-based structural health monitoring with special emphasis on composite materials". In: *The Shock and Vibration Digest* 38 (2006), pp. 295–324.

[118] V. Meruane and W. Heylen. "Structural damage assessment under varying temperature conditions". In: *Structural Health Monitoring* 11 (3 2012), 345–357. DOI: 10.1177/1475921711419995.

[119] P Cawley and R D Adams. "The location of defects in structures from measurements of natural frequencies". In: *The Journal of Strain Analysis for Engineering Design* 14.2 (1979), pp. 49–57. DOI: 10.1243/03093247V142049.

[120] E.P. Carden and P. Fanning. "Vibration based conditioning monitoring: a review". In: *Structural Health Monitoring* 3 (2004)), 355–377.

[121] Lieven N.A.J. and Ewins D.J. "Spatial correlation of mode shapes, the coordinate modal assurance criterion (COMAC)". In: *Proceedings of the 6th International Modal Analysis Conference*. Vol. 1. Kissimmee, Florida, USA, 1988.

[122] Magdalena Palacz and Marek Krawczuk. "Vibration parameters for damage detection in structures". In: *Journal of Sound and Vibration* 249.5 (2002), pp. 999–1010. ISSN: 0022-460X. DOI: https://doi.org/10.1006/jsvi.2001.3761.

[123] E. Parloo, P. Guillaume, and M. Van Overmeire. "Damage assessment using mode shape sensitivities". In: *Mechanical Systems and Signal Processing* 17.3 (2003), pp. 499–518. ISSN: 0888-3270. DOI: https://doi.org/10.1006/mssp.2001.1429.

[124] A.K. Pandey, M. Biswas, and M.M. Samman. "Damage detection from changes in curvature mode shapes". In: *Journal of Sound and Vibration* 145 (199), 321–332.

[125] A. Graps. "An introduction to wavelets". In: *IEEE Computational Science and Engineering* 2.2 (1995), pp. 50–61. DOI: 10.1109/99.388960.

[126] Norden Eh Huang. *Hilbert-Huang transform and its applications*. Vol. 16. World Scientific, 2014.

[127] Benoit Mandelbrot. "How Long Is the Coast of Britain? Statistical Self-Similarity and Fractional Dimension". In: *Science* 156.3775 (1967), pp. 636–638. DOI: 10.1126/science.156.3775.636. URL: https://www.science.org/doi/abs/10.1126/science.156.3775.636.

[128] Y.J. Yan, L. Cheng, Z.Y. Wu, and L.H. Yam. "Development in vibration-based structural damage detection technique". In: *Mechanical Systems and Signal Processing* 21.5 (2007), pp. 2198–2211. ISSN: 0888-3270. DOI: https://doi.org/10.1016/j.ymssp.2006.10.002.

[129] Diogo Montalvão, N. Maia, and A. Ribeiro. "A Review of Vibration-based Structural Health Monitoring with Special Emphasis on Composite Materials". In: *The Shock and Vibration Digest* 38 (July 2006), p. 295. DOI: 10.1177/0583102406065898.

[130] M. LINK and M. FRISWELL. "Generation of validated structural dynamic models—results of a benchmark study utilising the garteur sm-ag19 test-bed". In: *Mechanical Systems and Signal Processing* 17.1 (2003), pp. 9–20. ISSN: 0888-3270. DOI: https://doi.org/10.1006/mssp.2002.1534.

[131] J.E. Mottershead and M.I. Friswell. "Model Updating In Structural Dynamics: A Survey". In: *Journal of Sound and Vibration* 167.2 (1993), pp. 347–375. ISSN: 0022-460X. DOI: https://doi.org/10.1006/jsvi.1993.1340.

[132] Reza Jafarkhani and Sami F. Masri. "Finite Element Model Updating Using Evolutionary Strategy for Damage Detection". In: *Computer-Aided Civil and Infrastructure Engineering* 26.3 (2011), pp. 207–224. DOI: https://doi.org/10.1111/j.1467-8667.2010.00687.x.

[133] J.R. Wu and Q.S. Li. "Structural parameter identification and damage detection for a steel structure using a two-stage finite element model updating method". In: *Journal of Constructional Steel Research* 62.3 (2006), pp. 231–239. ISSN: 0143-974X. DOI: https://doi.org/10.1016/j.jcsr.2005.07.003.

[134] M. I. Friswell, D. J. Inman, and D. F. Pilkey. "Direct Updating of Damping and Stiffness Matrices". In: *AIAA Journal* 36.3 (1998), pp. 491–493. DOI: https://doi.org/10.2514/2.396.

[135] John E. Mottershead, Michael Link, and Michael I. Friswell. "The sensitivity method in finite element model updating: A tutorial". In: *Mechanical Systems and Signal Processing* 25.7 (2011), pp. 2275–2296. ISSN: 0888-3270. DOI: https://doi.org/10.1016/j.ymssp.2010.10.012.

[136] James M. W. Brownjohn and Pin-Qi Xia. "Dynamic Assessment of Curved Cable-Stayed Bridge by Model Updating". In: *Journal of Structural Engineering* 126.2 (2000), pp. 252–260. DOI: 10.1061/(ASCE)0733-9445(2000)126:2(252).

[137] Christopher M Bishop and Nasser M Nasrabadi. *Pattern recognition and machine learning*. Vol. 4. 4. Springer, 2006.

[138] Christopher M Bishop et al. *Neural networks for pattern recognition*. Oxford university press, 1995.

[139] Norhisham Bakhary, Hong Hao, and Andrew J. Deeks. "Structure Damage Detection Using Neural Network with Multi-Stage Substructuring". In: *Advances in Structural Engineering* 13.1 (2010), pp. 95–110. DOI: 10.1260/1369-4332.13.1.95.

[140] João P. Santos, Christian Crémona, Luís Calado, Paulo Silveira, and André D. Orcesi. "On-line unsupervised detection of early damage". In: *Structural Control and Health Monitoring* 23.7 (2016), pp. 1047–1069. DOI: https://doi.org/10.1002/stc.1825.

[141] Young-Jin Cha and Zilong Wang. "Unsupervised novelty detection–based structural damage localization using a density peaks-based fast clustering algorithm". In: *Structural Health Monitoring* 17.2 (2018), pp. 313–324. DOI: 10.1177/1475921717691260.

[142] Siheng Chen, Fernando Cerda, Piervincenzo Rizzo, Jacobo Bielak, James H. Garrett Jr., and Jelena Kovačević. "Semi-supervised multiresolution classification using adaptive graph filtering with application to indirect bridge structural health monitoring". In: *IEEE Transactions on Signal Processing* 62.11 (2014), 2879 – 2893. DOI: 10.1109/TSP.2014.2313528.

[143] T.J. Rogers, K. Worden, R. Fuentes, N. Dervilis, U.T. Tygesen, and E.J. Cross. "A Bayesian non-parametric clustering approach for semi-supervised Structural Health Monitoring". In: *Mechanical Systems and Signal Processing* 119 (2019), pp. 100–119. ISSN: 0888-3270. DOI: https://doi.org/10.1016/j.ymssp.2018.09.013.

2 Operational modal analysis in the time domain

Chapter abstract

Despite the wide variety of methods presented in the previous part, there are still challenges for which a stable and reliable solution for modal analysis has not yet been proposed. One such problem is the undetermined situation when the number of measurements is less than the number of active modes. Another, no less important problem is the presence of external harmonic excitations, which can be confused with modal parameters of system.

This chapter presents an improvement of the existing modal identification technique based on the PARAllel FACtor (PARAFAC) decomposition in the time domain. Recently proposed for operational modal analysis, PARAFAC decomposition based methods have been proven to be efficient for underdetermined problems and problems with the presence of harmonic excitations. The third-order tensor of the covariance of responses is decomposed into components corresponding to structural modes or harmonic components. The modal parameters are then deduced from the auto-covariance function of each component, and the distinction between the structural mode and the harmonic component is based on its kurtosis value. However, no criterion about the length of the auto-covariance function was given in the literature.

The study of the thesis showed that this length is important and should be chosen depending on the decomposed components, as an insufficient length of the auto-covariance function can lead to inaccurate results. To overcome this limitation, an enhanced procedure of the PARAFAC decomposition-based method for modal analysis in the time domain has been proposed. The minimum length of auto-covariance functions using natural periods and damping ratios is proposed to distinguish between harmonics and structural modes accurately. This procedure has been confirmed by numerical simulations and experimental tests.

2.1 An enhanced method for modal analysis in the time domain (Article 1)

INSTITUT DE FRANCE
Académie des sciences

Comptes Rendus
Mécanique

Duc-Tuan Ta, Thien-Phu Le and Michael Burman

Operational modal identification based on parallel factor decomposition with the presence of harmonic excitation

Volume 349, issue 3 (2021), p. 435-452

<https://doi.org/10.5802/crmeca.90>

Les Comptes Rendus. Mécanique *sont membres du Centre Mersenne pour l'édition scientifique ouverte*
www.centre-mersenne.org

Comptes Rendus
Mécanique
2021, 349, nº 3, p. 435-452
https://doi.org/10.5802/crmeca.90

Short paper / *Note*

Operational modal identification based on parallel factor decomposition with the presence of harmonic excitation

Duc-Tuan Ta *, [a], **Thien-Phu Le** [a] **and Michael Burman** [a]

[a] Université Paris-Saclay, Univ Evry, LMEE, 91020, Evry, France
E-mails: ductuan.ta@uni-evry.fr (D.-T. Ta), thienphu.le@univ-evry.fr (T.-P. Le), michael.burman@univ-evry.fr (M. Burman)

Abstract. One of the main difficulties of the operational modal analysis is to deal with underdetermined problems in which the number of sensors is less than the number of active modes. In the last decade, methods based on the PARAllel FACtor (PARAFAC) decomposition have attracted a lot of attention in the field of modal analysis because it has been proven that these methods can deal with underdetermined cases, as well as the presence of harmonic excitations. Moreover, in combination with kurtosis value as a harmonic indicator, this makes them more efficient in distinguishing between harmonic and structural components. However, it can lead to distorted results as it does not take into account the variation in the length of the covariance functions of the modal coordinates. Since the kurtosis values are estimated from these covariance functions, the length of the latter directly affects the kurtosis. To overcome this limit, the present study proposes to introduce the choice of the length of these functions based on their frequency and damping coefficient. This change improves the existing method by more efficient separating between harmonics and modal components. The proposed procedure is validated using numerical simulations, followed by ambient vibration measurements.

Keywords. Modal analysis, PARAFAC decomposition, Covariance function, Harmonic, Kurtosis.
Manuscript received 24th March 2021, revised 16th July 2021, accepted 19th July 2021.

1. Introduction

In recent decades, operational modal analysis (OMA) has been significantly developed, and it plays a vital role in the engineering fields. This is an identification technique that uses only structural responses without knowing the input excitation information [1]. It is a challenging task to measure the input excitations of mechanical systems and sometimes even impossible. Therefore, the input excitation is frequently considered as Gaussian white noise. However, this assumption is not always validated in reality because of the existence of periodic excitations. Moreover, the presence of input excitations such as harmonic ones can cause errors in the modal

* Corresponding author.

identification process. Therefore, harmonic excitations should be detected and isolated from the estimation of the structure's modal parameters.

Emerged in the audio domain for sources demixing from the audio records [2], the blind source separation (BSS) techniques have widely deployed in different research areas [3–8]. Castiglione *et al.* [9] recently proposed a solution to the BSS approach based on multi-filters designed in the frequency domain. The method's main idea is to divide a large underdetermined problem in the frequency axis into several overdetermined or determined problems in sub-bands. The modal parameters can then be estimated in the sub-bands. Thus, the method can handle the issue of severely underdetermined scenarios. In OMA, these techniques are used for finding latent sources from registered signals of systems without using any information about the mixing process. The state of the art in BSS for OMA has been comprehensively treated in [10].

The main challenge for applying the BSS techniques in OMA is when the number of measurement signals (or sensors) is less than that of latent sources—an underdetermined case. This problem can be encountered in many practical applications with limited measurements, for example, for complex structures or in the presence of harmonic excitations, when the measurement signals may be insufficient compared to the number of hidden sources.

There are some well-known indicators used in OMA to distinguish between the harmonic components and the structural components. Initially pointed out in study [11], kurtosis value has been widely used to distinguish between harmonic and modal responses [12–17]. If a component is pure harmonic, the graph of its probability density function (PDF) will have two peaks with the kurtosis value of 1.5. Otherwise, the PDF of a pure structural mode response will have a normal distribution with the kurtosis value equal to 3. Another effective tool to distinguish a structural component from a harmonic one is the modal assurance criterion (MAC) [18]. If a linear relationship exists between the two modal vectors, the MAC value will be near 1. If they are linearly independent, the MAC value will be near zero. In addition to the above-mentioned techniques, there is a direct approach for distinguishing harmonic components. This method proposes to consider them as zero-damping modes, while the damping ratio of the real pole of the structural component varies between 0.1% and 2% [12]. However, this method would not be effective when the structural modes have very low damping or the harmonic frequencies are very close to the structural frequencies [16].

The PARAFAC decomposition technique [19] was recently employed in operation modal analysis as one of the BSS family methods. It has been proven to effectively treat different types of excitations such as ambient vibrations, earthquakes, or human-induced vibrations [20–27]. It was showed that the method could handle a system with many modes, in which each mode has a different damping level [22, 27]. A simplified description of these methods can be summarized in three steps. At the first step, the covariance matrices of system responses are used to construct a third-order tensor. The PARAFAC technique is then used to decompose this third-order tensor into a sum of triple vectors' outer products. And finally, the obtained decomposition products like the mixing matrix and the auto-covariance matrix are used to estimate the system modal parameters.

Among the PARAFAC decomposition technique applications, Sadhu *et al.* [25] proposed a new approach based on a multiple-rank PARAFAC decomposition. In order to distinguish between sources corresponding to harmonic components or structural modes, the average kurtosis value is used. The authors proved that this approach is efficient for modal identification under the presence of multiple harmonic excitations.

However, the PARAFAC decomposition results in the auto-covariance functions of modal coordinates rather than direct modal coordinates. Because of the decaying feature of the auto-covariance functions of modal coordinates [28], the kurtosis values depend on the lengths of these functions. As a consequence, the insufficient length of the auto-covariance function can

cause inaccuracy when using kurtosis value as a harmonic indicator. Hence, for OMA, the length of the auto-covariance function needs to be considered when using kurtosis value as a harmonic indicator in PARAFAC decomposition-based methods.

To the best of our knowledge, there have been no studies on the influence of the length of the auto-covariance function on its kurtosis value.

This work takes advantage of previous studies. A modified procedure of the PARAFAC decomposition-based method is presented for the OMA. The minimum length of auto-covariance functions using natural periods and damping factors are suggested to distinguish between harmonic and modal components accurately. This modification allows to effectively distinguishing separated structural modes and harmonic ones. The efficiency in the performance of the proposed procedure has been verified using numerical and experimental tests. The rest of the paper is organized as follows. Section 2 describes the techniques of BSS and PARAFAC decomposition, Section 3 formulates a proposed procedure. The validation of the proposed procedure is presented in Section 4. Finally, Section 5 presents a conclusion.

2. Theoretical formulation

2.1. *Instantaneous mixing model and PARAFAC decomposition*

A linear instantaneous mixing model

$$\mathbf{x}(t) = \mathbf{A}\mathbf{s}(t) + \mathbf{n}(t) = \sum_{i}^{n_s} \mathbf{A}_i \mathbf{s}_i(t) + \mathbf{n}(t), \tag{1}$$

where $\mathbf{x}(t) = [x_1(t), x_2(t), \ldots, x_{n_x}(t)]^T$ is n_x output measurements, $\mathbf{s}(t) = [s_1(t), s_2(t), \ldots, s_{n_s}(t)]^T$ contains n_s latent sources, $\mathbf{n}(t)$ is the noisy vector, and $\mathbf{A}_i$ is the ith column of the unknown mixing matrix $\mathbf{A}$. BSS aims to obtain the latent sources $\mathbf{s}(t)$ from the output measurement $\mathbf{x}(t)$ only. Depending on the relation between the number of measurement sensors and the number of sources, BSS problems can be classified as overdetermined case, when $n_x > n_s$, determined case, when $n_x = n_s$, or underdetermined case, when $n_x < n_s$.

Consider a classically damped system with n degrees of freedom subjected to excitation $\mathbf{f}(t)$ as follows:

$$\mathbf{M}\ddot{\mathbf{x}}(t) + \mathbf{C}\dot{\mathbf{x}}(t) + \mathbf{K}\mathbf{x}(t) = \mathbf{f}(t), \tag{2}$$

where $\mathbf{x}(t)$ is the vector of displacements; $\mathbf{M}$, $\mathbf{C}$, $\mathbf{K}$ are mass, damping, and stiffness matrix, respectively.

The displacement $\mathbf{x}(t)$ can be represented in the form of a modal superposition of the vibration modes

$$\mathbf{x}(t) = \mathbf{\Phi}\mathbf{q}(t), \tag{3}$$

where $\mathbf{\Phi}$ is the mode shape matrix and $\mathbf{q}(t)$ is a column vector of modal coordinates.

Consider the similarity between (1) and (3), the modal coordinates $\mathbf{q}(t)$ and the mode shape matrix $\mathbf{\Phi}$ can be considered as the sources and the mixing matrix without the presence of noise, respectively.

The noise term $\mathbf{n}(t)$ in (1) is an additive noise assumed to be white. Therefore, its effect in the covariance function is zero at the time-lag τ_k different from zero. The covariance matrix $\mathbf{C}_\mathbf{x}(\tau_k)$ of vibration measurements $\mathbf{x}(t)$ evaluated at time-lag τ_k can be written as follows:

$$\mathbf{C}_\mathbf{x}(\tau_k) = E\{\mathbf{x}(t)\mathbf{x}^T(t+\tau_k)\} = \mathbf{\Phi}\mathbf{C}_\mathbf{q}(\tau_k)\mathbf{\Phi}^T. \tag{4}$$

The auto-covariance matrix $\mathbf{C}_\mathbf{q}(\tau_k)$ of modal coordinates (sources) at a time-lag τ_k is defined as

$$\mathbf{C}_\mathbf{q}(\tau_k) = E\{\mathbf{q}(t)\mathbf{q}^T(t+\tau_k)\} \tag{5}$$

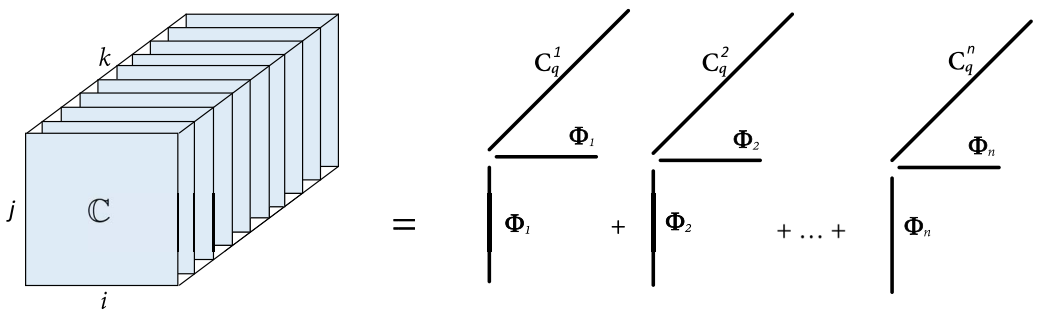

Figure 1. Geometric interpretation for PARAFAC decomposition [33].

and

$$C_{\mathbf{q}}^{ij}(\tau_k) = E\{q_i(t)q_j{}^T(t+\tau_k)\} = C_{\mathbf{q},k}^{ij}. \tag{6}$$

The modal coordinates are considered to be mutually uncorrelated $C_{\mathbf{q},k}^{ij} = 0 \ \forall i \neq j$.

In the case of a 2-DOF system, $\mathbf{x}(t) = [x_1(t), x_2(t)]^T$. The covariance matrix of the responses at a time-lag τ_k is represented as follows:

$$\begin{bmatrix} C_{\mathbf{x},k}^{11} & C_{\mathbf{x},k}^{12} \\ C_{\mathbf{x},k}^{21} & C_{\mathbf{x},k}^{22} \end{bmatrix} = \begin{bmatrix} \phi_{11} & \phi_{12} \\ \phi_{21} & \phi_{22} \end{bmatrix} \begin{bmatrix} C_{\mathbf{q},k}^{11} & 0 \\ 0 & C_{\mathbf{q},k}^{22} \end{bmatrix} \begin{bmatrix} \phi_{11} & \phi_{21} \\ \phi_{12} & \phi_{22} \end{bmatrix}, \tag{7}$$

where

$$C_{\mathbf{x},k}^{ij} = \phi_{i1}\phi_{j1}C_{\mathbf{q},k}^{11} + \phi_{i2}\phi_{j2}C_{\mathbf{q},k}^{22} = \sum_{r=1}^{2} \phi_{ir}\phi_{jr}C_{\mathbf{q},k}^{rr}. \tag{8}$$

For a general n-DOF system, the correlation between response signals at a time-lag τ_k can be represented by the following equation

$$C_{\mathbf{x},k}^{ij} = \sum_{r=1}^{n} \phi_{ir}\phi_{jr}C_{\mathbf{q},k}^{rr}. \tag{9}$$

Equation (9) can be treated by the joint approximate diagonalization technique employed in conventional second-order blind identification [4]. However, this method is only applicable to determined or overdetermined cases.

In order to deal with the underdetermined problem, Lathauwer and Castaing [29] introduced a simultaneous matrix diagonalization technique. A third-order tensor $\mathbb{C}$ constructed from the covariance matrices $\mathbf{C}_{\mathbf{x}}(\tau_k)$ can be treated by a PARAFAC decomposition [19]. This decomposition gives a mixing matrix and a matrix containing auto-covariance functions of modal coordinates.

The third-order tensor $\mathbb{C}$ can be decomposed to n rank-one tensors as follows:

$$\mathbb{C} = \sum_{r=1}^{n} \mathbf{\Phi}_r \circ \mathbf{\Phi}_r \circ \mathbf{C}_{\mathbf{q}}^r \Leftrightarrow C_{\mathbf{x},k}^{ij} = \sum_{r=1}^{n} \phi_{ir}\phi_{jr}C_{\mathbf{q},k}^{rr}, \tag{10}$$

where $\circ$ denotes the tensor outer product, and $\mathbf{\Phi}_r$ and $\mathbf{C}_{\mathbf{q}}^r$ is the rth column of $\mathbf{\Phi}$ and $\mathbf{C}_{\mathbf{q}}$, respectively.

As a consequence that tensor decomposition can be used to estimate mixing matrix $\mathbf{\Phi}$ and auto-covariance functions of modal coordinates in matrix $\mathbf{C}_{\mathbf{q}}$. Several algorithms have been developed to fit a PARAFAC model, which can be classified into three categories: alternating algorithms, derivative-based algorithms, and non-iterative algorithms [30–32]. The geometric interpretation for the above equation can be represented as shown in Figure 1 [33].

Unlike singular value decomposition used for matrix cases, PARAFAC decomposition offers an additional advantage: it gives a unique decomposition even if its rank order is greater than the smallest dimension of the tensor. This property of PARAFAC decomposition can be utilized

Table 1. Number of identifiable sources with the number of measurements [34]

Number of measurements n_x	2	3	4	5	6	7	8	9	10
Number of identifiable sources $n_{\max}$	2	4	6	10	15	20	26	33	41

to deal with underdetermined cases in BSS. Stegeman *et al.* [34] derived the uniqueness for the decomposition if the inequality equation between the number of measurements n_x and the number of latent sources n_s is satisfied:

$$\frac{n_s(n_s-1)}{2} \leq \frac{n_x(n_x-1)}{4}\left(\frac{n_x(n_x-1)}{2}+1\right) - \frac{n_x!}{(n_x-4)!4!}(n_x)_{(n_x\geq 4)}, \tag{11}$$

where

$$\begin{aligned}(n_x)_{\{n_x\geq 4\}} &= 0 \quad \text{if } n_x < 4\\ (n_x)_{\{n_x\geq 4\}} &= 1 \quad \text{if } n_x \geq 4.\end{aligned} \tag{12}$$

The relationship between the number of measurements and the maximal number of identifiable sources extracted using the PARAFAC decomposition is presented in Table 1.

2.2. *PARAFAC decomposition for modal analysis*

In BSS, the conventional kurtosis value can be used to distinguish modal responses and harmonic components. Besides, it has also been applied to a decay signal or the auto-covariance functions of modal responses [25, 35]. The kurtosis value of a zero-mean random variable x is defined as follows:

$$k = \frac{E\{x^4\}}{\left(E\{x^2\}\right)^2}, \tag{13}$$

where E is the expectation operator.

For sampled data with K samples, the expectation can be computed statistically as follows:

$$E\{x\} = \frac{1}{K}\sum_{k=0}^{K} x(k). \tag{14}$$

The existing PARAFAC decomposition can deal with underdetermined cases, and it also works well with the presence of harmonic excitations. In the case of harmonic excitations, kurtosis values of separated auto-covariance functions can be used to distinguish between the harmonic components and structural modes.

The main steps for modal analysis of the PARAFAC decomposition-based method can be presented as follows [25]:

- Step 1: Collect responses $\mathbf{x}(t)$.
- Step 2: Build a third-order tensor $\mathbb{C}$ from $\mathbf{C}_{\mathbf{x}}(\tau_k)$ using (4).
- Step 3: Perform rank $R = 2 : n_{\max}$ PARAFAC decomposition of the tensor $\mathbb{C}$ to obtain $\mathbf{C}_{\mathbf{q}}$ and mixing matrix $\mathbf{A}$. Estimate frequencies $\boldsymbol{f}$, damping ratios $\boldsymbol{\xi}$, and kurtosis values $\boldsymbol{\kappa}$ from $\mathbf{C}_{\mathbf{q}}$.
- Step 4: Build a stability diagram and calculate the average kurtosis values $\boldsymbol{k}$ at the estimated frequencies from the results in step 3.
- Step 5: Determine the number of active modes R_r, identify structural modes corresponding to the average kurtosis values $k \geq 3$, and harmonic components with $k < 3$ from the stability diagram.
- Step 6: Use the results of rank R_r PARAFAC decomposition and obtain modal parameters by eliminating harmonic components.

Table 2. Modal parameters of the numerical system are estimated with the proposed procedure under different kinds of excitations

Mode		1	2	3	4
Exact	f (Hz)	1.24	3.59	6.81	
	ξ (%)	1.31	0.50	0.34	
Initial displacement	f (Hz)	1.24	3.59	6.81	
	ξ (%)	1.29	0.51	0.38	
	Kurtosis	3.9	3.9	3.9	
	Nature	Struct	Struct	Struct	
Random noise	f (Hz)	1.24	3.59	6.81	
	ξ (%)	1.42	0.46	0.38	
	Kurtosis	4.0	3.9	4.0	
	Nature	Struct	Struct	Struct	
Presence of harmonics	f (Hz)	1.24	3.59	6.81	10.00
	ξ (%)	1.42	0.46	0.39	0.00
	Kurtosis	4.0	3.9	4.1	1.5
	Nature	Struct	Struct	Struct	*Harmonic*

The kurtosis values are estimated with $T_L^i = (40T_i)/(\xi_i)$.

In the method, the modal parameters can be extracted from the auto-covariance functions using the logarithmic decrement method in the time domain or the single-mode curve fitting method in the frequency domain.

2.3. *Illustration*

Consider an example of a 3-DOF mass–spring–damper system with the mass matrix **M** and the stiffness matrix **K**:

$$\mathbf{M} = \begin{bmatrix} 2 & 0 & 0 \\ 0 & 2 & 0 \\ 0 & 0 & 2 \end{bmatrix}; \quad \mathbf{K} = \begin{bmatrix} 200 & -360 & 120 \\ -360 & 2000 & -1300 \\ 120 & -1300 & 2600 \end{bmatrix}.$$

The damping matrix **C** is calculated through a proportional damping model $\mathbf{C} = 0.2\mathbf{M} + 0.00005\mathbf{K}$. The three exact natural frequencies and the three damping ratios are presented in Table 2.

The exact mode shape matrix is as follows:

$$\mathbf{\Phi} = \begin{bmatrix} 1.0000 & 1.0000 & 1.0000 \\ 0.2480 & -3.1550 & -6.8089 \\ 0.0816 & -2.6650 & 8.4359 \end{bmatrix}.$$

The system is subjected to an initial displacement $x_3(0) = 1$ with zero velocity. Responses are simulated for a duration of 50 s with a sampling rate of 200 Hz. The responses of 3 DOFs of the system are presented in Figure 2a. For the illustration, the covariance matrix is calculated with the total of 3000 time-lag points (15 s).

Following the steps of the existing PARAFAC decomposition-based method, a stability diagram is built with different rank R PARAFAC decomposition values ranging from 2 to 4 (corresponding to three signals).

Three average kurtosis values corresponding to three active modes in the diagram are shown in Figure 2b. The first two kurtosis values are less than 3. This means that these two first frequencies belong to harmonic excitation, according to step 5. This is an incorrect result since

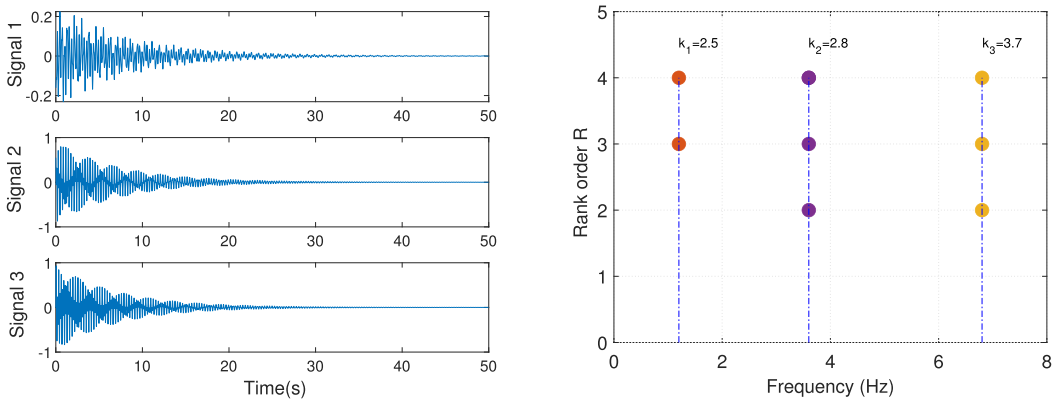

(a) Simulated signals **(b)** Stability diagram

Figure 2. Responses (left) and stability diagram obtained from the PARAFAC decomposition-based method (right).

these active modes are the structural modes in this example. This is due to the lengths of auto-covariance functions used for calculating kurtosis values are not sufficient. The existing PARAFAC decomposition-based method does not give a rule for choosing the length of the auto-covariance of the modal coordinates. To overcome this limitation and improve the existing method, the presented study proposes to select the length of the auto-covariance function while using the kurtosis value as a harmonic indicator.

3. Enhanced procedure for the PARAFAC decomposition-based method

The previous illustration shows that it is necessary to have an adequate length of auto-covariance function for accurate modal identification and an efficient distinction of structural modes and harmonic components. Since the decaying feature of the auto-covariance function [28] this decaying feature causes a variation of the auto-covariance function's statistical characteristic when the length of the auto-covariance function changes. Therefore, using kurtosis value as a harmonic indicator to distinguish between harmonic components and modal ones needs to consider the length of auto-covariance functions in PARAFAC decomposition-based methods in the OMA.

Kurtosis is well-known as a measure of the "tailedness" of the probability distribution that differs from the tails of a normal distribution. The modal coordinate has a normal distribution, and its kurtosis value equals 3. However, the decaying nature of the auto-covariance function makes the graph of its distribution being more narrow near the peak when the length of the auto-covariance functions is longer. It means that an auto-covariance function's kurtosis value becomes more than 3 if its length is longer than a certain value. The auto-covariance function of a harmonic component has a different feature than that of the modal coordinate's auto-covariance function. The kurtosis value of the auto-covariance function of a harmonic component is about 1.5 regardless of the length of its auto-covariance function.

3.1. *The effect of signal length on kurtosis value*

Under free vibration, the modal coordinate is the response of a single degree of freedom system that has a form as follow:

$$q_i(t) = A_i \mathrm{e}^{-2\xi\pi f_{ni} t} \sin(2\pi f_{di} t + \theta_i), \tag{15}$$

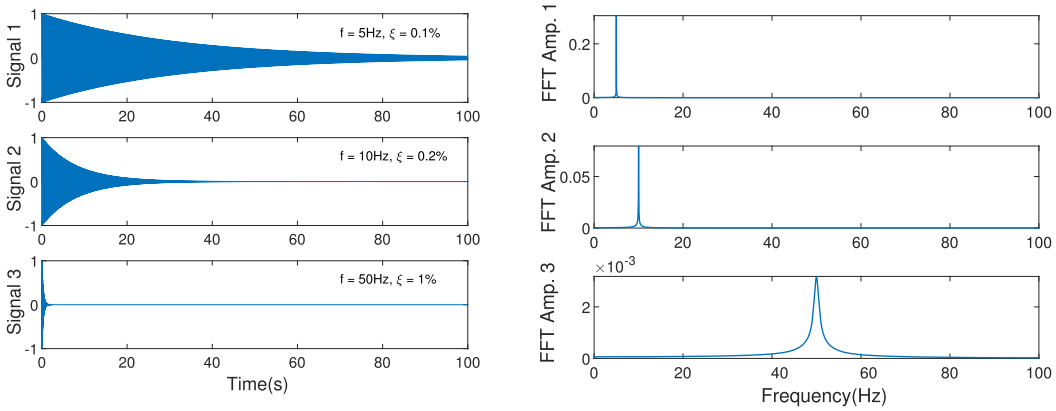

(a) Time domain

(b) Frequency domain

Figure 3. Three decaying signals.

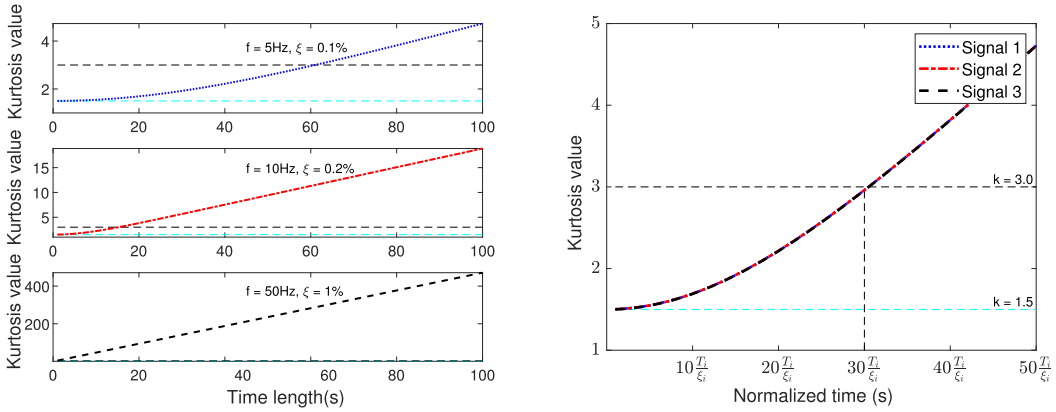

(a) **(b)**

Figure 4. Kurtosis with length variation of the decaying signals.

where f_{ni}, ξ_i, θ_i, and A_i are the natural frequency, the damping ratio, the phase, and the amplitude of the ith mode, respectively.

It was proven that the auto-covariance functions of responses have a decaying form [36] that is similar to those in (15). Thus, the auto-covariance functions can be treated as free vibration signals [37].

Decaying vibration signals with different natural frequencies and damping ratios are used to illustrate the influence of their length on kurtosis value. These signals last for 100 s, as seen in Figure 3.

It takes about 60 s for the kurtosis value to become equal to 3 for the first signal in Figure 4a. Less than this duration, its kurtosis values will be smaller than 3. However, less time is needed for the second and the third ones to their kurtosis values higher than 3.

Because of the decaying feature of these signals, not only the kurtosis value depends on the natural period, but it also depends on the signal's damping ratio. The kurtosis value of the auto-covariance function increases in the function of the period T_i and increases inversely in the damping ratio ξ_i function.

Therefore, this study considers the simultaneous influence of frequency and the damping coefficient on the kurtosis values. Figure 4b draws kurtosis values in a function of t_i with t_i defined in (16)

$$t_i = \frac{T_i}{\xi_i}, \tag{16}$$

where ξ is in percentage value, T_i is in second.

According to the numerical simulations that were carried out, one can conclude that the kurtosis reaches a value of 3 after approximately $30t_i$. Figure 4b shows that the kurtosis value reaches 3 in about $30t_i$ for the given example. Consequently, the auto-covariance functions' length should be at least $30t_i$, as presented in (17)

$$T_L^i > 30t_i = \frac{30T_i}{\xi_i}. \tag{17}$$

In the case of an auto-covariance function with a damping ratio identified smaller than 0.1%, the length of auto-covariance functions is selected by (18)

$$T_L^i > 30t_i = \frac{30T_i}{0.1}. \tag{18}$$

In this study, kurtosis values estimated with a time length $T_L^i = 40t_i$ is used for distinguishing between harmonic components and structural modes.

3.2. *The improvement procedure*

The above choice of the time length of the auto-covariance functions is integrated into the proposed procedure.

Here are the proposed steps for the PARAFAC decomposition-based method in OMA.

- Step 1: Collect responses $\mathbf{x}(t)$.
- Step 2: Build a third-order tensor $\mathbb{C}$ from $\mathbf{C_x}(\tau_k)$.
- Step 3: Perform rank $R = 2 : n_{\max}$ PARAFAC decomposition of the tensor $\mathbb{C}$ to obtain $\mathbf{C_q}$ and mixing matrix $\mathbf{A}$. Estimate frequencies $\mathbf{f}$ from $\mathbf{C_q}$.
- Step 4: Build a stability diagram and determine the number of active modes R_r.
- Step 5: Use the result of rank R_r PARAFAC decomposition. Recognize harmonic components with kurtosis value $k \approx 1.5$, or structural modes with $k \geq 3.0$ based on a choice of the time length of auto-covariance functions as follows:

$$\begin{cases} T_L^i > \dfrac{30T_i}{\xi_i} & \text{if } \xi_i \geq 0.1(\%) \\ T_L^i > \dfrac{30T_i}{0.1} & \text{if } \xi_i < 0.1(\%). \end{cases} \tag{19}$$

- Step 6: Obtain modal parameters by eliminating harmonic components.

4. Application

To validate the effectiveness of the proposed procedure, numerical and experimental tests were carried out for various excitation cases.

4.1. *Numerical simulations*

The numerical model used in Section 2.3 will be reutilized in this part. Modal identifications are performed for different cases like initial displacement, white noise excitation, and white noise accompanied by a harmonic excitation.

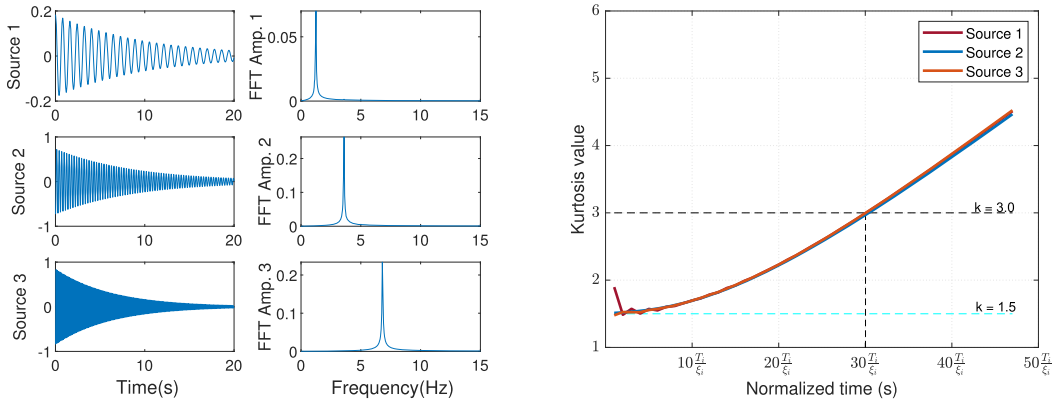

(a) Auto-covariance functions **(b)** Kurtosis vs. normalized time

Figure 5. Auto-covariance functions and kurtosis in the case of an initial displacement.

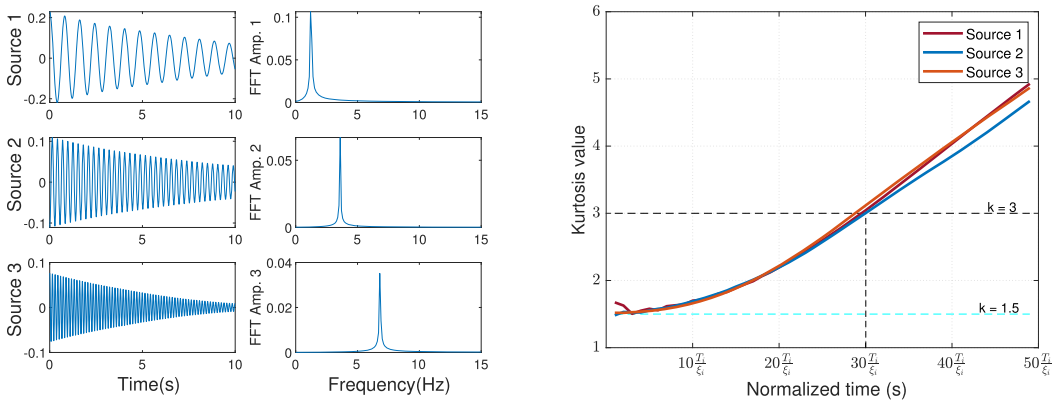

(a) Auto-covariance functions **(b)** Kurtosis vs. normalized time

Figure 6. Auto-covariance functions and kurtosis values in the case of random noise.

4.1.1. *The numerical system subjected to an initial displacement*

The proposed procedure was applied to the simulated responses used in Section 2.3. Three auto-covariance functions corresponding to rank $R = 3$ PARAFAC decomposition are shown in Figure 5a.

To illustrate the proposed procedure's effectiveness, the curves of kurtosis values corresponding to different lengths of the auto-covariance functions are presented in Figure 5b. One can realize that auto-covariance functions' lengths should be longer than $30 \times (T_i)/(\xi_i)$ to make kurtosis values higher than 3, as seen in Figure 5b. The identified modal parameters are the same as the exact ones, as seen in Table 2.

4.1.2. *The numerical system subjected to random noise excitation*

In this numerical test, random excitations were applied at all three DOFs of the system. The responses in the displacements of three DOFs were obtained by integrating the motion equation with the Runge–Kutta algorithm. The sampling rate was 200 Hz for a duration of 600 s.

The proposed procedure was then applied to this case. Three auto-covariance functions corresponding to rank $R = 3$ PARAFAC decomposition are shown in Figure 6a. The curves of

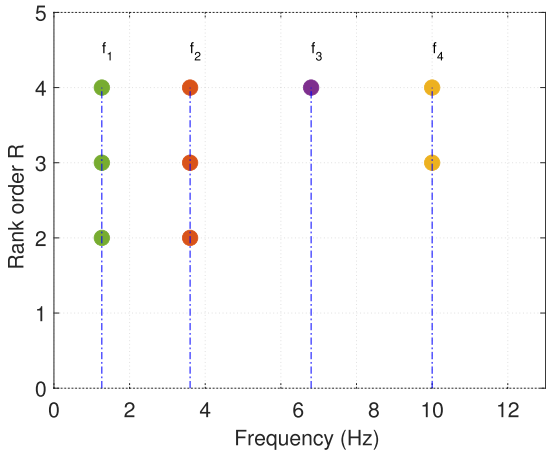

Figure 7. Stability diagram in the case of random noise accompanied by harmonic excitation.

kurtosis values corresponding to their different lengths are presented in Figure 6b. One can realize that auto-covariance functions' lengths should be longer than $30 \times (T_i)/(\xi_i)$ to make kurtosis higher than 3, as seen in Figure 6b. The identified modal parameters are close to the exact ones, as shown in Table 2.

4.1.3. *The numerical system subjected to random noise accompanied by a harmonic excitation*

In this numerical test, random excitations accompanied by a harmonic excitation were applied at all three DOFs of the system. The displacement of three DOFs was obtained by integrating the motion equation with the Runge–Kutta algorithm. The sampling rate was 200 Hz for a duration of 600 s.

The proposed procedure is now implemented to identify the modal parameters of the system. A stability diagram is built from different values of rank R PARAFAC decompositions, as seen in Figure 7. One can see that there are four active modes in this case.

The auto-covariance functions corresponding to rank $R = 4$ PARAFAC decomposition are shown in Figure 8a. The curves of kurtosis values corresponding to their different lengths are presented in Figure 8b. The figure shows that the first three components' kurtosis values (corresponding to source 1, source 2, and source 3) are higher than 3.0 when lengths of auto-covariance functions are longer than $30 \times (T_i)/(\xi_i)$. It means that these components belong to the structural modes. The last component (corresponding to source 4) with a kurtosis value of 1.5 corresponds to harmonic excitation. The MAC diagram shows a good correlation, as presented in Figure 9. The modal parameters are presented in Table 2, and they are close to the exact ones.

4.2. *Experimental tests*

To validate the proposed procedure's efficiency, a series of experimental tests were carried out, as shown in Figure 10. The tests were conducted for a steel cantilever beam with Young's modulus $E = 200{,}000$ MPa, and density $\rho = 7850$ kg/m^3. The cantilever beam of 0.8 m in length, 0.04 m in width, and 0.006 m in height were used for experimental tests under different excitation patterns. The responses of the cantilever beam were recorded at a sampling rate of 2048 Hz.

Initially, an analytical computation of the first five natural frequencies of the considered beam was performed. Its analytical frequencies are given in Table 3. To obtain a reference

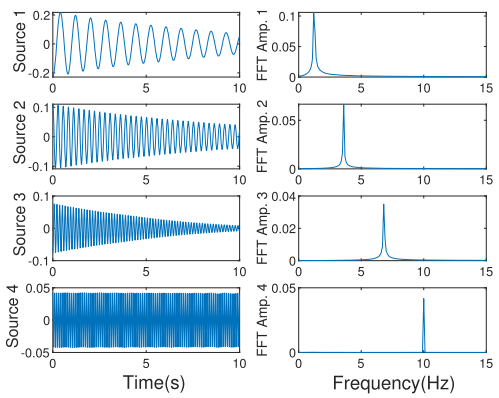

(a) Auto-covariance functions

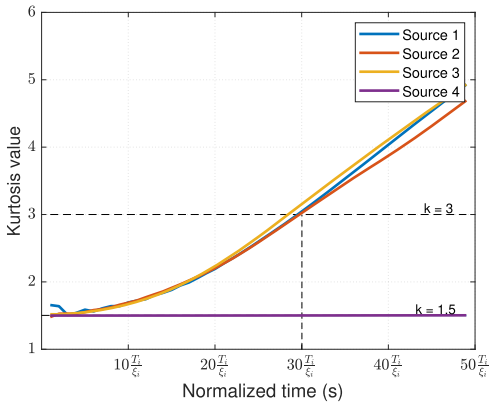

(b) Kurtosis vs. normalized time

Figure 8. Auto-covariance functions and kurtosis values in the case of random noise accompanied by harmonic excitation.

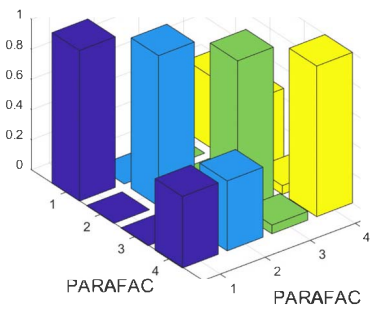

(a) Auto MAC before harmonic component removal

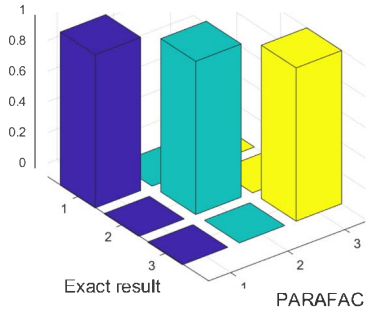

(b) Cross MAC after harmonic component removal

Figure 9. Mode shape comparison in the case of random noise accompanied by harmonic excitation.

Table 3. Modal parameters of the cantilever beam are estimated by the proposed procedure under different kinds of excitations, and kurtosis values are estimated with $T_L^i = (40T_i)/(\xi_i)$

Mode		1	2	3	4	5	6
Analytical	f (Hz)	7.64	47.90	134.14	262.85	433.52	
B&K software	f (Hz)	7.28	46.82	131.43	260.86	427.86	
	ξ (%)	1.23	0.28	0.45	0.66	0.17	
Gaussian noise	f (Hz)	7.32	46.73	131.23	260.44	428.00	
	ξ (%)	1.38	0.35	0.52	0.63	0.12	
	Kurtosis	3.8	3.9	3.8	3.9	4.0	
	Nature	Struct	Struct	Struct	Struct	Struct	
Presence of harmonics	f (Hz)	7.28	19.99	46.54	130.60	259.88	427.81
	ξ (%)	1.11	0.00	0.32	0.52	0.63	0.13
	Kurtosis	3.8	1.5	3.9	3.8	3.8	3.8
	Nature	Struct	*Harmonic*	Struct	Struct	Struct	Struct

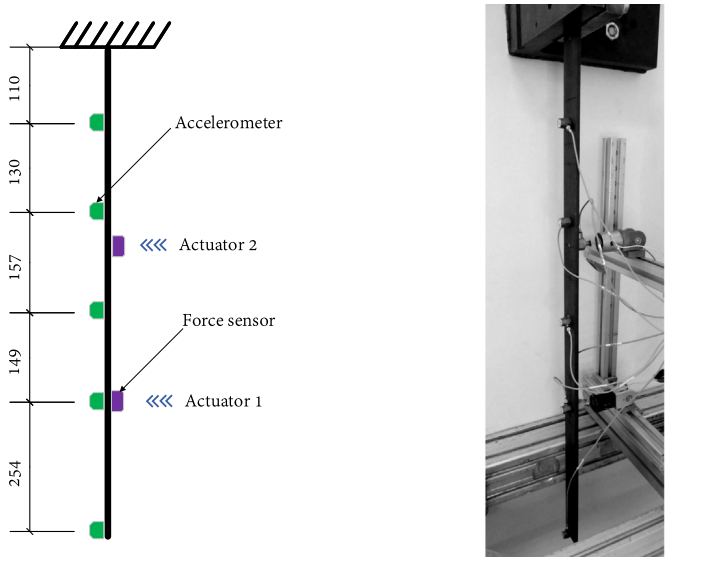

(a) Schematic model **(b)** Experimental setup

Figure 10. The cantilever beam and test point locations.

model, a classical experimental modal analysis was performed using a shaker at a location on the cantilever beam. The time responses were recorded using five B&K Type 4533-B-001 accelerometers mounted along the length of the cantilever beam. A B&K Type 8230-001 force transducer is also used to collect the input excitation, as shown in Figure 10. The commercial B&K Connect™ software acquires signals from the force sensor and the accelerators for input–output modal identification. The results of modal parameter identification are given in Table 3.

Two following experimental examples are considered to demonstrate the efficiency of the proposed procedure on actual measurements. The first example represents a determined case when the measurements equal the number of the structural modes. The second example illustrates an underdetermined problem where five sensors are used to separate six components: five structural modes and a harmonic component.

4.2.1. *The structure subjected to Gaussian noise excitation*

In this experiment, an actuator was used to create a band-limited Gaussian noise excitation with a 0–500 Hz pass-band.

The proposed procedure was then applied to the measurement data. A stability diagram is built with different rank R PARAFAC decomposition values ranging from 2 to 10 (corresponding to five measurement signals). The diagram shows that there are five active modes, as seen in Figure 11.

Five auto-covariance functions corresponding to rank $R = 5$ PARAFAC decomposition are shown in Figure 12a. The curves of kurtosis values estimated with different lengths of the auto-covariance functions are presented in Figure 12b. All kurtosis values of the auto-covariance functions are higher than 3.0 when their lengths are longer than $30 \times (T_i)/(\xi_i)$. Hence, it means that these active modes belong to the cantilever beam.

These results are compared to those identified by the software, as shown in Table 3. These estimated modal parameters match well with those identified by the software. The MAC shows

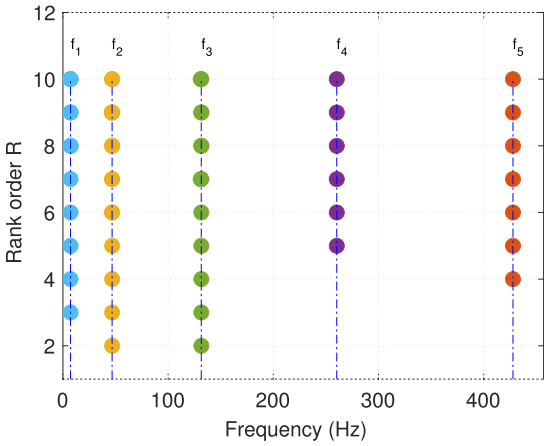

Figure 11. Stability diagram in the case of Gaussian noise excitation.

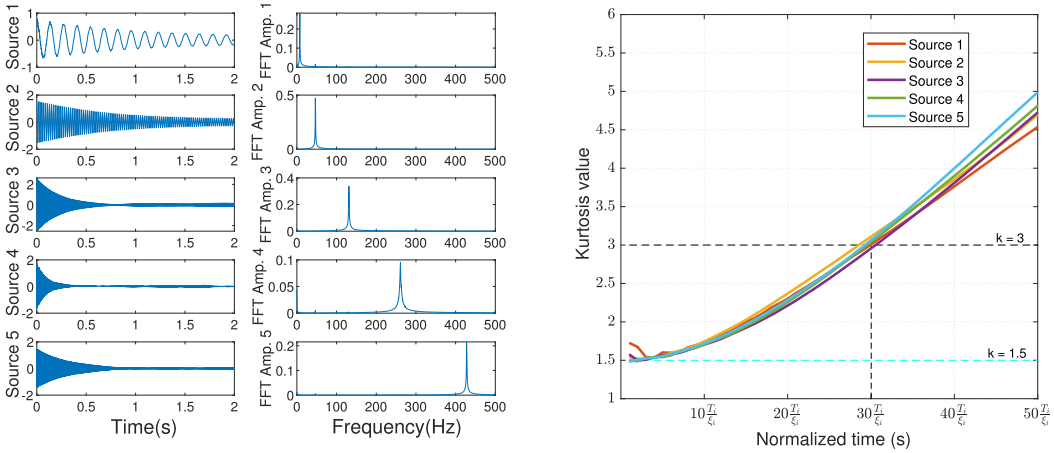

(a) Auto-covariance functions

(b) Kurtosis vs. normalized time

Figure 12. Auto-covariance functions and kurtosis values in the case of Gaussian noise excitation.

a good correlation between the structural mode shapes obtained by two different methods with the auto-correlation coefficients approximate 1, as seen in Figure 13.

4.2.2. *The structure subjected to Gaussian noise accompanied by a harmonic excitation*

In this experiment, in addition to a band-limited Gaussian noise excitation with a pass-band of 0 to 500 Hz, the cantilever beam was also subjected to a harmonic excitation at 20 Hz.

The proposed procedure was then applied to the measurement data. A stability diagram is built with different values of rank R PARAFAC decomposition ranging from 2 to 10. There are six active modes, as found in Figure 14. These six auto-covariance functions corresponding to rank $R = 6$ PARAFAC decomposition are shown in Figure 15a.

The curves of kurtosis values estimated with different lengths of the auto-covariance functions are presented in Figure 15b. The second separated component belongs to the harmonic excitation because this component's kurtosis values remain the same with the different lengths of its auto-covariance function. Its kurtosis value is approximately 1.5 at the time length of

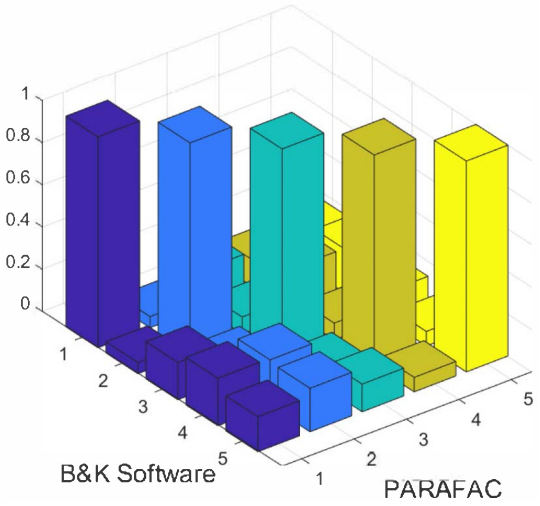

Figure 13. Mode shape comparison in the case of Gaussian noise excitation.

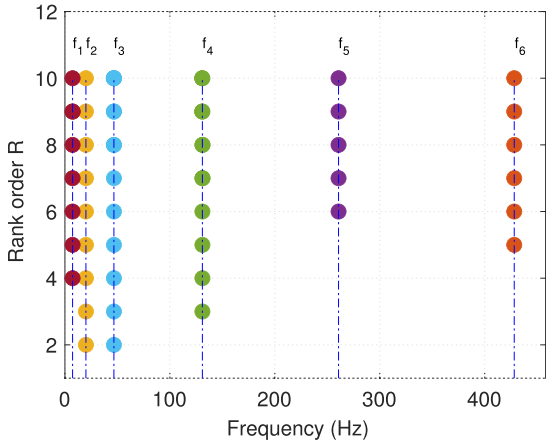

Figure 14. Stability diagram in the case of Gaussian noise accompanied by harmonic excitation.

$T_L^i = 40 \times (T_2)/(\xi_2)$. Other kurtosis values of the remaining auto-covariance functions are about 3.0 when their lengths are longer than a duration $T_L^i = 30 \times (T_i)/(\xi_i)$. The kurtosis values of these components with $T_L^i = 40 \times (T_i)/(\xi_i)$ are about 3.8, as given in Table 3. It means that these remaining active modes belong to the cantilever beam. The identified results are presented in Table 3. The MAC comparison is presented in Figure 16. It shows a good correlation.

5. Conclusions

The discussed method based on the PARAFAC decomposition has proven to be an effective tool for modal analysis in underdetermined cases. This method can also distinguish harmonic components and structural modes using kurtosis values estimated from the auto-covariance functions of modal coordinates. However, there was no explicit proposition for the choice of the length of the auto-covariance function, which led to an erroneous result when this length was insufficient.

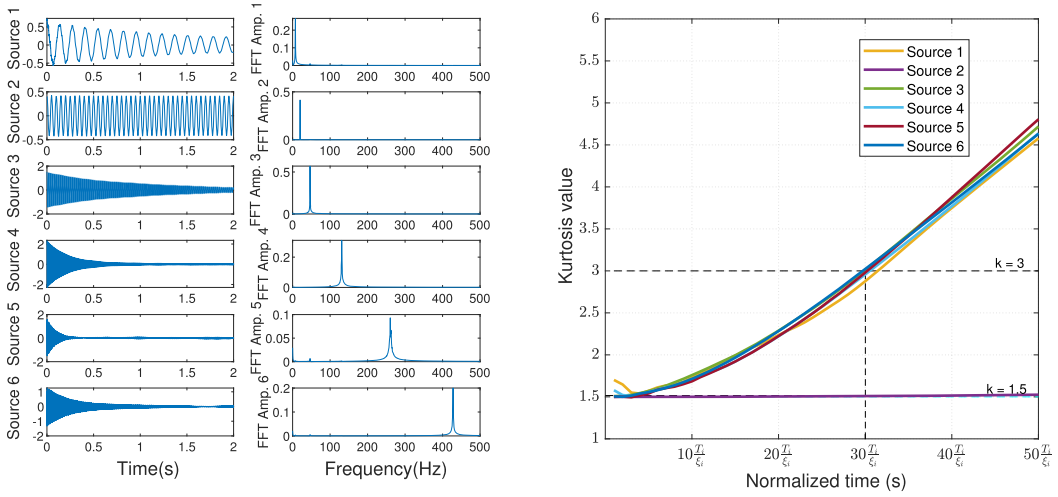

(a) Auto-covariance functions **(b)** Kurtosis vs. normalized time

Figure 15. Auto-covariance functions and kurtosis values in the case of Gaussian noise accompanied by harmonic excitation.

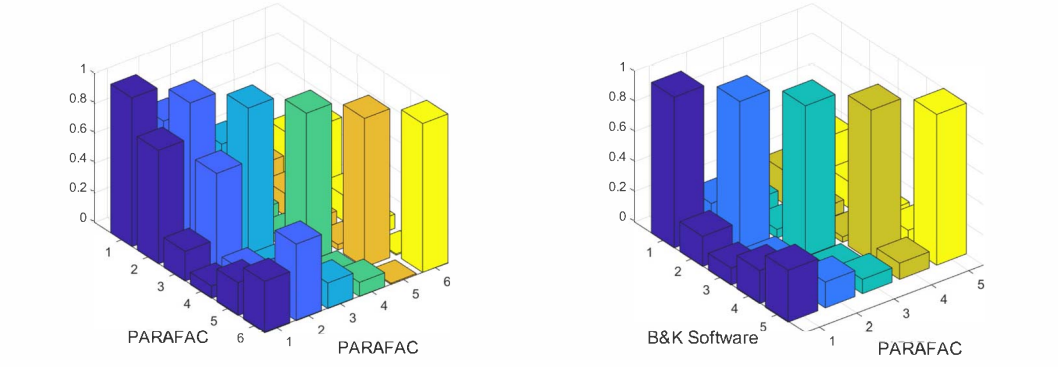

(a) Auto MAC before harmonic component removal **(b)** Cross MAC after harmonic component removal

Figure 16. Mode shape comparison in the case of Gaussian noise accompanied by harmonic excitation.

This study illustrates the dependence of the kurtosis values on the lengths of the auto-covariance functions. The presented work allows one to make a conclusion about this length based on the modal period T_i and the damping ratio ξ_i. It turned out that for the correct separation of structural modes and harmonic components, the length of these auto-covariance functions must be greater than $30T_i/\xi_i$.

The proposed procedure was applied to numerical examples and then confirmed by experimental tests. To estimate the kurtosis values, the length of the auto-covariance function was fixed at $40T_i/\xi_i (> (30T_i)/(\xi_i))$.

For the numerical simulation part, the responses from the 3-DOF system under (i) random excitation and (ii) random excitation accompanied by harmonic excitation were processed in accordance with the proposed procedure. The revealed modal parameters are very close to the exact ones when the calculated values of kurtosis for the structural modes is ($k = 3.9$–4.1) and for the harmonic component is $k \approx 1.5$).

In the experimental test section, the proposed procedure is applied to the responses of the cantilever beam under (i) random excitation and (ii) random excitation mixed with harmonic excitation. The identified modal parameters by the proposed method are in good agreement with the reference ones obtained using the B&K software. In the presence of harmonic excitation, the calculated kurtosis values for the structural modes are close to 4.0, and for the harmonic component is approximate 1.5.

These validation tests confirm the effectiveness of the proposed method for use in OMA for underdetermined cases in general and cases with the presence of harmonic excitations, in particular.

Acknowledgment

The first author gratefully acknowledges the French Government's funding through the scholarship to undertake this work.

References

[1] L. Zhang, R. Brincker, P. Andersen, "An overview of operational modal analysis: major development and issues", in *Proceedings of the 1st International Operational Modal Analysis* (Copenhagen), Aalborg Universitet, 2005.

[2] J.-F. Cardoso, "Blind signal separation: statistical principles", *Proc. IEEE* **86** (1998), p. 2009-2025.

[3] P. Comon, "Independent component analysis, a new concept?", *Signal Process.* **36** (1994), no. 3, p. 287-314.

[4] A. Belouchrani, K. Abed-Meraim, J.-F. Cardoso, E. Moulines, "A blind source separation technique using second-order statistics", *IEEE Trans. Signal Process.* **45** (1997), p. 434-444.

[5] A. Hyvärinen, E. Oja, "Independent component analysis: algorithms and applications", *Neural Netw.* **13** (2000), no. 4, p. 411-430.

[6] P. P. Pokharel, U. Ozertem, D. Erdogmus, J. C. Principe, "Recursive complex BSS via generalized eigendecomposition and application in image rejection for BPSK", *Signal Process.* **88** (2008), no. 6, p. 1368-1381.

[7] S. Xie, L. Yang, J.-M. Yang, G. Zhou, Y. Xiang, "Time-frequency approach to underdetermined blind source separation", *IEEE Trans. Neural Netw. Learn. Syst.* **23** (2012), no. 2, p. 306-316.

[8] P. Bofill, M. Zibulevsky, "Underdetermined blind source separation using sparse representations", *Signal Process.* **81** (2001), no. 11, p. 2353-2362.

[9] R. Castiglione, J. Antoni, L. Garibaldi, "Separation and identification of structural modes in largely underdetermined scenarios using frequency banding", *J. Sound Vib.* **414** (2018), p. 192-217.

[10] A. Sadhu, S. Narasimhan, J. Antoni, "A review of output-only structural mode identification literature employing blind source separation methods", *Mech. Syst. Signal Process.* **94** (2017), p. 415-431.

[11] T. Lago, "The difference between harmonics and stochastic narrow band responses", in *Presentation at the SVIBS Symposium* (Stockholm), Structural Vibration Solution, 1997.

[12] V. Gagnol, T.-P. Le, P. Ray, "Modal identification of spindle-tool unit in high-speed machining", *Mech. Syst. Signal Process.* **25** (2011), p. 2388-2398.

[13] N.-J. Jacobsen, P. Andersen, R. Brincker, "Eliminating the influence of harmonic components in operational modal analysis", in *The International Modal Analysis Conference IMAC-XXIV* (Orlando, USA), Society for Experimental Mechanics, 2007.

[14] J. Antoni, "The spectral kurtosis: a useful tool for characterising non-stationary signals", *Mech. Syst. Signal Process.* **20** (2006), p. 282-307.

[15] J. Antoni, "Blind separation of vibration components: Principles and demonstrations", *Mech. Syst. Signal Process.* **19** (2005), p. 1166-1180.

[16] C. Rainieri, G. Fabbrocino, G. Manfredi, M. Dolce, "Robust output-only modal identification and monitoring of buildings in the presence of dynamic interactions for rapid post-earthquake emergency management", *Eng. Struct.* **34** (2012), p. 436-446.

[17] R. Brincker, P. Andersen, N. B. Møller, "An indicator for separation of structural and harmonic modes in output-only modal testing", in *Proceedings of SPIE—The International Society for Optical Engineering* (Madrid, Spain), vol. 2, Aalborg University, 2000.

[18] R. Allemang, "The modal assurance criterion—twenty years of use and abuse", *Sound Vib.* **37** (2003), p. 14-21.

[19] R. A. Harshman, *Foundations of the PARAFAC Procedure: Models and Conditions for an Explanatory Multi-modal Factor Analysis*, University of California, Los Angeles, 1970.

[20] J. Antoni, S. Chauhan, "An alternating least squares (ALS) based blind source separation algorithm for operational modal analysis", in *Proceedings of the 29th IMAC, A Conference and Exposition on Structural Dynamics* (New York, USA), Conference Proceedings of the Society for Experimental Mechanics Series, vol. 3, Springer, 2011, https://doi.org/10.1007/978-1-4419-9299-4_15.

[21] S. I. McNeill, "Extending blind modal identification to the underdetermined case for ambient vibration", in *ASME 2012 International Mechanical Engineering Congress and Exposition* (Texas, USA), The American Society of Mechanical Engineers, 2012, https://doi.org/10.1115/IMECE2012-93140.

[22] F. Abazarsa, S. F. Ghahari, F. Nateghi, E. Taciroglu, "Response-only modal identification of structures using limited sensors", *Struct. Control Health Monit.* **20** (2013), p. 987-1006.

[23] F. Abazarsa, F. Nateghi, S. F. Ghahari, E. Taciroglu, "Blind modal identification of non-classically damped systems from free or ambient vibration records", *Earthq. Spectra* **29** (2013), p. 1137-1157.

[24] F. Abazarsa, F. Nateghi, S. F. Ghahari, E. Taciroglu, "Extended blind modal identification technique for nonstationary excitations and its verification and validation", *J. Eng. Mech.* **142** (2015), p. 1-19.

[25] A. Sadhu, A. Goldack, S. Narasimhan, "Ambient modal identification using multi-rank parallel factor decomposition", *Struct. Control Health Monit.* **22** (2015), p. 595-614.

[26] A. Sadhu, B. Hazra, S. Narasimhan, "Decentralized modal identification of structures using parallel factor decomposition and sparse blind source separation", *Mech. Syst. Signal Process.* **41** (2013), p. 396-419.

[27] P. Friesen, A. Sadhu, "Performance of tensor decomposition-based modal identification under nonstationary vibration", *Smart Mater. Struct.* **26** (2017), p. 1-19.

[28] D. E. Newland, *An Introduction to Random Vibrations and Spectral Analysis*, Longman Group Limited, London, 1975.

[29] L. D. Lathauwer, J. Castaing, "Blind identification of underdetermined mixtures by simultaneous matrix diagonalization", *IEEE Trans. Signal Process.* **56** (2008), p. 1096-1105.

[30] G. Tomasi, R. Bro, "A comparison of algorithms for fitting the PARAFAC model", *Comput. Statist. Data Anal.* **50** (2006), no. 7, p. 1700-1734.

[31] P. Comon, X. Luciani, A. de Almeida, "Tensor decompositions, alternating least squares and other tales", *J. Chemom.* **23** (2009), p. 393-405.

[32] L. Lathauwer, D. Nion, "Decompositions of a higher-order tensor in block terms—Part III: alternating least squares algorithms", *SIAM J. Matrix Anal. Appl.* **30** (2008), p. 1067-1083.

[33] A. Smilde, R. Bro, P. Geladi, *Multi Way Analysis—Applications in Chemical Sciences*, John Wiley Sons, Ltd, England, 2004.

[34] A. Stegeman, J. M. F. T. Berge, L. D. Lathauwer, "Sufficient conditions for uniqueness in Candecomp/Parafac and Indscal with random component matrices", *Struct. Control Health Monit.* **71** (2006), p. 219-229.

[35] S. McNeill, D. Zimmerman, "Relating independent components to free-vibration modal responses", *Shock Vib.* **17** (2010), p. 161-170.

[36] G. James, T. Carne, J. Laufer, "The natural excitation technique (NExT) for modal parameter extraction from operating structures", *J. Anal. Exp. Modal Anal.* **10** (1995), p. 260-277.

[37] B. Hazra, A. Roffel, S. Narasimhan, M. Pandey, "Modified cross-correlation method for the blind identification of structures", *J. Eng. Mech.* **136** (2010), p. 889-897.

3 Operational modal analysis in the frequency domain

Chapter abstract

The work presented in Chapter 2 to improve the existing modal analysis method based on the PARAFAC decomposition led to a better understanding of the performance of this mathematical tool, its capabilities and limitations for applications in the time domain. It has been noted that due to the nature of this decomposition, the number of identifiable modes is higher then the number of measured signals. Moreover, the PARAFAC decomposition in time-domain leads to covariance matrices of real values when its frequency-domain decomposition yields the PSD functions of the complex values. And it was shown in Table 1.1 that the PARAFAC decomposition in the frequency domain has more identifiable modes than in the time domain. This fact led to the idea of using the PARAFAC decomposition in the frequency domain for modal analysis to reveal complex modes, which is difficult to achieve in the time domain. To the best of authors' knowledge, there are no studies in the literature of modal identification method based on PARAFAC decomposition in the frequency domain.

This chapter presents the development of a novel method for modal identification based on PARAFAC decomposition in the frequency domain. Using the PARAFAC decomposition, a third-order tensor constructed from Power Spectral Density (PSD) of responses is decomposed into rank-1 tensors which can be structural modes or harmonic components. The auto-PSD function of each rank-1 tensor is then used to identify modal parameters, while spectral kurtosis values are used for the distinction of structural modes and harmonics. Detailed analytic development of the method is presented together with its practical step-by-step application procedure. The performance of the proposed method has been investigated for proportional/non-proportional damping, closely spaced modes, underdetermined cases and in the presence of harmonic excitations.

3.1 A novel method for modal analysis in the frequency domain (Article 2)

A novel method for modal analysis using parallel factor decomposition in the frequency domain

Abstract

Current study presents a new method for output only modal identification in the frequency domain. This work was inspired by the challenges of modern modal analysis when it comes to underdetermined problems, when the number of measurements is less than the number of active modes, or there are harmonic excitations. The proposed method based on parallel factor (PARAFAC) decomposition technique, which is used to decompose a third-order tensor constructed from power spectral density (PSD) matrices of response signals. This decomposition leads directly to mode shapes and auto-PSD matrices of the modal coordinates. Natural frequencies and damping ratios are then estimated from the auto-PSD functions. And the spectral kurtosis is used to distinguish disturbance modes from structural ones. Numerical simulation and experimental tests validate the effectiveness of the proposed method when applied to determined and underdetermined problems in modal analysis. It shows correct results in identifying mechanical systems with normal modes, with complex modes, closely-spaced modes and for cases with the presence of harmonic excitations.

Keywords: Modal identification, PARAFAC decomposition, frequency domain, power spectral density, harmonic excitation

1. Introduction

Operational modal analysis (OMA) aims to identify modal characteristics using only vibration responses of structures under ambient excitation [1, 2]. It offers many advantages for modal identification of mechanical systems as it does not require to measure external excitation and allows to estimate modal parameters under actual boundary condition.

Various modal identification methods have been developed for mechanical systems in OMA. They perform identification either in the time domain [3–6] or in the frequency domain [7, 8]. In general, these identification methods are aimed at information physically related to structures from correlation functions or spectral densities. Time domain identification methods extract this physical information from the correlation functions, while frequency domain identification methods extract it from the spectral density functions [9].

Blind source separation (BSS) has attracted considerable interest over the last decade in OMA as a non-parametric alternative to modal characteristic identification from output-only measurements [10]. The main purpose of the BSS is to identify sources from simultaneous recordings [11]. Many identification methods have been proposed. For example, one of the first methods used in BSS was called independent component analysis (ICA) [12–14], which assumed that the sources were statistically independent. Among various other techniques, there is a technique called second order blind identification (SOBI) [15], which uses a significant temporal structure of sources. However, these methods require a number of sources equal to or less than the number of measurements, which called a determined or an overdetermined problem. This limited the use of BSS methods for underdetermined problems. Therefore, various other BSS methods and variations have been proposed in the literature to deal with underdetermined cases. The state of the art in BSS for operational modal analysis has been comprehensively reviewed and discussed in [16]. Two main approaches seem to be the most efficient for handling underdetermined cases: the first uses the sparsity of sources, and the second involves tensor decomposition.

The idea of employing sparsity for underdetermined problems have been described in [17]. Sparsity means having a representation domain in which sources tend to occupy different regions of space with reduced overlap. Sparsity can be achieved in the frequency or time-frequency domain using Fourier transform [18], short-time Fourier transform [19], wavelet packet transform [20], etc when they are not directly achievable in the time domain. And then, mixing matrix is estimated through clustering algorithms, such as K-means clustering, hierarchical clustering, fuzzy C-mean clustering [21–23], etc. From the estimated mode shapes, the modal coordinates can be recovered by methods such as the least square method [24], l_1-norm [23]. However, the accuracy of the estimated mode shape of these methods depends on the clustering technique, and the recovered modal coordinates are less precise in the case of poor clustering performance.

In the second approach, tensor decomposition based methods provide a relatively straightforward solution to underdetermined BSS problems. It does not require statistical independence or the sparsity of sources. A parallel factor (PARAFAC) decomposition of a tensor was introduced in [25, 26]. This is a multi-linear algebra tool. Several algorithms have been developed to adapt to the PARAFAC model, which can be classified into three categories: alternating algorithms, derivative based algorithms and non-iterative algorithms [27–29]. The first algorithm is more popular because it is easier to implement, ensuring convergence. Modal identification methods based on the PARAFAC decomposition have been studied to solve undetermined cases, even in the presence of harmonic excitations. In the time domain, covariance matrices with several time lags are used to construct a third-order tensor. Then the tensor is decomposed into a mixing matrix and an auto-covariance matrix of latent sources [30–38]. Besides, Ta et al. [30] defined a

minimum length of auto-covariance functions to distinguish harmonic components for PARAFAC decomposition-based methods in the time domain.

To the best of our knowledge, there have been no studies using PARAFAC decomposition in the frequency domain for modal identification.

This present work employs the PARAFAC decomposition technique in the frequency domain. First, the third-order tensor is constructed from PSD matrices of response signals. Next, perform a decomposition to obtain mode shapes and an auto-PSD matrix of modal coordinates in the frequency domain. Then, the frequencies and damping ratios can be determined from the estimated auto-PSD functions of the modal coordinates.

The effectiveness of the proposed method is validated by numerical examples followed by experimental tests for determined and underdetermined cases. The performance of the method is investigated with proportional damping and non-proportional damping. The ability to cope with the presence of harmonic excitation is verified, which is known to be more challenging in BSS. Furthermore, tests are used to confirm the ability of the present method to deal with closely spaced modes.

The rest of the article is organized as follows. Section 2 presents the problem PARAFAC decomposition application in frequency domain. A procedure for modal analysis is revealed. Section 3 presents numerical and experimental tests that were carried out to confirm the effectiveness of the proposed method. Finally, Section 4 summarizes the results.

2. PARAFAC decomposition-based modal identification

2.1. Tensor and PARAFAC decomposition

Tensor representation is an adequate form to express data in many situations for instance, scores of air indicators on different time points and locations, correlation functions of responses from different channels and different time lags and so on. The use of tensor representation allows moreover to consider data as multidimensional that can be processed using multi-linear algebra tools, more efficient and powerful than linear algebra ones (e.g. principal component analysis) [39].

A complex-valued vector $\mathbf{t} = t_i \in \mathbb{C}^{n_1}$ is a first-order tensor while a complex-valued matrix $\mathbf{T} = t_{ij} \in \mathbb{C}^{n_1 \times n_2}$ is a second-order tensor. In general, a complex-valued pth-order tensor is written as $\mathbb{T} = t_{ij\ldots p} \in \mathbb{C}^{n_1 \times n_2 \times \ldots \times n_p}$ where $n_1 \times n_2 \times \ldots \times n_p$ are respectively the size of p dimensions indiced by $i\, j \ldots p$.

In this work, the focus is limited to third order tensors noted by $\mathbb{T} = t_{ijk} \in \mathbb{C}^{n_1 \times n_2 \times n_3}$. An illustration of a third order tensor as a parallelepiped is given in Figure 1. When one index is fixed, a third order tensor is reduced to matrices also called slices and when two indices are fixed, it reduced to vectors also called fibers. *Matricization* is the way to transform

a tensor to matrices and and then use efficient tools (singular value decomposition for instance) devoted to matrices for data processing.

Using parallel factor decomposition (PARAFAC) a third order tensor can be decomposed into a sum of outer products of triple vectors as follows [40]:

$$\mathbb{T} = \sum_{r=1}^{R} \mathbf{a}_r \circ \mathbf{b}_r \circ \mathbf{c}_r = \sum_{r=1}^{R} \mathbb{T}_r \Leftrightarrow t_{ijk} = \sum_{r=1}^{R} a_{ir} b_{jr} c_{kr} \tag{1}$$

where $\circ$ denotes the tensor outer product and R is the number of rank-1 tensor $\mathbb{T}_r$ present in $\mathbb{T}$ of rank R. This is termed as a trilinear model of $\mathbb{T}$, $\mathbb{T} = [[\mathbf{A}, \mathbf{B}, \mathbf{C}]]$ with the matrices $\mathbf{A} = [\mathbf{a}_1, \mathbf{a}_2, ..., \mathbf{a}_R]$, $\mathbf{B} = [\mathbf{b}_1, \mathbf{b}_2, ..., \mathbf{b}_R]$, and $\mathbf{C} = [\mathbf{c}_1, \mathbf{c}_2, ..., \mathbf{c}_R]$.

The factor matrices $\mathbf{A}, \mathbf{B}, \mathbf{C}$ can be obtained by optimizing the following cost function:

$$\min_{\mathbf{A},\mathbf{B},\mathbf{C}} \left\| \mathbb{T} - \sum_{r=1}^{R} \mathbf{a}_r \circ \mathbf{b}_r \circ \mathbf{c}_r \right\|^2 \tag{2}$$

The fundamental technique of PARAFAC was introduced in reference [25] and also called canonical decomposition [26]. Several algorithms have been developed to fit a PARAFAC model, which can be classified into three categories: alternating least square algorithm, derivative based algorithms, and non-iterative algorithms [27, 28]. In this work, the alternating least square algorithm is applied because of its simpler implementation, and guaranteed convergence [31, 40, 41].

A unique PARAFAC decomposition is obtained if the Kruskal condition [42] is satisfied:

$$k_{\mathbf{A}} + k_{\mathbf{B}} + k_{\mathbf{C}} \geq 2R + 2 \tag{3}$$

where $k_{\mathbf{A}}, k_{\mathbf{B}}$ and $k_{\mathbf{C}}$ are $k-$rank of the matrices $\mathbf{A}, \mathbf{B}$ and $\mathbf{C}$ respectively, where $k-$rank is defined as maximum number k such that every set of k columns of the matrix is linearly independent.

2.2. Formulation for the PARAFAC decomposition in the frequency domain

The motion equation of a n-DOF linear system subjected to external forces can be written as follows:

$$\mathbf{M}\ddot{\mathbf{x}}(t) + \mathbf{C}\dot{\mathbf{x}}(t) + \mathbf{K}\mathbf{x}(t) = \mathbf{f}(t) \tag{4}$$

where $\mathbf{M}$, $\mathbf{C}$, and $\mathbf{K}$ denote the $n \times n$ mass, damping, and stiffness matrices, respectively. $\mathbf{f}(t)$ is the $n \times 1$ vector of applied forces, and $\mathbf{x}(t)$ is the $n \times 1$ vector of displacements.

The displacement $\mathbf{x}(t)$ can be represented in the form of a modal superposition of the vibration modes:

$$\mathbf{x}(t) = \mathbf{\Phi}\mathbf{q}(t) = \sum_{r=1}^{n} \boldsymbol{\phi}_r q_r(t) \tag{5}$$

where $\mathbf{\Phi}$ is the $n \times n$ mode shape matrix and $\mathbf{q}(t)$ is a $n \times 1$ column vector of modal coordinates.

The correlation function (CF) matrix $\mathbf{C}^{\mathbf{x}}(\tau)$ of vibration measurements $\mathbf{x}(t)$ evaluated at time-lag τ can be written as follows:

$$\mathbf{C}^{\mathbf{x}}(\tau) = E\left\{\mathbf{x}(t)\mathbf{x}^T(t+\tau)\right\} = \mathbf{\Phi}\mathbf{C}^{\mathbf{q}}(\tau)\mathbf{\Phi}^T \tag{6}$$

where the $n \times n$ CF matrix $\mathbf{C}^{\mathbf{q}}(\tau)$ of modal coordinates is expressed as follows:

$$\mathbf{C}^{\mathbf{q}}(\tau) = E\left\{\mathbf{q}(t)\mathbf{q}^T(t+\tau)\right\} \tag{7}$$

with

$$C_{ij}^{\mathbf{q}}(\tau) = E\left\{q_i(t){q_j}^T(t+\tau)\right\} \tag{8}$$

Fourier transform of both sides of Eq. (6) gives corresponding PSD matrices:

$$\mathbf{G}^{\mathbf{x}}(f) = \mathbf{\Phi}\mathbf{G}^{\mathbf{q}}(f)\mathbf{\Phi}^H \tag{9}$$

In Eq. (9), the values of the cross-correlation functions of the measurements are complex values, while the values of the autocorrelation part are positive real values. In operational conditions, excitations are assumed to be white noise and uncorrelated processes. $\mathbf{G}^{\mathbf{q}}(f)$ is thus diagonal and it leads to the following approximation:

$$\mathbf{G}^{\mathbf{x}}(f) = \mathbf{\Phi}\mathbf{G}^{\mathbf{q}}(f)\mathbf{\Phi}^H \approx \sum_{r=1}^{n} \boldsymbol{\phi}_r \boldsymbol{\phi}_r^H g_{rr}^{\mathbf{q}}(f) \tag{10}$$

where $\mathbf{G}^{\mathbf{x}}(f)$ and $g_{rr}^{\mathbf{q}}(f)$ are respectively the $n \times n$ PSD matrix of the responses and the r^{th} diagonal component of the $n \times n$ auto-PSD matrix of the modal coordinates $\mathbf{G}^{\mathbf{q}}(f)$.

The frequency domain decomposition (FDD) technique was introduced by Brincker et al. [7] that is based on the singular value decomposition (SVD) of the spectral density matrices $\mathbf{G}^{\mathbf{x}}(f)$ in Eq. (10) evaluated in discretized frequencies f_k. For each frequency f_k, the processing is independent and it gives the corresponding singular values and singular vectors. The abscissa of the peaks in the first singular values in function of frequencies f_k indicate natural frequencies and associated singular vectors at these frequencies gives

estimates of mode shapes. The enhanced frequency domain decomposition (EFDD) [43] proposed to identify the modal damping using a piece of singular values around a mode. The selection of the piece is based on the similarity of singular vectors of adjacent frequencies using MAC values.

In the FDD method, at a frequency neighborhood, the estimated mode shapes given by SVD are orthogonal and the number of identified modes is limited by the number of sensors (i.e. the smallest dimension of the PSD matrix). Moreover, the PSD matrices are considered separately and the relationship between them are not clearly exploited.

In contrast to the FDD method based on SVD, we propose to consider the PSD as a third-order tensor $\mathbb{G}$ and to apply the PARAFAC decomposition to identify modal parameters. The tensor $\mathbb{G}$ is obtained in stacking $\mathbf{G}^{\mathbf{x}}(f)$ sampled in n_f frequencies. The dimension of $\mathbb{G}$ is thus $n \times n \times n_f$ or in practice $n_x \times n_x \times n_f$ where n_x is the number of measurement channels. Figure 1 gives an illustration of $\mathbb{G}$ with indices: $i = 1 \dots n_x$, $j = 1 \dots n_x$ and $k = 1 \dots n_f$.

Equation (10) can be rewritten for every frequency f_k

$$\mathbf{G}^{\mathbf{x}}(f_k) = \sum_{r=1}^{n} \boldsymbol{\phi}_r \boldsymbol{\phi}_r^H g_{rr}^{\mathbf{q}}(f_k) \tag{11}$$

and the (i, j, k) component of the third-order tensor $\mathbb{G}$ of responses $\mathbf{x}(t)$ is thus computed by

$$g_{ij}^{\mathbf{x}}(f_k) = g_{ijk}^{\mathbf{x}} = \sum_{r=1}^{n} \phi_{ir} \phi_{jr}^* g_r^{\mathbf{q}}(f_k) = \sum_{r=1}^{n} \phi_{ir} \phi_{jr}^* g_{rk}^{\mathbf{q}} \tag{12}$$

By comparison between Equation (12) and Equation (1), it can be deduced

$$g_{ijk}^{\mathbf{x}} = \sum_{r=1}^{n} \phi_{ir} \phi_{jr}^* g_{rk}^{\mathbf{q}} \Leftrightarrow \mathbb{G}^{\mathbf{x}} = \sum_{r=1}^{n} \mathbb{G}_r{}^{\mathbf{x}} = \sum_{r=1}^{n} \boldsymbol{\phi}_r \circ \boldsymbol{\phi}_r^* \circ \boldsymbol{g}_r{}^{\mathbf{q}} \tag{13}$$

Recall that $\boldsymbol{\phi}_r$ is the r^{th} column vector of mode shape matrix $\boldsymbol{\Phi}$ and $\mathbf{g}_r^{\mathbf{q}}$ is the vector evaluated at n_f frequencies of the r^{th} component auto-PSD modal coordinate. The Equation (13) gives the foundation of our proposed method. By using the PARAFAC decomposition of $\mathbb{G}^{\mathbf{x}}$ under the condition of unique decomposition as given in Equation(3), the mode shapes are estimated from $\boldsymbol{\phi}_r$ while natural frequencies and damping ratios are deduced from $\mathbf{g}_r^{\mathbf{q}}$.

It is worth to note that the PARAFAC decomposition offers a unique decomposition even if its rank order is greater than the smallest dimension of the tensor. Therefore, this decomposition can be utilized to handle underdetermined cases. For the complex form of

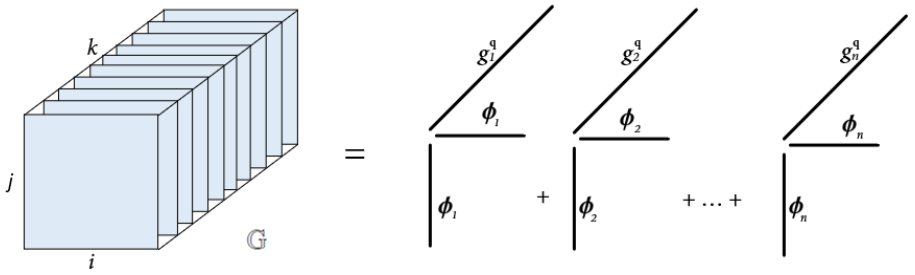

Fig. 1. Geometric interpretation for PARAFAC decomposition [44]

the PSD tensor, the constrained decomposition in Eq. (1) is essentially unique under the following condition [44]:

$$2n_s(n_s - 1) \leq n_x^2(n_x - 1)^2 \tag{14}$$

where n_x is the number of measurements and n_s is the maximum number of identifiable sources.

The relationship between the number of measurements and the maximum number of identifiable sources (i.e., modes or components) extracted by PARAFAC decomposition is given in Table. 1. It can be noted that the number of identifiable modes for complex tensor cases is higher than for real-valued tensors.

Table 1
Source separation capability for PARAFAC decomposition [44]

Number of measurements n_x	2	3	4	5	6	7	8
Number of identifiable modes $n_s^{\max}$ (real-valued case)	2	4	6	10	15	20	26
Number of identifiable modes $n_s^{\max}$ (complex-valued case)	2	4	9	14	21	30	40

2.3. Harmonic detection in the frequency domain

In the OMA, system is generally assumed to be excited by a random broadband signal. However, in many applications, periodic forces generated by unbalanced masses of rotating parts or electric actuators may cause harmonic components in the responses. Extra terms relative to the harmonic excitations are thus added in the Equation(13). These components need to be detected and eliminated in the modal identification process [45]. A direct approach for processing these harmonic components is to consider them as zero-damping modes [46]. Kurtosis value was also used in time domain to distinguish modal

responses from periodic excitations [47, 48]. In frequency domain, the spectral kurtosis (SK) of a signal is defined as the kurtosis value of its frequency component. It has been applied to the detection of harmonics [49–52]. A remarkable advantage of this approach is that the information for each frequency component can be indicated in the frequency range of interest.

Let $X(f)$ be the discrete Fourier transform (DFT) of signal $x(t)$. The original SK can be defined as follows [49]:

$$SK(f) = \frac{E\left\{|X(f)|^4\right\} - 2\left[E\left\{|X(f)|^2\right\}\right]^2}{\left[E\left\{|X(f)|^2\right\}\right]^2} \tag{15}$$

where $E\{.\}$ denotes the operator of expectation and $|.|$ represents the modulus operator.

In practice, the signal $x(t)$ is divided into M blocks to obtain an unbiased estimator of the SK by using the k-statistics:

$$SK(f) = \frac{M}{M-1}\left[\frac{(M+1)\sum_{i=1}^{M}\left|X^i(f)\right|^4}{\left(\sum_{i=1}^{M}|X^i(f)|^2\right)^2} - 2\right] \tag{16}$$

where the vector $X^i(f)$ is a DFT of the i-th block.

According to the statistical characteristic [49], the SK of a synthetic signal always equals to –1 for the harmonic frequency. However, this value for a random process equals to zero. In the case of $\mathbf{x}(t)$ mixing with a harmonic signal, its SK can be comprehensively described as:

$$\begin{cases} SK(f) = -1, & f = f_h \\ SK(f) = 0, & f \neq f_h \end{cases} \tag{17}$$

where f_h is a harmonic frequency.

Consequently, harmonic components and structural modes will be detected and confirmed by estimating the values of SK at each frequency through Eq. (16) and Eq. (17).

2.4. Proposed procedure for modal analysis

The procedure for modal analysis using PARAFAC decomposition in the frequency domain is proposed as follows:

Step 1. Collect responses $\mathbf{x}(t)$.

Step 2. Estimate the third-order PSD tensor $\mathbb{G}^{\mathbf{x}}$ from $\mathbf{x}(t)$.

Step 3. Build a stability diagram and determine the number of active modes R.

Methods based on the PARAFAC decomposition require a prior knowledge of the number of active modes. The order of rank R of the decomposition is chosen equal to the number of operating modes. This is essential to determine the correct rank. In order to determine the actual value of the rank order, the present study applies a PARAFAC decomposition with several ranks to obtain a stability diagram. The actual rank R will be determined from the stability diagram. This step is done as follows:

- Perform multi-rank $R_i = 2 : n_s^{max}$ PARAFAC decomposition of tensor $\mathbb{G}^{\mathbf{x}}$ to estimate mode shape matrix $\mathbf{\Phi}_{(i)}$ and auto-PSD matrix $\mathbf{G}^{\mathbf{q}}_{(i)}$ corresponding to the rank R_i decomposition.

- Find the dominant frequency in each auto-PSD function in the estimated $\mathbf{G}^{\mathbf{q}}_{(i)}$

- Draw the stability diagram of the identified frequencies with $R_i = 2 : n_s^{max}$

- Determine the number of active modes R equals to the minimum rank order when the number of identified frequencies becomes stable.

Step 4. Use the results of the rank R decomposition to estimate the frequencies and damping ratios from $\mathbf{g}^{\mathbf{q}}_r$ using a optimization procedure.

Each separated mode can be interpreted as a 1-DOF system. The theoretical formula of an auto-PSD function of the r^{th} mode can be written as follows:

$$\hat{\mathbf{g}}^{\mathbf{q}}_r(f) = \frac{A_r}{\left(f_r^2 - f\right)^2 + 4 f_r^2 f^2 \xi_r^2} \tag{18}$$

where f_r and ξ_r are the modal frequency and the damping ratio of the k^{th} mode, respectively and A_r is a constant.

The frequency and the damping ratio can be identified by solving the optimization problem. Each auto-PSD function estimated in the previous step is treated as the input for the optimization procedure as follows:

$$\hat{A}_r, \hat{f}_r, \hat{\xi}_r = \underset{A_r, f_r, \xi_r}{\arg\min} \left\| \hat{\mathbf{g}}^{\mathbf{q}}_r(f) - \mathbf{g}^{\mathbf{q}}{}_r(f) \right\|_2 \tag{19}$$

where $\|.\|_2$ denotes the L2-norm (Euclidean norm). $\hat{\mathbf{g}}^{\mathbf{q}}_r(f)$ and $\mathbf{g}^{\mathbf{q}}{}_r(f)$ are the theoretical formula and the estimated auto-PSD of the r^{th} mode, respectively.

The frequency values identified in the previous step are reutilized. The damping ratio can be estimated preliminarily by the half power bandwidth method. They can be considered as the initial values for the optimization procedure.

Step 5. Detect harmonic components by evaluating spectral kurtosis values at the frequencies identified in step 4.

- The SK value of the signal is -1 for the harmonic frequency and its value is close to zero for a structural mode.

Step 6. Obtain modal parameters by eliminating harmonic components.

The Modal Assurance Criterion (MAC) [53] can be used to check the colinearity between mode shapes $\boldsymbol{\phi}_i$ and $\boldsymbol{\phi}_j$ as follows :

$$\mathrm{MAC}_{ij} = \frac{\left|\boldsymbol{\phi}_i^H \boldsymbol{\phi}_j\right|^2}{(\boldsymbol{\phi}_i^H \boldsymbol{\phi}_i)(\boldsymbol{\phi}_j^H \boldsymbol{\phi}_j)} \tag{20}$$

When exact mode shapes are known, MAC values are also used to evaluate the quality of identified mode shapes.

3. Validation

3.1. Theoretical power spectral density

In this section, different mass-spring-damper systems are examined to validate the proposed method. The different modal parameters are defined to take into account various problems in modal identification, such as real-valued normal mode and complex modes.

3.1.1. A proportionally damped system

Consider an example of a 2-DOF system with the mass matrix $\mathbf{M}$, the stiffness matrix $\mathbf{K}$ and the corresponding mode shape matrix $\mathbf{\Phi}$.

$$\mathbf{M} = \begin{bmatrix} 2 & 0 \\ 0 & 2 \end{bmatrix}; \mathbf{K} = \begin{bmatrix} 800 & -800 \\ -800 & 2400 \end{bmatrix}; \mathbf{\Phi} = \begin{bmatrix} 1.0000 & 1.0000 \\ 0.4142 & -2.4142 \end{bmatrix}$$

The damping matrix $\mathbf{C}$ is calculated through a proportional model $\mathbf{C} = 0.2\mathbf{M}+0.00005\mathbf{K}$. Two exact natural frequencies and the two damping ratios are presented in Table. 2.

The third-order tensor $\mathbb{G}^{\mathbf{x}}$ is estimated under white noise excitation according to the theoretical formula from the reference [54] with 524288 frequency lines and a sampling rate of 512 Hz. The components of this theoretical PSD tensor are shown in Fig. 2:

The theoretical PSD tensor is processed by the proposed method to obtain a mode shape matrix and a matrix containing the auto-PSD functions of modal coordinates. Two estimated auto-PSD functions with rank $R = 2$ PARAFAC decomposition are shown in Fig. 3a.

The modal frequencies and damping ratios are identified using the optimization procedure described in Step 4. In Fig. 3b, the red-dash line shows the PSD curves plotted by the identified values.

The identification results are shown in Table. 2 together with exact modal parameters. The identified frequencies and the damping ratios are the same as the exact ones. The mode shapes are also exactly estimated. This confirms the efficiency of the procedure proposed when it is applied to the exact third-order PSD tensor by the theoretical formula.

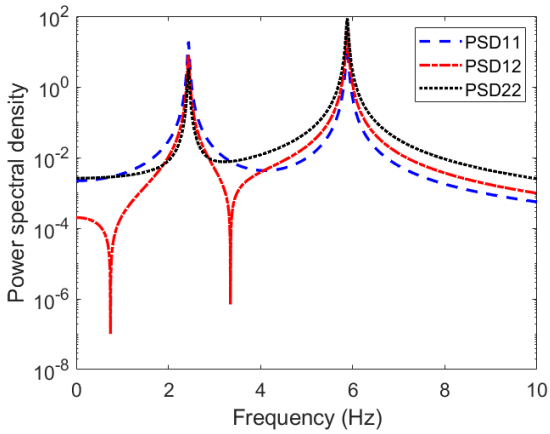

Fig. 2. Theoretical PSD curves of the 2-DOF system

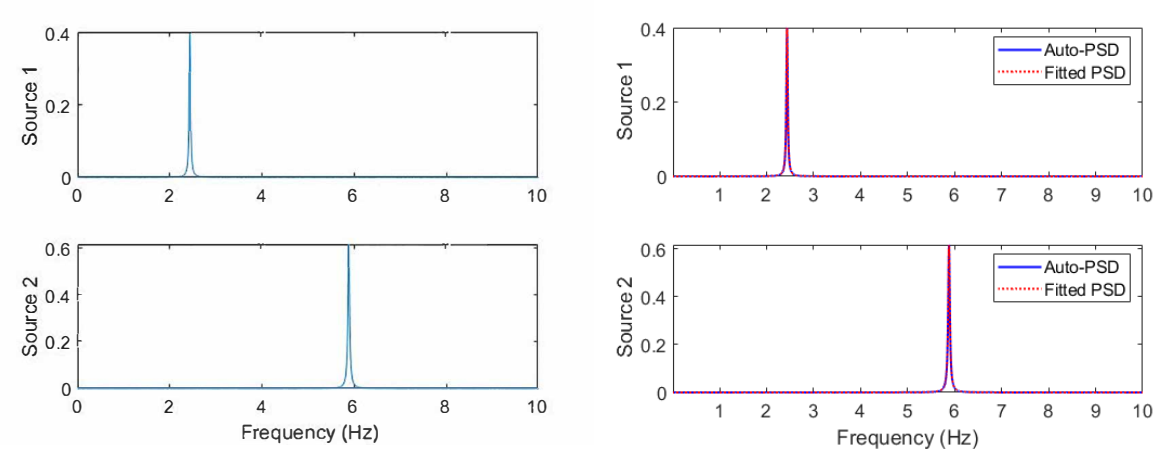

(a) Auto-PSD functions

(b) Estimation of modal parameters

Fig. 3. The identified sources from the 2-DOF system

Table 2
The identified results from the 2-DOF system

Mode	Frequency (Hz)		Damping ratio (%)		MAC
	Exact	Identified	Exact	Identified	
1	2.44	2.44	0.69	0.69	1.00
2	5.88	5.88	0.36	0.36	1.00

3.1.2. A non-proportionally damped system

To demonstrate the capabilities of the proposed method for identifying complex modes, this study uses a non proportionately damped 4-DOF model taken from the reference [55]. The mass, stiffness, and damping matrices of the model are as follows:

$$\mathbf{M} = \begin{bmatrix} 1 & 0 & 0 & 0 \\ 0 & 1 & 0 & 0 \\ 0 & 0 & 0.5 & 0 \\ 0 & 0 & 0 & 0.3 \end{bmatrix}; \mathbf{K} = \begin{bmatrix} 2 & -1 & 0 & 0 \\ -1 & 2 & -1 & 0 \\ 0 & -1 & 2 & -1 \\ 0 & 0 & -1 & 1 \end{bmatrix}; \mathbf{C} = \begin{bmatrix} 0.04 & -0.02 & 0 & 0 \\ -0.02 & 0.03 & -0.01 & 0 \\ 0 & -0.01 & 0.02 & -0.01 \\ 0 & 0 & -0.01 & 0.01 \end{bmatrix}$$

The complex mode shapes are presented in Table. 3. The exact modal frequencies and the exact modal damping ratios of the system are presented in Table. 4.

The theoretical PSD tensor is estimated with 524288 frequency points. The four auto-PSD curves are presented in Fig. 4.

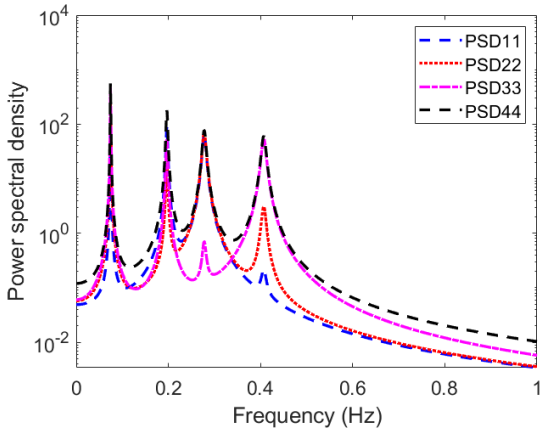

Fig. 4. Theoretical auto-PSD curves of the 4-DOF system

Fig. 5a shows the identified auto-PSD functions by PARAFAC decomposition in frequency domain. Fig. 5b presents the auto-PSD functions obtained by optimization procedure (in red) with ones from figure 5a (in blue). The curves are coincide. The identified results for the plots presented on Fig. 5 are shown in Table. 3 and Table. 4. It can be seen that the identified parameters are the same as the exact values. This confirms that the method is capable of dealing with complex modes.

3.2. Numerical examples

3.2.1. Well-separated modes

The effectiveness of the proposed method is investigated here using data from a numerical system. This test uses a simple 3 DOF system (Fig. 6) with a mass matrix **M**, a stiffness matrix **K**, and a corresponding mode shape matrix **Φ**.

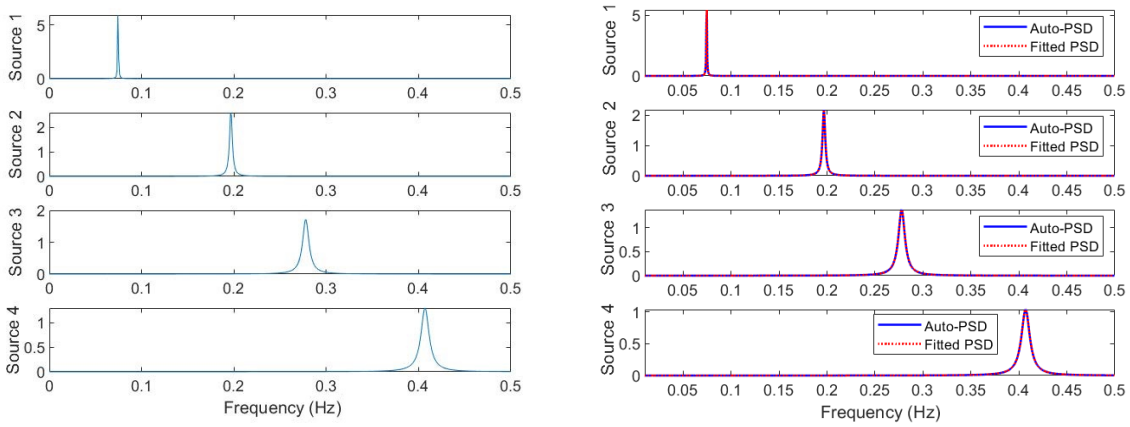

(a) Auto-PSD functions

(b) Estimation of modal parameters

Fig. 5. The identified sources from the 4-DOF system

Table 3
The complex modes of the 4-DOF system

Mode	1	2	3	4
Exact	1.00 + 0.00i	1.00 - 0.00i	1.00 - 0.00i	1.00 + 0.00i
	1.78 + 0.00i	0.47 + 0.01i	-1.05 + 0.02i	-4.53 + 0.16i
	2.17 + 0.00i	-0.78 - 0.00i	0.09 - 0.01i	19.59 - 0.88i
	2.32 + 0.00i	-1.43 - 0.01i	1.09 - 0.02i	-20.35 + 0.93i
Identified	1.00 + 0.00i	1.00 - 0.00i	1.00 - 0.00i	1.00 + 0.00i
	1.78 + 0.00i	0.47 + 0.01i	-1.05 + 0.02i	-4.53 + 0.16i
	2.17 + 0.00i	-0.78 - 0.00i	0.09 - 0.01i	19.59 - 0.88i
	2.32 + 0.00i	-1.43 - 0.01i	1.09 - 0.02i	-20.35 + 0.93i

Table 4
Frequencies and damping ratios estimated from the 4-DOF system

Mode		1	2	3	4
Exact	f (Hz)	0.07	0.20	0.28	0.41
	ξ (%)	0.45	0.86	1.48	1.30
Identified	f (Hz)	0.07	0.20	0.28	0.41
	ξ (%)	0.45	0.86	1.48	1.30
MAC		1.00	1.00	1.00	1.00

The damping matrix is calculated through a proportional model $\mathbf{C} = 0.2\mathbf{M}+0.00005\mathbf{K}$. The exact values of the natural frequencies and the damping ratios are presented in Table.

5.

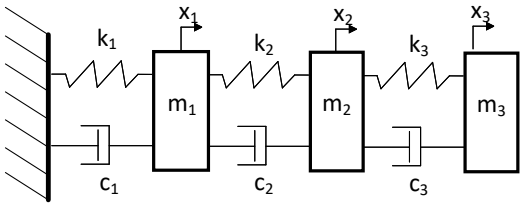

Fig. 6. The 3-DOF numerical system

$$\mathbf{M} = \begin{bmatrix} 2 & 0 & 0 \\ 0 & 2 & 0 \\ 0 & 0 & 2 \end{bmatrix}; \mathbf{K} = \begin{bmatrix} 800 & -800 & 0 \\ -800 & 2400 & -1600 \\ 0 & -1600 & 4000 \end{bmatrix}; \mathbf{C} = \begin{bmatrix} 0.44 & -0.04 & 0.00 \\ -0.04 & 0.52 & -0.08 \\ 0.00 & -0.08 & 0.60 \end{bmatrix}$$

In this test, random excitations accompanied by harmonic excitation were applied to all three DOFs of the system. Newmark algorithm was used to obtain time responses. In this simulation, the sampling rate was 200Hz and the total response time was 1200s. The responses of the system are shown in Fig. 7a.

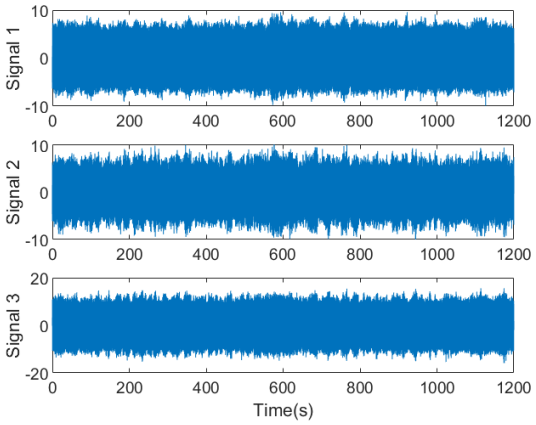

(a) Simulated signals

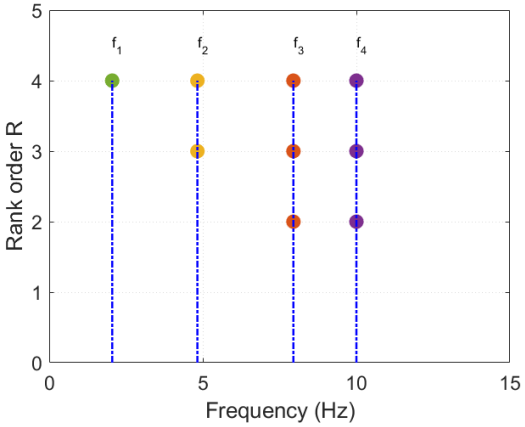

(b) Stability diagram

Fig. 7. Simulated signals and stability diagram in the case of random noise accompanied by harmonic excitation

The stability diagram is drawn for PARAFAC decomposition for rank $R_i = 2 : 4$ as shown in Fig. 7b. The diagram shows that there are four active modes. The four auto-PSD functions estimated by PARAFAC decomposition of rank $R = 4$ are presented in Fig. 8a.

The PSD curves obtained by the optimization are plotted in Fig. 8b (in red) with one from Fig. 8a (in blue).

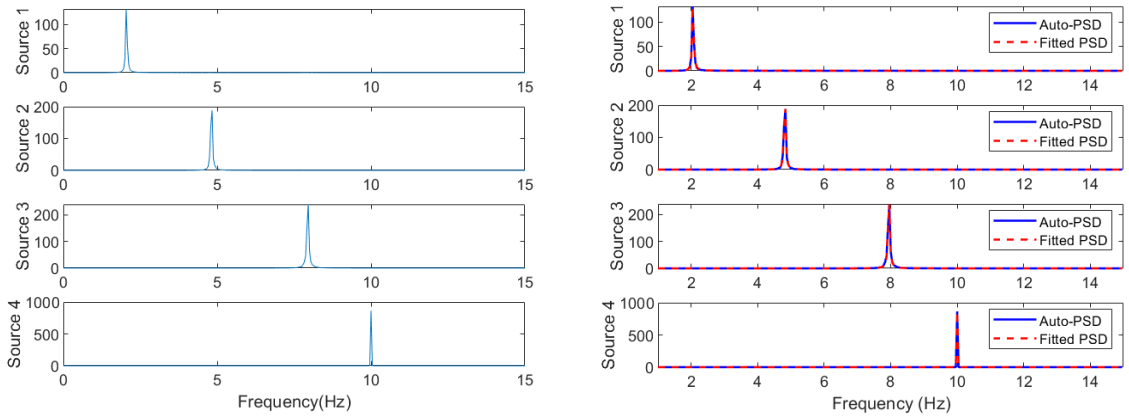

(a) Auto-PSD functions **(b)** Estimation of modal parameters

Fig. 8. Separated sources in the case of random noise accompanied by harmonic excitation

Fig. 9 presents the spectral kurtosis corresponding to the identified frequencies. It can be seen from the figure that the first three components (corresponding to source 1, 2, and 3) with average SK values are approximately equal to zero, which corresponds to structural modes. However, the last component (corresponding to source 4) with an average SK of about -1.0, corresponds to harmonic excitation.

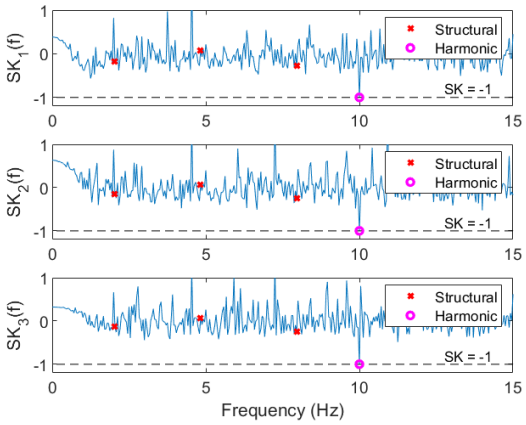

Fig. 9. Spectral kurtosis at each frequency of the simulated signals

The estimated modal parameters are presented in Table. 5. They are close to the exact ones. This confirms the effectiveness of the proposed procedure for a numerical system subjected to white noise excitation accompanied by harmonic excitation.

Table 5
Results estimated from the numerical system

Mode		1	2	3	4
Exact	f (Hz)	2.05	4.82	7.98	10.00
	ξ (%)	0.81	0.41	0.32	-
Identified	f (Hz)	2.05	4.82	7.95	10.00
	ξ (%)	0.78	0.37	0.42	0.01
	SK value	0	0	0	-1
	Nature	Struct	Struct	Struct	*Harmonic*
MAC		1.00	1.00	1.00	

3.2.2. Closely-spaced modes

The property of closely spaced modes frequently appears in practical engineering structures. To demonstrate the capabilities of the proposed method for identifying closely spaced modes, a 3-DOF model is taken from [56]. The mass, stiffness, and damping matrices of the model are as follows:

$$\mathbf{M} = \begin{bmatrix} 1 & 0 & 0 \\ 0 & 2 & 0 \\ 0 & 0 & 1 \end{bmatrix}; \mathbf{K} = \begin{bmatrix} 5 & -1 & 0 \\ -1 & 4 & -3 \\ 0 & -3 & 3.5 \end{bmatrix}; \mathbf{C} = \begin{bmatrix} 0.0894 & -0.0084 & 0.0003 \\ -0.0084 & 0.1301 & -0.0244 \\ 0.0003 & -0.0244 & 0.0772 \end{bmatrix}$$

Free decay is simulated with initial condition $\mathbf{x}(0) = [0, 0, 0]^T$ and $\mathbf{v}(0) = [0, 1, 0]^T$. The responses are shown in Figure 10. In this example, modes 2 and 3 are quite closely spaced.

The stability diagram is shown in Fig 11 and it indicates the number of active modes $R = 3$. The estimated auto-PSD functions of modal responses are shown in Fig. 12a, from which the modal frequencies and damping ratios are estimated (shown in Table. 6). The PSD curves obtained by the optimization are plotted in Fig. 12b. These values are well identified. The identified mode shapes fit the exact ones, with MAC values higher than 0.99.

3.3. Experimental tests

3.3.1. Cantilever beam

The proposed method of modal identification is now verified with an experimental test shown in Fig. 13. The test was carried out on a steel cantilever beam with Young's

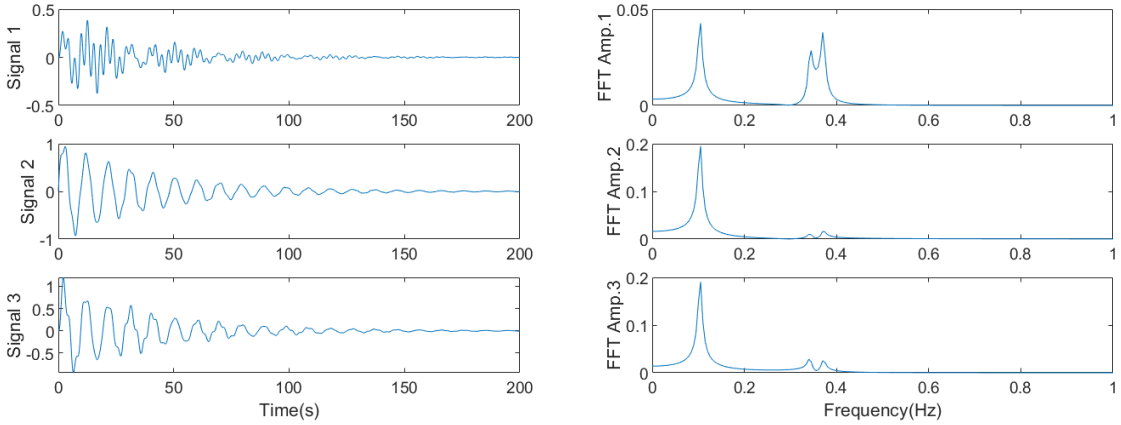

Fig. 10. Simulated signals and corresponding Fourier spectrums with closely-space modes

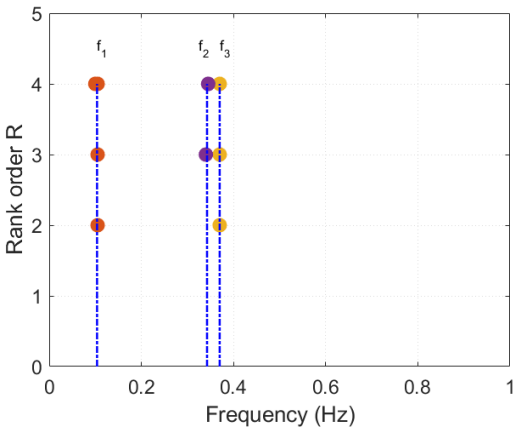

Fig. 11. Stability diagram

modulus E = 200GPa and a density of ρ = 7850kg/m^3. The dimensions of the cantilever beam are as follows: length 1005mm, width 42mm and height 10mm.

To obtain a reference model, a classical experimental modal analysis was performed. The time responses were recorded using five B&K Type 4533-B-001 accelerometers mounted along the length of the cantilever beam. A B&K Type 8230-001 force transducer was used to collect the input excitation as shown in Fig. 13(at the place of actuator 1). The commercial B&K Connect^{TM} software was used to acquire both the input excitation and the output responses. The modal parameters were determined using Rational Fraction Polynomial

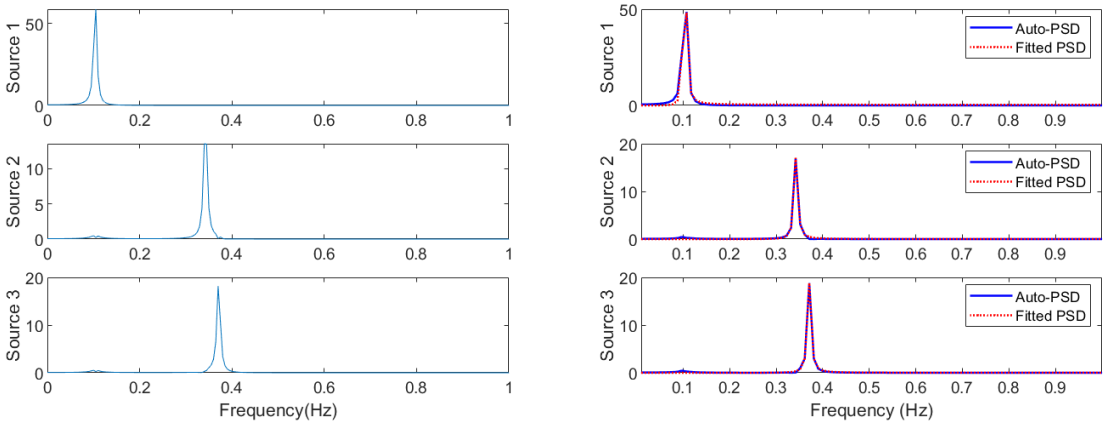

(a) Auto-PSD functions **(b)** Estimation of modal parameters

Fig. 12. Separated sources in the case of the system with closely-space modes

Table 6
Results estimated from the closely-spaced modes system

Mode		1	2	3
Exact	f (Hz)	0.10	0.34	0.37
	ξ (%)	3.83	1.16	1.07
Identified	f (Hz)	0.10	0.34	0.37
	ξ (%)	3.83	1.23	1.17
MAC		1.00	0.999	0.999

(RFP) method implemented in the software. The identified mode shapes are shown in Eq. (21) and identified natural frequencies and damping ratios are given in Table. 7. These results are used as reference values to check the accuracy of the proposed method. In this experiment, in addition to an ambient excitation, the cantilever beam was also excited by a harmonic frequency of 20Hz (at the place of actuator 2). The responses were recorded with a sampling rate of 2048Hz. Fig. 14 shows the acceleration responses at the locations of the sensors on the beam.

Stability diagram of five measurement signals obtained by performing several PARAFAC decompositions with $R_i = 2 : 7$. When performing a decomposition for rank $R = 7$, seven auto-PSD functions are given. However, two of them have the same dominant peak at the same frequency. This means that only six frequencies are identified by the decomposition for rank $R = 7$. The stability diagram indicates that there are six active modes in this test (Fig. 15a). In addition, to simulate the underdetermined case, the stability diagrams using only four sensors is also shown in Fig. 15b. One more time, the stability diagram indicates

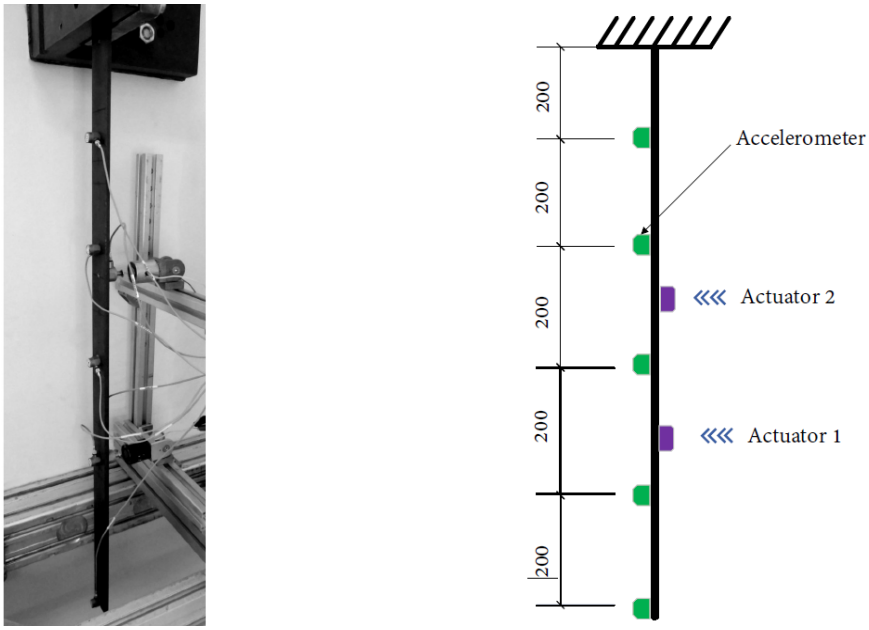

(a) Cantilever beam **(b)** Schematic model

Fig. 13. The cantilever beam and test point locations

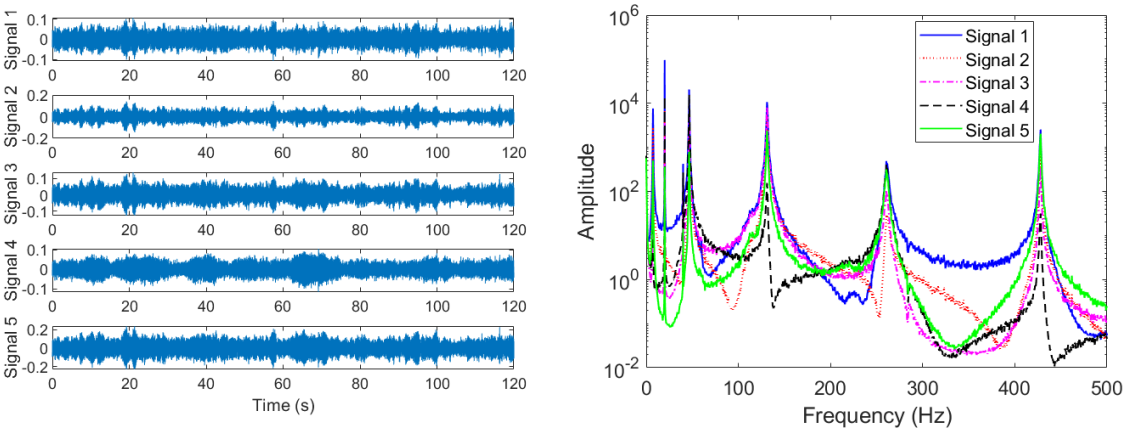

(a) Time domain **(b)** Frequency domain

Fig. 14. Five measurement signals of the cantilever beam

six active modes.

Six estimated auto-PSD functions of PARAFAC decomposition for rank $R = 6$ are shown in Fig. 16. The modal frequencies and the damping ratios are estimated from these

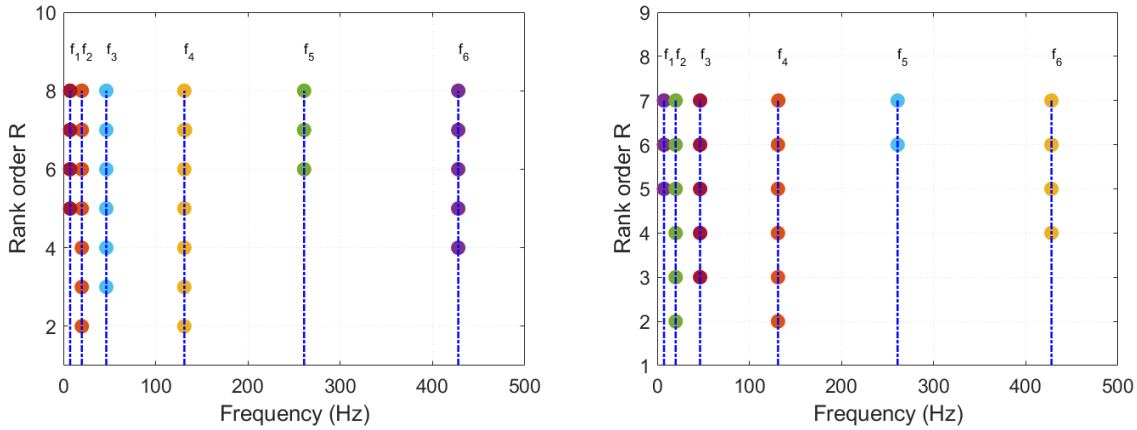

(a) Using five sensors **(b)** Using four sensors

Fig. 15. Stability diagrams

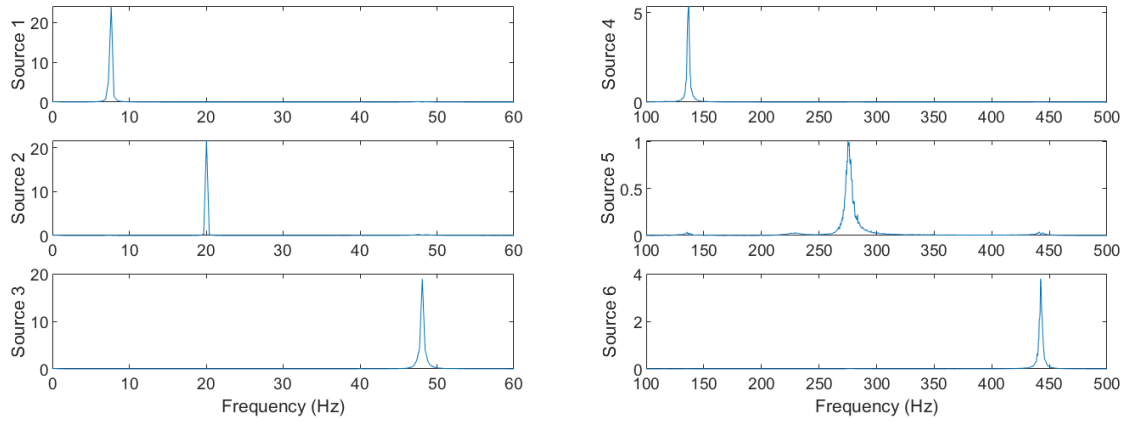

Fig. 16. Separated auto-PSD functions in the case of random noise accompanied by harmonic excitation

estimated functions. They are plotted in Fig. 17 together with the corresponding identified auto-PSD curves. The identified results are presented in Table.7. The results agree with the modal parameters identified by the RFP method in the software.

The plots of the SK value of the first and fifth measured signals for different frequencies are shown in Fig. 18. It can be seen that the second separated component belongs to the harmonic excitation because its SK values in the five measurement signals are equal to -1.0. This second mode also has a zero identified damping value. The other components have mean SK values close to zero. This means that these frequencies correspond to the

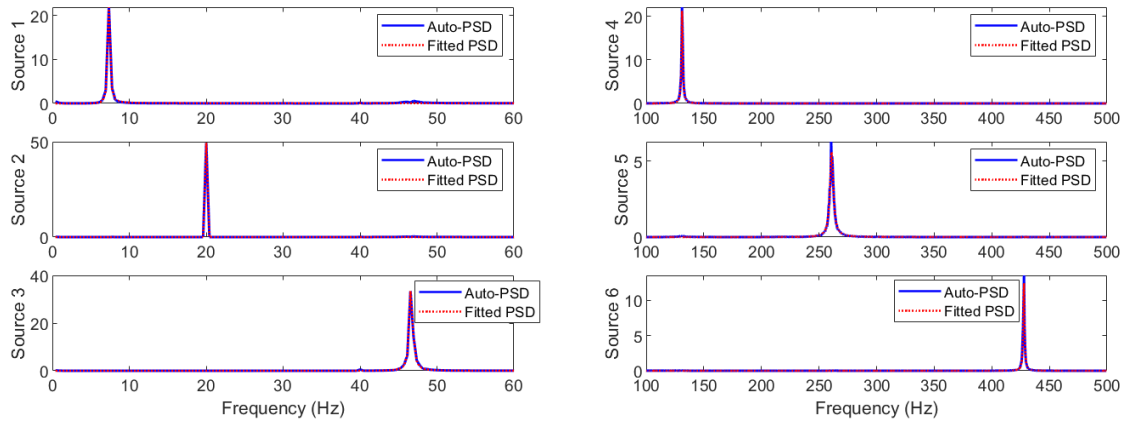

Fig. 17. Estimation of modal parameters of the cantilever beam

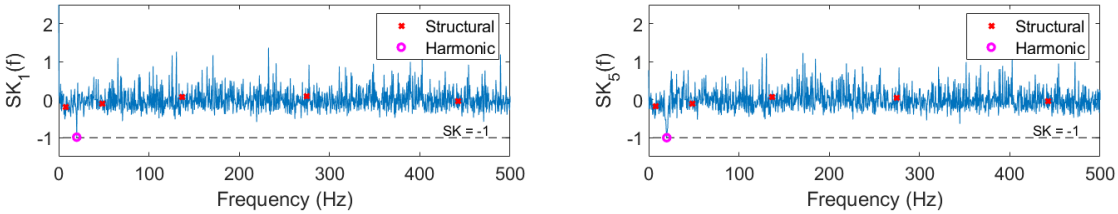

Fig. 18. Spectral kurtosis at each frequency of the measurement signals

structural modes.

The estimated mode shapes using PARAFAC decomposition are presented in Eq. (22) for five sensors and Eq. (23) for 4 sensors respectively. The structural mode shape plots are depicted in Figure. 19. The continuous blue lines represent the analytical mode shapes and the red asterisks represent the results obtained from the proposed method.

$$\mathbf{A_{RFP}} = \begin{bmatrix} 0.1725 & -0.3794 & 0.6935 & -1.0027 & 0.6005 \\ 0.2698 & -0.7120 & 0.4873 & 0.4719 & -0.7356 \\ 0.4943 & -0.5681 & -0.5248 & 0.4392 & 0.7818 \\ 0.7440 & 0.0930 & -0.4077 & -0.7186 & -0.6527 \\ 1.0000 & 1.0000 & 1.0000 & 1.0000 & 1.0000 \end{bmatrix} \tag{21}$$

$$\mathbf{A}^{(5)}_{\mathbf{PARAFAC}} = \begin{bmatrix} 0.1723 & -0.0297 & -0.3791 & 0.6935 & -1.2693 & 0.6006 \\ 0.2689 & 0.0000 & -0.7116 & 0.4874 & 0.5866 & -0.7369 \\ 0.4944 & 0.2130 & -0.5679 & -0.5249 & 0.4746 & 0.7829 \\ 0.7438 & 0.5805 & 0.0932 & -0.4076 & -0.9281 & -0.6558 \\ 1.0000 & 1.0000 & 1.0000 & 1.0000 & 1.0000 & 1.0000 \end{bmatrix} \tag{22}$$

$$\mathbf{A}^{(4)}_{\mathbf{PARAFAC}} = \begin{bmatrix} 0.1724 & -0.0293 & -0.3790 & 0.6932 & -1.0079 & 0.5974 \\ 0.2692 & -0.0001 & -0.7112 & 0.4870 & 0.3650 & -0.7317 \\ 0.4942 & 0.2127 & -0.5673 & -0.5247 & 0.4299 & 0.7794 \\ 1.0000 & 1.0000 & 1.0000 & 1.0000 & 1.0000 & 1.0000 \end{bmatrix} \tag{23}$$

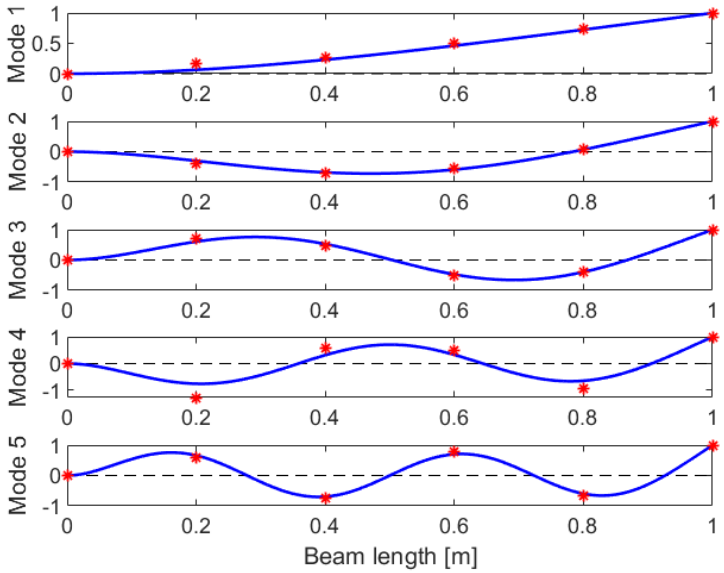

Fig. 19. Mode shapes of the experimental cantilever beam

Table 7
Results estimated from the experimental beam

Mode		1	2	3	4	5	6
RFP	f (Hz)	7.55	-	48.11	136.57	274.17	442.52
	$\xi(\%)$	0.72	-	0.33	0.70	1.12	0.30
5 sensors	f (Hz)	7.56	20.04	48.09	136.63	275.08	442.57
	$\xi(\%)$	0.73	0.00	0.40	0.72	1.09	0.29
	MAC	1.00	-	1.00	1.00	0.99	1.00
4 sensors	f (Hz)	7.56	20.00	48.09	136.64	275.12	442.56
	$\xi(\%)$	0.66	0.02	0.35	0.71	1.08	0.28
	SK value	≈ 0	-1	≈ 0	≈ 0	≈ 0	≈ 0
	Nature	Struct	*Harmonic*	Struct	Struct	Struct	Struct

Besides, four out of five measurement signals (1, 2, 3, 5) are also used for modal identification to show the effectiveness of the proposed method. The identified results

are tabulated in Table.7. The estimated partial mode shapes are shown in Eq. (23). The identified parameters match well with the references.

These obtained results confirm the effectiveness of the proposed procedure in under-determined problems as well as with the presence of harmonic excitation.

3.3.2. Two-story aluminum frame

In order to test the proposed method with an experimental test of very close modes, a two-storey laboratory frame (shown in Fig. 20a) is considered, measuring 19cm x 30cm in plan with a story height of 31cm. First, a classical modal analysis based on the RFP method is performed with the input and output signals. These identified modal parameters by the RFP method are the used as reference values.

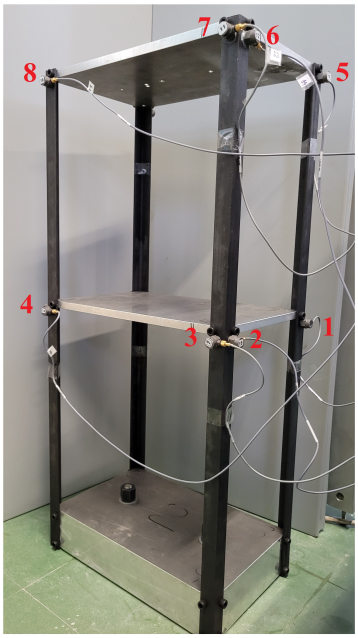

(a) Two-story frame

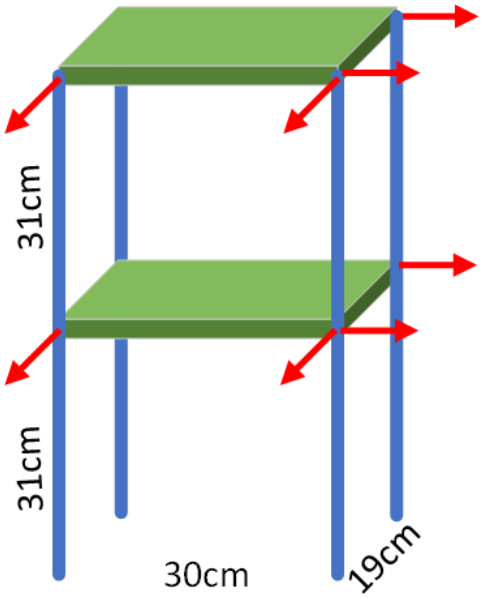

(b) Schematic model

Eight B&K Type 4533-B-001 accelerometers are attached to the frame to measure the vibration response of the frame in two horizontal directions. Vibration responses were measured with a sampling rate of 2048 Hz. The auto-PSD functions of the vibration signals are shown in Fig. 21. It should be noted that modes 1 and 2 closely spaced. It is also the same for modes 4 and 5.

The signals is processed by the proposed method in two situations : (i) eight signals and (ii) four signals only . The stability diagrams for 8 sensors and 4 sensors are shown in Fig. 22a and Fig. 22b, respectively. They indicate clearly the present of six active

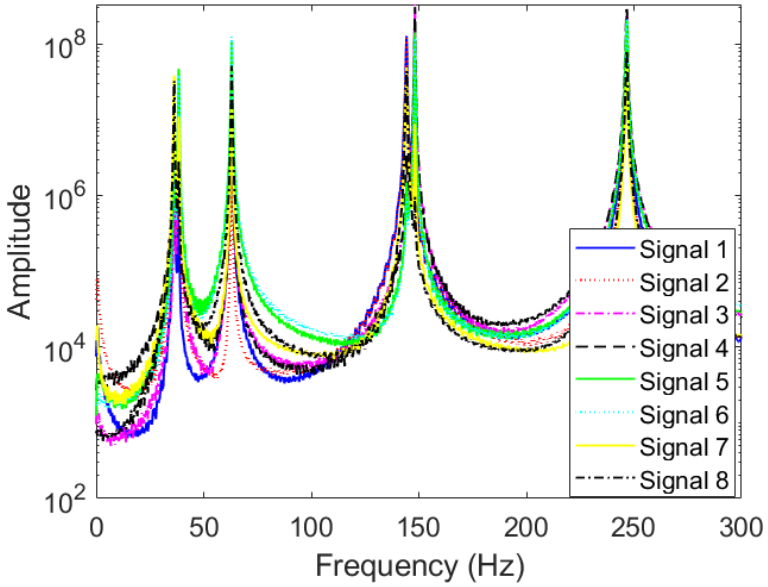

Fig. 21. The auto-spectral density functions of measured signals

modes in the signals. The six estimated auto-PSD functions of PARAFAC decomposition for rank $R = 6$ are shown in Fig. 23. It can be seen that they are effectively separated by the PARAFAC decomposition. These functions are also plotted in Fig. 24 together with its corresponding identified curve in red dashed line. The identified modal parameters are presented in Table.8. The results match well with the modal parameters identified by the classical RFP method implemented in the B&K Pulse software. The estimated mode shapes are plotted in the Fig. 25. Besides, the FDD method is also applied for comparisons with the proposed method in this test. The comparison of the estimated mode shapes is presented in Fig. 26.

Furthermore to simulate an underdetermined case, only four sensors (1,2,7,8) are used for the proposed method. The identified results given in in Table.8 confirm that the proposed method can give a good performance in underdetermined cases.

4. Conclusion

This paper presents a novel method for output-only modal identification in the frequency domain. The method is based on the PARAFAC decomposition of the third-order PSD tensor of responses. Decomposed components along sensor dimension allow to identified mode shapes while the ones along the frequency dimension give auto-PSD functions of modal coordinates. The application of an optimization procedure on these functions

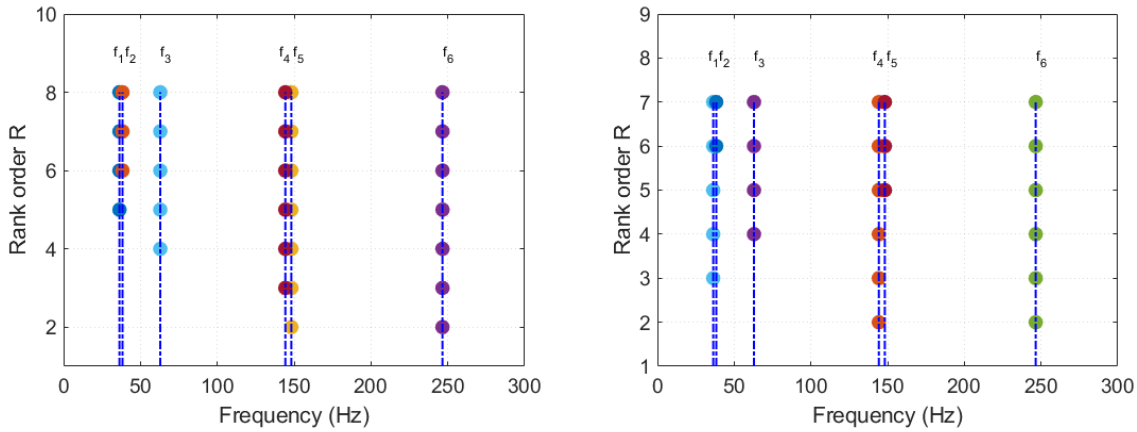

(a) Using eight sensors **(b)** Using four sensors

Fig. 22. Stability diagrams

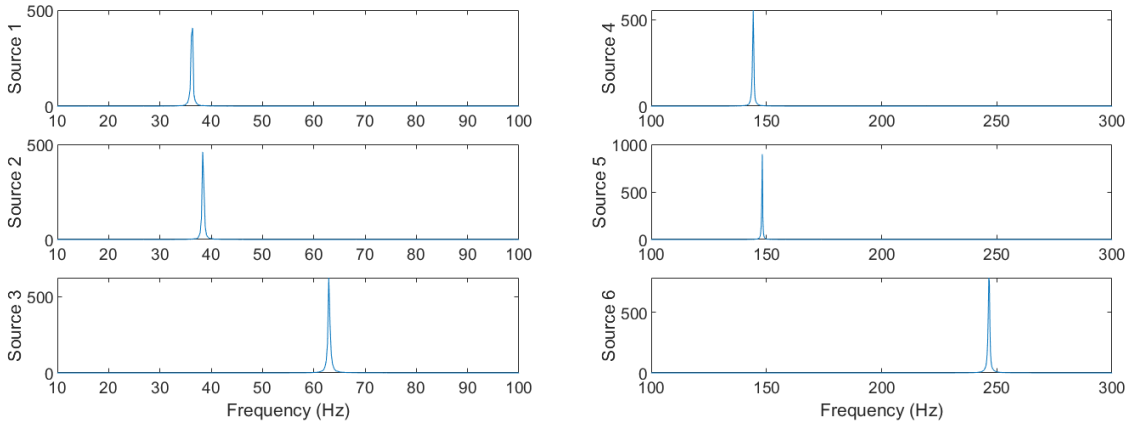

Fig. 23. Separated auto-PSD functions

gives natural frequencies and damping ratios. The use of a stability diagram allows to recognize the exact number of active modes. A practical step-by-step procedure of the proposed method has been proposed.

The validity of the proposed method was verified using simulated responses and experimental tests. Proportional and non-proportional damping examples showed that the application of the PARAFAC decomposition in frequency domain gives the proposed method the capacity identifying complex modes and moreover it is more efficient in comparison with real-valued tensors as the case of time domain.

Closely and very closely-spaced modes tests were also tested. Identified results by

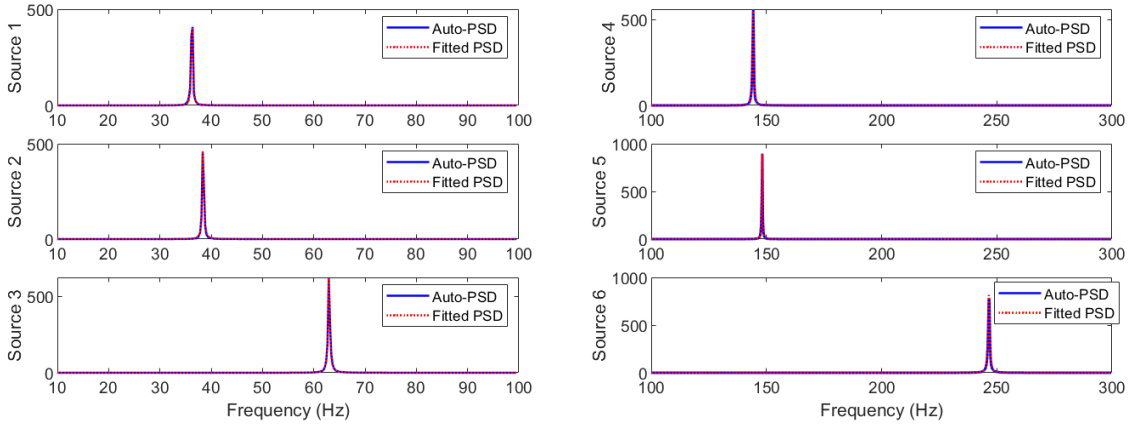

Fig. 24. Estimation of modal parameters of the frame

Table 8
Results estimated from the frame

Mode		1	2	3	4	5	6
RFP	f (Hz)	36.25	38.44	63.00	144.24	148.14	246.71
	$\xi(\%)$	0.55	0.38	0.32	0.31	0.13	0.25
FDD	f (Hz)	36.27	38.41	62.96	144.28	148.20	246.64
	$\xi(\%)$	0.44	0.46	0.32	0.20	0.17	0.14
8 sensors	f (Hz)	36.27	38.39	62.96	144.30	148.19	246.63
	$\xi(\%)$	0.43	0.42	0.30	0.21	0.10	0.14
4 sensors	f (Hz)	36.26	38.42	62.97	144.26	148.16	246.62
	$\xi(\%)$	0.35	0.42	0.31	0.21	0.11	0.15

the proposed method are all in good agreement exact values or reference values of the input-output RFP method.

The proposed method was also efficient in underdetermined cases when the number of signal channels was reduced in comparison with number of active modes. The quality of identified results are quite unchanged when a half of signal channels were removed (8 sensors v.s. 4 sensors) for the case of two-storey frame.

In presence of harmonic excitations, by using the spectral kurtosis values, the proposed method can easily distinguish structural modes from harmonic components.

The proposed method should be thus a performance method for operational modal analysis.

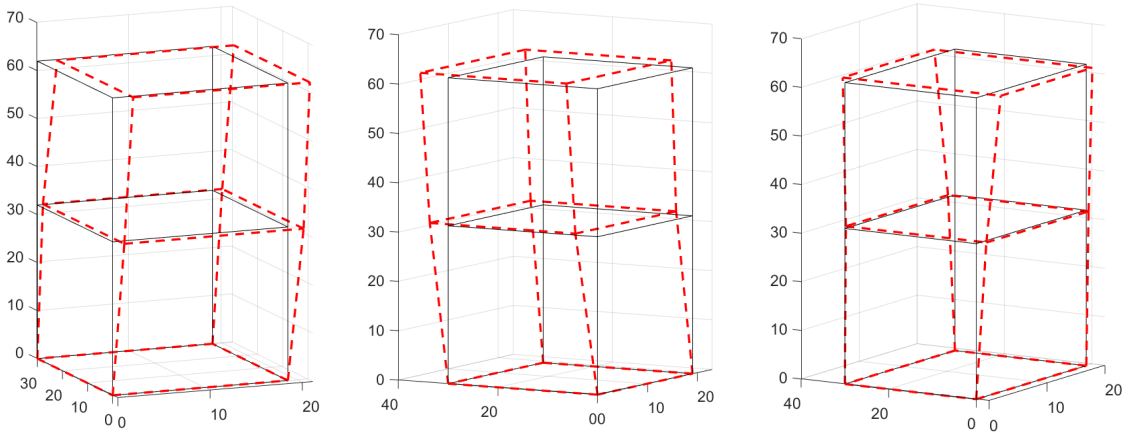

(a) 1st mode (lateral) **(b)** 2nd mode (lateral) **(c)** 3rd mode (torsional)

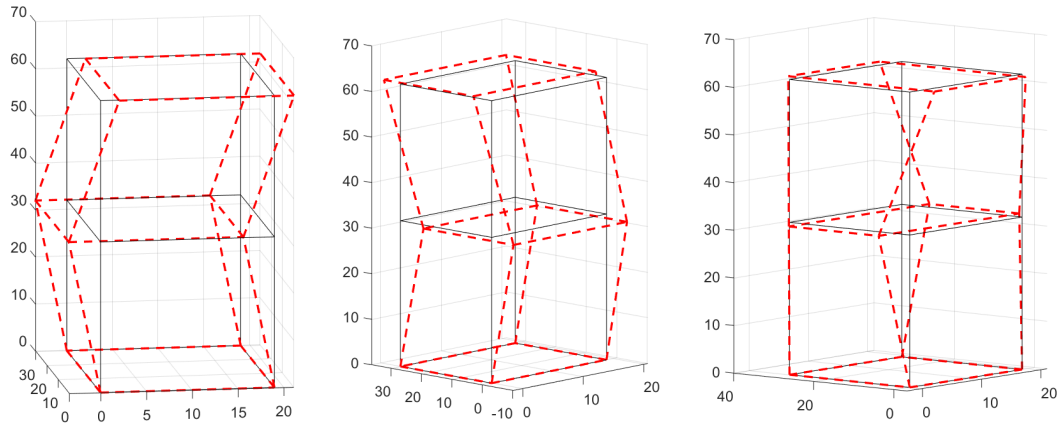

(d) 4th mode (lateral) **(e)** 5th mode (lateral) **(f)** 6th mode (torsional)

Fig. 25. The identified mode shapes of the frame

5. Acknowledgments

We acknowledge with gratitude the funding provided by the French government in the form of a fellowship that has helped to carry out this work.

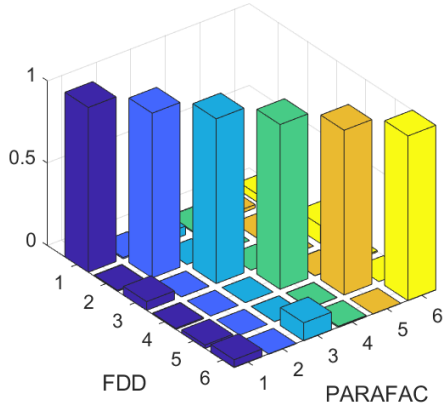

Fig. 26. Cross MAC

References

[1] L. Zhang, R. Brincker, P. Andersen, An overview of operational modal analysis: Major development and issues, in: Proceedings of the 1st International Operational Modal Analysis, Aalborg Universitet, Copenhagen, 2005, pp. 179–190.

[2] R. Brincker, P. H. Kirkegaard, Special issue on operational modal analysis, Mechanical Systems and Signal Processing 24 (2010) 1209–1212. doi:https://doi.org/10.1016/j.ymssp.2010.03.005.

[3] B. Peeters, G. De Roeck, Reference-based stochastic subspace identification for output-only modal analysis, Mechanical Systems and Signal Processing 13 (1999) 855–878. doi:https://doi.org/10.1006/mssp.1999.1249.

[4] D. Bonnecase, M. Prevosto, A. Benveniste, Application of a multidimensional arma model to modal analysis under natural excitation, in: Proceedings of the 8th International Modal Analysis Conference (IMAC), Florida, US, 1994, p. 382–388.

[5] S. Ibrahim, E. Mikulcik, A method for the direct identification of vibration parameters from the free response, in: Computer Science, 1977, p. 183–196.

[6] R. S. Pappa, K. B. Elliott, A. Schenk, Consistent-mode indicator for the eigensystem realization algorithm, Journal of Guidance, Control, and Dynamics 16 (1993) 852–858. doi:https://doi.org/10.2514/3.21092.

[7] R. Brincker, L. Zhang, P. Andersen, Output-only modal analysis by frequency domain decomposition, in: Proceedings of ISMA25: 2000 International Conference on

Noise and Vibration Engineering, Katholieke Universiteit, Leuven, 2000, pp. 717–723.

[8] B. Peeters, H. Auweraer, P. Guillaume, J. Leuridan, The polymax frequency-domain method: a new standard for modal parameter estimation?, Shock and Vibration 11 (2004) 395–409.

[9] R. Brincker, C. E. Ventura, Introduction to Operational Modal Analysis, John Wiley and Sons, 2015. doi:10.1002/9781118535141.

[10] J. Antoni, Blind separation of vibration components: Principles and demonstrations, Mechanical Systems and Signal Processing 19 (2005) 1166–1180. URL: https://doi.org/10.1016/j.ymssp.2005.08.008.

[11] A. Cichocki, S.-i. Amari, Adaptive blind signal and image processing: learning algorithms and applications, John Wiley & Sons, 2002.

[12] P. Comon, Independent component analysis, a new concept?, Signal Processing 36 (1994) 287 – 314. doi:https://doi.org/10.1016/0165-1684(94)90029-9.

[13] A. Hyvärinen, E. Oja, Independent component analysis: algorithms and applications, Neural Networks 13 (2000) 411–430. doi:https://doi.org/10.1016/S0893-6080(00)00026-5.

[14] J.-F. Cardoso, Blind signal separation: statistical principles, in: Proceedings of the IEEE, volume 86, IEEE, 1998, pp. 2009 – 2025. doi:https://doi.org/10.1109/5.720250.

[15] A. Belouchrani, K. Abed-Meraim, J.-F. Cardoso, E. Moulines, A blind source separation technique using second-order statistics, in: IEEE Transactions on Signal Processing, volume 45, IEEE, 1997, pp. 434–444. doi:https://doi.org/10.1109/78.554307.

[16] A. Sadhu, S. Narasimhan, J. Antoni, A review of output-only structural mode identification literature employing blind source separation methods, Mechanical Systems and Signal Processing 94 (2017) 415–431. doi:https://doi.org/10.1016/j.ymssp.2017.03.001.

[17] P. Bofill, M. Zibulevsky, Underdetermined blind source separation using sparse representations, Signal Processing 81 (2001) 2353–2362. URL: https://doi.org/10.1016/S0165-1684(01)00120-7.

[18] R. Castiglione, J. Antoni, L. Garibaldi, Separation and identification of structural modes in largely underdetermined scenarios using frequency banding, Journal of Sound and Vibration 414 (2018) 192–217. doi:https://doi.org/10.1016/j.jsv.2017.10.033.

[19] F. Amini, Y. Hedayati, Underdetermined blind modal identification of structures by earthquake and ambient vibration measurements via sparse component analysis, Journal of Sound and Vibration 366 (2016) 117–132. doi:https://doi.org/10.1016/j.jsv.2015.10.028.

[20] Y. Li, A. Cichocki, S. Amari, Sparse component analysis for blind source separation with less sensors than sources, in: 4th International Symposium on Independent Component Analysis and Blind Signal Separation, 2003, p. 89–94.

[21] K. Yu, K. Yang, Y. Bai, Estimation of modal parameters using the sparse component analysis based underdetermined blind source separation, Mechanical Systems and Signal Processing 45 (2014) 302–316. doi:https://doi.org/10.1016/j.ymssp.2013.11.018.

[22] X.-J. Yao, T.-H. Yi, C. Qu, H.-N. Li, Blind modal identification using limited sensors through modified sparse component analysis by time-frequency method, Computer-Aided Civil and Infrastructure Engineering 33 (2018) 769–782. doi:https://doi.org/10.1111/mice.12372.

[23] Y. Yang, S. Nagarajaiah, Output-only modal identification with limited sensors using sparse component analysis, Journal of Sound and Vibration 332 (2013) 4741–4765. doi:https://doi.org/10.1016/j.jsv.2013.04.004.

[24] W. Guan, L. Dong, Y. Cai, J. Yan, Y. Han, Sparse component analysis with optimized clustering for underdetermined blind modal identification, Measurement Science and Technology 30 (2019) 125011 (16pp). doi:https://doi.org/10.1088/1361-6501/ab3054.

[25] R. A. Harshman, Foundations of the PARAFAC Procedure: Models and Conditions for an explanatory Multi-modal Factor Analysis, University of California at Los Angeles, 1970.

[26] J. Carroll, J. Chang, Analysis of individual differences in multidimensional scaling via an n-way generalization of "eckart-young" decomposition, Psychometrika 35 (1970) 283–319. doi:https://doi.org/10.1007/BF02310791.

[27] G. Tomasi, R. Bro, A comparison of algorithms for fitting the parafac model, Computational Statistics and Data Analysis 50 (2006) 1700 – 1734. doi:https://doi.org/10.1016/j.csda.2004.11.013.

[28] P. Comon, X. Luciani, A. de Almeida, Tensor decompositions, alternating least squares and other tales, Journal of Chemometrics 23 (2009) 393–405. doi:https://doi.org/10.1002/cem.1236.

[29] L. Lathauwer, D. Nion, Decompositions of a higher-order tensor in block terms—part iii: Alternating least squares algorithms, SIAM J. Matrix Analysis Applications 30 (2008) 1067–1083.

[30] D.-T. Ta, T.-P. Le, M. Burman, Operational modal identification based on parallel factor decomposition with the presence of harmonic excitation, Comptes Rendus. Mécanique 349 (2021) 435–452. doi:10.5802/crmeca.90.

[31] J. Antoni, S. Chauhan, An alternating least squares (als) based blind source separation algorithm for operational modal analysis, in: Modal Analysis Topics, volume 3 of *Conference Proceedings of the Society for Experimental Mechanics Series*, Springer, New York, United States, 2011, pp. 179–187. doi:https://doi.org/10.1007/978-1-4419-9299-4_15.

[32] F. Abazarsa, F. Nateghi, S. F. Ghahari, E. Taciroglu, Blind Modal Identification of Non-Classically Damped Systems from Free or Ambient Vibration Records, Earthquake Spectra 29 (2013) 1137–1157. doi:https://doi.org/10.1193/031712EQS093M.

[33] F. Abazarsa, S. F. Ghahari, F. Nateghi, E. Taciroglu, Response-only modal identification of structures using limited sensors, Structural Control and Health Monitoring 20 (2013) 987–1006. doi:https://doi.org/10.1002/stc.1513.

[34] P. Friesen, A. Sadhu, Performance of tensor decomposition-based modal identification under nonstationary vibration, Smart Materials and Structures 26 (2017) 035024. doi:https://doi.org/10.1088/1361-665X/aa5438.

[35] S. I. McNeill, Extending blind modal identification to the underdetermined case for ambient vibration, in: ASME 2012 International Mechanical Engineering Congress and Exposition, The American Society of Mechanical Engineers, Texas, USA, 2012, pp. 241–252. doi:https://doi.org/10.1115/IMECE2012-93140.

[36] A. Sadhu, A. Goldack, S. Narasimhan, Ambient modal identification using multi-rank parallel factor decomposition, Structural Control and Health Monitoring 22 (2015) 595–614. doi:https://doi.org/10.1002/stc.1706.

[37] A. Sadhu, B. Hazra, S. Narasimhan, Decentralized modal identification of structures using parallel factor decomposition and sparse blind source separation, Mechanical Systems and Signal Processing 41 (2013) 396–419. doi:https://doi.org/10.1016/j.ymssp.2013.06.031.

[38] F. Abazarsa, F. Nateghi, S. F. Ghahari, E. Taciroglu, Extended blind modal identification technique for nonstationary excitations and its verification and validation, Journal of Engineering Mechanics 124 (2015) 1–19. doi:https://doi.org/10.1061/(ASCE)EM.1943-7889.0000990.

[39] A. Smilde, R. Bro, P. Geladi, Multi-way Analysis: Applications in Chemical Sciences, Wiley, Uk, 2004.

[40] R. Bro, Parafac. tutorial and applications, Chemometrics and Intelligent Laboratory Systems 38 (1997) 149–171. doi:https://doi.org/10.1016/S0169-7439(97)00032-4.

[41] D. Nion, L. De Lathauwer, An enhanced line search scheme for complex-valued tensor decompositions. application in ds-cdma, Signal Processing 88 (2008) 749–755. doi:https://doi.org/10.1016/j.sigpro.2007.07.024.

[42] J. B. Kruskal, Three-way arrays: rank and uniqueness of trilinear decompositions, with application to arithmetic complexity and statistics, Linear Algebra and its Applications 18 (1977) 95–138. doi:https://doi.org/10.1016/0024-3795(77)90069-6.

[43] R. Brincker, C. Ventura, P. Andersen, Damping estimation by frequency domain decomposition, volume 1, 2001.

[44] L. D. Lathauwer, J. Castaing, Blind identification of underdetermined mixtures by simultaneous matrix diagonalization, IEEE Transactions on Signal Processing 56 (2008) 1096 – 1105. doi:https://doi.org/10.1109/TSP.2007.908929.

[45] N.-J. Jacobsen, P. Andersen, R. Brincker, Eliminating the influence of harmonic components in operational modal analysis, in: The International Modal Analysis Conference IMAC-XXIV: A Conference & Exposition on Structural Dynamics, Society for Experimental Mechanics, 2007.

[46] V. Gagnol, T.-P. Le, P. Ray, Modal identification of spindle-tool unit in high-speed machining, Mechanical Systems and Signal Processing (2011) 2388–2398. doi:https://doi.org/10.1016/j.ymssp.2011.02.019.

[47] T. Lago, The difference between harmonics and stochastic narrow band responses, in: Presentation at the SVIBS symposium, Structural Vibration Solution, Stockholm, 1997.

[48] R. Brincker, P. Andersen, N. B. Møller, An indicator for separation of structural and harmonic modes in output-only modal testing, in: Proceedings of SPIE - The International Society for Optical Engineering, Aalborg University, Madrid, Spain, 2000.

[49] V. Vrabie, P. Granjon, C. Serviere, Spectral kurtosis: from definition to application, in: Proceedings of the 6th IEEE NSPI Grado-Trieste, Italy, 2003.

[50] J.-L. Dion, I. Tawfiq, G. Chevallier, Harmonic component detection: Optimized spectral kurtosis for operational modal analysis, Mechanical Systems and Signal Processing 26 (2012) 24–33. doi:https://doi.org/10.1016/j.ymssp.2011.07.009.

[51] T. Wang, Z. Xia, L. Zhang, Detection and removal of harmonic components in operational modal analysis, Journal of Vibroengineering 19 (2017) 5278–5289. doi:https://doi.org/10.21595/jve.2017.17725.

[52] J. Antoni, The spectral kurtosis: a useful tool for characterising non-stationary signals, Mechanical Systems and Signal Processing 20 (2006) 282–307. doi:https://doi.org/10.1016/j.ymssp.2004.09.001.

[53] R. Allemang, The modal assurance criterion - twenty years of use and abuse, Sound and Vibration 37 (2003) 14–23.

[54] T.-P. Le, Use of the morlet mother wavelet in the frequency-scale domain decomposition technique for the modal identification of ambient vibration responses, Mechanical Systems and Signal Processing 95 (2017) 488–505. doi:https://doi.org/10.1016/j.ymssp.2017.03.045.

[55] T.-P. Le, Dynamical monitoring of structures using continuous wavelet analysis, Thesis, Ecole des Ponts ParisTech, 2003.

[56] S. McNeill, D. Zimmerman, A framework for blind modal identification using joint approximate diagonalization, Mechanical Systems and Signal Processing 22 (2008) 1526–1548. doi:https://doi.org/10.1016/j.ymssp.2008.01.010.

4 Single damage detection

Chapter abstract

As discussed in Chapter 1, the damage detection procedure is an indispensable tool for ensuring structure integrity and safety in the process of Structural Health Monitoring. This is just as important as modal analysis presented in previous chapters. The challenges in damage detection procedure are to detect the presence, location and extent of structural damage, especially in the early stage of its formation. In addition, an important part of this procedure is damage diagnostics, which reflects information about the safety of the structure.

As modal parameters like natural frequencies, mode shapes and its curvatures are highly depend on health state of structure, the most of existing methods for detection of a single damage are based on this fact. They assume a simplified heuristic expression between the change in beam stiffness and its impact on the natural frequency shift and mode shape curvature. Then they produce a curve for each mode, expressing the severity of damage and its location. In plotting several curves of identified modes, the stiffness change and its location are deduced manually from the coordinates of the intersection of these curves. However, these methods can give inaccurate results of damage identification when these curves do not have the same intersection point. In addition, it is important to note that the variation in modal parameters comes not only from the appearance of a stiffness change, as the main assumption of all these methods, but also from a local change in the mass of the structure.

This chapter presents an efficient method for the rapid detection and quantification of single local damage in like-beam structures using identified modal parameters. Damage can be viewed as a localized change in mass and/or stiffness. The presented explicit analytical expression provides a relationship between local changes in the mass and stiffness of a beam and its natural frequency shift and mode shape. Based on the proposed expression, linear regression is applied to obtain accurate results of the change in masse/stiffness of the beam. The effectiveness of the proposed procedure was confirmed by numerical simulations followed by experiment verification.

4.1 Single damage detection using natural frequency shifts and mode shapes (Article 3)

Single damage detection using natural frequency shift, mode shapes and curvatures

Abstract

The article presents a procedure for detecting changes in the beam structures using dynamic analysis. This procedure allows to determine the location of structural changes in the beam and the degree of their severity by analyzing the variations of natural frequencies, the mode shapes and the curvatures of the intact and damaged states. For damage identification, a simplified relationship between local changes in mass and/or stiffness and variations in natural frequency is established. These local changes are represented by damage coefficients, which are estimated by linear regression along the structure. The criterion for determining the location of the damage is defined as the position at which the error in estimating these coefficients is the smallest. Then, the type of damage and its severity are determined by analyzing the values of these estimated coefficients. The effectiveness of the proposed procedure was confirmed by numerical simulations followed by experiment verification.

Keywords: Structural modification, single damage identification, frequency shift, mode shape

1. Introduction

The past few decades have seen a rapid growth in the development of structural health monitoring tools thanks to tremendous technological advances. Consequently, the detection of structural damage has now become one of the important parts of assessing the condition of engineering structures. Since damage can cause changes in the dynamic behavior of structures [1, 2], it is obvious that these unnoticed and untreated structural changes can have serious consequences.

Structural damage detection by monitoring the dynamic behavior of structures using modal parameters has been the subject of numerous studies [3, 4]. Changes in dynamic characteristics such as natural frequencies, mode shapes, and damping ratios are the most common parameters used in damage detection. However, damping ratios are less commonly used for damage detection than changes in natural frequencies or mode shapes as it is sensitive to environmental factors such as humidity and temperature [5].

Studies based on comparisons of modal shapes and their curvature before and after damage exploit the fact that these parameters are sensitive to the presence of damage [6–9]. Studies [10, 11] show that the use of additional modal parameters, in combination with mode shapes and their derivatives, can provide a more reliable assessment of damage identification. However, these methods mainly depend on the number of measurement points for accurate damage assessment, which is often difficult to achieve in real conditions. Also, techniques using only mode shapes or their derivatives are limited to identifying the location of the damage, without assessing the severity.

Damage detection methods using frequency shift has been introduced in many studies as natural frequencies are independent of the measurement site and can be measured more accurately than mode shape and damping [12]. Thus, Patil and Maiti [13] developed a crack detection technique that uses a rotational spring model to simulate the crack effect in the beam, with the damage index being an indicator of how much strain energy is stored in the spring. Dahak et al. [14] presented a study where the damaged zone was distinguished by the classification of the first four frequencies of the structure. Sha et al. [15] developed a damage detection method that combines relative natural frequency changes and Bayesian inference to detect damage in beams. Surace and Bovsunovskii [16] used the ratios between natural frequencies of different modes as a characteristic of damage. Gillich and Praisach [17] discovered the damage location through a pattern recognition problem of measured frequency changes. Le et al. [18] used a first-order estimate between the relative frequency variation and the damage parameters to determine the damage. In addition, in [10, 11, 19] the use of the relationship between natural frequency variation and modal curvature for damage detection was discussed.

Significant improvements in computing power and advances in sensor technology have enabled machine learning techniques to be used in damage detection applications. Lee [20] constructed a set of training patterns of a neural network for damage detection in pipe-type beams using changes in natural frequencies. Other methods such as bee algorithm [21], hybrid optimization [22] and particle swarm optimization [23] have been applied for damage detection. In general, these methods are effective but cause computational burden while trying to get convergence of the damage identification algorithm.

Among the above studies, methods using natural frequency shift seem to be simple, accurate and convenient for single crack detection in beams. These methods are based on using natural frequency shift and modal curvature to produce contour lines along the entire length of the beam. The intersection of these contour lines then serves to manually locate the damage by visual identification of these intersections. However, damage identification becomes less accurate when several of these contour lines do not have a mutual intersection point [10, 11, 19]. In addition, it is important to note that variation in modal parameters occurs not only from the appearance of a crack, but also from a local change in the mass

of the structure.

Summarizing the above, this work is aimed at establishing a simplified relationship between changes in natural frequency and local changes in the stiffness and mass of the beam, either separately or simultaneously. Based on this relation, a procedure for detecting a single damage in beams is introduced. This procedure can be used to simultaneously detect and quantify local changes in the mass and/or stiffness of a beam. Numerical examples and experimental tests were used to validate this procedure.

The rest of the article is organized as follows. First, a general dynamic analysis is discussed in Section 2. Then, damage analysis and a proposed procedure for damage identification are introduced in Section 3. Next, the focus of the work shifts to the application of proposed procedure to numerical and experimental tests with different boundary conditions in Section 4 and Section 5. Finally, a conclusion is given in Section 6.

2. Theoretical formulation

Consider an Euler–Bernoulli beam with the following equation of motion:

$$\frac{\partial^2}{\partial x^2}\left(EI(x)\frac{\partial^2 y(x,t)}{\partial x^2}\right) - P\frac{\partial^2 y(x,t)}{\partial x^2} + \mu(x)\frac{\partial^2 y(x,t)}{\partial t^2} = 0 \tag{1}$$

where $y(x,t)$ is the displacement of the beam at a coordinate x at time t. P, μ and $EI(x)$ are axial force, the mass per unit length and bending stiffness, respectively.

The solution of Eq. (1) is obtained by separation of variables. Suppose that the displacement can be represented as two parts: one depending on the position x and the other depending on time t as follows:

$$y(x,t) = \phi_i(x)y(t) \tag{2}$$

After substituting Eq. (2) into Eq. (1) and some mathematical rearrangements, the following equation is obtained:

$$\left(EI(x)\phi_i''(x)\right)'' - P\phi_i''(x) - \lambda_i\mu(x)\phi_i(x) = 0 \tag{3}$$

where λ_i and ϕ_i are eigenvalue and mode shape of the i^{th} mode, respectively.

Multiplying Eq.(3) by any function $u(x)$ that satisfies the same boundary conditions as the modes and continuing the mathematical transformations of this equation (presented in Appendix A), one can arrive at the following equation:

$$\int_0^L EI(x)\phi_i''(x)u''(x)dx + P\int_0^L \phi_i'(x)u'(x)dx - \lambda_i\int_0^L \mu(x)\phi_i(x)u(x)dx = 0 \tag{4}$$

Consider two cases when function $u(x)$ satisfies the same boundary conditions as the modes:

Case 1. When $u(x) = \phi_i(x)$, expression (4) becomes:

$$\int_0^L EI(x)\phi_i''^2(x)dx + P\int_0^L \phi_i'^2(x)dx - \lambda_i \int_0^L \mu(x)\phi_i^2(x)dx = 0 \tag{5}$$

Defining the parameter γ_i as:

$$\gamma_i = \frac{\int_0^L EI(x)\phi_i''^2(x)dx}{P\int_0^L \phi_i'^2(x)dx} \tag{6}$$

allows to express the eigenvalue λ_i as a function of bending stiffness:

$$\lambda_i = \frac{1+\gamma_i}{\gamma_i}\frac{\int_0^L EI(x)\phi_i''^2(x)dx}{\int_0^L \mu(x)\phi_i^2(x)dx} \tag{7}$$

When $P = 0$, expression (7) becomes:

$$\lambda_i = \frac{\int_0^L EI(x)\phi_i''^2(x)dx}{\int_0^L \mu(x)\phi_i^2(x)dx} \tag{8}$$

Case 2. When $u(x) = \phi_j(x)$, the modes are orthogonal with respect to the mass density $\mu(x)$:

$$\int_0^L \mu(x)\phi_i(x)\phi_j(x)dx = 0;\ \forall i \neq j \tag{9}$$

Thus, Eq. (4) becomes:

$$\int_0^L EI(x)\phi_i''(x)\phi_j''(x)dx + P\int_0^L \phi_i'(x)\phi_j'(x)dx = 0 \tag{10}$$

If the axial force $P = 0$, Eq. (10) turns out to:

$$\int_0^L EI(x)\phi_i''(x)\phi_j''(x)dx = 0 \tag{11}$$

The above equation represents the orthogonality of the curvatures with respect to the bending stiffness.

3. Damage analysis

Consider a change due to a local variation in bending stiffness $\Delta EI(x)$ and/or mass $\mu(x)$:

$$\overline{EI}(x) = EI(x) + \Delta EI(x) \tag{12}$$

$$\overline{\mu}(x) = \mu(x) + \Delta\mu(x) \tag{13}$$

These modifications are assumed to be sufficiently small to make a first-order approximation in this work. These variations cause new natural frequencies, eigenvalues and mode shapes.

$$\overline{f_i}(x) = f_i(x) + \Delta f_i(x) \tag{14}$$

$$\overline{\lambda_i}(x) = \lambda_i(x) + \Delta\lambda_i(x) \tag{15}$$

$$\overline{\phi_i}(x) = \phi_i(x) + \Delta\phi_i(x) \tag{16}$$

The change in mode shape $\Delta\phi_i(x)$ can be expressed using the basis of the normal modes $\left\{\phi_j\right\}_{j=1}^{\infty}$, as follows:

$$\Delta\phi_i(x) = \sum_{j=1}^{\infty} \eta_{ij}\phi_j(x) \tag{17}$$

The changed mode shape $\overline{\phi_i}(x)$ and eigenvalue $\overline{\lambda_i}(x)$ must satisfy Eq. (4):

$$\int_0^L \left(\overline{EI}(x)\overline{\phi}_i''(x)u''(x) + P\overline{\phi}_i'(x)u'(x) - \overline{\lambda}_i\overline{\mu}(x)\overline{\phi}_i(x)u(x)\right)dx = 0 \tag{18}$$

By subtraction between Eq. (18) and Eq. (4) with $u(x) = \phi_i(x)$ given in Appendix B, one can get:

$$\int_0^L \Delta EI(x)\phi_i''^2(x)dx - \lambda_i \int_0^L \Delta\mu(x)\phi_i^2(x)dx - \Delta\lambda_i \int_0^L \mu(x)\phi_i^2(x)dx \approx 0 \tag{19}$$

From (7) and (19), the relative variation of the eigenvalue can be expressed as:

$$\frac{\Delta\lambda_i}{\lambda_i} \approx \frac{\gamma_i}{1+\gamma_i} \frac{\int_0^L \Delta EI(x)\phi_i''^2(x)dx}{\int_0^L EI(x)\phi_i''^2(x)dx} - \frac{\int_0^L \Delta\mu(x)\phi_i^2(x)dx}{\int_0^L \mu(x)\phi_i^2(x)dx} \tag{20}$$

The variations in mass and stiffness are assumed to be local and around x_0 on the interval Ω of length ΔL with $\Delta L << L$.

$$\int_0^L \Delta EI(x)\phi_i''^2(x)dx \approx \left(\int_\Omega \Delta EI(x)dx\right)\phi_i''^2(x_0) \tag{21}$$

$$\int_0^L \Delta\mu(x)\phi_i^2(x)dx \approx \left(\int_\Omega \Delta\mu(x)dx\right)\phi_i^2(x_0) \tag{22}$$

From the expression $\lambda_i = (2\pi f_i)^2$, one can obtain (see details in Appendix C):

$$\frac{\Delta\lambda_i}{\lambda_i} \approx 2\frac{\Delta f_i}{f_i} \tag{23}$$

From Eq. (20), the relative variation of each natural frequency can be expressed as:

$$\frac{\Delta f_i}{f_i} \approx \frac{\gamma_i}{1+\gamma_i} \frac{\left(\int_\Omega \Delta EI(x)dx\right)\phi_i''^2(x_0)}{2\int_0^L EI(x)\phi_i''^2(x)dx} - \frac{\left(\int_\Omega \Delta\mu(x)dx\right)\phi_i^2(x_0)}{2\int_0^L \mu(x)\phi_i''^2(x)dx} \tag{24}$$

The bending stiffness and the density are assumed to be initially constant ($EI(x) = EI$ and $\mu(x) = \mu$). The variations on the interval Ω are assumed to be $\Delta EI(x) = \Delta EI$ and $\Delta\mu(x) = \Delta\mu$. Thus, the relative variation of each natural frequency can be rewritten as:

$$\frac{\Delta f_i}{f_i} \approx \frac{\gamma_i}{1+\gamma_i} \frac{\Delta EI \Delta L}{2EI} \frac{\phi_i''^2(x_0)}{\left\|\phi_i''\right\|_2^2} - \frac{\Delta\mu\Delta L}{2\mu} \frac{\phi_i^2(x_0)}{\left\|\phi_i\right\|_2^2} \tag{25}$$

When the axial force P tends to be zero, γ_i tends to infinity in (6). Thus, the above equation becomes:

$$\frac{\Delta f_i}{f_i} \approx \delta_{\mathrm{K}} \frac{\phi_i''^2(x_0)}{\left\|\phi_i''\right\|_2^2} + \delta_{\mathrm{M}} \frac{\phi_i^2(x_0)}{\|\phi_i\|_2^2} \tag{26}$$

where $\delta_{\mathrm{K}} = \dfrac{\Delta EI \Delta L}{2EI}$ and $\delta_{\mathrm{M}} = -\dfrac{\Delta\mu\Delta L}{2\mu}$ represent the relative local variation of bending stiffness and mass, respectively.

It can be seen that the natural frequency of the beam varies with a local changes in stiffness and/or mass.

In the case of a change in bending stiffness due to damage and neglecting the influence of mass change, Eq. (26) becomes:

$$\frac{\Delta f_i}{f_i} \approx \delta_{\mathrm{K}} \frac{\phi_i''^2(x_0)}{\left\|\phi_i''\right\|_2^2} \tag{27}$$

Eq. (27) represents the relationship between the relative frequency shift and the mode shape curvature of the intact state of a beam. A similar form of this relationship was used for damage detection in [11, 17, 19, 24]. However, these studies do not consider the effect of a local mass change, which can lead to false identification results.

In the case of the mass change only, the relative change of the natural frequency in Eq. (26) can be rewritten as:

$$\frac{\Delta f_i}{f_i} \approx \delta_{\mathrm{M}} \frac{\phi_i^2(x_0)}{\left\|\phi_i\right\|_2^2} \tag{28}$$

Eq. (28) represents the relationship between the relative frequency shift and the mode shape of the intact state.

Finally, for damage location identification, the relationship in (26) is transformed into the following form:

$$\delta_{\mathrm{K}} \frac{\phi_i''^2(x_0) f_i}{\left\|\phi_i''\right\|_2^2 \Delta f_i} + \delta_{\mathrm{M}} \frac{\phi_i^2(x_0) f_i}{\left\|\phi_i\right\|_2^2 \Delta f_i} - 1 \approx 0 \tag{29}$$

δ_{K} and δ_{M} are considered constants, depending only on the degree of the local changes. These local changes in the stiffness and/or mass of the damaged element should be taken as a general physical measure of the severity of the damage, rather than its geometric shape. For example, cracks often have an irregular shape, whose dimensions cannot be accurately determined.

Summing up the presented analysis of the damage identification in the beam, first of all, the location of the damage is identified, followed by an assessment of the degree of its severity. The detailed steps for the proposed damage identification procedure are presented in the Table. 1.

Table 1
Modification identification procedure

1) Divide the beam into $x_k = 0, ..., \mathrm{L}$
2) For each location x_k:
- Compute the following values for all n modes: $X_{i,k} = \dfrac{\phi_i''^2(x_k) f_i}{\left\|\phi_i''\right\|_2^2 \Delta f_i}$, $Y_{i,k} = \dfrac{\phi_i^2(x_k) f_i}{\left\|\phi_i\right\|_2^2 \Delta f_i}$;
- Do linear regression of all n modes $(X_{1,k}, Y_{1,k}), ..., (X_{n,k}, Y_{n,k})$: $f(X, Y) = \delta_{\mathrm{K}} X + \delta_{\mathrm{M}} Y - 1$
- Calculate coefficients $(\delta_{\mathrm{K}}^k, \delta_{\mathrm{M}}^k)$ and the error $\varepsilon_k = \dfrac{\sum_{i=1}^{n} (\delta_{\mathrm{K}}^k X_i + \delta_{\mathrm{M}}^k Y_i - 1)^2}{n}$
3) Draw ε_k. The minimum value ε_{min} indicates the location of the modification at x_0.
4) The damage coefficients $(\delta_{\mathrm{K}}, \delta_{\mathrm{M}})$ are determined from the corresponding values $(\delta_{\mathrm{K}}^k, \delta_{\mathrm{M}}^k)$ at the identified damage location x_0.
5) Consequently, the change in mass and/or in stiffness are identified.

4. Numerical tests

In this section, the proposed procedure is validated by analyzing the model simulated in ANSYS APDL. The numerical tests were carried out for a steel beam of Young's modulus E = 2e11Pa, and density ρ = 7850kg/m^3. The beam of 1000mm in length, 40mm in width, and 6mm in height were used for these simulations. The tests were performed with

different scenarios under different boundary conditions. These scenarios are chosen to check the efficiency of the proposed procedure when different structural modifications are present: increase/decrease in mass/stiffness at different locations.

4.1. Clamped-simply supported beams

Six cases are considered with different modification parameters for a damage simulation in a clamped-simply supported beam. x_0, b_0, and h_0 are the position, width, and height at local modification, respectively. The interval Ω is 2mm for all simulations of local changes. These cases are summarized in Table 2.

In cases, 1 to 4, the geometric dimensions of these beams are the same as those in the intact state. Only local mass density is modified in the first two cases. This change is equivalent to about 15% local mass increase in the first case, and about 20% local mass decrease in the second case. In cases 3 and 4, only the local elastic modulus is adjusted to change the bending stiffness by a 10% decrease and a 5% increase while keeping the mass density constant. Examples of cross-sectional reduction are given in cases 5 and 6, which leads to a change in both the mass density and the bending stiffness. Equivalent changes in local stiffness and mass are calculated for each case. In each case, the first five modal frequencies of the cantilever beam were used for calculations. These data are presented in Table 3.

By following the steps presented in Table 1, the calculated error values are plotted. The minimum values ε_{min} of these curves indicate the modified location. The identified location of changes in mass and bending stiffness are shown in Figures 1 and 2, respectively. The red dashed line marks the actual position of the modification on the beam. Fig. 3 shows the determined result of the damage location in the case of local change in cross-section geometry.

The results of determining the extent of the modifications are given in Table. 4. It can be seen that they are very close to the data chosen for simulations in determining both the location and the degree of the modifications.

4.2. Cantilever beams

Six cases are considered with different modification parameters for cantilever beam. These cases are summarized in Table 5. The local modulus of elasticity was changed to decrease the bending stiffness by 5% and increase it by 10% for cases 1 and 2, respectively.

In the third case, the local mass increase is 10%, and in the fourth case, the local mass loss is 20%. The changes in both the mass density and the elastic modulus due to the reduction of the cross-section are given in cases 5 and 6. The first five frequencies for these cases are presented in Table. 6.

Table 2
Scenarios for numerical tests for clamped-simply supported beam.

Case No.	x_0 (mm)	b_0 (mm)	h_0 (mm)	E_0 (Pa)	ρ_0(kg/m^3)	$\frac{\Delta EI}{EI}$ (%)	$\frac{\Delta\mu}{\mu}$ (%)
Intact	-	40	6	2e11	7850	-	-
1	300	40	6	2e11	9030	-	15.03
2	600	40	6	2e11	6280	-	-20.00
3	300	40	6	1.8e11	7850	-10.00	-
4	500	40	6	2.1e11	7850	5.00	-
5	400	35	6	2e11	7850	-12.5	-12.5
6	700	40	5.8	2e11	7850	-9.67	-3.33

Table 3
Frequencies for numerical tests for clamped-simply supported beam.

Case No.	Natural frequency (Hz)				
	Mode 1	Mode 2	Mode 3	Mode 4	Mode 5
Intact	21.4530	69.5181	145.0328	247.9883	378.3667
1	21.4506	69.4947	145.0058	247.9878	378.2834
2	21.4627	69.5207	145.0701	248.0546	378.3798
3	21.4528	69.5059	145.0157	247.9878	378.3049
4	21.4543	69.5190	145.0446	247.9920	378.3970
5	21.4549	69.5189	145.0323	247.9789	378.3640
6	21.4507	69.5105	145.0327	247.9667	378.3145

The results of determining the modification sites are shown in Figs. 4, 6, and 7 for the local mass change, local stiffness change and local cross-section reduction, respectively. The actual modified positions are marked with red dashed lines. It can be seen that the minimum values ε_{min} of these curves coincide with the actual modification positions. However, these figures have two symmetric minima due to the relationship between the mode shape and the curvature of the cantilever beam given in Eq. (D.12).

The proposed procedure provides information about two possible modification positions: the actual location of the modification and its fictitious counterpart on the symmetrical part. The actual modification site can be clarified if additional information about the modification is known i.e. change in mass or stiffness. It can be easily detected by comparing the difference between the mode shapes of the modified state and those of the intact

Table 4
Results estimated from numerical tests for clamped-simply supported beam.

Case No.	Exact value			Identified value		
	x_0 (mm)	$\frac{\Delta EI}{EI}$ (%)	$\frac{\Delta\mu}{\mu}$ (%)	x_0 (mm)	$\frac{\Delta EI}{EI}$ (%)	$\frac{\Delta\mu}{\mu}$ (%)
1	300	-	15.03	301.3	0.47	15.41
2	600	-	-20.00	600.6	0.77	-19.17
3	300	-10.00	-	300.3	-10.64	0.46
4	500	5.00	-	498.5	5.20	0.48
5	400	-12.50	-12.50	402.4	-14.44	12.65
6	700	-9.67	-3.33	698.7	-10.60	-3.05

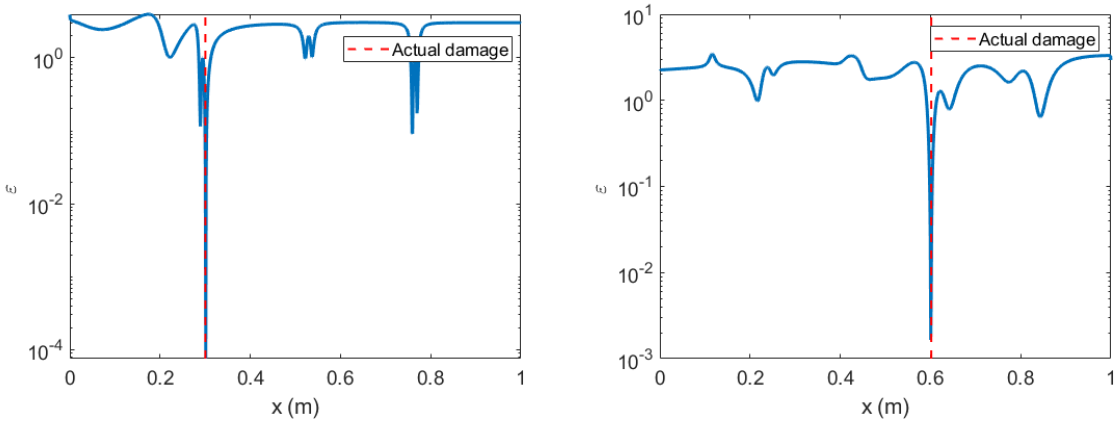

Fig. 1. Damage detection for changes in mass for case 1 (left) and case 2 (right)

state [6].

The example of reduction in stiffness was considered in the first case. The proposed procedure detects the actual reduction in stiffness on the left side of the beam. In addition, it detects in a pseudo-symmetric position on the right side of the beam an increase in mass. This is because the extra mass at that location can cause the same change in natural frequency.

An example of using a modal curvature comparison between modified and intact state to determine the actual position can be seen in Fig. 5 for cases 1 and 2. The results of determining the extent of the modifications are given in Table. 7. They are very close to the exact ones.

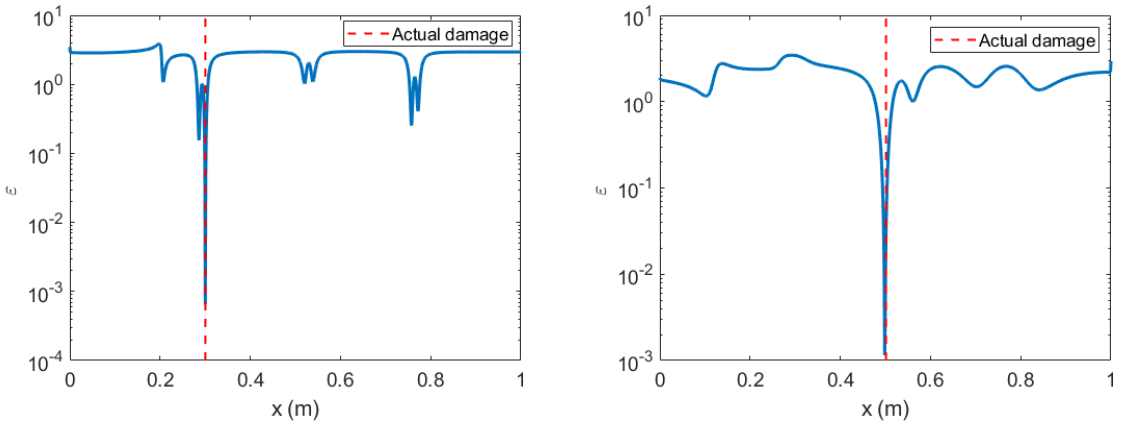

Fig. 2. Damage detection for changes in stiffness for case 3 (left) and case 4 (right)

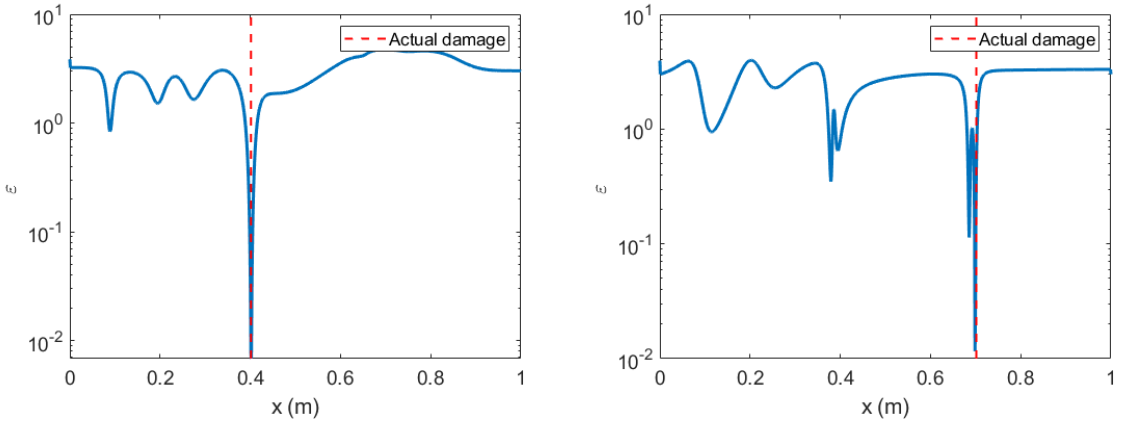

Fig. 3. Damage detection for changes in cross-section for case 5 (left) and case 6 (right)

4.3. Clamped-clamped beams

This section describes six numerical tests for a pinched beam with the following local modifications. In the first case, a local decrease in mass density by about 5% is considered. In the second case, a local increase in stiffness by 10% is considered. In the third case, the local elastic modulus and mass density are reduced by about 5% and 10%, respectively. In the fourth case, the same parameters are increased by 10% and approximately 15%, respectively. In the fifth and sixth cases, local changes in the mass density and elastic modulus of 12.5% occur due to variations in the cross-section. The parameters of each case are presented in Table. 8. The first five frequencies for all these cases are given in

Table 5
Scenarios for numerical tests for cantilever beam.

Case No.	x_0 (mm)	b_0 (mm)	h_0 (mm)	E_0 (Pa)	ρ_0(kg/m^3)	$\frac{\Delta EI}{EI}$ (%)	$\frac{\Delta\mu}{\mu}$ (%)
Intact	-	40	6	2e11	7850	-	-
1	300	40	6	1.9e11	7850	-5.00	-
2	800	40	6	2.2e11	7850	10.00	-
3	300	40	6	2e11	8640	-	10.06
4	400	40	6	2e11	6280	-	-20.00
5	400	35	6	2e11	7850	-12.50	-12.50
6	450	40	5.5	2e11	7850	-22.97	-8.33

Table 6
Frequencies for numerical tests for cantilever beam.

Case No.	Natural frequency (Hz)				
	Mode 1	Mode 2	Mode 3	Mode 4	Mode 5
Intact	4.8923	30.6579	85.8373	168.1903	277.9952
1	4.8919	30.6573	85.8295	168.1849	277.9919
2	4.8925	30.6589	85.8486	168.2250	278.0398
3	4.8923	30.6545	85.8176	168.1780	277.9897
4	4.8925	30.6694	85.8564	168.2038	278.1032
5	4.8918	30.6590	85.8382	168.1885	277.9850
6	4.8917	30.6519	85.8351	168.1619	277.9668

Table. 9.

The results of determining the modification sites are illustrated in Figs. 8, 9, and 10. It can be seen that these curves have two symmetric minima. The actual modified positions are marked with red dashed lines and coincide with one of the minimum values ε_{min}. In contrast to the symmetry of the results for cantilever beams, which is due to the relationship between mode shape and curvature, the reason for the symmetry of solutions in this case is related to the symmetry of the mode shapes and curvatures. Thus, the same local changes at the two symmetry positions will give the same frequency shifts.

However, when the change happens in the middle of the beam (case 4), the identified results are unique as shown in Fig. 9.

The actual modification site can be found by comparing the difference between the

Table 7
Results estimated from numerical tests for cantilever beam.

Case No.	Exact value			Identified value		
	x_0 (mm)	$\frac{\Delta EI}{EI}$ (%)	$\frac{\Delta\mu}{\mu}$ (%)	x_0 (mm)	$\frac{\Delta EI}{EI}$ (%)	$\frac{\Delta\mu}{\mu}$ (%)
1	300	-5.00	-	301.0	-5.28	-0.02
2	800	10.00	-	799.8	8.17	-1.77
3	300	-	10.06	301.0	0.11	10.15
4	400	-	-20.00	399.9	0.40	-19.68
5	400	-12.5	-12.5	400.7	-14.19	-12.43
6	450	-22.97	-8.33	447.4	-21.88	-9.67

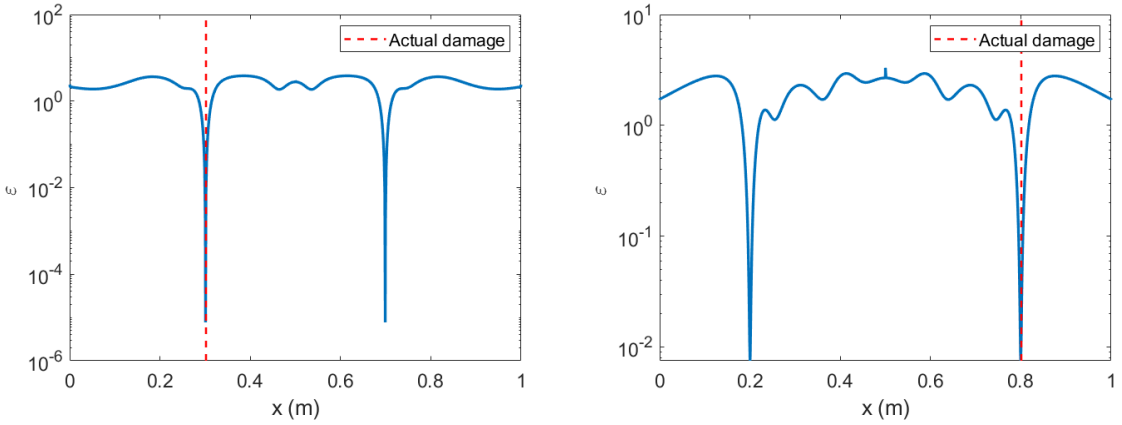

Fig. 4. Damage detection for changes in stiffness for case 1 (left) and case 2 (right)

mode shapes of the modified state and those of the intact state as shown in Fig. 11.

Table. 10 presents the results determining the extent of the modifications. The identified parameters are very close to the exact ones. These results of numerical tests confirm the effectiveness of the proposed technique.

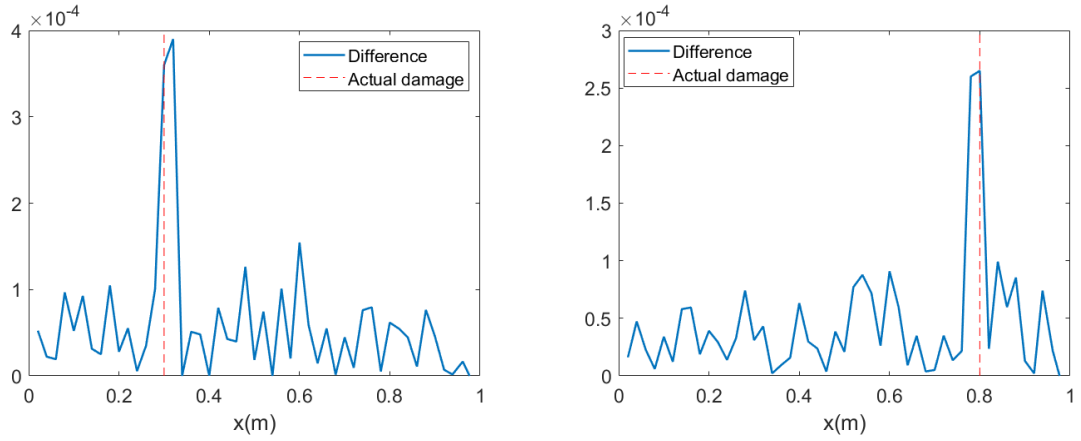

Fig. 5. Actual modification detection in curvature changes for case 1 (left) and case 2 (right).

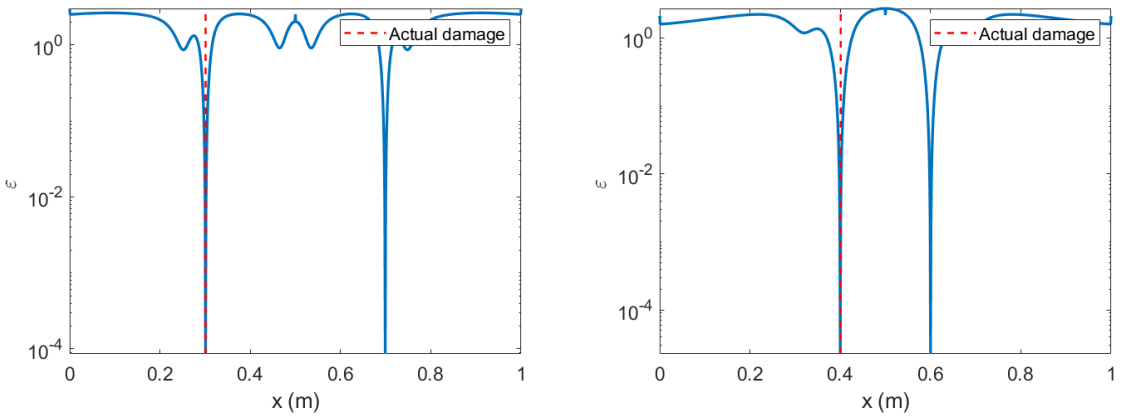

Fig. 6. Damage detection for changes in mass for case 3 (left) and case 4 (right)

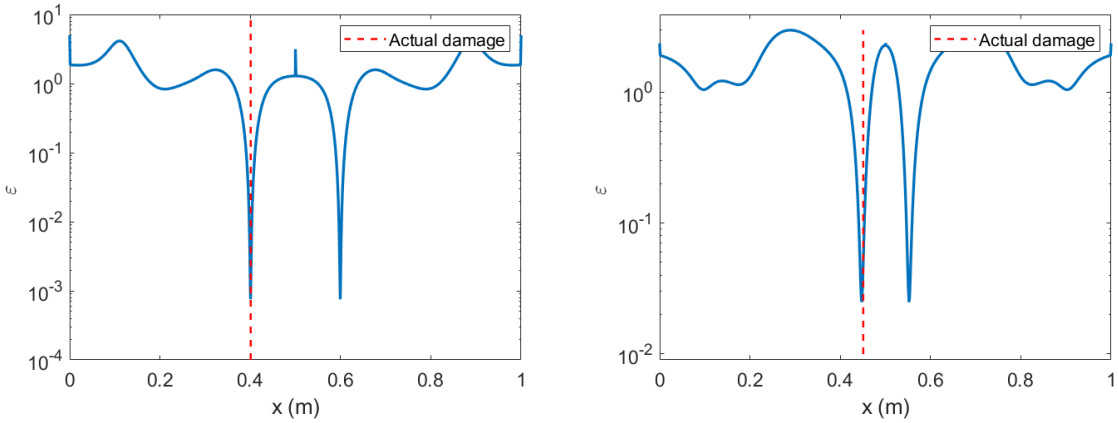

Fig. 7. Damage detection for changes in cross-section for case 5 (left) and case 6 (right)

Table 8
Scenarios for numerical tests for clamped-clamped beam.

Case No.	x_0 (mm)	b_0 (mm)	h_0 (mm)	E_0 (Pa)	ρ_0(kg/m^3)	$\frac{\Delta EI}{EI}$ (%)	$\frac{\Delta \mu}{\mu}$ (%)
Intact	-	40	6	2e11	7850	-	-
1	200	40	6	2e11	7460	-	-4.97
2	400	40	6	2.2e11	7850	10.00	-
3	300	40	6	1.9e11	7070	-5.00	-9.94
4	500	40	6	2.2e11	9030	10.00	15.03
5	350	35	6	2e11	7850	-12.5	-12.5
6	450	45	6	2e11	7850	12.5	12.5

Table 9
Frequencies for numerical tests for clamped-clamped beam.

Case No.	Natural frequency (Hz)				
	Mode 1	Mode 2	Mode 3	Mode 4	Mode 5
Intact	31.1303	85.8074	168.2035	278.0186	415.2543
1	31.1308	85.8136	168.2225	278.0427	415.2637
2	31.1333	85.8147	168.2101	278.0682	415.2562
3	31.1335	85.8188	168.2105	278.0206	415.2885
4	31.1226	85.8073	168.1846	278.0185	415.2054
5	31.1338	85.8083	168.2037	278.0103	415.2432
6	31.1256	85.8067	168.2011	278.0156	415.2495

Table 10
Results estimated from numerical tests for clamped-clamped beam.

Case No.	Exact value			Identified value		
	x_0 (mm)	$\frac{\Delta EI}{EI}$ (%)	$\frac{\Delta\mu}{\mu}$ (%)	x_0 (mm)	$\frac{\Delta EI}{EI}$ (%)	$\frac{\Delta\mu}{\mu}$ (%)
1	200	0.00	-4.97	201.0	1.36	-4.08
2	400	10.00	0.00	400.0	9.41	0.26
3	300	-9.94	-5.00	300.0	-9.77	-5.06
4	500	10.00	15.03	496.0	10.24	16.20
5	350	-12.5	-12.5	349.0	-14.03	-12.29
6	450	12.5	12.5	450.0	11.35	12.69

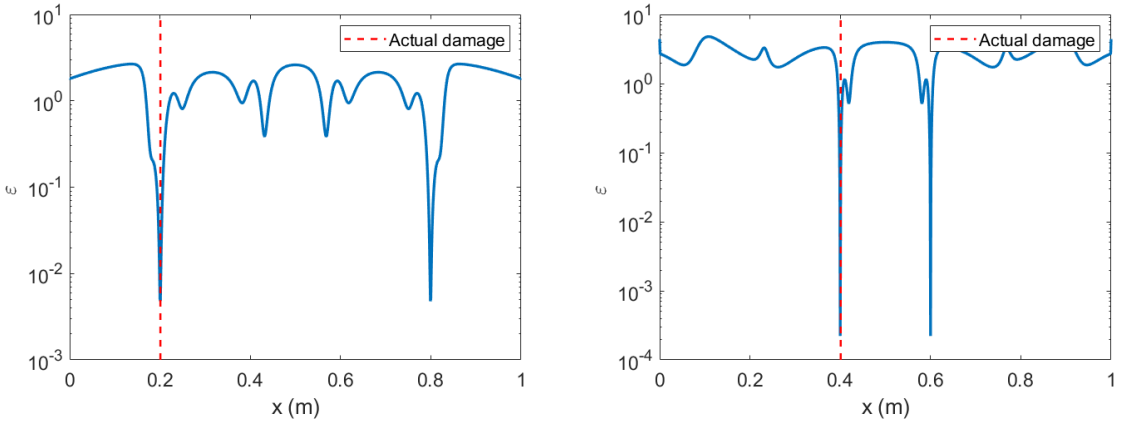

Fig. 8. Damage detection for changes in mass for case 1 (left) and stiffness for case 2 (right)

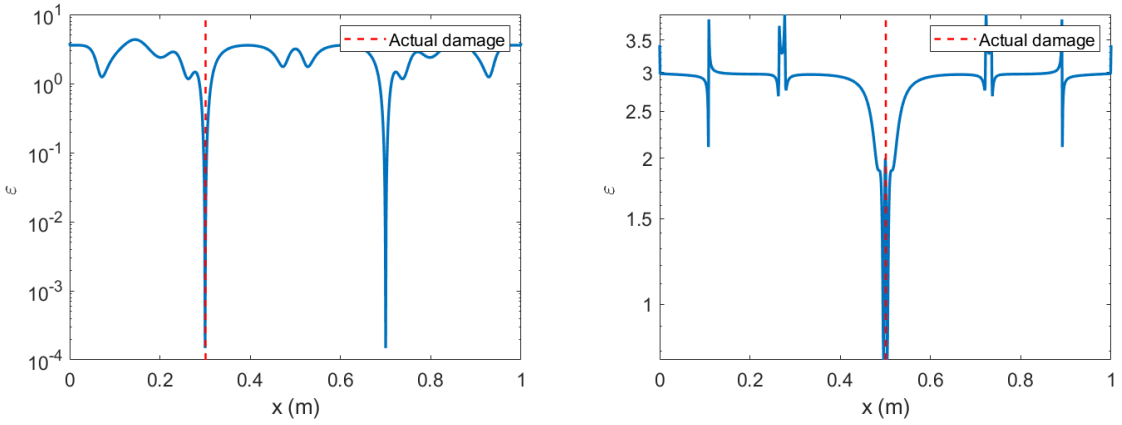

Fig. 9. Damage detection for both stiffness and mass changes for case 3 (left) and case 4 (right)

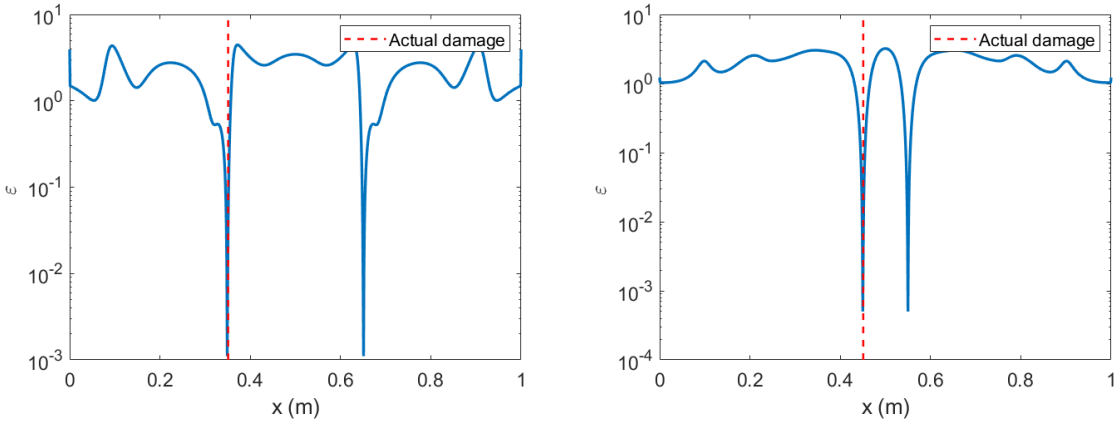

Fig. 10. Damage detection for changes in cross-section for case 5 (left) and case 6 (right)

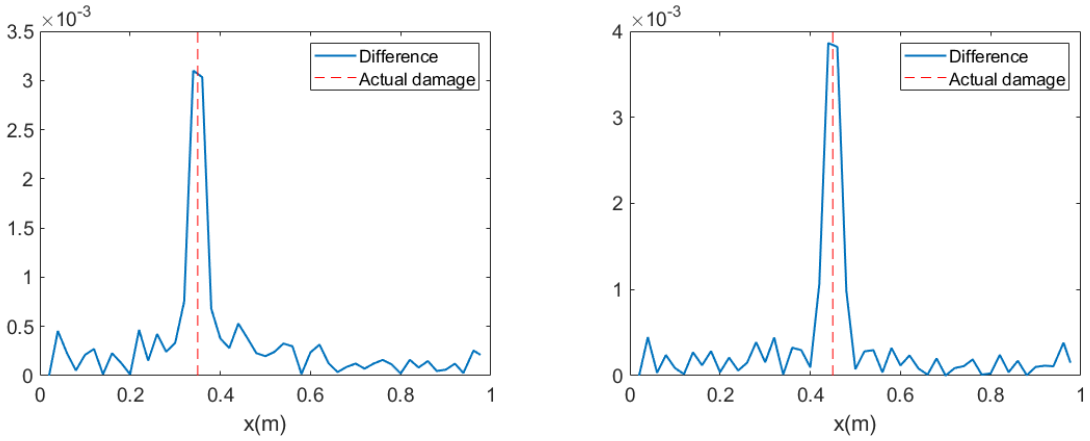

Fig. 11. Actual modification detection in curvature changes for case 5 (left) and case 6 (right).

It has been shown that the exact location can be determined without doubt by using additional information, such as the difference between the mode shapes or curvatures of the intact state and those of the modified state, or just by visualization of possible damage locations of the structures.

5. Experimental tests

Steel cantilever beams were used to verify the proposed damage identification procedure. Tested beams have the following physical parameters: length L = 1005mm, width B = 40mm and height H = 10mm. The material of the beams has Young's modulus E = 200GPa, and density ρ = 7850kg/m^3. Experimental tests were considered for two scenarios: one is for identifying an additional mass, and the other is for identifying a cross-section reduction. The experimental setup is shown in Figure. 12.

In the first scenario two experimental tests were carried out. At the first test, a 10g rectangular magnet was attached to a chosen location on the beam, without changing local stiffness. This change corresponds to a local mass increase of $\Delta m_1/m \approx 0.32\%$. For the second test, another 10g magnet was attached to the first one, which corresponds to an increase of $\Delta m_2/m \approx 0.63\%$. These mass changes are given in Table. 11.

For this testing scenario, the natural frequencies of both intact and modified states were obtained by classical testing performed by the commercial B&K Connect^{TM} software. The identified frequencies of the beams are given in Table. 12. In both cases, the mode shape and the curvature of the intact state are calculated using the analytic formula in Eqs. (D.10) and (D.11).

The results of identified locations of mass changes are shown in Fig. 13. These figures have two symmetric minima due to the relationship between the mode shape and the curvature of the cantilever beam. The results of determining the degree of the modifications are given in Table. 13. The obtained results are in a good agreement with the actual values of the localization of modifications and their quantitative assessment.

In the second scenario, the proposed damage identification procedure was applied to the case of the cross-section reduction where the damage was fabricated by a milling. The produced cut is about 2mm wide and 5mm depth (about 12.5% stiffness loss and 12.5% mass loss per unit length). It was located at a distance of 220mm from the support. The identified localization of the cross-section drop is located at 228mm from the support as represented in Fig. 14. The estimated damage by the proposed procedure for this experimental test is 14.1% in stiffness and 5.6% in mass per unit length. The identified results in two scenarios are in agreement with the actual ones, which validates the proposed procedure.

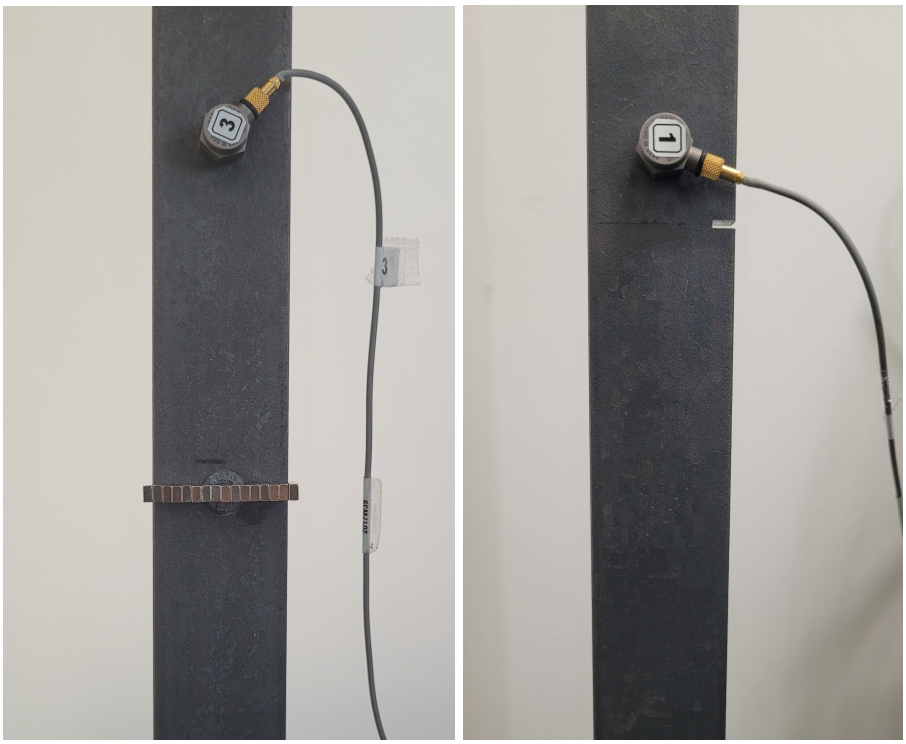

(a) Add mass **(b)** Reduce cross-section

Fig. 12. Experimental setup for cantilever beams

Table 11
Variations in mass for experimental tests for a cantilever beam.

Case No.	x_0 (mm)	Added mass (g)	$\frac{\Delta m}{m}$ (%)
1	300	10	0.32
2	300	20	0.63

Table 12
Frequencies of experimental tests for cantilever beams.

Case No.	Natural frequency (Hz)				
	Mode 1	Mode 2	Mode 3	Mode 4	Mode 5
Intact	7.7691	48.3655	137.3496	277.2691	445.6196
1	7.7688	48.2876	136.8765	276.9507	445.5082
2	7.7679	48.2078	136.4057	276.6315	445.3966
3	7.7674	48.3689	137.3397	277.2396	445.5758

Table 13
Results obtained from experimental tests on a cantilever beam.

Case No.	Actual value		Identified value	
	x_0 (mm)	$\frac{\Delta m}{m}$ (%)	x_0 (mm)	$\frac{\Delta m}{m}$ (%)
1	300	0.32	305.7	0.31
2	300	0.63	303.8	0.61

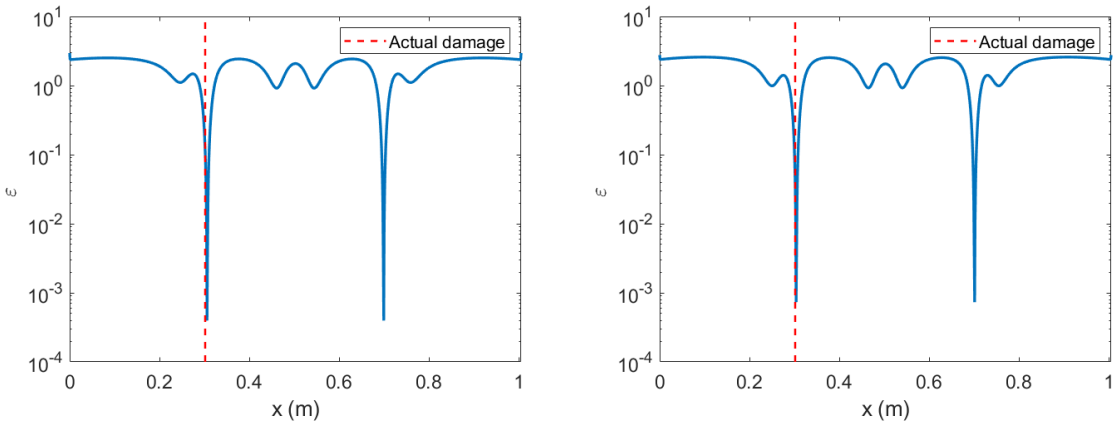

(a) Case 1 **(b)** Case 2

Fig. 13. Damage detection for changes in mass

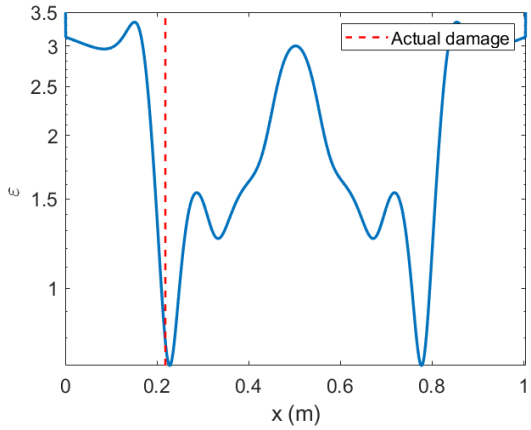

Fig. 14. Damage detection for a change in cross-section

Similarly, the exact location can be determined by using additional information, such as the difference between the mode shapes or curvatures of the intact state and those of the modified one, or just by visualization of possible damaged locations of the structures.

6. Conclusion

This work presents a procedure for localization and quantification of a single structural damage, which can be modeled as local modification in stiffness and mass of a structure. To identify damage, a simplified relationship was established between local changes in mass and/or stiffness and changes in natural frequency. These local changes in mass and stiffness were represented by damage coefficients, which were estimated by linear regression along the structure. The criterion for determining the location of damage was the position in which the error in estimating these coefficients was the least. Then, to quantify the type of damage and its severity, the values of the estimated coefficients mentioned above used.

To validate the procedure, it was numerically tested on cantilever beams with local variations in mass, stiffness or cross-section. These numerical tests were carried out on beams with various boundary conditions. All tested scenarios showed accurate identification of locations and quantification of modeled structural variations. The procedure has been found to offer the following benefits: (i) it localizes the modification site, the extent of change in mass and stiffness; (ii) it requires only natural frequency shifts and intact mode shapes of the intact state that are easily achievable in practice; (iii) it provides a unique solution for identification of modifications in clamped-simply supported beams. Despite all of the above, it does not unambiguously determine the position of damage for cases of cantilever beams and clamped-clamped beams. Due to the symmetry in the boundary

conditions for clamped-clamped beams and the relationship between the mode shapes and the curvatures in cantilever beams, the given procedure identifies two possible modification positions: the real one and the fictitious one. But it was shown that the exact location can be determined without a doubt by using additional information, such as the difference between the mode shapes or curvatures of the intact state and those of the modified one or just by a simple visualization of the structures. Finally, this damage identification procedure was experimentally tested on cantilever beams with local variations in mass and cross section. All tested scenarios showed accurate identification of locations and quantification of structural variations.

In conclusion, the numerical and experimental results show that the proposed procedure can localize and quantify the local variations in mass and stiffness in beams under different boundary conditions.

7. Acknowledgments

We acknowledge with gratitude the funding provided by the French government in the form of a fellowship that has helped to carry out this work.

Appendix A.

Multiplying Eq. (3) by a function $u(x)$ and then taking an integration by part leads to the following relation:

$$\int_0^L \left(EI(x)\phi_i''(x)\right)'' u(x)dx - \int_0^L P\phi_i''(x)u(x)dx - \int_0^L \lambda_i\mu(x)\phi_i(x)u(x)dx = 0 \tag{A.1}$$

The first two parts of Eq. (A.1) are transformed as follows:

$$\begin{aligned}\int_0^L \left(EI(x)\phi_i''(x)\right)'' u(x)dx &= \left[\frac{\partial}{\partial x}\left(EI(x)\phi_i''(x)\right)u(x)\right]_0^L - \int_0^L \left(EI(x)\phi_i''(x)\right)' u'(x)dx \\ &= \left[\frac{\partial}{\partial x}\left(EI(x)\phi_i''(x)\right)u(x)\right]_0^L - \left[EI(x)\phi_i''(x)u'(x)\right]_0^L + \int_0^L EI(x)\phi_i''(x)u''(x)dx\end{aligned} \tag{A.2}$$

and

$$-\int_0^L P\phi_i''(x)u(x)dx = -\left[P\phi_i'(x)u(x)\right]_0^L + \int_0^L P\phi_i'(x)u'(x)dx \tag{A.3}$$

From the above transformations, Eq. (A.1) can be expressed as follows:

$$\int_0^L \left(EI(x)\phi_i''(x)u''(x) + P\phi_i'(x)u'(x) - \lambda_i\mu(x)\phi_i(x)u(x) \right) dx + C = 0 \tag{A.4}$$

where C depends on the boundary condition.

$$C = \left[\frac{\partial}{\partial x} \left(EI(x)\phi_i''(x) \right) u(x) \right]_0^L - \left[EI(x)\phi_i''(x)u'(x) \right]_0^L - \left[P\phi_i'(x)u(x) \right]_0^L \tag{A.5}$$

The quantity C is zero for any function $u(x)$ satisfying the same boundary conditions as the modes for beams satisfying one of the most common boundary conditions such as clamped-simply supported beam ($\phi_i(0) = \phi_i'(0) = \phi_i(L) = \phi_i''(L) = 0$), clamped-free beam ($\phi_i(0) = \phi_i'(0) = \phi_i''(L) = \phi_i'''(L) = 0$ and $P = 0$), clamped-clamped beam ($\phi_i(0) = \phi_i'(0) = \phi_i(L) = \phi_i'(L) = 0$).

$$\int_0^L \left(EI(x)\phi_i''(x)u''(x) + P\phi_i'(x)u'(x) - \lambda_i\mu(x)\phi_i(x)u(x) \right) dx = 0 \tag{A.6}$$

or

$$\int_0^L EI(x)\phi_i''(x)u''(x)dx + P\int_0^L \phi_i'(x)u'(x)dx - \lambda_i \int_0^L \mu(x)\phi_i(x)u(x)dx = 0 \tag{A.7}$$

Appendix B.

Performing subtraction between Eq. (18) and Eq. (4) with $u(x) = \phi_i(x)$ gives:

$$\begin{aligned} &\int_0^L \left(\overline{EI}(x)\overline{\phi_i''}(x) - EI(x)\phi_i''(x) \right)\phi_i''(x)dx + P\int_0^L \left(\overline{\phi_i'}(x) - \phi_i'(x) \right)\phi_i'(x)dx \\ &+ \int_0^L \left(\lambda_i\mu(x)\phi_i(x) - \overline{\lambda_i}\overline{\mu}(x)\overline{\phi_i}(x) \right)\phi_i(x)dx = 0 \end{aligned} \tag{B.1}$$

The parts of the above equation can be approximated as follows:

$$\int_0^L \left(\overline{EI}(x)\overline{\phi_i''}(x) - EI(x)\phi_i''(x) \right)\phi_i''(x)dx \approx \int_0^L EI(x)\Delta\phi_i''(x)\phi_i''(x)dx + \int_0^L \Delta EI(x)\phi_i''^2(x)dx \tag{B.2}$$

$$P\int_0^L \left(\overline{\phi_i'}(x) - \phi_i'(x)\right)\phi_i'(x)dx = P\int_0^L \Delta\phi_i'(x)\phi_i'(x)dx \tag{B.3}$$

and

$$\begin{aligned}&\int_0^L \left(\lambda_i\mu(x)\phi_i(x) - \overline{\lambda_i}\overline{\mu}(x)\overline{\phi_i}(x)\right)\phi_i(x)dx \approx \\ &-\int_0^L \lambda_i\mu(x)\Delta\phi_i\phi_i(x)dx - \int_0^L \lambda_i\Delta\mu(x)\phi_i^2(x)dx - \int_0^L \Delta\lambda_i\mu(x)\phi_i^2(x)dx\end{aligned} \tag{B.4}$$

From the above approximate transformations, Eq. (B.1) becomes:

$$\begin{aligned}&\int_0^L EI(x)\Delta\phi_i''(x)\phi_i''(x)dx + P\int_0^L \Delta\phi_i'(x)\phi_i'(x)dx - \int_0^L \lambda_i\mu(x)\Delta\phi_i\phi_i(x)dx + \\ &+\int_0^L \Delta EI(x)\phi_i''^2(x)dx - \int_0^L \lambda_i\Delta\mu(x)\phi_i^2(x)dx - \int_0^L \Delta\lambda_i\mu(x)\phi_i^2(x)dx \approx 0\end{aligned} \tag{B.5}$$

Combining with Eq. (10) and Eq. (17), the above equation can be transformed to:

$$\begin{aligned}&\eta_{ii}\left(\int_0^L EI(x)\phi_i''^2(x)dx + P\int_0^L \phi_i'^2(x)dx - \lambda_i\int_0^L \mu(x)\phi_i^2(x)dx\right) + \\ &+\left(\int_0^L \Delta EI(x)\phi_i''^2(x)dx - \lambda_i\int_0^L \Delta\mu(x)\phi_i^2(x)dx - \Delta\lambda_i\int_0^L \mu(x)\phi_i^2(x)dx\right) \approx 0\end{aligned} \tag{B.6}$$

The first part of the above equation is zero because of Eq. (5). Thus:

$$\int_0^L \Delta EI(x)\phi_i''^2(x)dx - \lambda_i\int_0^L \Delta\mu(x)\phi_i^2(x)dx - \Delta\lambda_i\int_0^L \mu(x)\phi_i^2(x)dx \approx 0 \tag{B.7}$$

Appendix C.

The eigenvalue can be written as:

$$\lambda = (2\pi f)^2 \tag{C.1}$$

Taking a derivative of λ with respect to f, one gets:

$$\frac{\partial\lambda}{\partial f} = (2\pi)^2 2f \tag{C.2}$$

$$\partial\lambda = (2\pi)^2\, 2f\, \partial f \tag{C.3}$$

Dividing both sides by λ, the above equation becomes:

$$\frac{\partial\lambda}{\lambda} = \frac{(2\pi)^2\, 2f}{\lambda}\, \partial f \tag{C.4}$$

$$\frac{\partial\lambda}{\lambda} = \frac{(2\pi)^2\, 2f}{(2\pi f)^2}\, \partial f \tag{C.5}$$

Simplifying the right part of the above equation, one gets:

$$\frac{\partial\lambda}{\lambda} = \frac{2\partial f}{f} \tag{C.6}$$

or

$$\frac{\Delta\lambda}{\lambda} \approx \frac{2\Delta f}{f} \tag{C.7}$$

Appendix D. Vibrations of beams under different boundary conditions

In this part, free vibration of beams is investigated analytically under four different boundary conditions.

For an intact beam with $EI(x) = EI$ and $\mu(x) = \mu$, the mode shape $\phi(x)$ is represented by the following form:

$$\phi_i(x) = a_1 \sin(\alpha_i x) + a_2 \cos(\alpha_i x) + a_3 \sinh(\alpha_i x) + a_4 \cosh(\alpha_i x) \tag{D.1}$$

with

$$\alpha_i = \sqrt[4]{\frac{\rho A \omega_i^2}{EI}} \tag{D.2}$$

The first three derivatives of Eq. (D.1) are given as follows:

$$\begin{cases} \phi_i(x) = a_1 \sin(\alpha_i x) + a_2 \cos(\alpha_i x) + a_3 \sinh(\alpha_i x) + a_4 \cosh(\alpha_i x) \\ \phi_i'(x) = \alpha_i \left(a_1 \cos(\alpha_i x) - a_2 \sin(\alpha_i x) + a_3 \cosh(\alpha_i x) + a_4 \sinh(\alpha_i x)\right) \\ \phi_i''(x) = \alpha_i^2 \left(-a_1 \sin(\alpha_i x) - a_2 \cos(\alpha_i x) + a_3 \sinh(\alpha_i x) + a_4 \cosh(\alpha_i x)\right) \\ \phi_i'''(x) = \alpha_i^3 \left(-a_1 \cos(\alpha_i x) + a_2 \sin(\alpha_i x) + a_3 \cosh(\alpha_i x) + a_4 \sinh(\alpha_i x)\right) \end{cases} \tag{D.3}$$

where the constants a_1, a_2, a_3, a_4 depends on the boundary conditions,

Appendix D.1. Clamped-simply supported beam

The boundary conditions satisfied by a clamped-simply supported beam are as follows: $\phi_i(0) = 0$, $\phi_i'(0) = 0$, $\phi_i(L) = 0$ and $\phi_i''(L) = 0$. The a_1, a_2, a_3, a_4 of the beam can be represented as follows:

$$a_1 = -a_3;\ a_2 = -a_4;\ a_3 \sinh(\alpha_i L) + a_4 \cosh(\alpha_i L) = 0 \tag{D.4}$$

Substituting the above conditions into Eq. (D.3), after some mathematical operations, the value α_i for the mode n^{th} is determined from the characteristic equation as follows:

$$\sin(\alpha_i L)\cosh(\alpha_i L) - \sinh(\alpha_i L)\cos(\alpha_i L) = 0 \tag{D.5}$$

The mode shape and curvature of the clamped-simply supported beam are given as followed:

$$\phi_i(x) = a_1(\sin(\alpha_i x) - \sinh(\alpha_i x) - \tanh(\alpha_i)(\cos(\alpha_i x) - \cosh(\alpha_i x))) \tag{D.6}$$

$$\phi_i''(x) = -a_1\alpha_i^2(\sin(\alpha_i x) + \sinh(\alpha_i x) - \tanh(\alpha_i)(\cosh(\alpha_i x) + \cos(\alpha_i x))) \tag{D.7}$$

The first five mode shapes and mode shape curvatures of the clamped-simply supported beam are shown in Fig. D.15.

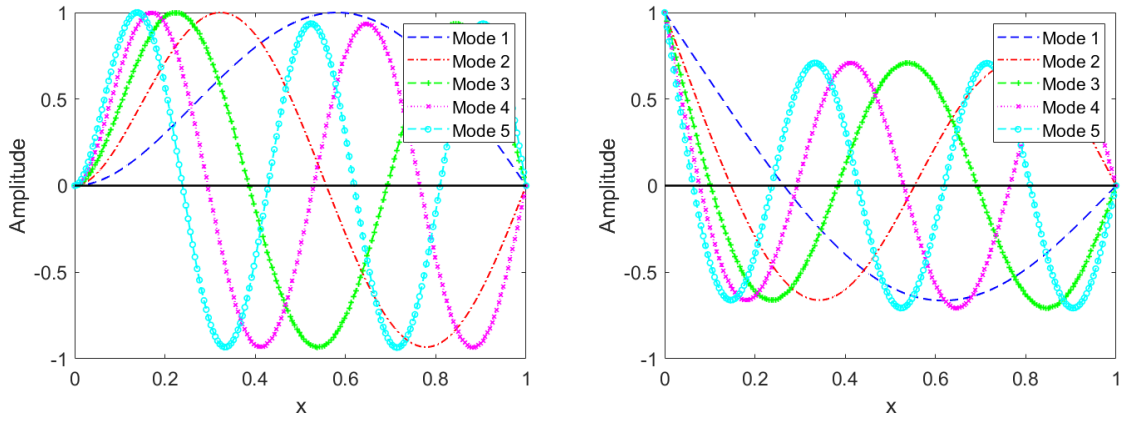

Fig. D.15. Mode shape (left) and curvature (right) of a clamped-simply supported beam

Appendix D.2. Cantilever beam

Applying the boundary condition of a cantilever beam (clamped-free beam): $\phi_i(0) = 0$, $\phi_i'(0) = 0$, $\phi_i''(L) = 0$ and $\phi_i'''(L) = 0$. The constants a_1, a_2, a_3, a_4 can be determined as follows:

$$a_1 = -a_3;\ a_2 = -a_4;\ a_1 = -a_2\frac{\cos(\alpha_i L) + \cosh(\alpha_i L)}{\sin(\alpha_i L) + \sinh(\alpha_i L)} \tag{D.8}$$

The values α_i for modes can be determined from the following characteristic equation:

$$1 + \cos(\alpha_i L)\cosh(\alpha_i L) = 0 \tag{D.9}$$

Substituting Eq. (D.8) into Eq. (D.3), the mode shape and curvature are defined as:

$$\phi_i(x) = a_1\left(\sin(\alpha_i x) - \sinh(\alpha_i x) + \frac{\sin(\alpha_i L) + \sinh(\alpha_i L)}{\cos(\alpha_i L) + \cosh(\alpha_i L)}(\cosh(\alpha_i x) - \cos(\alpha_i x))\right) \tag{D.10}$$

$$\phi_i''(x) = a_1\alpha_i^2\left(-\sin(\alpha_i x) - \sinh(\alpha_i x) + \frac{\sin(\alpha_i L) + \sinh(\alpha_i L)}{\cos(\alpha_i L) + \cosh(\alpha_i L)}(\cos(\alpha_i x) + \cosh(\alpha_i x))\right) \tag{D.11}$$

From Eqs. (D.10) and (D.11), the first five mode shapes and mode shape curvatures of the cantilever beam are shown in Fig. D.16.

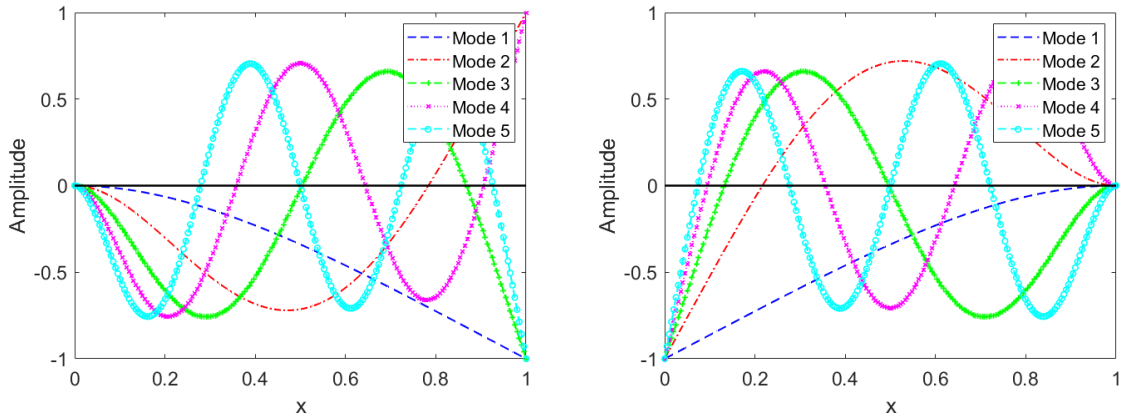

Fig. D.16. Mode shape (left) and curvature (right) of a cantilever beam

There is a relationship between the mode shape and the curvature of the cantilever beam as follows:

$$\phi_i''(x) = (-1)^{i+1}\alpha_i^2\phi_i(L - x) \tag{D.12}$$

The sign of the right part in (D.12) depends on the roots α_i of the equation (D.9). This relationship can be observed graphically in Fig. D.16 and demonstrated later in this section.

From (26) and (D.12), it should be noted that an increase in mass or a decrease in stiffness at the point of symmetry results in the same frequency change in the cantilever beam.

- **Demonstration for the relation** (D.12)

Denote $C = \dfrac{\sin(\alpha_i L) + \sinh(\alpha_i L)}{\cos(\alpha_i L) + \cosh(\alpha_i L)}$, Eq. (D.10) can be written as follows:

$$\begin{aligned}
&\frac{\phi_i(L-x)}{a_1} = \sin(\alpha_i L - \alpha_i x) - \sinh(\alpha_i L - \alpha_i x) + C\left[\cosh(\alpha_i L - \alpha_i x) - \cos(\alpha_i L - \alpha_i x)\right] \\
&= \sin(\alpha_i L)\cos(\alpha_i x) - \cos(\alpha_i L)\sin(\alpha_i x) - \sinh(\alpha_i L)\cosh(\alpha_i x) + \cosh(\alpha_i L)\sinh(\alpha_i x) \\
&+C\left[\cosh(\alpha_i L)\cosh(\alpha_i x) - \sinh(\alpha_i L)\sinh(\alpha_i x)\right] - C\left[\cos(\alpha_i L)\cos(\alpha_i x) + \sin(\alpha_i L)\sin(\alpha_i x)\right] \\
&= \left[-\cos(\alpha_i L) - C\sin(\alpha_i L)\right]\sin(\alpha_i x) + \left[\cosh(\alpha_i L) - C\sinh(\alpha_i L)\right]\sinh(\alpha_i x) + \\
&+\left[\sin(\alpha_i L) - C\cos(\alpha_i L)\right]\cos(\alpha_i x) + \left[-\sinh(\alpha_i L) + C\cosh(\alpha_i L)\right]\cosh(\alpha_i x) + \\
&= C_1\sin(\alpha_i x) + C_2\sinh(\alpha_i x) + C_3\cos(\alpha_i x) + C_4\cosh(\alpha_i x)
\end{aligned} \tag{D.13}$$

$$\frac{\phi_i(L-x)}{a_1} = C_1\sin(\alpha_i x) + C_2\sinh(\alpha_i x) + C_3\cos(\alpha_i x) + C_4\cosh(\alpha_i x) \tag{D.14}$$

Where

$$\begin{aligned}
C_1 &= -\cos(\alpha_i L) - C\sin(\alpha_i L) = -\cos(\alpha_i L) - \frac{\sin(\alpha_i L) + \sinh(\alpha_i L)}{\cos(\alpha_i L) + \cosh(\alpha_i L)}\sin(\alpha_i L) \\
C_1 &= -\frac{\cos^2(\alpha_i L) + \cos(\alpha_i L)\cosh(\alpha_i L) + \sin^2(\alpha_i L) + \sin(\alpha_i L)\sinh(\alpha_i L)}{\cos(\alpha_i L) + \cosh(\alpha_i L)} \\
C_1 &= -\frac{\cos^2(\alpha_i L) + \sin^2(\alpha_i L) + \cos(\alpha_i L)\cosh(\alpha_i L) + \sin(\alpha_i L)\sinh(\alpha_i L)}{\cos(\alpha_i L) + \cosh(\alpha_i L)} \\
C_1 &= -\frac{1 + \cos(\alpha_i L)\cosh(\alpha_i L) + \sin(\alpha_i L)\sinh(\alpha_i L)}{\cos(\alpha_i L) + \cosh(\alpha_i L)} \\
C_1 &= -\frac{\sin(\alpha_i L)\sinh(\alpha_i L)}{\cos(\alpha_i L) + \cosh(\alpha_i L)}
\end{aligned} \tag{D.15}$$

$$
\begin{aligned}
C_2 &= \cosh(\alpha_i L) - C\sinh(\alpha_i L) = \cosh(\alpha_i L) - \frac{\sin(\alpha_i L) + \sinh(\alpha_i L)}{\cos(\alpha_i L) + \cosh(\alpha_i L)}\sinh(\alpha_i L) \\
C_2 &= \frac{\cos(\alpha_i L)\cosh(\alpha_i L) + \cosh^2(\alpha_i L) - \sin(\alpha_i L)\sinh(\alpha_i L) - \sinh^2(\alpha_i L)}{\cos(\alpha_i L) + \cosh(\alpha_i L)} \\
C_2 &= \frac{\cosh^2(\alpha_i L) - \sinh^2(\alpha_i L) + \cos(\alpha_i L)\cosh(\alpha_i L) - \sin(\alpha_i L)\sinh(\alpha_i L)}{\cos(\alpha_i L) + \cosh(\alpha_i L)} \\
C_2 &= \frac{1 + \cos(\alpha_i L)\cosh(\alpha_i L) - \sin(\alpha_i L)\sinh(\alpha_i L)}{\cos(\alpha_i L) + \cosh(\alpha_i L)} \\
C_2 &= -\frac{\sin(\alpha_i L)\sinh(\alpha_i L)}{\cos(\alpha_i L) + \cosh(\alpha_i L)}
\end{aligned}
\tag{D.16}
$$

$$
\begin{aligned}
C_3 &= \sin(\alpha_i L) - C\cos(\alpha_i L) = \sin(\alpha_i L) - \frac{\sin(\alpha_i L) + \sinh(\alpha_i L)}{\cos(\alpha_i L) + \cosh(\alpha_i L)}\cos(\alpha_i L) \\
C_3 &= \frac{\sin(\alpha_i L)\cos(\alpha_i L) + \sin(\alpha_i L)\cosh(\alpha_i L) - \sin(\alpha_i L)\cos(\alpha_i L) - \cos(\alpha_i L)\sinh(\alpha_i L)}{\cos(\alpha_i L) + \cosh(\alpha_i L)} \\
C_3 &= \frac{\sin(\alpha_i L)\cosh(\alpha_i L) - \cos(\alpha_i L)\sinh(\alpha_i L)}{\cos(\alpha_i L) + \cosh(\alpha_i L)}
\end{aligned}
\tag{D.17}
$$

$$
\begin{aligned}
C_4 &= -\sinh(\alpha_i L) + C\cosh(\alpha_i L) = -\sinh(\alpha_i L) + \frac{\sin(\alpha_i L) + \sinh(\alpha_i L)}{\cos(\alpha_i L) + \cosh(\alpha_i L)}\cosh(\alpha_i L) \\
C_4 &= \frac{-\cos(\alpha_i L)\sinh(\alpha_i L) - \sinh(\alpha_i L)\cosh(\alpha_i L) + \sin(\alpha_i L)\cosh(\alpha_i L) + \sinh(\alpha_i L)\cosh(\alpha_i L)}{\cos(\alpha_i L) + \cosh(\alpha_i L)} \\
C_4 &= \frac{\sin(\alpha_i L)\cosh(\alpha_i L) - \cos(\alpha_i L)\sinh(\alpha_i L)}{\cos(\alpha_i L) + \cosh(\alpha_i L)}
\end{aligned}
\tag{D.18}
$$

Eq. (D.14) can be represented as follows:

$$
\begin{aligned}
\frac{\phi_i(L-x)}{a_1} = &-\frac{\sin(\alpha_i L)\sinh(\alpha_i L)}{\cos(\alpha_i L) + \cosh(\alpha_i L)}[\sin(\alpha_i x) + \sinh(\alpha_i x)] + \\
&\frac{\sin(\alpha_i L)\cosh(\alpha_i L) - \cos(\alpha_i L)\sinh(\alpha_i L)}{\cos(\alpha_i L) + \cosh(\alpha_i L)}[\cos(\alpha_i x) + \cosh(\alpha_i x)]
\end{aligned}
\tag{D.19}
$$

With α_i being the root of (D.9), the following equality can be proved by squaring both sides of it:

$$
\begin{cases}
\dfrac{\sin(\alpha_i L)\sinh(\alpha_i L)}{\cos(\alpha_i L) + \cosh(\alpha_i L)} = (-1)^{i+1} \\
\dfrac{\sin(\alpha_i L)\cosh(\alpha_i L) - \cos(\alpha_i L)\sinh(\alpha_i L)}{\cos(\alpha_i L) + \cosh(\alpha_i L)} = (-1)^{i+1}\dfrac{\sin(\alpha_i L) + \sinh(\alpha_i L)}{\cos(\alpha_i L) + \cosh(\alpha_i L)}
\end{cases}
\tag{D.20}
$$

From (D.20), Eqs. (D.19) becomes:

$$
\phi_i(L-x) = (-1)^{i+1} a_1 \left(-\sin(\alpha_i x) - \sinh(\alpha_i x) + \frac{\sin(\alpha_i L) + \sinh(\alpha_i L)}{\cos(\alpha_i L) + \cosh(\alpha_i L)}(\cos(\alpha_i x) + \cosh(\alpha_i x)) \right)
\tag{D.21}
$$

From (D.11) and (D.21), the relation (D.12) are verified.

Appendix D.3. Clamped-clamped beam

Apply the boundary condition of the clamped-clamped beam: $\phi_i(0) = 0$, $\phi_i(L) = 0$, $\phi_i'(0) = 0$ and $\phi_i'(L) = 0$, one gets:

$$a_1 = -a_3;\ a_2 = -a_4;\ a_1 = a_2 \frac{\cosh(\alpha_i L) - \cos(\alpha_i L)}{\sin(\alpha_i L) - \sinh(\alpha_i L)} \tag{D.22}$$

The root α_i of the characteristic equation of the fixed beam is given below:

$$1 - \cos(\alpha_i L)\cosh(\alpha_i L) = 0 \tag{D.23}$$

Substitute Eq. (D.22) into Eq. (D.3), the mode shape and the curvature are as follows:

$$\phi_i(x) = a_1 \left(\sin(\alpha_i x) - \sinh(\alpha_i x) + \frac{\sin(\alpha_i L) - \sinh(\alpha_i L)}{\cosh(\alpha_i L) - \cos(\alpha_i L)} (\cos(\alpha_i x) - \cosh(\alpha_i x)) \right) \tag{D.24}$$

$$\phi_i''(x) = -a_1 \alpha_i^2 \left(\sin(\alpha_i x) + \sinh(\alpha_i x) + \frac{\sin(\alpha_i L) - \sinh(\alpha_i L)}{\cosh(\alpha_i L) - \cos(\alpha_i L)} (\cos(\alpha_i x) + \cosh(\alpha_i x)) \right) \tag{D.25}$$

Fig. D.17 presents the first five mode shapes and curvatures of the clamped-clamped beam, determined with relation D.24 and D.25, respectively.

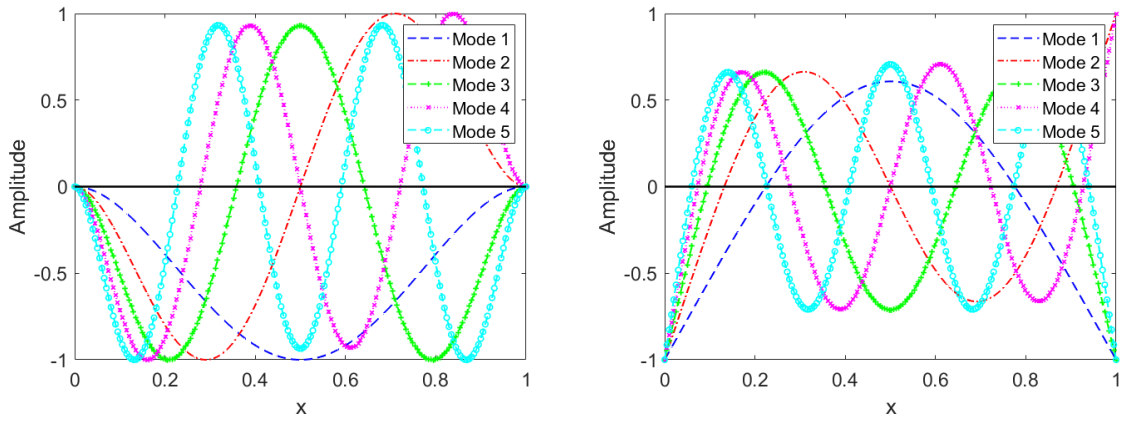

Fig. D.17. Mode shapes (left) and curvatures (right) of a clamped-clamped beam

References

[1] S. W. Doebling, C. R. Farrar, M. B. Prime, D. W. Shevitz, Damage identification and health monitoring of structural and mechanical systems from changes in their vibration characteristics: a literature review, Technical Report (1996).

[2] H. P. Chen, Y.-Q. Ni, Structural Health Monitoring of Large Civil Engineering Structures, John Wiley & Sons Ltd, UK, 2018. doi:https://doi.org/10.1002/9781119166641.

[3] O. Avci, O. Abdeljaber, S. Kiranyaz, M. Hussein, M. Gabbouj, D. J. Inman, A review of vibration-based damage detection in civil structures: From traditional methods to machine learning and deep learning applications, Mechanical Systems and Signal Processing 147 (2021) 107077. doi:https://doi.org/10.1016/j.ymssp.2020.107077.

[4] R. Hou, Y. Xia, Review on the new development of vibration-based damage identification for civil engineering structures: 2010–2019, Journal of Sound and Vibration 491 (2021) 115741. doi:https://doi.org/10.1016/j.jsv.2020.115741.

[5] A. Rytter, Vibrational Based Inspection of Civil Engineering Structures, Ph.D. thesis, University of Aalborg, Denmark, 1993.

[6] A. Pandey, M. Biswas, M. Samman, Damage detection from changes in curvature mode shapes, Journal of Sound and Vibration 145 (1991) 321–332. doi:https://doi.org/10.1016/0022-460X(91)90595-B.

[7] M. M. A. Wahab, G. D. Roeck, Damage detection in bridges using modal curvatures: Application to a real damage scenario, Journal of Sound and Vibration 226 (1999) 217–235. doi:https://doi.org/10.1006/jsvi.1999.2295.

[8] E. Carden, P. Fanning, Vibration based conditioning monitoring: a review, Structural Health Monitoring 3 (2004)) 355–377.

[9] R. Gorgin, Damage identification technique based on mode shape analysis of beam structures, Structures 27 (2020) 2300–2308. doi:https://doi.org/10.1016/j.istruc.2020.08.034.

[10] D. Capecchi, J. Ciambella, A. Pau, F. Vestroni, Damage identification in a parabolic arch by means of natural frequencies, modal shapes and curvatures, Meccanica 51 (2016) 467–476. doi:https://doi.org/10.1007/s11012-016-0510-3.

[11] M. Dahak, N. Touat, M. Kharoubi, Damage detection in beam through change in measured frequency and undamaged curvature mode shape, Inverse Problems in Science and Engineering 27 (2018) 1–26. doi:https://doi.org/10.1080/17415977.2018.1442834.

[12] Y.-S. Lee, M.-J. Chung, A study on crack detection using eigenfrequency test data, Computers & Structures 77 (2000) 327–342. doi:https://doi.org/10.1016/S0045-7949(99)00194-7.

[13] D. Patil, S. Maiti, Experimental verification of a method of detection of multiple cracks in beams based on frequency measurements, Journal of Sound and Vibration 281 (2005) 439–451. doi:10.1016/j.jsv.2004.03.035.

[14] M. Dahak, N. Touat, N. Benseddiq, On the classification of normalized natural frequencies for damage detection in cantilever beam, Journal of Sound and Vibration 402 (2017) 70–84. doi:https://doi.org/10.1016/j.jsv.2017.05.007.

[15] G. Sha, M. Radzieński, M. Cao, W. Ostachowicz, A novel method for single and multiple damage detection in beams using relative natural frequency changes, Mechanical Systems and Signal Processing 132 (2019) 335 – 352. doi:https://doi.org/10.1016/j.ymssp.2019.06.027.

[16] C. Surace, A. Bovsunovskii, The use of frequency ratios to diagnose structural damage in varying environmental conditions, Mechanical Systems and Signal Processing 136 (2019). doi:https://doi.org/10.1016/j.ymssp.2019.106523.

[17] G.-R. Gillich, Z.-I. Praisach, Modal identification and damage detection in beam-like structures using the power spectrum and time–frequency analysis, Signal Processing 96 (2014) 29–44. doi:https://doi.org/10.1016/j.sigpro.2013.04.027.

[18] T. Le, N. Point, P. Argoul, G. Cumunel, Structural changes assessment in axial stressed beams through frequencies variation, International Journal of Mechanical Sciences 110 (2016) 41–52. doi:10.1016/j.ijmecsci.2016.02.008.

[19] S. S. B. Chinka, S. R. Putti, B. K. Adavi, Modal testing and evaluation of cracks on cantilever beam using mode shape curvatures and natural frequencies, Structures 32 (2021) 1386–1397. URL: https://www.sciencedirect.com/science/article/pii/S2352012421002290. doi:https://doi.org/10.1016/j.istruc.2021.03.049.

[20] J.-W. Lee, Crack identification method for tapered cantilever pipe-type beam using natural frequencies, International Journal of Steel Structures 16 (2016) 467–476. doi:https://doi.org/10.1007/s13296-016-6017-x.

[21] M.-T. Vakil-Baghmisheh, M. Peimani, M. H. Sadeghi, M. M. Ettefagh, Crack detection in beam-like structures using genetic algorithms, Applied Soft Computing 8 (2008) 1150–1160. doi:https://doi.org/10.1016/j.asoc.2007.10.003.

[22] S. A. Moezi, E. Zakeri, A. Zare, Structural single and multiple crack detection in cantilever beams using a hybrid cuckoo-nelder-mead optimization method, Mechanical Systems and Signal Processing 99 (2018) 805–831. doi:https://doi.org/10.1016/j.ymssp.2017.07.013.

[23] S. Khatir, K. Dekemele, M. Loccufier, T. Khatir, M. Abdel Wahab, Crack identification method in beam-like structures using changes in experimentally measured frequencies and particle swarm optimization, Comptes Rendus Mécanique 346 (2018) 110–120. doi:https://doi.org/10.1016/j.crme.2017.11.008.

[24] G.-R. Gillich, Z.-I. Praisach, Robust method to identify damages in beams based on frequency shift analysis, in: T. Kundu (Ed.), Health Monitoring of Structural and Biological Systems 2012, volume 8348, International Society for Optics and Photonics, SPIE, 2012, pp. 367 – 378. doi:https://doi.org/10.1117/12.915158.

5 Multiple damage detection

Chapter abstract

Continuing the topic covered in Chapter 4, a problem of a higher degree of complexity is considered, namely the problem of identifying multiple damages in engineering structures.

As discussed in Chapter 1, finite element methods (FEM) are a popular tool for structural design, dynamic analysis, and damage detection in civil engineering. In general, these finite element methods can provide baseline information that can then be compared to new information from a monitoring system to detect structural damage and predict the future performance. In particular, for damage detection, natural frequency shifts between a healthy state and a suspected damaged state are obtained by simulations using FEM. Comparison of the simulated and measured natural frequency shifts then allows damage to be identified, for example using an optimization step or Bayesian inference. However, despite the seemingly clear and understandable algorithm, there are a number of difficulties that must be taken into account when applying these methods. First, they require a large amount of computational time to process the data and update the model, which delay the identification process for real-time damage detection. Second, the performance of these methods largely depends on the accuracy of the FE model, namely discretization error and modeling error.

To overcome these shortcomings of FEM for multiple damage detection, this chapter extends the damage identification procedure presented previously for multiple damage detection. The simulated natural frequency shifts are obtained directly from the analytic expression established in the former chapter instead of using FEM. Then, the localization of damages is deduced based on the most probable locations given by the Bayesian reference. The damages identification becomes fast because the proposed procedure skips the computational costs associated with FEM simulations. However, it can introduce pseudo-damage locations that are symmetrical to the real damage ones. These pseudo-damage locations can be easily eliminated by using other available information such as measured modal shape. The proposed method has been confirmed by numerical and experimental tests.

5.1 A enhance method for multiple damage detection (Article 4)

Multiple damage detection on beams using relative natural frequency shifts and Bayesian inference

Abstract

Vibration based methods for detecting the location of damage in structures are generally based on changes in the dynamic characteristics of structures caused by damage, such as natural frequencies and mode shapes. The frequency based damage detection approach is one such technique, which uses natural frequency shifts between intact and damaged structure to locate damage. This paper presents a modified procedure for multiple damage detection based on a simplified relationship between relative natural frequency shift and damage. The proposed procedure allows to determine the locations of structural changes in beams and their severity by analyzing the variation of natural frequencies combined with Bayesian inference. The efficiency of the proposed method was validated by numerical simulation and then by experimental tests under different boundary conditions.

Keywords: Damage detection, frequency shift, mode shape curvature

1. Introduction

Structural damage detection is an essential part of monitoring the health of a structure. During operation, structures can accumulate damage caused by environmental and human factors. Damage is interpreted as a change in the geometrical or material properties of the structure, which can adversely affect the performance, safety and durability of the structure [1]. A structural failure can have catastrophic consequences if it is not detected or repaired in time. Structural damage induces changes in vibration characteristics such as frequencies, mode shapes and damping ratios [2]. The identification of structural damage based on change of these dynamic characteristics has been the subject of many studies [3, 4].

Among the many methods developed for damage detection, methods based on frequency variation are widely used [5–7]. This is because natural frequencies are easier and accurately to measure than mode shapes or damping ratios. The main drawback of these methods is that different damage locations can result in the same frequency change.

Many studies have attempted to detect single damage in beams. One of the first compact forms relating natural frequency and damage parameters was introduced in [8]. This

form was used for damage localization in beams by Narkis [9]. Similarly, Kam and Lee [10] used frequencies and mode shapes to identify a cracked element based on a simple reduced stiffness model. Lee and Chung [11] identified a crack in a cantilever beam by combining a finite element model with an analysis of the first four natural frequencies. Sayyad and Kumar [12] determined the location and the size of a damage using the first two natural frequencies by establishing the relationship between the natural frequencies, the location and the size of the crack. Lee [13] presented a method for determining the location and the extent of a crack in a tapered cantilever using natural frequency variations and neural networks. Dahak et al. [14] developed a damage detection procedure based on the classification of normalized frequencies in cantilever beams. An expression of the natural frequency variation and damage was derived in [15] and applied to single damage detection as a pattern recognition problem in [16]. The expression in [15] is also used to generate contour lines along the entire length of the beam, and the intersection of these contours is considered to be damage position [17–19]. Radzieński et al. [20] introduced a method for single damage detection using frequency shift and analytical mode shape. Le et al. [21] presented a single damage detection procedure based on the relationship between damage parameters and natural frequencies.

The identification of multiple damages is more difficult than that of single damage, and in recent decades this issue has received considerable attention [22]. Ostachowicz and Krawczuk [23] analyzed the influence of the location and depth of two cracks on the natural frequency of cantilever beams. Mazanoglu and Sabuncu [24] presented an algorithm that uses the map of natural frequency ratios to identify double cracks in beams. Xiang and Liang [25] developed a two-step hybrid method based on mode shape and frequency changes to detect two cracks in cantilever beams. Studies [26, 27] proposed probabilistic approaches to damage identification. Bayesian inference-based methods have been recognized as an effective approach to detecting structural damage [28–31]. Generalized procedures for the identification of multiple damages such as genetic algorithm [32] or optimization algorithm [33, 34] have been developed recently. Although these optimization methods are effective, they often take a long time to reach the convergence of the optimization procedures.

Among the above studies, the relationship between natural frequency shift and damage is used for many damage identification procedures [15–19, 21], but its applications are only limited to single damage detection.

This article uses the simplified relationship derived in chapter 4 and the procedure presented by Sha et al. [27] to detect multiple damages in structures. In this work, the simulated natural frequency shifts are obtained directly from the analytical expression given in a simplified relationship, instead of using the finite element method (FEM). The localization of damages is determined by the most probable locations obtained using the Bayesian

inference. The proposed procedure of damage identification becomes fast because it skips the computational cost associated with FEM simulations.

The remainder of this study is organized as follows. Section 2 presents a simplified relationship between relative natural frequency shift and damages and the modified procedure for multiple damage detection. The modified procedure is then validated by numerical tests in Section 3, followed by experimental tests in Section 4. Finally, a conclusion is given in Section 5.

2. Theoretical formulation

2.1. Theoretical background

In chapter 4, the relationship between natural frequency shift and damage at location x_0 is given as:

$$\frac{\Delta f_i}{f_i} = \frac{\overline{f_i} - f_i}{f_i} \approx \delta_{\mathrm{K}} \frac{\phi_i''^2(x_0)}{\left\|\phi_i''\right\|_2^2} + \delta_{\mathrm{M}} \frac{\phi_i^2(x_0)}{\|\phi_i\|_2^2} \tag{1}$$

where f_i and $\overline{f_i}$ are the natural frequencies of i^{th} mode of the intact and damaged states, respectively; $\delta_{\mathrm{K}} = \dfrac{\Delta EI \Delta L}{2EI}$ and $\delta_{\mathrm{M}} = -\dfrac{\Delta \mu \Delta L}{2\mu}$ represent the relative local variation of bending stiffness and mass, respectively; $\left\|\phi_i''\right\|_2^2 = \int_0^L \phi_i''^2(x)dx$ and $\|\phi_i\|_2^2 = \int_0^L \phi_i^2(x)dx$

In the case of damage due to only change of bending stiffness and neglecting the influence of mass change, a simpler expression for the natural frequency variation can be expressed as a function of squared modal curvature:

$$\frac{\Delta f_i}{f_i} \approx \zeta \phi_i''^2(x_0) \tag{2}$$

Where ζ represents the damage severity.

The expression (2) has been applied to damage detection in many studies [15, 16, 18–21]. However, these applications are limited to the detection of single damage in beam-like structures. In the case of structures with multiple damages, their identification becomes even more challenging. In the next part, expression (2) and Bayesian inference are combined to develop a fast procedure for multiple damage detection.

2.2. The damage detection procedure

This article partially uses the steps of the damage identification process presented in [27], but the natural frequency shifts are obtained directly from Equation (2). This work does not use the FEM as in the existing procedure, although the authors in [27] also mention the possibility of using Equation (2). The proposed identification of damages becomes fast as it skips the computational cost associated with FEM simulations.

Assuming that damages are independent events with $P(a,b) = P(a)*P(b)$ and the effect of multiple damages follows the principle of superposition. The procedure for multiple damage detection is as follows:

Step 1. Calculate relative frequency shift $\overline{\Delta f}^{o}_{i,j}$ from analytical formula (2) by varying damage location $x_j = 0 : L$.

Normalize the relative frequency shift to the range [0 1].

$$\overline{\delta f}^{o}_{i,j} = \frac{\overline{\Delta f}^{o}_{i,j} - \min_i(\overline{\Delta f}^{o}_{i,j})}{\max_i(\overline{\Delta f}^{o}_{i,j}) - \min_i(\overline{\Delta f}^{o}_{i,j})} \tag{3}$$

where $\overline{\Delta f}^{o}_{i,j}$ is the relative frequency shift of the i^{th} mode due to a damage occurring at location x_j.

Step 2. Calculate relative frequency shift from measured values.

$$\overline{\Delta f}_i = \frac{\overline{f}_i - f_i}{f_i} \tag{4}$$

Normalize the relative frequency shift to the range [0 1].
$\min_i$

$$\overline{\delta f}_i = \frac{\overline{\Delta f}_i - \min(\overline{\Delta \mathbf{f}})}{\max(\overline{\Delta \mathbf{f}}) - \min(\overline{\Delta \mathbf{f}})} \tag{5}$$

where $\overline{\Delta \mathbf{f}}$ contains the measured relative frequency shifts of modes.

Step 3. Denote the damage position function at location x_j with mode i as:

$$P_{i,j} = 1 - \left| \overline{\delta f}^{o}_{i,j} - \overline{\delta f}_i \right| \tag{6}$$

Step 4. Apply the Bayesian probability theory

The posterior probability of events $A_1, A_2, .., A_n$ after the relevant information is taken into account can be represented as follows [35]:

$$P(A_j|S_1, S_2, ..., S_m) = \frac{P(S_1, S_2, ..., S_m|A_j)P(A_j)}{P(S_1, S_2, ..., S_m)} \tag{7}$$

where m, n are the number of information S_i and the number of events A_j, respectively.

In the damage identification problem, each mode i is considered as an information S_i, and damage occurring at point j is considered as an independent event A_j. Suppose that n is the total number of locations of the beam, the prior probability of each event is $P(A_j) = 1/n$.

$$P(S_1, S_2, ..., S_m|A_j) = \prod_i^m P(S_i|A_j) \tag{8}$$

$$P(S_1, S_2, ..., S_m) = \sum_j^n P(S_1, S_2, ..., S_m|A_j)P(A_j) = \sum_j^n \left(\prod_i^m P(S_i|A_j)P(A_j) \right) \tag{9}$$

Substitute Eq. (8) and Eq. (9) into Eq. (7):

$$P(A_j|S_1, S_2, ..., S_m) = \frac{\prod_i^m P(S_i|A_j)P(A_j)}{\sum_j^n \left(\prod_i^m P(S_i|A_j)P(A_j) \right)} \tag{10}$$

The conditional probability of S_i is considered as $P(S_i|A_j) = P_{i,j}$. The posterior probability P_j in Eq. (10) can be simplified as follows:

$$P_j = \frac{\prod_i^m P_{i,j}}{\sum_j^n \left(\prod_i^m P_{i,j} \right)} \tag{11}$$

Step 5. Make a generalization for all boundary conditions

$$Q_j = \sqrt{P_j P_{n+1-j}} \tag{12}$$

Step 6. Normalize

$$Z_j = \frac{Q_j - \mu(\mathbf{Q})}{\delta(\mathbf{Q})} \tag{13}$$

where μ and δ are mean and standard deviation operators, respectively.

Step 7. Calculate probabilistic damage indicator (PDI)

$$\text{PDI} = \begin{cases} Z & \text{if } Z \geq 0 \\ 0 & \text{if } Z < 0 \end{cases} \tag{14}$$

The regions with PDI > 0 contain damage locations. Therefore, the peaks of this curve represent the highest possibility of damage locations.

Step 8. Estimate damage severity

When the effect of multiple damages follows the principle of superposition, the relative natural frequency shift can be represented as follows:

$$\overline{\Delta f_i} \approx \sum_{k=1}^{d} \zeta_k \, \phi_i''^2 \, (x_{0,k}) \tag{15}$$

where d is the number of identified damages. $x_{0,k}$ and ζ_k represents the location and the coefficient of the k^{th} damage, respectively.

Once the locations of the damages are determined, the damages coefficients ζ_k can be solved from m Equation (15) of m modes. The corresponding damage severity (depth) is estimated through an inverse method using the relationship between damage depth and damage coefficient obtained by numerical simulations.

2.3. The proposed augmentation procedure for measured mode shape

In general, damage detection methods based on mode shapes require many measurement points to improve the accuracy. However, in practical applications, a limited number of measurement points leads to low accuracy of this method. In order to overcome this limitation, a procedure is proposed to improve the lack of points for the measured mode shapes.

In experimental tests, analytical mode shapes and analytical curvatures can be interpolated from measured mode shapes. When measured mode shapes are used for damage detection, a procedure must be implemented to deal with a limited number of sensors.

It is known that the i^{th} mode shape and curvature function of an intact beam are expressed using five coefficients including a_1, a_2, a_3, a_4 and α.

$$\begin{cases} \phi_i(x) = a_1 \sin(\alpha_i x) + a_2 \cos(\alpha_i x) + a_3 \sinh(\alpha_i x) + a_4 \cosh(\alpha_i x) \\ \phi_i''(x) = \alpha_i^2 \left(-a_1 \sin(\alpha_i x) - a_2 \cos(\alpha_i x) + a_3 \sinh(\alpha_i x) + a_4 \cosh(\alpha_i x)\right) \end{cases} \tag{16}$$

where the coefficients a_1, a_2, a_3, a_4 and α depend on the boundary conditions,

From spatial points of measured mode shapes, the measured mode shapes are used to estimate the coefficients a_1, a_2, a_3, a_4 and α in (16). Since the relationship between the mode shapes and their coefficients is non-linear, an optimization procedure is used to estimate these coefficients from the measured points. Once these coefficients are obtained, the modal curvatures of the intact state can be calculated for any location x_j using Equation (16).

3. Numerical tests

In this section, the procedure is verified by the analysis of the simulated models using ANSYS Workbench (Fig. 1). The tests were carried out with different boundary conditions.

The numerical beams have a length of 800 mm, a width of 40mm, and a height of 6mm. Their physical properties are Young's modulus E = 200GPa, the density ρ = 7850kg/m^3, and the Poisson's ratio υ = 0.3.

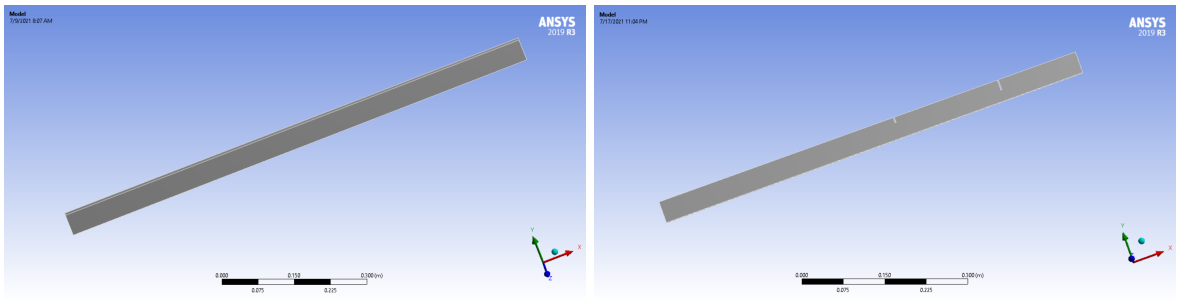

(a) Numerical intact beam **(b)** Numerical beam with damages

Fig. 1. Numerical beams simulated in ANSYS

3.1. Numerical cantilever beam

Five cases with different crack locations and crack depths in a cantilever beam are considered. Damage scenarios are shown in Table 1. x_k and s_k represent the damage location from the fixed-end and the damage depth of the k^{th} damage. All damages are simulated with a width of 2mm.

By following the steps mentioned in Section. 2.2, the probability curves of damage for each case are obtained, as shown in Figs. 2 and 3. Areas with probability values higher than zero may contain damaged locations. The identified damage locations are defined at the abcisse of the peaks of the curve. It can be seen from Fig. 3 that the accuracy of the proposed procedure can increase as the number of modes used increases. This method

Table 1
Damage scenarios of the numerical cantilever beams.

Case	Damage (mm)				Natural frequency (Hz)				
	x_1	s_1	x_2	s_2	Mode 1	Mode 2	Mode 3	Mode 4	Mode 5
Intact					7.6850	48.149	134.79	264.08	436.47
1	300.0	15.0			7.6375	47.838	133.83	263.86	431.64
2	513.3	20.0			7.6772	47.294	132.24	263.85	429.11
3	300.0	15.0	650.0	20.0	7.6471	47.672	131.84	257.66	422.86
4	400.0	25.0	650.0	20.0	7.6304	46.355	132.70	249.87	426.38
5	450.0	10.0	650.0	20.0	7.6804	47.734	132.70	257.15	426.54

gives symmetrical fake damage locations, but these false locations can be easily detected by comparing the difference between the modal curvature of the modified state and those of the intact state as shown in Fig. 4.

Once the damage location is determined, the damage severity ζ_k corresponding to its damage location can be estimated using Equation (15). For an accurate assessment of the damage depth, numerical simulations are carried out to establish the relationship between depths and their coefficients. The curve of this relationship is shown in Fig. 5. The damage depths are interpolated from adjacent values using cubic spline interpolation.

The identified results given in Table 2 represent damage locations and damage depths. It can be seen that they are close to the data selected for simulations in determining both the locations and the depths of the damages. Although the proposed procedure gives both the actual damages and the symmetrically false ones, it limits the number of possible locations containing damages. Fake damaged locations can be eliminated with additional information, such as the difference between the mode shapes or curvatures of the intact state and those of the modified one, or by visualization at possible damage locations on the structure.

3.2. Numerical clamped-clamped beam

Four cases were considered with different crack locations and crack depths of the clamped-clamped beams. Damage scenarios are given in Table 3.

By following the steps mentioned in Section. 2.2, the probability curves of damage for each case are presented in Fig. 6. Actual damages are always inside regions with high probability values. After the damage location is determined, the damage coefficients ζ_k corresponding to its damage locations are estimated. The curve for the relationship between damage depths and their coefficients is shown in Fig. 7. The damage depths are

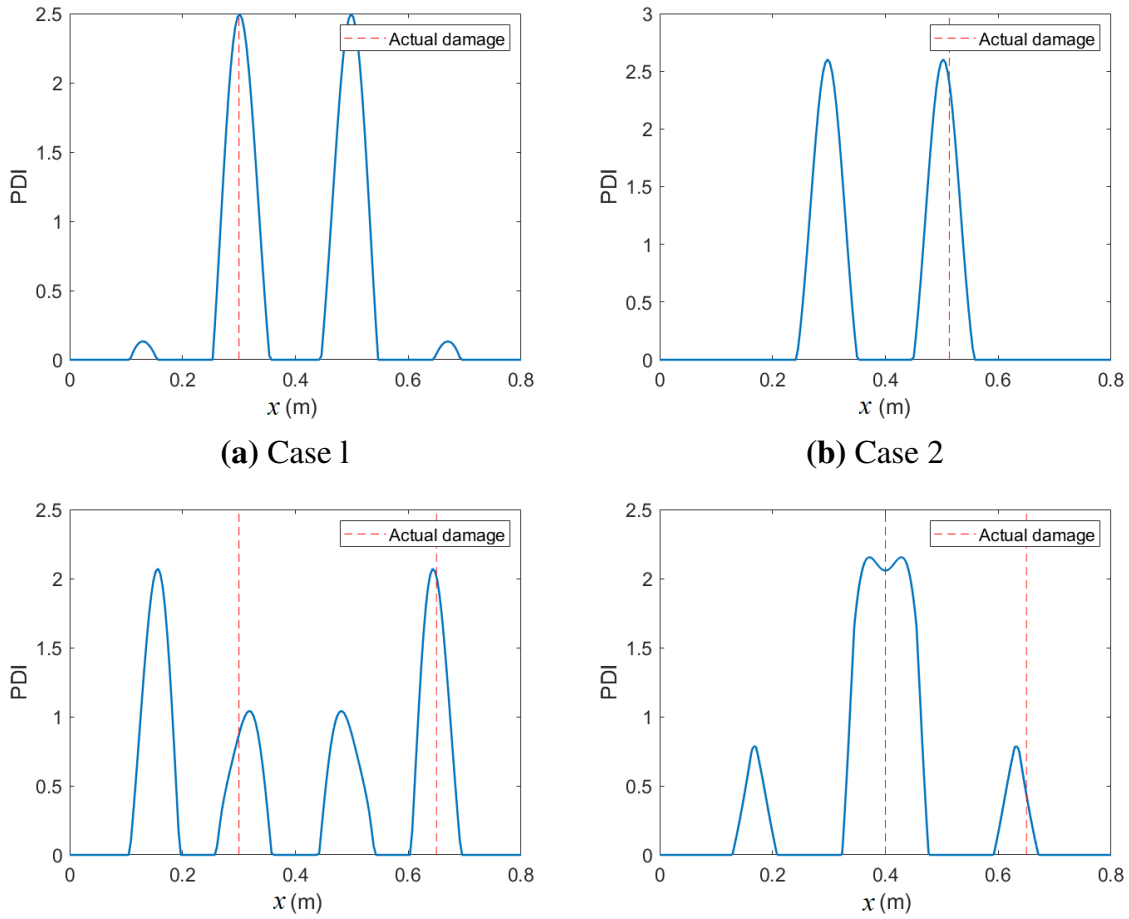

(a) Case 1 **(b)** Case 2

(c) Case 3 **(d)** Case 4

Fig. 2. Damage index in the numerical cantilever beams by using the first five modes

Table 2
Results identified from the numerical cantilever beams.

Case	x_1 (mm)	s_1 (mm)	x_2 (mm)	s_2 (mm)
1	301.1	14.2		
2	502.1	19.5		
3	318.7	14.1	643.8	19.6
4	428.4	23.9	630.2	19.2
5	455.7	9.5	638.2	19.6

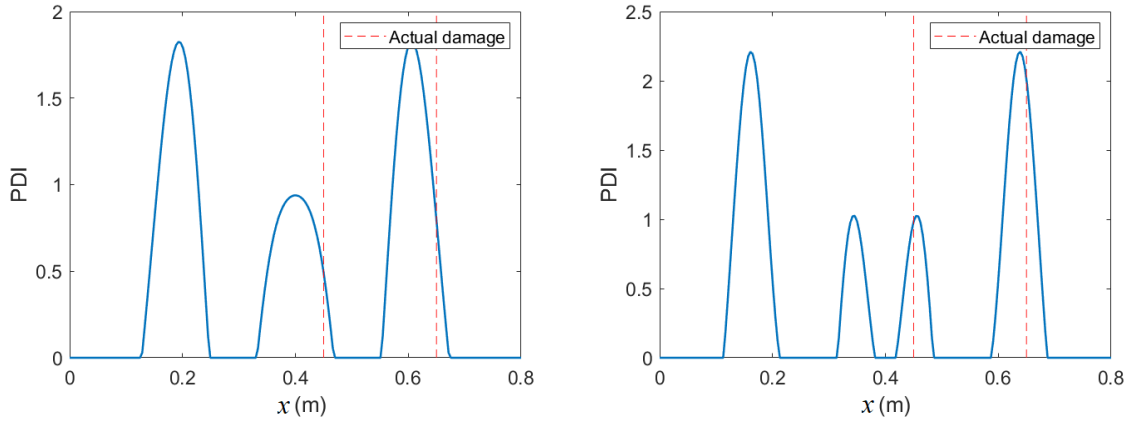

(a) Using the first four modes **(b)** Using the first five modes

Fig. 3. Damage index in the numerical cantilever beams in case 5

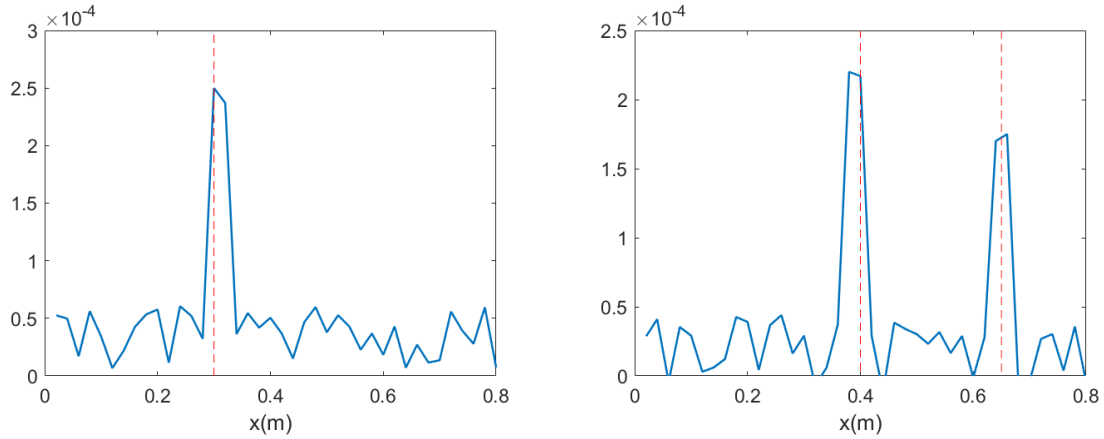

(a) Case 1 **(b)** Case 4

Fig. 4. Eliminate fake locations for case 1 (left) and case 4 (right)

interpolated from adjacent values using cubic spline interpolation. The results of determining the location and the depth of damage are given in Table 4. The identified results are close to the exact ones.

4. Experimental tests

This section uses experimental tests to verify the method's effectiveness in beams with different boundary conditions. The damage detection procedure is considered in two ap-

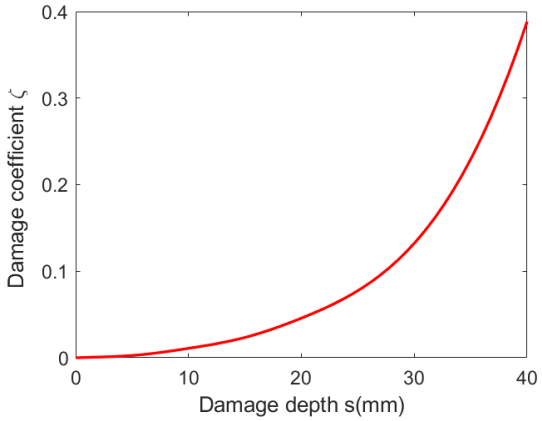

Fig. 5. Damage coefficient vs. damage depth in the numerical cantilever beam

Table 3
Damage scenarios of the numerical clamped-clamped beams.

Case	Damage (mm)				Natural frequency (Hz)					
	x_1	s_1	x_2	s_2	Mode 1	Mode 2	Mode 3	Mode 4	Mode 5	Mode 6
Intact					49.142	135.41	265.35	438.47	654.76	914.14
1	200.0	15.0			49.131	134.36	263.06	437.68	653.17	907.33
2	400.0	10.0			48.961	135.39	263.91	438.39	651.31	913.80
3	200.0	15.0	400.0	10.0	48.965	134.39	261.74	437.64	649.88	905.08
4	450.0	10.0	700.0	10.0	48.866	135.23	264.35	435.98	651.24	905.72

Table 4
Results identified from the numerical clamped-clamped beams.

Case	x_1 (mm)	s_1 (mm)	x_2 (mm)	s_2 (mm)
1	211.4	14.0		
2	399.6	10.3		
3	216.2	13.4	373.2	11.7
4	449.2	10.6	695.1	9.8

proaches: the first uses the analytical mode curvatures, and the second uses the mode curvatures derived from the measured mode shapes in the intact state.

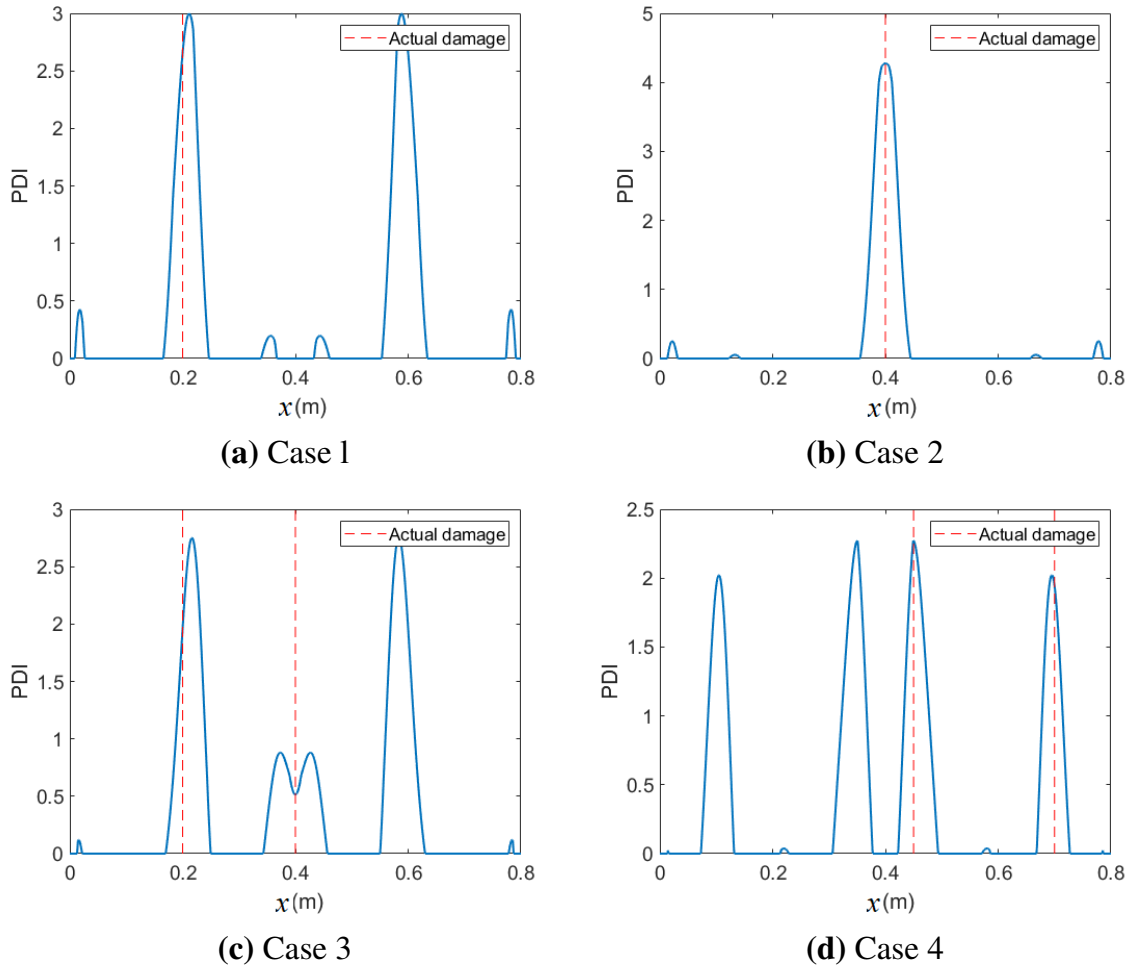

(a) Case 1 **(b)** Case 2

(c) Case 3 **(d)** Case 4

Fig. 6. Damage index in the numerical clamped-clamped beams using first six modes

4.1. Using analytical mode shape curvature

This section uses an example taken from the work of Gillich and Praisach [16]. The structure is a clamped-clamped beam: 1000mm in length, 50mm in width, and 5mm in height. The physical properties of the beam: density $\rho = 7850kg/m^3$, Young's modulus E = 200GPa. The transversal damage was placed at 0.6m from the fixed-end with 2mm wide and 30% depth. The measured frequencies are given in Table. 5.

In this test, mode shape measurements are not available, so the analytical mode curvatures are used for the damage detection procedure. The probability curves obtained by the proposed procedure are shown in Fig. 8. It can be seen that the accuracy of the probability curves is significantly improved when ten modes are used instead of five modes.

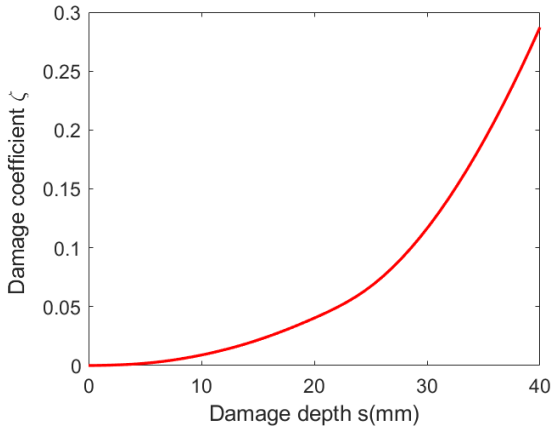

Fig. 7. Damage coefficient vs. damage depth in the numerical clamped-clamped beam

Table 5
Measured frequencies of the intact and damaged states of the clamped-clamped beam [16].

Case	Measured frequency (Hz)				
Intact	Mode 1	Mode 2	Mode 3	Mode 4	Mode 5
	26.099	71.926	140.991	233.070	348.205
	Mode 6	Mode 7	Mode 8	Mode 9	Mode 10
	486.420	647.735	832.155	1039.672	1270.254
Damaged	Mode 1	Mode 2	Mode 3	Mode 4	Mode 5
	25.929	71.493	140.579	230.016	348.130
	Mode 6	Mode 7	Mode 8	Mode 9	Mode 10
	481.188	643.729	829.675	1026.964	1269.934

4.2. Using experimental mode shape

In this section, an experimental test on a cantilever beam was designed to verify the applicability of the proposed procedure in the real structure. The beam have the following physical parameters: length L = 1005mm, width B = 42mm and height H = 10mm, Young's modulus E = 200GPa, and density ρ = 7850kg/m^3. Two damages of different depths were introduced into the lateral side. These damages have a width of 2mm.

To obtain natural frequencies and mode curvatures for the damage detection procedure, five Type 4533-B-001 accelerometers located along the beam length, were used for modal analysis. The masses of the selected accelerometers are relatively small in comparison with the mass of the beam, so the effect of these additional masses can be neglected. The

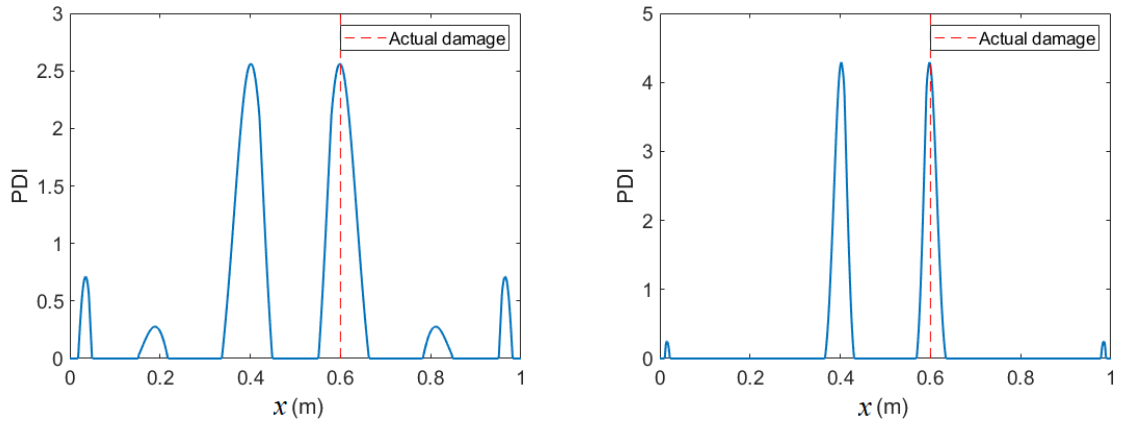

(a) Using five modes **(b)** Using ten modes

Fig. 8. Damage index in the beam by using the five modes (left) and ten modes (right)

experimental setup is shown in Fig. 9. Table. 6 shows the damage scenario and measured frequencies of the intact and damaged beams.

Table 6
Damage scenario of the experimental cantilever beam.

Case	Damage (mm)				Measured frequency (Hz)				
	x_1	s_1	x_2	s_2	1	2	3	4	5
Intact					7.7691	48.3655	137.3496	277.2691	445.6196
Damaged	500.0	10.0	750.0	15.0	7.7450	47.4729	134.6511	270.9963	445.5722

The relative natural frequency shift is used in addition to the mode curvature calculated from the measured mode shapes of the intact structure. The probability curves obtained by the proposed procedure are shown in Fig. 11. The red dashed line marks the actual positions of the damages on the beam. It shows the identified damage locations that are close to real ones. The corresponding damage coefficient is then estimated for each location.

In order to estimate the depth of these damages, the relationship between the damage coefficient and damage depth can be accomplished by numerical simulations. The curve for this relationship is shown in Fig. 12. The results of determining the damage parameters are presented in Table 7. These results confirm the effectiveness of the proposed procedure.

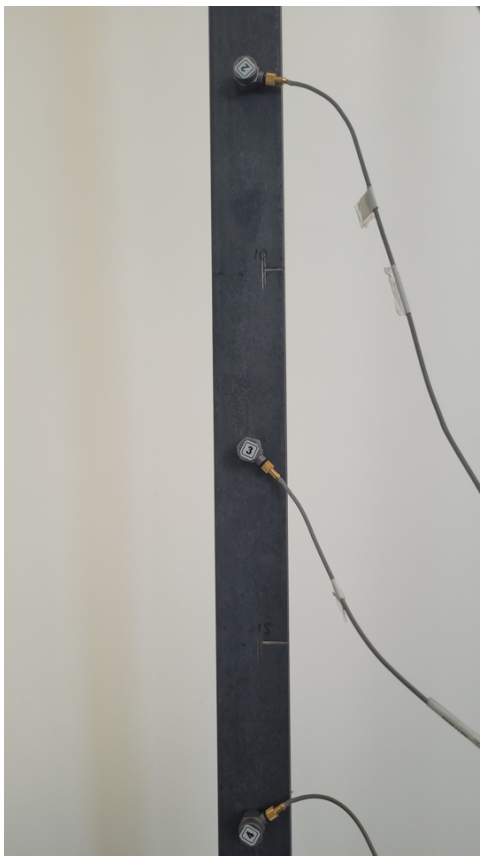

Fig. 9. Experimental setup for the cantilever beam

Table 7
Results identified from the experimental cantilever beam.

Case	x_1 (mm)	s_1 (mm)	x_2 (mm)	s_2 (mm)
1	493.9	8.9	741.4	13.8

5. Conclusion

This work extends the previous damage identification procedure to detect multiple damages. In this study, the simulated natural frequency shifts are obtained directly from the analytic expression established in the previous chapter instead of using finite element method. The proposed identification of damages becomes fast because it skips the computational costs associated with FEM simulations. However, the procedure gives pseudo-failure locations that are symmetrical to the actual failure locations. They can be easy to distinguish by comparing the difference between the mode shapes of the modified state

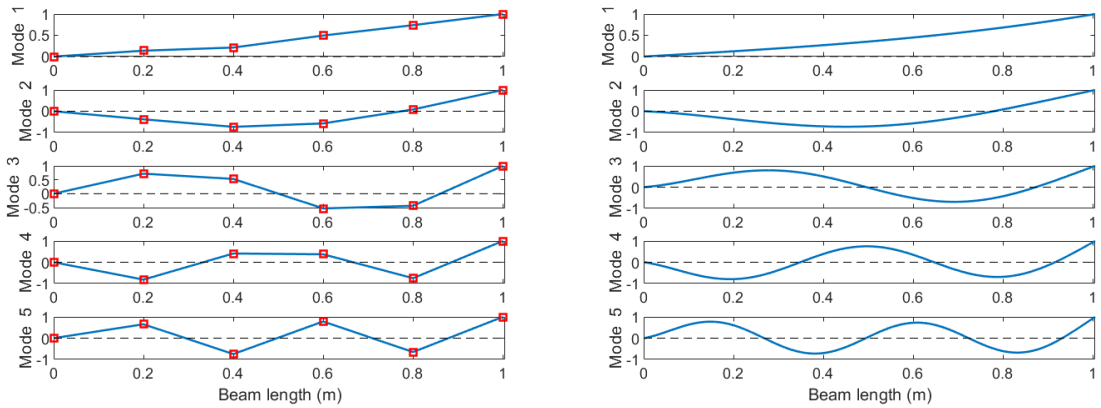

(a) Experimental mode shape **(b)** Augmented mode shape

Fig. 10. Experimental mode shape (left) and augmented mode shape (right) in the intact cantilever beam

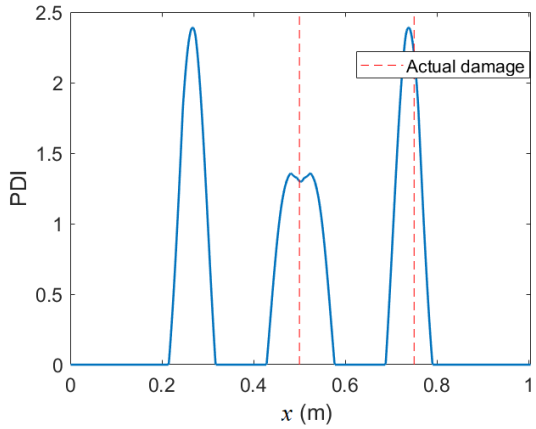

Fig. 11. Damage index in the experimental cantilever beam

and those of the intact state. Numerical simulations were carried out to confirm the effectiveness of the proposed method on the various types of beams. The proposed procedure has also been tested experimentally in two different approaches: the first using the analytical modal curvatures, the second using the modal curvatures derived from the measured mode shapes.

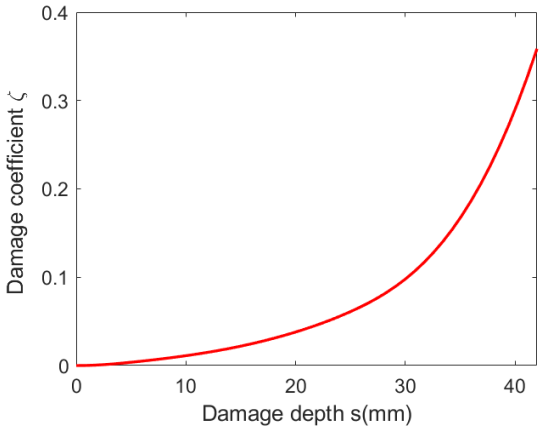

Fig. 12. Damage coefficient vs. damage depth in the experimental cantilever beam

6. Acknowledgments

The authors gratefully acknowledge the support of the French government in the form of a grant that has contributed to carry out this work.

References

[1] H.-P. Chen, Y.-Q. Ni, Introduction to Structural Health Monitoring, John Wiley & Sons, Ltd, 2018. doi:https://doi.org/10.1002/9781119166641.

[2] S. W. Doebling, C. R. Farrar, M. B. Prime, D. W. Shevitz, Damage identification and health monitoring of structural and mechanical systems from changes in their vibration characteristics: a literature review, Technical Report (1996). doi:10.2172/249299.

[3] O. Avci, O. Abdeljaber, S. Kiranyaz, M. Hussein, M. Gabbouj, D. J. Inman, A review of vibration-based damage detection in civil structures: From traditional methods to machine learning and deep learning applications, Mechanical Systems and Signal Processing 147 (2021) 107077. doi:https://doi.org/10.1016/j.ymssp.2020.107077.

[4] R. Hou, Y. Xia, Review on the new development of vibration-based damage identification for civil engineering structures: 2010–2019, Journal of Sound and Vibration 491 (2021) 115741. doi:https://doi.org/10.1016/j.jsv.2020.115741.

[5] O. Salawu, Detection of structural damage through changes in frequency: a review, Engineering Structures 19 (1997) 718–723. URL: https://www.sciencedirect.com/science/article/pii/S0141029696001496. doi:https://doi.org/10.1016/S0141-0296(96)00149-6.

[6] A. Morassi, M. Rollo, Identification of two cracks in a simply supported beam from minimal frequency measurements, Journal of Vibration and Control 7 (2001) 729–739. doi:10.1177/107754630100700507.

[7] F. B. Sayyad, B. Kumar, Identification of crack location and crack size in a simply supported beam by measurement of natural frequencies, Journal of Vibration and Control 18 (2012) 183–190. doi:10.1177/1077546310395979.

[8] R. Adams, P. Cawley, C. Pye, B. Stone, A vibration technique for non-destructively assessing the integrity of structures, Journal of mechanical engineering science 20 (1978) 93–100.

[9] Y. Narkis, Identification of crack location in vibrating simply supported beams, Journal of Sound and Vibration 172 (1994) 549–558. doi:https://doi.org/10.1006/jsvi.1994.1195.

[10] T. Kam, T. Lee, Detection of cracks in structures using modal test data, Engineering Fracture Mechanics 42 (1992) 381–387. doi:https://doi.org/10.1016/0013-7944(92)90227-6.

[11] Y.-S. Lee, M.-J. Chung, A study on crack detection using eigenfrequency test data, Computers & Structures 77 (2000) 327–342. doi:https://doi.org/10.1016/S0045-7949(99)00194-7.

[12] F. Sayyad, B. Kumar, Theoretical and experimental study for identification of crack in cantilever beam by measurement of natural frequencies, Journal of Vibration and Control 17 (2011) 1235–1240. doi:10.1177/1077546310384005.

[13] J.-W. Lee, Crack identification method for tapered cantilever pipe-type beam using natural frequencies, International Journal of Steel Structures 16 (2016) 467–476. doi:https://doi.org/10.1007/s13296-016-6017-x.

[14] M. Dahak, N. Touat, N. Benseddiq, On the classification of normalized natural frequencies for damage detection in cantilever beam, Journal of Sound and Vibration 402 (2017) 70–84. doi:https://doi.org/10.1016/j.jsv.2017.05.007.

[15] G.-R. Gillich, Z.-I. Praisach, Robust method to identify damages in beams based on frequency shift analysis, in: T. Kundu (Ed.), Health Monitoring of Structural and Biological Systems 2012, volume 8348, International Society for Optics and Photonics, SPIE, 2012, pp. 367–378. doi:https://doi.org/10.1117/12.915158.

[16] G.-R. Gillich, Z.-I. Praisach, Modal identification and damage detection in beam-like structures using the power spectrum and time–frequency analysis, Signal Processing 96 (2014) 29–44. doi:https://doi.org/10.1016/j.sigpro.2013.04.027.

[17] D. Capecchi, J. Ciambella, A. Pau, F. Vestroni, Damage identification in a parabolic arch by means of natural frequencies, modal shapes and curvatures, Meccanica 51 (2016) 2847–2859. doi:https://doi.org/10.1007/s11012-016-0510-3.

[18] S. S. B. Chinka, S. R. Putti, B. K. Adavi, Modal testing and evaluation of cracks on cantilever beam using mode shape curvatures and natural frequencies, Structures 32 (2021) 1386–1397. URL: https://www.sciencedirect.com/science/article/pii/S2352012421002290. doi:https://doi.org/10.1016/j.istruc.2021.03.049.

[19] M. Dahak, N. Touat, M. Kharoubi, Damage detection in beam through change in measured frequency and undamaged curvature mode shape, Inverse Problems in Science and Engineering 27 (2018) 1–26. doi:https://doi.org/10.1080/17415977.2018.1442834.

[20] M. Radzieński, M. Krawczuk, M. Palacz, Improvement of damage detection methods based on experimental modal parameters, Mechanical Systems and Signal Processing 25 (2011) 2169–2190. doi:https://doi.org/10.1016/j.ymssp.2011.01.007.

[21] T. Le, N. Point, P. Argoul, G. Cumunel, Structural changes assessment in axial stressed beams through frequencies variation, International Journal of Mechanical Sciences 110 (2016) 41–52. doi:10.1016/j.ijmecsci.2016.02.008.

[22] A. Sekhar, Multiple cracks effects and identification, Mechanical Systems and Signal Processing 22 (2008) 845–878. doi:https://doi.org/10.1016/j.ymssp.2007.11.008, special Issue: Crack Effects in Rotordynamics.

[23] W. Ostachowicz, M. Krawczuk, Analysis of the effect of cracks on the natural frequencies of a cantilever beam, Journal of sound and vibration 150 (1991) 191–201.

[24] K. Mazanoglu, M. Sabuncu, A frequency based algorithm for identification of single and double cracked beams via a statistical approach used in experiment, Mechanical Systems and Signal Processing 30 (2012) 168–185. doi:https://doi.org/10.1016/j.ymssp.2012.02.004.

[25] J. Xiang, M. Liang, Wavelet-based detection of beam cracks using modal shape and frequency measurements, Computer-Aided Civil and Infrastructure Engineering 27 (2012) 439–454. doi:https://doi.org/10.1111/j.1467-8667.2012.00760.x.

[26] S. Singh, R. Tiwari, Identification of a multi-crack in a shaft system using transverse frequency response functions, Mechanism and Machine Theory 45 (2010) 1813–1827. doi:https://doi.org/10.1016/j.mechmachtheory.2010.08.007.

[27] G. Sha, M. Radzieński, M. Cao, W. Ostachowicz, A novel method for single and multiple damage detection in beams using relative natural frequency changes, Mechanical Systems and Signal Processing 132 (2019) 335 – 352. doi:https://doi.org/10.1016/j.ymssp.2019.06.027.

[28] C.-W. Kim, Y. Zhang, Z. Wang, Y. Oshima, T. Morita, Long-term bridge health monitoring and performance assessment based on a bayesian approach, Structure and Infrastructure Engineering 14 (2018) 883–894. doi:https://doi.org/10.1080/15732479.2018.1436572.

[29] A. Jesus, P. Brommer, R. Westgate, K. Y. Koo, J. Brownjohn, I. Laory, Modular bayesian damage detection for complex civil infrastructure, Journal of Civil Structural Health Monitoring 9 (2019) 201–215. doi:https://doi.org/10.1007/s13349-018-00321-8.

[30] M. Uzun, H. Sun, D. Smit, O. Büyüköztürk, Structural damage detection using bayesian inference and seismic interferometry, Structural Control and Health Monitoring 26 (2019) 1–20. doi:https://doi.org/10.1002/stc.2445.

[31] X. Wang, R. Hou, Y. Xia, X. Zhou, Structural damage detection based on variational bayesian inference and delayed rejection adaptive metropolis algorithm, Structural Health Monitoring 20 (2020) 1518–1535. doi:https://doi.org/10.1177/1475921720921256.

[32] M.-T. Vakil-Baghmisheh, M. Peimani, M. H. Sadeghi, M. M. Ettefagh, Crack detection in beam-like structures using genetic algorithms, Applied Soft Computing 8 (2008) 1150–1160. doi:https://doi.org/10.1016/j.asoc.2007.10.003.

[33] S. A. Moezi, E. Zakeri, A. Zare, Structural single and multiple crack detection in cantilever beams using a hybrid cuckoo-nelder-mead optimization method, Mechanical Systems and Signal Processing 99 (2018) 805–831. doi:https://doi.org/10.1016/j.ymssp.2017.07.013.

[34] S. Khatir, K. Dekemele, M. Loccufier, T. Khatir, M. Abdel Wahab, Crack identification method in beam-like structures using changes in experimentally measured frequencies and particle swarm optimization, Comptes Rendus Mécanique 346 (2018) 110–120. doi:https://doi.org/10.1016/j.crme.2017.11.008.

[35] J. Joyce, Bayes' Theorem, in: E. N. Zalta (Ed.), The Stanford Encyclopedia of Philosophy, spring 2019 ed., Metaphysics Research Lab, Stanford University, 2019.

6 General conclusions and perspectives

Chapter abstract

This part summarizes the work and its results described in the previous chapters. It gives a brief discussion about the prospects and possible ways for improvements that can be applied in future studies of the proposed vibration-based methods for application in the process of structural health monitoring.

It briefly recalls the work presented earlier: (1) review of modern effective and popular methods of operational modal analysis, damage identification and existing problems; (2) improvement on the existing modal identification method that can deal with underdetermined cases in the time domain; (3) introduction of a new method of modal identification in the frequency domain; (4) development of a fast damage detection procedure based on a simplified relationship between damage and modal change; (5) presentation of an improved procedure for the detection of multiple damages in structures by replacing the computational costs associated with finite element modeling with a calculated developed analytical expression.

It then discusses some recommendations for future research that should be applied to improve the proposed methods and procedures for their use for modal identification as well as damage detection.

6.1 Conclusions

Structural health monitoring has always been a focus of research because the health and safety of structures depends on monitoring the occurrence, formation and propagation of structural damage. In the SHM system, the modal analysis and damage detection are the two most important components. This thesis has proposed a number of methods for modal analysis and damage detection used use in engineering structures. The main conclusions in this thesis are summarized in four major contributions, which are listed below:

1. The first contribution is an improvement of the existing modal identification technique based on the PARAFAC decomposition in the time domain. Recently proposed for operational modal analysis, PARAFAC decomposition based methods have been proven to

be efficient in underdetermined situations and in the presence of harmonic excitations. The third-order tensor of the covariance of responses is first decomposed into components corresponding to structural modes or harmonic deflections. The modal parameters are then deduced from the auto-covariance function of each component, and the distinction between the structural mode and the harmonic component is based on its kurtosis value. No criterion about the length of the auto-covariance function was given. However, the study of the thesis showed that this length should be chosen depending on the decomposed components, and an insufficient length of the auto-covariance function can lead to inaccurate results. To overcome this limitation, an enhanced procedure of the PARAFAC decomposition-based method for modal analysis in the time domain has been proposed. The minimum length of auto-covariance functions using natural periods and damping ratios is proposed to distinguish between harmonics and structural modes accurately.

2. The second contribution is the development of a novel method for modal identification based on PARAFAC decomposition in the frequency domain. Using the PARAFAC decomposition, a third-order tensor in frequency constructed from PSD of responses is first decomposed into rank-1 tensors that can be structural modes or harmonic components. The auto-PSD function of each rank-1 tensor is then used to identify modal parameters, while spectral kurtosis values are used for the distinction of structural modes and harmonics. Detailed analytic developments of the method are presented together with its practical step-by-step procedure. The performance of the proposed method has been investigated for proportional/non-proportional damping, closely spaced modes, underdetermined cases and in the presence of harmonic excitations. To the best of authors' knowledge, there was no similar modal identification method in the literature based on PARAFAC decomposition in frequency.

3. The third contribution is devoted to the proposal of an efficient method for the rapid detection and quantification of a single local change in the mass and/or stiffness of like-beam structures using identified modal parameters. Existing methods are based on a simplified heuristic expression between beam stiffness change alone and its impact on natural frequency shift and mode shape curvature to produce a curve for each mode expressing damage severity and damage location. In plotting several curves of identified modes, the stiffness change and its location are deduced manually from the coordinates of the intersection of these curves. The existing methods can however give inaccurate results of damage identification when the curves do not have the same intersection point. In addition, it is important to note that the variation in modal parameters occurs not only from the appearance of a stiffness change, but also from a local change in the mass of the structure. Therefore, the third contribution considers the relationship between local changes in the mass and/or stiffness of a beam and its natural frequency shift and mode shape, and explicitly gives an analytical expression. Based on the proposed expression, linear regression is applied to obtain accurate results of the change in the mass/stiffness of the beam. However, this proposed procedure identifies two possible modification positions: the real one and the fictitious one in cases of cantilever beams and clamped-clamped beams. But it was shown that the exact location can be determined without a doubt by using additional information, such as the difference between the mode shapes or curvatures of the intact state and those of the modified one.

4. The fourth contribution aims to extent the previously presented damage identification

procedure for multiple local changes in mass and/or stiffness. In general, natural frequency shifts between the healthy state and assumed damaged states are obtained by simulations using the Finite Element Method (FEM). Comparison between simulated and measured natural frequency shifts allows damage to be identified, for example, using an optimization step or Bayesian inference. In this contribution, the simulated natural frequency shifts are obtained directly from the analytic expression established in the former contribution instead of using FEM. The localization of damages is deduced based on the most probable locations given by the Bayesian inference. The proposed identification of damages becomes rapid because it skips the computational cost caused by FEM simulations. It can however introduce pseudo-damage locations that are symmetrical to the actual damage ones. These pseudo-damage locations can be easily eliminated by using other available information such as measured modal shape.

6.2 Perspectives

Despite some promising results were obtained and presented in this thesis, further works are always possible in order to enhance performance of proposed methods for modal identification as well as for damage detection. Below are some suggestions and ideas for further research that can enhance the proposed methods:

Modal identification

- The performance of the developed modal analysis method needs to be studied in more challenging situations, such as a structure that has several identical frequencies.
- PARAFAC decomposition-based methods in the time domain involve user selection of time-lag parameters to compute correlation matrices, but there is no optimal procedure for this selection. It is still necessary to develop a procedure for choosing such parameter and minimizing user intervention.
- In the proposed methods for mode analysis in this thesis, the stability graph is used to determine the number of active modes. However, this leads to multiple decompositions for the stability diagram. The problem of selecting the number of active modes without using stability diagram requests a development in future studies.
- The thesis considers the PARAFAC decomposition for third-order tensors in the time domain and frequency domain, but does not consider the decomposition in the time-frequency domain. Decomposition in the time-frequency domain can be used to examine the change in frequency over time. Therefore, it could be an interesting extension for modal analysis as well as damage detection.

Damage identification

- The use of mode shape comparison to eliminate the pseudo-failure locations can be resolved in simulation with a large number of mode shape points. In reality, the measurements are often limited. Therefore, the use of a limited number of measured points for eliminating the fake damage location is expected.
- The damage detection procedure proposed in the thesis detects damage based on natural frequency shifts, but it can produce symmetrical fake locations. This work does not

consider further information of the locations of measurements. Responses at different locations on structures contain different information, and thus responses at sites near the actual damage site have different information from responses at distant sites of the damaged area. Additional processing of the measured signals to eliminate spurious damage locations using the Hilbert transform should be considered.

- The proposed procedure for multiple damage detection in this thesis do not consider the use of change in mode shape between intact and damaged states for Bayesian inference in multiple damage detection. Therefore, the combination of changes in frequency and mode shape should be considered together for multiple damage detection using Bayesian inference.

A Résumé étendu en Français

La surveillance de la santé structurelle (SHM) des structures est primordiale pour une utilisation sûre et essentielle pour le développement durable. Parmi les méthodes existantes de SHM, les méthodes basées sur les mesures de vibration, sont les plus couramment utilisées. L'analyse modale opérationnelle (OMA) est très appropriée pour les structures réelles car elle offre plusieurs avantages : faible coût, utilisation normale des structures et surveillance continue. Cependant, elle présente quelques obstacles majeurs : (i) l'incertitude des paramètres modaux identifiés due à des excitations opérationnelles non mesurées et non contrôlées ; (ii) des problèmes de sous-détermination lorsque le nombre de réponses vibratoires mesurées est inférieur à celui des modes actifs ; (iii) la relation entre les endommagements exprimés par le changement des propriétés mécaniques comme la masse et la rigidité et le changement des paramètres modaux, n'est pas directe, et elle passe souvent par des étapes de recalage des modèles d'éléments finis, ce qui entraîne une charge importante de calcul ; (iv) en réalité, il peut y avoir des endommagements multiples dans une structure, et la détection de endommagements multiples n'est pas évidente. Par conséquent, les objectifs de cette thèse sont les suivants : (i) faire une analyse sur des méthodes efficaces et populaires pour l'analyse modale opérationnelle et pour l'identification des endommagements ; (ii) proposer des améliorations des méthodes existantes ou de nouvelles méthodes qui peuvent traiter les cas sous-déterminés ; (iii) développer une procédure de détection rapide des endommagements basée sur un lien simplifié entre les endommagements et les changements des paramètres modaux ; (iv) introduire une procédure améliorée pour la détection des dommages multiples dans les structures. Par rapport à ces objectifs, les résultats obtenus dans le cadre de cette thèse peuvent être résumés en quatre contributions principales suivantes : La première contribution est une amélioration de la technique d'identification modale existante basée sur la décomposition PARAllel FACtor (PARAFAC) dans le domaine temporel. Récemment proposée pour l'analyse modale opérationnelle, la méthode PARAFAC s'est avérée efficace dans des situations sous-déterminées et en présence d'excitations harmoniques. Le tenseur de troisième ordre de la covariance des réponses est d'abord décomposé en composantes correspondant aux modes structurels ou aux déflections harmoniques. Les paramètres modaux sont ensuite déduits de la fonction d'auto-covariance de chaque composante et la distinction entre un mode structurel et une composante harmonique est basée sur sa valeur de kurtosis. Aucun critère concernant la longueur de la fonction d'auto-covariance n'a été donné. Cependant, l'étude de la thèse a montré que cette longueur doit être choisie en fonction des composantes décomposées et qu'une longueur insuffisante de la

fonction d'auto-covariance peut conduire à des résultats inexacts. Afin de surmonter cette limitation, une procédure d'amélioration de la méthode PARAFAC existante a été proposée. Une longueur minimale des fonctions d'auto-covariance utilisant les périodes naturelles et les taux d'amortissement est suggérée pour distinguer avec précision les harmoniques des modes structurels. La deuxième contribution consiste à développer une nouvelle méthode d'identification modale basée sur la décomposition PARAFAC dans le domaine fréquentiel. En utilisant la décomposition PARAFAC, un tenseur d'ordre 3 en fréquence construit à partir de la densité spectrale de puissance (DSP) des réponses est d'abord décomposé en plusieurs tenseurs d'ordre de rang 1 qui peuvent être des modes structurels ou des composantes harmoniques. La fonction auto-PSD de chaque tenseur d'ordre 3 de rang 1 est ensuite utilisée pour identifier les paramètres modaux tandis que les valeurs de kurtosis spectral sont utilisées pour distinguer les modes structurels et les harmoniques. Les développements analytiques détaillés de la méthode sont présentés ainsi que sa procédure pratique étape par étape. La performance de la méthode proposée a été étudiée avec un amortissement proportionnel/non-proportionnel, des modes très rapprochés, des cas sous-déterminés et en présence d'excitations harmoniques. A notre connaissance, aucune méthode d'identification modale similaire basée sur la décomposition PARAFAC en fréquence n'existait dans la littérature. La troisième contribution est consacrée à la proposition d'une méthode rapide pour la détection et la quantification d'un changement local simple de la masse et/ou la rigidité de structures de type poutre en utilisant des paramètres modaux identifiés. Les méthodes existantes sont basées sur une expression heuristique simplifiée entre le changement seul de la rigidité d'une poutre et son impact sur le décalage de la fréquence naturelle et la courbure de la déformée modale pour produire une courbe correspondant à chaque mode exprimant la sévérité et la localisation des endommagements. En traçant plusieurs courbes de modes identifiés, le changement de rigidité et sa localisation sont déduits manuellement des coordonnées de l'intersection de ces courbes. Les méthodes existantes peuvent cependant donner des résultats inexacts de l'identification des endommagements lorsque les courbes n'ont pas le même point d'intersection. En outre, il est important de noter que la variation des paramètres modaux ne résulte pas seulement de l'apparition d'un changement de rigidité, mais aussi d'un changement local de la masse de la structure. Par conséquent, dans la troisième contribution, la relation entre les changements locaux de masse et/ou de rigidité d'une poutre et son décalage de fréquence naturelle et sa déformée modale est examinée et une expression analytique est explicitement donnée. Sur la base de l'expression proposée, une régression linéaire est appliquée pour obtenir des résultats précis du changement de masse et/ou rigidité des poutres. La quatrième contribution vise à étendre la procédure précédente d'identification des endommagements pour de multiples changements locaux de masse et/ou de rigidité. En général, les décalages de fréquence naturelle entre l'état sain et les états supposés endommagés sont obtenus par des simulations utilisant la méthode des éléments finis (FEM). La comparaison entre les décalages de fréquence naturelle simulés et ceux mesurés permet ensuite l'identification des endommagements en utilisant une étape d'optimisation ou une inférence Bayésienne par exemple. Dans cette contribution, les décalages de fréquence naturelle simulés sont obtenus directement à partir de l'expression analytique établie dans la contribution précédente au lieu d'utiliser la méthode des éléments finis. La localisation des dommages est déduite sur la base des emplacements les plus probables donnés par la référence Bayésienne. L'identification des endommagements proposée devient rapide car elle évite le coût de calcul causé par les simulations FEM. Elle peut cependant introduire des emplacements de pseudo-endommagements qui sont symétriques à ceux des endommagements

réels. Ces emplacements de pseudo-endommagements peuvent être facilement éliminés en utilisant d'autres informations disponibles telles que les déformées modales mesurées. Toutes les contributions ci-dessus ont été validées par des simulations numériques et des tests expérimentaux au laboratoire. Bien que de bons résultats aient été obtenus dans cette thèse, des travaux supplémentaires sont toujours possibles pour améliorer leur performance/précision pour l'analyse modale opérationnelle ainsi que pour l'identification des endommagements. Quelques idées sur les perspectives de la thèse sont donc proposées.

université PARIS-SACLAY
ÉCOLE DOCTORALE
Sciences mécaniques et énergétiques, matériaux et géosciences (SMEMAG)

Titre: Suivi de santé structurale basé sur l'identification modale opérationnelle

Mots clés: structure, analyse modale, détection de dommages, vibration, excitation harmonique.

Résumé: La surveillance de la santé structurelle (SHM) des structures est primordiale pour une utilisation sûre et essentielle pour le développement durable. L'analyse modale opérationnelle (OMA) pour SHM est appropriée pour les structures réelles car elle offre plusieurs avantages : faible coût, utilisation normale des structures et surveillance continue. Cependant, elle présente quelques obstacles majeurs : (i) excitations non mesurées; (ii) problèmes de sous-détermination; (iii) relation entre les endommagements et le changement des paramètres modaux, n'est pas directe; (iv) identification difficile des endommagements multiples. Par conséquent, les objectifs de la thèse sont : (i) faire une analyse sur des méthodes efficaces et populaires pour l'analyse modale opérationnelle et pour l'identification des endommagements ; (ii) proposer des améliorations des méthodes existantes ou de nouvelles méthodes qui peuvent traiter les cas sous-déterminés ; (iii) développer une procédure de détection rapide des endommagements; (iv) introduire une procédure améliorée pour la détection des dommages multiples. Les résultats obtenus dans le cadre de cette thèse peuvent être résumés en quatre contributions principales suivantes :

La première contribution est une amélioration de la technique d'identification modale existante basée sur la décomposition PARAllel FACtor (PARAFAC) dans le domaine temporel. Le tenseur de troisième ordre de la covariance des réponses est décomposé en composantes correspondant aux modes structurels ou aux déflections harmoniques. Une longueur minimale des fonctions d'auto-covariance utilisant les périodes naturelles et les taux d'amortissement est suggérée pour distinguer avec précision les harmoniques des modes structurels.

La deuxième contribution consiste à développer une nouvelle méthode d'identification modale basée sur la décomposition PARAFAC dans le domaine fréquentiel. En utilisant la décomposition PARAFAC, un tenseur d'ordre 3 en fréquence construit à partir de la densité spectrale de puissance (DSP) des réponses est d'abord décomposé en plusieurs tenseurs d'ordre de rang 1 qui peuvent être des modes structurels ou des composantes harmoniques. La fonction auto-PSD de chaque tenseur d'ordre 3 de rang 1 est ensuite utilisée pour identifier les paramètres modaux tandis que les valeurs de kurtosis spectral sont utilisées pour distinguer les modes structurels et les harmoniques. La performance de la méthode proposée a été étudiée avec un amortissement proportionnel/non-proportionnel, des modes très rapprochés, des cas sous-déterminés et en présence d'excitations harmoniques.

La troisième contribution est consacrée à la proposition d'une méthode rapide pour la détection et la quantification d'un changement local simple de la masse et/ou la rigidité de structures de type poutre en utilisant des paramètres modaux identifiés. La relation entre les changements locaux de masse et/ou de rigidité d'une poutre et son décalage de fréquence naturelle et sa déformée modale est examinée et une expression analytique est explicitement donnée. Sur la base de l'expression proposée, une régression linéaire est appliquée pour obtenir des résultats précis du changement de masse et/ou rigidité des poutres.

La quatrième contribution vise à étendre la procédure précédente d'identification des endommagements pour de multiples changements locaux de masse et/ou de rigidité. La comparaison entre les décalages de fréquence naturelle obtenus directement à partir de l'expression analytique établie dans la contribution précédente au lieu d'utiliser la méthode des éléments finis et ceux mesurés permet ensuite l'identification des endommagements en utilisant une inférence Bayésienne. L'identification des endommagements proposée devient rapide car elle évite le coût de calcul causé par les simulations FEM.

Toutes les contributions ci-dessus ont été validées par des simulations numériques et des tests expérimentaux au laboratoire.

Université Paris-Saclay
Espace Technologique / Immeuble Discovery
Route de l'Orme aux Merisiers RD 128 / 91190 Saint-Aubin, France

université PARIS-SACLAY
ÉCOLE DOCTORALE
Sciences mécaniques et énergétiques, matériaux et géosciences (SMEMAG)

Title: Structural health monitoring based on operational modal analysis

Keywords: structure, modal analysis, damage detection, vibration, harmonic excitation

Abstract: Structural health monitoring (SHM) is primordial for safe use and is essential for sustainable development. Among existing methods for SHM, vibration-based methods are the most commonly used. Operational modal analysis (OMA) is suitable for real structures as it offers several advantages: low cost, normal use of structures, and continuous monitoring. However, it has some main obstacles: (i) uncertainty in identified modal parameters due to unmeasured and uncontrolled operational excitations; (ii) underdetermined problems when the number of measured responses is less than that of active modes; (iii) the relationship between the damage in terms of change in mechanical properties like mass and stiffness and the change in modal parameters, is not straightforward, and it often goes through finite element update steps resulting in computational burden; (iv) in reality, there may be several damages in a structure, and the detection of multiple damages is not obvious. Therefore, the objectives of the thesis are: (i) overview of efficient and popular methods for operational modal analysis and damage identification; (ii) propose improvements to existing methods or a novel method that can deal with underdetermined cases; (iii) develop a procedure for rapid damage detection based on a simplified relationship between damage and changes in modal parameters; (iv) introduce an enhanced procedure for multiple damage detection in structures. To achieve these objectives, the obtained results of the thesis can be briefly summarized in the following four contributions.

The first contribution is an improvement of the existing modal identification technique based on the PARAllel FACtor (PARAFAC) decomposition in time domain. The third-order tensor of the covariance of responses is first decomposed into components corresponding to structural modes or harmonic components. A minimum length of autocovariance functions using natural periods and damping factors is suggested to distinguish between harmonics and structural modes accurately.

The second contribution is the development of a novel method for modal identification based on PARAFAC decomposition in frequency domain. Using the PARAFAC decomposition, a third-order tensor in frequency constructed from Power Spectral Density (PSD) of responses is first decomposed into rank-1 tensors that can be structural modes or harmonic components. The auto-PSD function of each rank-1 tensor is then used to identify modal parameters, while spectral kurtosis values are used for the distinction of structural modes and harmonics.

The third contribution is devoted to the proposal of an efficient method for the rapid detection and quantification of a single local change in the mass and/or stiffness of like-beam structures using identified modal parameters. This contribution considers the relationship between local changes in the mass and/or stiffness of a beam and its natural frequency shift and mode shape, and explicitly gives an analytical expression. Based on the proposed expression, linear regression is applied to obtain accurate results of the change in the mass/stiffness of the beam.

The fourth contribution aims to extent the previous damage identification procedure for multiple local changes in mass and/or stiffness. Comparison between natural frequency shifts obtained directly from the analytic expression established in the former contribution instead of using FEM and measured ones allows multiple damages to be identified using Bayesian inference. The proposed identification of damages becomes rapid because it skips the computational cost caused by FEM simulations. All the above contributions have been validated by numerical simulations and experimental laboratory tests.

Université Paris-Saclay
Espace Technologique / Immeuble Discovery
Route de l'Orme aux Merisiers RD 128 / 91190 Saint-Aubin, France